Chapter 2: Observations: Atmosphere and Surface

Coordinating Lead Authors: Dennis Hartmann (USA), Albert Klein Tank (Netherlands), Matilde Rusticucci (Argentina)

Lead Authors: Lisa Alexander (Australia), Stefan Broennimann (Switzerland), Yassine Abdul-Rahman Charabi (Oman), Frank Dentener (EU / Netherlands), Ed Dlugokencky (USA), David Easterling (USA), Alexey Kaplan (USA), Nzioka John Muthama (Kenya), Brian Soden (USA), Peter Thorne (USA / UK), Martin Wild (Switzerland), Panmao Zhai (China)

Contributing Authors:

Review Editors: Jim Hurrell (USA), Jose Marengo (Brazil), Fredolin Tangang (Malaysia), Pedro Viterbo (Portugal)

Date of Draft: 15 April 2011

Notes: TSU Compiled Version

Table of Contents

Executive Summary

[PLACEHOLDER FOR FIRST ORDER DRAFT]

2.1 Introduction

In this chapter, we assess the scientific literature on atmospheric and surface observations since the AR4 (IPCC, 2007a). The most likely changes are indentified based on current knowledge, following the new IPCC AR5 uncertainty guidance [reference needed].

As described in the AR4, the climate varies over all spatial and temporal scales: from the diurnal cycle to El Niño to multi-decadal and millennial variations. In this chapter, the changes are examined for the period with instrumental observations, since about 1860. The reference climate period is generally 1961–1990. For many variables derived from satellite data, information is only available for the post 1979 period. For this recent period, use is also made of dynamical reanalyses datasets of the global atmosphere.

The global mean surface temperature remains an important climate change metric for several reasons. First, the global mean surface temperature has traditionally been used to measure warming and has been monitored for several decades now. Using global mean temperature, the variability associated with regional variability is averaged out, giving a larger signal to noise ratio. Secondly, a readily link with global mean radiative forcing of the climate system exists, and as such global temperature plays a key role in the mitigation policy framework. Third, alternative measures of climate change, such as ocean heat content (see Chapter 3), can be fully assessed for recent years only due to a lack of observations prior to 2005.

In addition to changes in temperature, this chapter considers changes in the hydrological cycle, and in atmospheric composition, radiation budget, atmospheric circulation, and extreme events.

Besides global averages of climate variables, this chapter also focuses on a limited number of preferred patterns (or modes) of variability, which determine the main seasonal and longer-term climate anomalies at the regional scale. These patterns arise from the differential effects on the atmosphere of land and ocean, mountains, and anomalous heating, such as occurs during El Niño events. The regional response to global warming can be complex and perhaps even counter-intuitive, such as changes in planetary waves in the atmosphere that result in regional cooling (Trenberth et al., 2007).

Changes in time-averages of climate variables are assessed, as well as changes in variability and extremes. Extremes of weather and climate, such as droughts and wet spells, are important because of their large impacts on society and the environment. The nature of variability at different spatial and temporal scales is vital to our understanding of extremes.

The chapter uses the word ‘trend’ to designate a generally monotonic change in the level of a variable (IPCC, 2007a). Where numerical values are given, they are equivalent linear trends, though more complex changes in the variable will often be clear from the description. The chapter also assesses the physical consistency across different observations, which helps to provide additional confidence in trends.

[START BOX 2.1 HERE]

Box 2.1: Uncertainty in Observational Records

The vast majority of historical weather observations were never intended for climate research. Measurements have changed in nature over time as data demands, observing practices and technologies have changed. These changes almost always alter the characteristics of the measurements, changing their mean, their variability or both such that it is necessary to process the raw measurements before they can be considered useful for assessing the true evolution of the climate. This is true of all observing techniques that measure physical atmospheric characteristics. The uncertainty in observational records encompasses instrumental errors, errors of representivity (e.g., related to exposure, observing frequency, local time of observation, measurement geometry, and instrument environment) as well as errors due to physical changes in the

instrumentation (such as station relocations or new satellites). All further processing steps (gridding, interpolating, averaging) have their own particular uncertainties. For instance, changes in the in-situ observing network or irregular spacing of stations may cause errors in a spatially averaged series.

There is no unique, unambiguous, solution to identify and account for non-climatic artefacts in the vast majority of records which means we cannot be absolutely certain as to how the climate system changed. The only exception is certain atmospheric composition and flux measurements that are directly traceable through an unbroken, well-characterized measurement chain to internationally recognized absolute measurement standards. Such records, including the CO_2 record (Keeling, 1976), can be considered an accurate record of the true changes in the measure and as sensed by the instrument, although this obviously does not preclude non-instrumental effects. This is very much the exception to the norm.

Uncertainty in dataset production for all remaining variables falls into two distinct classes – parametric uncertainty and structural uncertainty. Parametric uncertainty is the range of estimates that arises solely through varying a restricted subset of methodological choices for which no rigorous basis exists. For example, when adjusting for an apparent break in a time series whether to use 2, 3 or 5 years of data either side to estimate this adjustment. But the overall methodological framework is not substantially questioned or varied in assessing parametric uncertainty. In contrast, structural uncertainty involves questioning fundamental assumptions about the choice of methodological framework. This uncertainty is most easily ascertained from having multiple independent groups assess the same data as they will have distinct approaches. It follows that structural uncertainty is almost always larger than parametric uncertainty and arguably more useful in assessing our knowledge of the true changes in climate. Therefore whenever multiple published estimates exist for a given parameter we have included them wherever possible to ensure an honest assessment of the state of our knowledge. Box 2.1, Table 1 consolidates the types of uncertainty that are present in climate analysis.

Many of the analyses we have assessed include a published estimate of parametric or structural uncertainty and this is far more the case now than it was at the time of AR4 (Trenberth et al., 2007). It is important to note that these constitute a very broad range of approaches. Great care should therefore be taken in comparing the uncertainty ranges where they are quoted as it invariably does not constitute a like-for-like comparison. In general studies that have been formulated and assessed against a comprehensive error model accounting for multiple potential error sources in a rigorous manner yield larger uncertainty ranges than those that consider a more restricted subset. This yields an apparent paradox in interpretation as naively lower uncertainty should be associated with a better product. However, in many cases this would be an incorrect inference as the smaller uncertainty range may instead reflect that the published estimate considered only a subset of the plausible set of sources of uncertainty. Where this is likely to cause confusion we clarify which approach was used to calculate published estimates of uncertainty and how comprehensive the error consideration was.

Furthermore, commonly trends are calculated from these datasets as a way to summarize them in a single number. But the climate system does not behave linearly so fitting a linear trend adds additional uncertainty. There is a further complication that is sometimes overlooked in assigning confidence intervals to such estimates. The atmosphere does not vary entirely randomly so there are fewer independent samples than there are time steps in the series. If today is anomalously warm then more likely than not tomorrow will be likewise. So, the uncertainty estimate needs to be inflated to reflect the fact that fewer independent samples exist. There is a rich and often confusing literature in this regard but the basic issue being addressed by all these approaches is that outlined above. In an annex to this chapter we have considered various options and alighted on an approach to calculating trends and their uncertainties that we employ throughout the chapter whenever we calculate them ourselves. This choice is a balance between applicability, comprehensibility and statistical elegance and is not meant to imply that this should be used universally. Using a common approach with a few standard trend periods is primarily designed to facilitate intercomparisons of results from different areas of the chapter.

Box 2.1, Table 1: Examples of types of uncertainty relevant for climate research.

Degree of processing	Type of uncertainty	Example
Station time series	Measurement uncertainty	Instrument calibration

	Procedural uncertainty	Change in standards (e.g., shelter), reporting
	Representivity in time and space	Station relocation, change in observation times
Homogenization	Structural uncertainty	All possible correction strategies
	Parametric uncertainty	Choices and parameters in a selected correction strategy
Averages and products	Coverage uncertainty	Gaps in time and space
	Representivity in time and space	Over-/underrepresentation of urbanized areas
	Structural uncertainty	All possible gridding and averaging strategies
	Parametric uncertainty	Choices and parameters in a selected gridding or averaging strategy
Trend calculation	Structural uncertainty	All possible trend methods
	Parametric uncertainty	Parameters in selected trend method

[END BOX 2.1 HERE]

2.2 Changes in Temperature

[PLACEHOLDER FOR FIRST ORDER DRAFT]

2.2.1 Land Surface Temperature

AR4 concluded global land surface temperatures had increased, particularly rapidly so since the 1970s. Warming was noted to be greatest in winter and spring over the Northern Hemisphere extra-tropics. Urban Heat Island effects were concluded to be real local phenomena but their impact on the global average trend much smaller than the trend itself. Diurnal Temperature Range was concluded to have narrowed with minimum increasing faster than maximum; but significant multi-decadal variability was highlighted. Since AR4 substantial developments have occurred including the production of revised global and regional estimates. These innovations have improved understanding of data issues and uncertainties and allowed better understanding of regional changes. However, the key findings in AR4 remain essentially unaffected.

Observations are available for most of the global land surface since the mid-1800s to early 1900s. Availability reduces recently due in part to data latencies. Some regions such as deserts and other extreme environments have never been adequately sampled (Figure 2.1). Non-digital temperature records continue to be found in various country archives and are being digitized.

[INSERT FIGURE 2.1 HERE]
Figure 2.1: Station availability for the GHCN monthly network for the late 19th century, the 1961–90 period of maximum station density and most recent decade.

Improvements have been made to the two main historical global data sets of land-based station observations, the Global Historical Climatology Network Version 3 (GHCN V3; (Lawrimore, 2011) and CRUTEM3 (Brohan et al., 2006). There remain some differences in station inventories and sources used.

GHCN V3 improvements, described in Lawrimore (2011), include elimination of “duplicate” time series for many stations, updating station data with the most recent data, the application of enhanced quality assurance procedures (Durre et al., 2010) and the application of a new pairwise homogenization approach for individual station time series (Menne and Williams, 2009). GISS continues to provide an estimate based upon GHCN but with different station inclusion criteria, additional night light adjustments and a distinct gridding and infilling method (Hansen et al., 2010).

Similarly, the CRUTEM3 data set has undergone improvements through updating of station time series, and additional quality assurance. Since CRUTEM3 is provided in gridded form, enhancements were made to the gridding technique.

The long-term variations and trends of available global land surface estimates are in broad agreement (Figure 2.2). As discussed extensively in AR4 differences generally arise from different methods used to spatially average station data into one global number (Vose et al., 2005b; [Easterling et al., 2011]). Land temperature evolution exhibits inter-annual, decadal and interdecadal variability that is grossly similar across all datasets. Uncertainties arising from choice of dataset do not impact the conclusion that global land surface temperatures have increased.

[INSERT FIGURE 2.2 HERE]
Figure 2.2: Global land surface temperature time series evolution estimates from 1880 to present.

[PLACEHOLDER FOR FIRST ORDER DRAFT] Regional analyses

2.2.1.1 Diurnal Variation

[A paper updating Vose et al., 2005a on mx/mn/dtr, adding 6 more years of data through 2010, is being done by Russ Vose and will be submitted by Summer 2011 and results available for the FOD. The next paragraph is a placeholder for those results.]

[PLACEHOLDER FOR FIRST ORDER DRAFT] The quasi-global annual trend in maximum and minimum surface air temperature for the period 1950–2010 is ?? per decade for maximum temperature and ?? per decade for minimum temperature (Figure 2.2). The diurnal temperature range (DTR: maximum minus minimum temperature) trends are ?? per decade (will say something about the character of DTR changes in relation to max/min much like the AR4 where the DTR time series flattens after about 1985). Spatial coverage in Vose et al. (2005a) and reported in AR4 for the period 1950–2004 was approximately 71% of the global land area and for Vose et al. (2011) for the period 1950–2010 coverage is approximately XX% of the global land area....

Regionally some differences have been reported. Makowski et al. (2009) find that the long-term trend of annual DTR in Europe over 1950–2005 changed from a decrease to an increase in the 1970s in Western Europe and 1980s in Eastern Europe. Roy and Balling (2005) found significant increases in both maximum and minimum temperatures for India, but little change in DTR over 1931–2002.

A number of studies have related changes in the DTR to changes in other variables. Zhou et al. (2009a) compared spatial trends in DTR to trends in precipitation, cloud cover, and leaf-area index (LAI), finding that decreasing trends in DTR correlated with increasing precipitation, cloud cover, and LAI, with stronger decreases in DTR in drier areas. Shiu et al. (2009) examined DTR, humidity and precipitation in Taiwan finding that decreases in night time relative humidity were related to increasing night time temperatures over 1961–2005. Jackson and Forster (2010) found that cloud cover, soil moisture, distance inland, solar radiation, and elevation along with vegetation type explained most of the seasonal and geographical variance in DTR, with vegetation and cloud cover having the strongest relationship.

AR4 discussed a so-called “weekend” effect in DTR for a number of regions including the USA, China, Japan, and Mexico [(Forster and Solomon, 2004)]. Since then similar effects have been found for Germany (Baumer and Vogel, 2007), China (Ho et al., 2009a; [Gong et al., 2006]), Tibet [(You et al., 2009)], Korea [(Kim et al., 2009)], southern Europe (Sanchez-Lorenzo et al., 2008b), and all Europe (Laux and Kunstmann, 2008). In each case the DTR for week days and weekend days is significantly different, in most cases greater on the weekend.

2.2.1.2 Urban Heat Islands and Land Use Effects

Estimates of large-scale temperature change have either avoided urban observing sites, or adjusted their data to match regional rural trends (Menne and Williams, 2009; [Parker, 2010]). Accordingly, Trenberth et al. 2007) concluded that “Urban heat islands are real but local, and have not biased the large-scale trends”. AR4 adopted Brohan et al. (2006)’s urban warming uncertainty of 0.06°C per century for global land surface air temperature trend.

Urban heat islands form because the modified surface affects the storage and transfer of heat. Therefore rural land-use change, such as clearance of forest for agriculture, also influences surface air temperature. Examples of regional modification of temperature were discussed in AR4. However attempts to estimate the effects of regional land-use changes, by comparing observations with a first-generation reanalysis (Box 2.2) were shown to be flawed.

Hansen et al. (2010) used satellite-based nightlight radiances to estimate the worldwide influence on land surface air temperature of local urban development down to 1 km granuality. Adjusting trends in lit areas to match neighbouring dark areas only reduced the global 1900–2009 temperature change (averaged over land and ocean) from 0.71°C to 0.70°C. Over the contiguous USA the temperature change was reduced by 0.07°C. [Efthymiadis and Jones (2010)] estimated an upper limit on urban influence of 0.02°C per decade, or about 15% of the total trends, in 1951–2009 from trends of coastal land and sea surface temperature.

McKitrick and Michaels (2007) analysed surface air temperature trend fields in terms of national socioeconomic and geographical indicators. They discounted atmospheric circulation as a driver because they found different relationships of the indicators with free-tropospheric temperature trends. But atmospheric circulation affects surface and tropospheric temperature patterns differently, weakening their conclusion that about half the trend in global-average land surface air temperature in 1980–2002 resulted from land-surface changes and faults in the observations.

[Wang et al. (2010)] used five-yearly 100m resolution Landsat images for 1980–2005 to measure areal urban growth in China. The influence on the national-average temperature trend was estimated to be 0.10°C/decade during 1980–2009 by reference to trends at stations with negligible urban growth within 20km, accounting for 21% of the total national warming. This estimate is similar to those of Ren et al. (2008) for north China for 1961–2000 on a population basis and Jones et al. (2008) for east China for 1951–2004 by reference to ocean surface temperatures. It is much smaller than McKitrick and Michaels (2007)'s estimate for China (about 0.3°C/decade) implicit in their Figure 4. It is much larger than the 0.01°C/decade estimate for northeast China for 1954–2005 made by [Li et al. (2010)] who only classified high-population sites as urban. Fujibe (2009) implicitly ascribes about 25% of warming trends in Japan in 1979–2006 to urban development.

[INSERT FIGURE 2.3 HERE]
Figure 2.3: Fall et al. (2010)'s Figure 6 comparing (inverted) "Observations minus Reanalysis" temperature trends (°C per decade) over the USA with the Hansen et al. (2001) nightlight-based urban.

Improved reanalyses have been used to estimate the urban and land-use signature in observed surface air temperature trends. Fall et al. (2010) found that the North American Regional Reanalysis, which does not assimilate observed surface air temperatures, generated overall surface air temperature trends for 1979–2003 similar to the US Historical Climatology Network over the USA; the geographical pattern of observations-minus-reanalysis trends was in good qualitative agreement with Hansen et al. (2001)'s nightlights-based adjustments (Figure 2.3). Observations-minus-reanalysis trends were most positive for barren and urban areas, in accord with Lim et al. (2008)'s results using the NCEP/NCAR and ERA-40 reanalyses, and negative in agricultural areas. Land-use changes to urban or barren (agriculture) caused observations-minus-reanalysis warming (cooling) respectively as expected from changes in surface heat fluxes. [Hu et al. (2010)] compared 4 reanalyses with surface air temperatures in eastern China, ascribing nearly a third of the overall warming in 1979–2008 to land-use changes. The influence of land-use change was greater at night, explaining nearly half of the observed decrease in frequency of nights colder than the 10th percentile.

2.2.2 Sea Surface Temperature

AR4 concluded that warming was strongly evident at all latitudes in Sea Surface Temperatures (SST) over each ocean. Significant spatio-temporal structures including the El Nino phenomenon in the Pacific and a hemispheric asymmetry in the Atlantic and their impact upon atmospheric circulation highlighted. Since AR4 there have been a number of new estimates of SST evolution and a step change in availability of metadata as well as improvements in data completeness. Whilst these new products and information have helped highlight and quantify uncertainties, they do not alter the conclusion that global SSTs have increased since the late 19th century.

2.2.2.1 Advances in Data and Understanding of Errors

Most historical SST observations arise from ships, with buoy measurements and satellite data becoming a significant contribution in the 1980s. Digital archives such as the International Comprehensive Ocean-Atmosphere Data Set [ICOADS, currently version 2.5; [Woodruff et al., 2011]] are constantly enriched as paper archives are imaged and digitised (Brohan et al., 2009). Improvements in the understanding of marine data have been expedited by the use of metadata such as WMO Publication 47 International List of Selected and Supplementary Ships (Kent et al., 2007) and the availability of observer instructions and other related documents. Data coverage prior to the second half of the nineteenth century is extremely poor (with little or no data prior to 1800), so pre-1850 SST data has not been widely used (Figure 2.7).

Since AR4 it has been increasingly recognized that the traditional definition of the "bulk" SST which assumes that the surface layer is well-mixed is valid only for night-time conditions or when surface winds are strong. In many cases, the surface layer will be stratified and its measured temperature will depend on the depth at which the measurement was made (Figure 2.4, Donlon et al. (2007)). The effect is significant for relatively shallow buoy observations (Kennedy et al. (2007) and for all satellite measurements. Converting measurements at different depths to the foundation SST (at 10 m depth) or reliably screening out measurements affected by surface stratification, though theoretically possible, still represent substantial challenges [(Merchant et al., 2008)].

[INSERT FIGURE 2.4 HERE]
Figure 2.4: Thermal structure of the ocean surface layer (adopted from Donlon et al. (2007) by GHRSST participants; https://www.ghrsst.org/SST-Definitions.html; [precise attribution needs to be].

Early data were systematically biased cold because they were made using canvas or wooden buckets that, on average, lost a great deal of heat to the air as they were hauled to the deck. This has long been recognized, and various "bucket correction" schemes developed, which use simplified physical modelling of measuring bucket's heat exchange with the air (Folland and Parker, 1995; Rayner et al., 2006) or statistical modelling based on the difference between measured SST and night marine air temperature (NMAT) observations (Smith and Reynolds, 2002). Prior to AR4 this was the only artefact adjusted in SST products. From about 1920 the situation became more complex. Some ships began making measurements of engine room intake (ERI) water. Despite the greater depth from which the water was taken, proximity to the hot engine often biased these measurements warm [(Kent et al., 2010)]. During 1950–1980, bucket designs improved, and heat losses became much smaller. Since the 1980s, many measurements have been made by drifting and moored buoys. The buoy measurements tend to be more reliable than those from ships, with smaller biases and measurement errors [(Kennedy et al., 2011a)]. Because of the prevalence of the ERI measurements, the overall ship SST data tend to be biased warm compared to the buoy data by 0.12-0.18K on average ([Emery et al., 2001]; Reynolds et al., 2010; [Kennedy et al., 2011a,c]).

Although less important than systematic biases for long-term trend analyses, random measurement errors play an important role in the understanding of small scale features and at times when data are sparse. Kent and Challenor (2006), [O'Carroll (2008)] and [Kennedy et al., 2011a] made estimates of the random measurement uncertainties in ship and buoy data. Ship data were found to be less reliable, on average, than buoy observations. Random sampling and measurement errors were shown to be twice as large in the global average when calculated appropriately to account for both correlated and uncorrelated aspects for HadSST3 [(Kennedy et al., 2011b,c)] as in the HadSST2 data set used in AR4 which erroneously estimated all sampling errors to be uncorrelated.

[INSERT FIGURE 2.5 HERE]
Figure 2.5: Fractional contribution to the global average SST from different measurement methods. The blue area represents bucket observations. The green area, engine inlet and hull contact sensor observations. The red area shows the contribution of moored and drifting buoys and the yellow area represents those observations that cannot be identified.

Temporal and spatial variations in relative contributions of different measurement methods to the total database (Figure 2.5) create a time-varying systematic bias in the mean SST (Figure 2.6), which is adjusted in HadSST3 [(Kennedy et al., 2011c)]. These adjustments are responsible for small but noticeable

differences in the global estimates of the SST from HadSST2 and HadSST3 prelim data sets (Figure SST4), the largest being the one due to the ERI-to-bucket transition at the end of World War II (Thompson et al., 2008). Their effect on linear trend estimates for periods of the order of a century is quite small, both globally (Table 2.1) and locally (Figure 2.7). It should be noted that there has not yet been any kind of independent re-estimation of biases in the SST record after 1941 so the structural component of the uncertainty has not been fully explored.

[INSERT FIGURE 2.6 HERE]

Figure 2.6: Effect of observational platform biases on global mean SST [(from Kennedy et al., 2011c)].

[INSERT FIGURE 2.7 HERE]

Figure 2.7: Global means of annually averaged anomalies from marine surface temperature data sets. See Table 2.2 for descriptions of the data sets. Anomalies for all data sets are computed with regards to a common estimate of 1961–1990 climatological normals for SST (Table 2.1, Smith and Reynolds, 1998). To aid visual comparison, the results for the night marine air temperature data set (MOHMAT4.3N) have been shifted up by 1.2°C.

Table 2.1: Data Sets of SST and NMAT Observations used in Subsection 2.2.2. These data sets belong to the following categories: as a database of in situ observations; gridded data sets of climate anomalies (with bucket or bias corrections applied as deemed necessary by their authors); globally complete interpolated data sets based on the latter products; and gridded data sets of the higher resolution that exist for the satellite data period. A data set of climatological normals used in Figure 2.4 is listed too. Temporal trends (in °C per decade) in annual averages of global mean anomalies are computed from the data contained in these data sets for 1891–2006 period (except where indicated otherwise) using ordinary least squares regression. Their uncertainties are given as two standard deviation of regression coefficients (correspond to 95% confidence interval for normal distributions).

Data set	Abbr.	Period	Space-Time Grid Resolution	Reference	Bucket / bias corr.	Trend α in annual global means for 1891–2006: $\alpha \pm 2\sigma$, °C/decade	Comment
Historical Database of In Situ Observations							
International Comprehensive Ocean – Atmosphere Data Set	ICOADS, v2.5	1662 – present; 1800 – present, 1960 – present	individual reports; 2°x2° monthly summaries; 1°x1° monthly summaries	Woodruff et al. (2011)	No	Not applicable w/o bucket corrections	Only 2°x2° monthly summaries for SST are used here
Gridded Data Sets of Observed Climate Anomalies							
U.K.M.O. Hadley Centre SST, v.2	HadSST2	1850 – present	5°x5° monthly	Rayner et al. (2006); Rayner et al. (2006)	Yes	0.062 ± 0.007	Will be superseded by HadSST2
U.K.M.O. Hadley Centre SST, prelim v.3	HadSST3 prelim	1850 – 2006	5°x5° monthly	[Kennedy et al. (2011bc)]	Yes	0.059 ± 0.007	Preliminary version produced in Dec 2010
U.K.M.O. Hadley Centre NMAT, v.4.3	MOHMAT4.3N	1856 – 2007?	5°x5° monthly	Rayner et al. (2003)	Yes	0.057 ± 0.008 (1891–2005)	Ends mid-2007 on hadobs.metoffice.com ; newer version is expected for AR5
Globally Complete Objective Analyses (Interpolated Products) of Historical SST Records							
U.K.M.O. Hadley Centre Interpolated SST, v.1	HadISST1	1870 – present	1°x1° monthly	Rayner et al. (2003); bucket correction: Folland and Parker (1995)	Yes	0.046 ± 0.005	newer version is expected for AR5; uses satellite data from 1981
JMA Centennial in-situ Observation Based Estimates of variability of SST	COBE SST	1891 – present	1°x1° monthly	[Ishii et al. (2005)]; bucket correction: Folland and Parker (1995)	Yes	0.050 ± 0.005	uses satellite data from 1981
NOAA Extended Reconstruction of SST, v.3b	ERSSTv3b	1854 – present	2°x2° monthly	Smith et al. (2008); bucket correction:	Yes	0.056 ± 0.006	V.3 is published but n/a; v.3b is different by excluding the satellite data : only

				Smith and Reynolds (2002)			website info
Higher Resolution Gridded Data Sets for Satellite Data Period							
NOAA Optimum Interpolation SST Analysis, v.2	NCEP OI SST, v.2	Nov 1981 – present	1°x1° monthly and weekly	Reynolds et al. (2002)	N/a	0.094 ± 0.03 (1982–2006)	Legacy product
NOAA Optimum Interpolation Daily SST Analysis, v.2	NCDC Daily OI SST, v.2	Sep 1981 – present	0.25°x0.25° daily	Reynolds et al. (2007)	N/a	Not computed yet	To be used for ZOD or later versions
U.K. NCOF Operational SST and Sea Ice Analysis and Reanalysis	OSTIA SST	1985 – present	0.05°x0.05° daily	[Donlon et al. (2011)]	N/a	Not computed yet	To be used for ZOD or later versions
U.K. (A)TSR Reprocessing for Climate	ARC SST	1991 – present	1 km pixels, 0.1°x0.1° grid averages, daily grids from day and night specific overflight times	Merchant et al. (2008)	N/a	Not computed yet	To be used for ZOD or later versions
Climatological Normals							
NCEP OI 1961–1990 SST monthly climatology	NCEP OI 61–90 SST monthly climatology	1961–1990 climatological average (12 monthly fields)	1°x1° monthly	Smith and Reynolds (1998)	N/a	Not applicable	Used as a common climatology for computing anomalies in **Figure 2.2.5**

Although noisier than SST, marine air temperatures are physically related and provide an independent measure of marine temperature change. Biases due to solar heating mean that night time observations (NMAT) having been used preferentially in climate analyses; further adjustments have been applied to account for the change in deck heights and the use of non-standard practices during World War II. Progress has been made on the analytical correction of solar heating biases in recent data (Berry and Kent, 2009; Berry et al., 2004). Although the known biases in NMAT and SST are largely independent it is possible that other biases are correlated via changes in the observational data set. Figure 2.8 illustrates that different versions of bucket corrections shift pre-1940 global means of observational data sets (HadSST2, HadSST3prelim) and interpolated products (HadISST1, COBE SST, ERSSTv3b) from the ICOADS SST values into the vicinity of the NMAT (MOHMAT4.3N).

[INSERT FIGURE 2.8 HERE]

Figure 2.8: Linear trends for 1891–2006 period in the annual means of uninterpolated gridded data sets of marine surface temperature observations. MOHMAT4.3N trend is through 2005. See Table 2.2.1 and references therein for data set details. Trends are computed by ordinary least squares (OLS). In white areas computed trends were not different from zero at 5% significance level.

2.2.2.2 Interpolated SST Products and Their Trends

Gridded analyses of historical SST (interpolated data sets) depend on their "analysis" method (e.g., how missing data are inferred and how existing data are smoothed) as well as on the underlying set of observations, their quality control (QC) and bias correction procedures. SST analyses such as HadISST (Rayner et al., 2003), ERSSTv3b (Smith et al., 2008) and COBE [(Ishii et al., 2005)], use statistical methods to fill areas of missing data. At the time of writing HadISST1 remains unchanged from AR4 (will be updated methodologically in 2011). The low-frequency analysis of ERSST has been optimised in version 3 to reproduce long-term trends in the data with greater fidelity; its further modification resulted in the most current version ERSSTv3b.

Linear trend estimates for three interpolated globally-complete gridded SST analyses are shown in Figure 2.9. Since the statistical interpolation reduces the effect of sampling error on the computed statistics, the trend patterns of analyzed products (Figure 2.9) are much smoother than those of uninterpolated ones (Figure 2.8), although the overall patterns are similar.

[INSERT FIGURE 2.9 HERE]

Figure 2.9: Linear trends for 1891–2006 period in the annual means of interpolated globally complete SST data sets. See Table 2.2.1 and references therein for data set details. Trends are computed by OLS. In white areas computed trends were not different from zero at 5% significance level.

HadISST1 and COBE SST resemble each other because these products are based on observational datasets to which similar bucket correction schemes (Folland and Parker, 1995) were applied, while ERSST3b used a different bias correction scheme (Smith and Reynolds, 2002). Differences in the overall 1891–2006 trend patterns for interpolated data sets are driven mostly by the data differences in the first half of the trend period (1891–1948). In the later half, 1949–2006, trend estimates are much more similar to each other (Figure 2.10), although their patterns are less uniform than those in Figure 2.9: features of multidecadal climate in North Pacific and North Atlantic Oceans variability are much more prominent in 57-year linear trend patterns than they are in 114-year trend patterns.

[INSERT FIGURE 2.10 HERE]
Figure 2.10: Linear trends for 1949–2006 period in the annual means of interpolated globally complete ("analyzed") SST data sets. See Table 2.2.1 and references therein for data set details. Trends are computed by OLS. In white areas computed trends were not different from zero at 5% significance level.

2.2.2.2 Satellite SST Products

Since the early 1980s, satellites have been a hugely valuable resource. Satellite observations can suffer from both intra-satellite and inter-satellite biases with spatially- or temporally-dependent patterns [(Donlon et al., 2011) and references therein]. Corrections of these biases (e.g., in AVHRR-based SST products) usually require some use of in situ data. Once the biases are corrected, however, an unprecedented spatial and temporal resolution is achieved for the global SST field. The period of record now extends to 30 years for the AVHRR data (Figure 2.5) and about half of that for other types of sensors. Moreover, accumulated satellite data from the dual-view radiometers, ATSR-1,2 (Along-Track Scanning Radiometer), and (A)ATSR, has a potential to provide satellite-based SST estimates with a few km footprint that are accurate and virtually independent of in situ data. The along track scanning radiometer instruments were designed to fulfil the needs of climate researchers [(Llewellyn-Jones et al., 2001)]. [O'Carroll et al. (2008), Corlett et al. (2006) and Barton (2007)] showed that biases and errors from ATSR retrievals were significantly lower than those from other satellite instruments. Such a product may allow a thorough validation of bias-correction schemes for various kinds of in situ data (Figure 2.11).

[INSERT FIGURE 2.11 HERE]
Figure 2.11: Consistency of bias corrections to the in situ SST data with independent satellite observations: (top) Co-located monthly, 5º area global average SST anomalies August 1991 to December 2007 (relative to 1961–1990) for the ATSR instruments (red) and HadSST2 (black, Rayner et al., 2006). D3 retrievals were used where they were available, but between 1992 and 1996 D2 retrievals from the ATSR-1 instrument were used. The dashed black line is an estimate of the HadSST2 time series corrected for the bias between drifting buoys and ships. (bottom) Fractional contribution of drifting buoy observations to the global average calculated by taking the area weighted average of the fraction of drifting buoy observations in each grid box. The correction is shown on the right-hand axis.

2.2.3 Global Combined Surface Temperature

AR4 considered analyses from NASA GISS, NOAA's NCDC and the HadCRUT product. These were concluded to be consistent within their stated uncertainties and to exhibit centennial scale warming which had accelerated in the most recent period. All three groups have updated their analysis. These updates have not substantially altered the conclusion that the world is warming on multi-decadal timescales and that this warming rate has increased since the 1970s.

2.2.3.1 Advances in Combined Surface Temperature Analysis

[PLACEHOLDER FOR FIRST ORDER DRAFT: HadCRUT paragraph to describe changes hopefully will see text of paper(s) before first order draft but not available at present time so this placeholder heads up that a paragraph will be introduced here.]

[PLACEHOLDER FOR FIRST ORDER DRAFT: to be updated by FOD when planned NCDC merged product paper currently in draft is available.] The product from NOAA's NCDC has been updated to incorporate GHCNv.3 land data detailed in Section 2.2.1. For the marine component ERSST3b is a variant on the documented v3 (Smith et al., 2008) which removes the satellite data from more recent decades which was discovered to have a relative bias compared to in-situ data in certain regions. The merging of land and SST components and infilling technique has remained unchanged with the exception that observed very high latitude land data which had been removed in the infilling step has now been reinstated in the final fields.

Rather than undertaking a fundamentally distinct homogeneity assessment exercise NASA GISS use data products prepared by others with some additional adjustments and a methodologically distinct station selection, merging and averaging technique. Since AR4 they have undertaken several updates and a published sensitivity analysis focussed primarily around their urban heat island adjustments approach (Section 2.2.1.2) and choice of product and method for merging pre-satellite era and satellite era SSTs (Hansen et al., 2010). Over land this analysis utilized a combination of raw GHCN data and adjusted USHCN data. In addition Antarctic data from a separate dedicated Antarctic archive that has been quality controlled but not adjusted were used. For SST several alternative datasets or combinations of datasets were considered and these choices had an impact of the order 0.04K over the period of record. An improved concatenation of pre-satellite era and satellite era products was discussed which removed a small apparent cooling bias in recent times. It was stressed that such choices did not substantially alter conclusions regarding the rate of warming. [PLACEHOLDER FOR FIRST ORDER DRAFT: In 2011 the land record component was updated to include the homogenized GHCN v.3 series incorporating the USHCN v.2 adjustments technique globally.]

[PLACEHOLDER FOR FIRST ORDER DRAFT: Planned Met Office poor-mans structural uncertainty through merging candidate sst and land products under different approaches likely to be discussed either here or in following section in FOD assuming done on that timescale].

2.2.3.2 Synthesis of Global Surface Temperature Estimates

Global mean surface temperatures have increased since the late 19th century (Figure 2.12). Warming has not been linear; most warming occurred in two periods – 1900–1940 and 1970 onwards. Starting in the 1980s each decade has been warmer than all preceding decades in the record by a larger amount than can be accounted for by recognized uncertainties in the data products (Figure 2.13). Furthermore, each year in these decades has been warmer than the average of the preceding decade.

Differences between datasets are much smaller than both inter-annual variability and the long-term trend (Figure 2.12). However, there are interesting decadal timescale differences. Much interest has focussed on differences in the period since 1998 and the oft-repeated meme 'has global warming stopped?', discussed in detail in the context of model behaviour and natural variability in Chapter 10. During this period HadCRUT3 exhibits little trend whilst the remaining products show a warming trend. Hansen et al. (2010) contend that this relates primarily to different approaches to infill for missing data, arguing that recent warming has been under-estimated in HadCRUT as it does not adequately account for rapid northern polar region warming. This is corroborated by Simmons et al. (2010) in comparing HadCRUT to spatially complete ERA reanalyses products. Subsampling to HadCRUT fields led to excellent agreement but a systematic under-estimation vis-à-vis spatially complete sampling of ERA. This solely reflects upon how the different groups choose to attempt to account for the issue of incomplete sampling in estimating a truly global mean rather than on fundamental dataset quality. The HadCRUT dataset, which is the most conservative in undertaking no interpolation but rather folds this aspect into its uncertainty estimation instead, is consistent with the remaining datasets within its uncertainty estimates. Differences between datasets are larger in earlier periods that have received less focus. They are particularly large prior to c.1945 when observational sampling is much more incomplete.

[INSERT FIGURE 2.12 HERE]
Figure 2.12: Global mean time series at annual resolution from a straight average of the three data products, plus offset from this differences between products. Right hand panel shows decadally averaged values.

[INSERT FIGURE 2.13 HERE]
Figure 2.13: Decadal mean anomalies and associated uncertainties based upon Brohan et al. (2006) uncertainty model for HadCRUT3. Anomalies are relative to a 1961–1990 climatology period. Use of NCDC or GISS plus their uncertainties would yield grossly similar results and a similar conclusion that each of the last three decades in turn has been significantly warmer than all preceding decades in the record.

Warming has been far from globally uniform. Early 20th century warming was dominated by Northern Hemisphere polar and mid-latitude region warmth, whilst the more recent warming has been much more global but again with a maximum in the extra-tropical Northern Hemisphere (Figure 2.14). High frequency variability is greatest in polar regions with a minimum in the sub-tropics. Temperature changes in high Southern latitudes are highly uncertain owing in part to very poor observational coverage and the challenging physical measurement environment.

[INSERT FIGURE 2.14 HERE]
Figure 2.14: Hovmuller plot of surface anomalies from HadCRUT3 on an annual basis (left hand panel) and decadally averaged (right hand panel). Anomalies are relative to a 1961–1990 climatology.

Since 1901 almost all of the globe has experienced warming (Figure 2.15). This warming is greater over land than ocean in general although the SE contiguous United States, Central Africa, SE Asia, Australia and Patagonia have exhibited little or no net warming. The only ocean region not to have exhibited warming is the North Atlantic south of Greenland. Warming is generally greater in mid- to high-latitude regions. Over the recent period of rapid warming again most of the globe has exhibited warming at the surface. Exceptions are Australia, parts of SE Asia, much of the Southern Ocean and the Eastern Pacific. [PLACEHOLDER FOR FIRST ORDER DRAFT: Text to go here on comparison of the three datasets if we go multipanel here – see Figure comment.]

[INSERT FIGURE 2.15 HERE]
Figure 2.15: Global mean trend maps from NCDC surface record for 1901–2010 (left hand panel) and 1979–2010.

Trends in surface temperature over the recent period of warming have been far from seasonally invariant in some regions (Figure 2.16). Particularly marked is seasonal trend variation over much of Siberia with a cooling in winter and rapid warming in both spring and autumn. Noting the lack of significance, this may reflect end-point effects on trend estimation given the large interannual variability in winter half year temperatures in the region. More muted seasonal variations also exist for much of Western Canada and Alaska with spring and summer cooling and winter warming. Trends are generally greater in winter and spring than summer and autumn in the Northern Hemisphere whilst Southern Hemisphere trends overall are more seasonally invariant.

[INSERT FIGURE 2.16 HERE]
Figure 2.16: Seasonality of trends from the NCDC surface temperature analysis over the period since 1979.

2.2.4 Soil Temperature

[PLACEHOLDER FOR FIRST ORDER DRAFT]

2.2.5 Upper Air Temperature Including Stratosphere

Radiosonde records extend back to the early 20th century but most analysis consider 1958 onwards. Temperatures, measured as the balloon ascends, are reported on distinct levels. Satellites have monitored tropospheric and lower stratospheric temperature trends since late 1978 through the Microwave Sounding Unit (MSU) and its follow on Advanced Microwave Sounding Unit (AMSU) since 1998. These measures of upwelling radiation represent bulk atmospheric temperature (Figure 2.2.17). The ‘Mid-Tropospheric’ (MT) MSU channel that most directly corresponds to the troposphere has 10-15% of its signal from both the skin temperature of the Earth’s surface and the stratosphere. Two alternative approaches have been suggested for removing the stratospheric component based upon differencing of view angles and statistical recombination

with LS (Fu et al., 2004; Spencer and Christy, 1992). On the MSU satellite series in addition there was a Stratospheric Sounding Unit (SSU) that measured at higher altitudes (Seidel, 2011).

[INSERT FIGURE 2.17 HERE]
Figure 2.17: Vertical weighting functions for satellite temperature retrievals discussed in this chapter. The dashed line indicates the typical maximum altitude achieved in the historical radiosonde record.

Understanding of free atmosphere temperature trends has evolved substantially since inception of the IPCC process and particularly rapidly since AR4 (Thorne, 2011b; Christy et al., 2011). Previous ARs highlighted the presence of significant uncertainty and possibility of hitherto unidentified issues (Thorne, 2011b). Despite this AR4 concluded that globally the troposphere was warming at a rate indistinguishable from reported surface trends over the common period of record. Trends in the tropics were concluded to be more uncertain although even this region was concluded to be warming. Globally, the stratosphere was concluded to be cooling over the satellite era starting in 1979. These conclusions remain essentially unaltered despite the advancements detailed below.

2.2.5.1 Advances in Radiosonde Records

For AR4 only two published estimates that had assessed homogeneity issues existed – RATPAC (Free et al., 2005) and HadAT (Thorne et al., 2005b). Three additional estimates now exist using novel and distinct approaches in addition to a systematic effort to understand uncertainty in the HadAT product. These advances significantly modify understanding of the structural uncertainty (Thorne et al., 2005a). Trend estimates from these various products over their common period of record are summarized in Figure 2.m.

[INSERT FIGURE 2.18 HERE]
Figure 2.18: Radiosonde product global temperature trend estimates from four datasets (symbols) and the estimated structural uncertainty in the HadAT product from Thorne et al. (2011a) (Box whiskers denote median estimator, 25-75th percentile and range) over the common period of record 1958–2003. All trend estimates are from median of pairwise slopes technique. Global averages were created by calculating zonal means and then weighting zonal anomalies by cos(lat). The four best estimates used are HadAT2 (Δ), IUK (□), RICH (+) and RAOBCORE (◊).

A group at University of Vienna have produced a suite of products: RAOBCORE / RICH. Data at the individual observation resolution are compared to analysis increment time series from ERA-40 (Uppala et al., 2005) using a Standard Normal Homogeneity Test variant (Haimberger, 2007) to ascertain breakpoints. Two distinct approaches to bias adjustments yield: i) RAOBCORE which uses the analysis increment field; and ii) RICH which uses apparently homogeneous neighbour segments. Uncertainties arising from readily apparent non-stationarity of the analysis increment field for RAOBCORE have been addressed by several variants and sensitivity studies (Haimberger, 2004, 2007; Haimberger et al., 2008). The RICH product has only an indirect dependency on this field as the adjustments are neighbour based.

Sherwood and colleagues developed an iterative universal kriging approach, commonly used in geostatistics, for radiosonde data (Sherwood, 2007) and applied this to a global network (Sherwood et al., 2008) to create IUK. Breakpoints were derived hierarchically looking first at evidence for breaks in 00Z-12Z series, then breaks in the series with twice daily measures, and finally those with once daily ascents. Breakpoint detection was undertaken at the monthly timescale and, unlike all other methods, made no recourse to metadata. The adjustment included fitting the resulting raw data at the observation resolution to a set of basis functions that include spatial and temporal information inferred from the entire global network and breakpoint locations plus a noise term that iterated to a best fit, minimizing the noise term. They concluded that issues likely remained in the deep tropics even after homogenisation. Recourse to metadata and the analog cases used in the HadAT work (Titchner et al., 2009) increased confidence in the product (Sherwood et al., 2008).

The original HadAT algorithm (Thorne et al., 2005b) included substantial human input. Although this has advantages, there are distinct drawbacks over reproducibility and the ability to assess fundamental uncertainties. The group created an automated version of HadAT, pulling out a large number of non-rigorously based methodological steps as system tunable parameters and created an ensemble (McCarthy et

al., 2008). They then created four distinct analog worlds that shared the spatio-temporal sampling of the real-world and, crucially, known error structures. Running the ensemble against these analogs enabled a degree of benchmarking and a reassessment of likely real-world trends (Titchner et al., 2009). This permitted a lower bound estimate but no upper bound. In a final analysis step, in collaboration with IUK, RATPAC, and RAOBCORE teams more wide ranging methodological choices were examined (Thorne, 2011a). The largest impact was varying the input data temporal resolution from seasonal averages down to pentad (5-day average) resolution. A subset of results from this analysis that exhibited consistent behaviour across all four analogs was used under a conditional probability framework to yield an estimate of the likely solution range. This includes all other radiosonde datasets for global mean trends over the common period of record (Figure 2.18).

2.2.5.2 Advances in MSU Satellite Records

AR4 considered estimates produced from three groups: UAH (University of Alabama in Huntsville); RSS (Remote Sensing Systems) and VG2 (Vinnikov and Grody). Of these only UAH and RSS products have been updated. A new product termed STAR has been produced since AR4.

The UAH group, aided by citizen scientists, removed an apparent seasonal cycle artefact in the latter part of their record related to the introduction of AMSU [reference needed / J. Christy, xxxx] in version 5.3. In 2011 the climatological baseline used was changed to 1981–2010 to produce version 5.4. Both had negligible impact on trend estimates.

Version 3.2 of the RSS product (Mears and Wentz, 2009a, 2009b) incorporated a subset of AMSU instruments (which had been included in UAH since (Christy et al., 2003). Given the non-coincidence of the radiance bands it was concluded an instantaneous correction is required to merge MSU and AMSU as they sense slightly different layers. This issue is two-fold in that there will also be a systematic long-term impact unless trends are vertically isothermal, which they are not (Mears, 2011). Using HadAT data the impact was estimated to be no more than 5% of the trend. Several additional changes were introduced in v.3.2 with the two most significant being accounting for latitudinal error structure dependencies, and a more physical handling of instrument body temperature effect issues in response to Grody et al. (2004). In early 2011 version 3.3 was released which incorporated all the AMSU instruments and led to a de-emphasising of the last MSU instrument which still after 15 years remained operational, slight trend reduction over the post-1998 period, and a reduction in apparent noise. [PLACEHOLDER FOR FIRST ORDER DRAFT: they are transitioning to 3.3 so some words on this will be needed for FOD once the new version is documented. Figures use 3.3.]

RSS also produced a comprehensive model of their parametric (internal) uncertainty (Mears, 2011) employing a Monte Carlo approach considering all processing choices that yielded non-negligible impacts at any time or space scale allowing inter-dependencies to be fully expressed. As the processing is linear any errors in early steps cascade through remaining steps. For large-scale trends dominant effects were intersatellite offset determinations and, for tropospheric channels, diurnal drift. RSS diurnal drift adjustment is driven by data from a climate model. Use of two alternative models yielded substantial sensitivity particularly in desert regions. Uncertainties were of the order 0.1K/decade at the global mean for both tropospheric channels and the stratospheric channel but smaller for the tropopause channel. At smaller space and timescales sampling effects tended to dominate.

The new STAR analysis used a fundamentally distinct approach for the critical inter-satellite warm target calibration step (Zou et al., 2006a). Satellites orbit in a pole-to-pole configuration. Near the poles they measure several times a day, whereas in the deep tropics it is about every other day. There are normally two satellites in operation phase separated so that they sense in local morning and afternoon in the ascending orbital node. Over most of the globe they never intersect. The exception is the polar regions where they quasi-regularly (typically once every 24 to 48 hours but this is orbital geometry dependent) sample in close proximity in space (< 111 km) and time (< 100 s). The STAR technique uses these Simultaneous Nadir Overpass (SNO) measures to characterize inter-satellite biases and the impact of instrument body temperature effects before accounting for diurnal drift. Suitably close samples in space and time yield inter-satellite error characteristics, although they remain two point comparisons between uncertain measures so cannot guarantee absolute accuracy.

Initially STAR considered solely MT (Channel 2) near-nadir measures since 1987 over the oceans (Zou et al., 2006a). It was subsequently expanded to include more view angles and TS (Channel 3) and LS (Channel 4) and multi-channel recombinations along the Fu et al. (2004) approach to remove stratospheric impacts (Zou et al., 2009). The consistency of recombined products was used to infer a degree of inter-channel consistency and build confidence. In version 1.2 the product was extended to 1979 and to include land (Zou and Wang, 2010). Additional processing to account for residual instrument body temperature effects building upon the UAH methodology and diurnal corrections based upon RSS were employed to enable these innovations. In version 2.0, STAR incorporated the AMSU observations inter-calibrated by the SNO method to extend to the present [reference needed / Zou, xxxx]. STAR exhibits more warming / less cooling at all levels than UAH and RSS. For MT and LS (Zou and Wang, 2010) conclude this does not primarily relate to use of the SNO technique but rather differences in remaining processing.

2.2.5.3 Intercomparisons Between Various Long-Term Products

Since AR4 there have been a number of intercomparisons. Because no dataset is directly traceable to absolute or even relative standards, and therefore there is no unimpeachable truth, such comparisons can never absolutely determine whether residual biases exist in any single product. What they can highlight is areas of disagreement between products and such information can potentially be used in combination with physical understanding to elucidate issues. Interpretation is complicated as most studies considered dataset versions that have since been superseded and it is unclear whether documented issues any longer pertain.

Several studies compared UAH and RSS products to raw / homogenized radiosonde station level data locally or regionally. Christy and Norris (2006) concluded that UAH was more reasonable than RSS when compared to VIZ manufactured radiosondes operated by the United States. Christy et al. (2007) drew similar conclusions for LT using tropical radiosonde stations operated by a mixture of countries and with a mix of instrumentation. Christy and Norris (2009) confirmed these general findings for Australian radiosonde data. The transition from NOAA-11 to NOAA-12 was identified as the primary period when the different comparisons consistently pointed towards an issue in RSS. Christy et al. (2007) noted that this coincided with Pinatubo and that RSS was the only product, either surface or tropospheric, that exhibited tropical warming immediately after the eruption when physically cooling would be expected. Christy (2010) later expanded this analysis incorporating additional new data products again concluding that RSS exhibited spurious warming. Randall and Herman (2008) came to similar findings independently. But these various studies also revealed other potential issues. MSU records were most uncertain when satellite orbits are drifting rapidly (Christy and Norris, 2006, 2009). It was cautioned that there were potential common residual biases in the MSU records. Drifts could not be explained as residual radiosonde artefacts by the comprehensive metadata gained for the VIZ and Australian networks.

Mears and Wentz (2009a) compared global, tropical and hemispheric RSS LT to UAH and the various radiosonde datasets. Noting the importance of subsampling in space and time (Free and Seidel, 2005) each comparison involved firstly spatio-temporal subsampling which increased series congruence (Mears and Wentz, 2009a). It was concluded impossible to ascertain anything unambiguously regarding MSU differences. Mears (2011) generalized this approach to other levels and incorporated both STAR and their internal uncertainty estimates. These uncertainties overlapped with other datasets only in approximately half of cases (Figure 2.2.24). It was therefore concluded that structural uncertainty was an important factor. Mears (2011) noted that there are potentially many intercomparison performance metrics and implications made critically depended on this choice. Specifically, UAH exhibited better trend agreement on average but also an outlier zonal trend structure with much greater equator to pole trend gradients than any other dataset.

A pair of papers compared reanalyses to observation-based estimates (Bengtsson and Hodges, 2011; Xu and Powell, 2010). Bengtsson and Hodges (2011) found evidence of a potential jump in RSS in 1993 over the tropical oceans, discussed earlier. Xu and Powell (2010) used an ensemble spread approach considering all radiosonde datasets and reanalyses, finding that the spread in reanalyses was greater than between radiosonde products, particularly in the stratosphere. However, much of this related to inclusion of early generation reanalyses products which had been heavily caveated for free atmosphere trend analysis [(Karl et al., 2006)]. Modern reanalyses products were in much greater concordance.

Several dataset papers or data-model comparisons compared trends of suites of estimates with one another (e.g., Douglass et al., 2008b; Santer et al., 2008; Sherwood et al., 2008; Titchner et al., 2009; Thorne, 2011a; Christy, 2010). Most have treated each observational estimate equally. Some analysis, however, have used deductive reasoning to discard or downplay certain datasets, often based upon published intercomparisons (Christy et al., 2011; Christy, 2010). This yields trend estimates that have one or more existing dataset outside the quoted range; in those approaches published precluding solutions which exhibit greatest warming rates. Whilst these products may well be implausible estimates of the single, unknown, real-world climate trajectory it is not scientifically possible to conclude so definitively for the reasons given in the introductory paragraph to this sub-section. Therefore in Section 2.2.5.7 no subsetting is undertaken.

2.2.5.4 GPS-RO Data and Intercomparisons with Datasets

Global Positioning System (GPS) radio occultation (RO) now represents a mature remote sensing technique ([GCOS, 2004]; Anthes et al., 2008; Hajj et al., 2004; Ho et al., 2009c; [Kuo et al., 2004; NRC, 2007; WMO, 2007]). The highly stable observations can be used as global references in orbit (Baringer et al., 2010). Currently, it represents the only self-calibrated SI traceable raw satellite measurements ([Ohring et al., 2007]; Baringer et al., 2010). The fundamental observation is time delay of the occulted signal's phase traversing the atmosphere. With a GPS receiver on board a low-Earth orbiting (LEO) satellite, the occulted signal's phase transmitted from GPS satellites, which are delayed and bent due to atmospheric refraction, can be detected. The traceability of the RO data is established by subsequently correcting and resolving the clocks of the GPS satellites and LEO satellites with a network of GPS ground receivers, whose clocks are tied to atomic clocks.

GPS RO measurements have several attributes that make them suited for climate studies: (i) they exhibit no satellite-to-satellite bias (Hajj et al., 2004; Ho et al., 2009c), (ii) they are of very high precision (Anthes et al., 2008; Foelsche et al., 2009; Ho et al., 2009c), (iii) they are not affected by clouds and precipitation, and (iv) they are insensitive to retrieval error when used to estimate inter-annual trends in the climate system (Ho et al., 2009d). GPS-RO observations can be used to derive atmospheric temperature profiles in the upper troposphere and lower stratosphere (UT/LS) (Hajj et al., 2004; Ho et al., 2009c; [Kuo et al., 2004]). With their quality unaffected by the surrounding environment (e.g., geo-location, day and night, etc.), these data have been used to identify systematic temperature biases for different radiosonde sensors (Kuo et al., 2005; Sun et al., 2010; [He et al., 2009; Ho et al., 2010]). [Ho et al., (2011a)] demonstrated that upper air temperature trends derived from radiosondes are highly dependent on sensor type.

Recently, Ho et al., (2009b; 2007; 2009c, [2011b]) used the high-resolution CHAMP and COSMIC temperature profiles (from about 60 m near the surface to about 1.5 km at 40 km) from 2001 to 2010 to simulate the AMSU LS temperature and used these data to calibrate LS from various AMSU missions. Regional trend estimates for this and the other MSU-based datasets are listed in Table 2.2. The time series agreement varies with latitude (Figure 2.19). LS anomalies from UAH and STAR generally agree well with those from RO calibrated AMSU.

[INSERT FIGURE 2.19 HERE]

Figure 2.19: LS anomalies of RSS, UAH, STAR, and RO_AMSU for a) the entire globe (82.5ºN–82.5ºS), b) 82.5ºN–60ºN, c) 60ºN–20ºN, d) 20ºN–20ºS, e) 20ºS–60ºS, and f) 60ºS–82.5ºS. The orange line indicates the mean trend for RO_AMSU.

Table 2.2: Trends for the period 200106–201008 of LS Tb anomalies (in K/decade) for RSS, UAH, STAR, RO_AMSU, RSS-RO_AMSU, UAH-RO_AMSU, and STAR-RO_AMSU for the global (82.5°N-82.5° S) and five latitudinal zones.

	RSS	UAH	STAR	RO_AMSU	RSS-RO_AMSU	UAH-RO_AMSU	STAR-RO_AMSU
82.5°N-82.5° S	-0.88	-0.44	-0.46	-0.54	-0.34	0.1	0.08
60°N – 82.5° N	-0.65	-0.21	-0.22	-0.22	-0.43	-0.01	0.0
20° N - 60° N	-0.17	-0.14	-0.15	-0.21	0.04	0.07	0.06

20° N - 20° S	-0.36	-0.21	-0.2	-0.37	0.01	0.16	0.17
20° S – 60° S	-0.81	-0.38	-0.40	-0.48	-0.33	0.1	0.08
60°S – 82.5° S	-3.2	-1.37	-1.53	-1.59	-1.66	0.22	0.06

2.2.5.5 Stratospheric Sounding Unit Data

The SSU instrument, carried upon the same satellites as MSU, senses temperatures at higher altitudes although with some overlap with LS (Figure 2.20). They provide the only long-term near-global temperature data above the lower stratosphere, sensing infra-red radiation, extending from the upper troposphere to the lower mesosphere (Randel et al., 2009; Seidel, 2011) with the series terminating in 2006. In theory five channels of AMSU should be able to continue this series (Kobayashi et al., 2009) but despite incipient efforts at an AMSU only record (Mo, 2009) and plans to merge, the current long-term series ends in 2006.

The raw record has three unique additional issues to those encountered in MSU dataset construction. The satellite carries a cell of CO_2 which tends to leak causing a spurious increase in observed temperatures. Compounding this the CO_2 content varies among SSU instruments (Kobayashi et al., 2009). At the higher altitudes sensed, large diurnal and semi-diurnal tides (due to absorption of solar radiation) require substantial corrections (Brownscombe et al., 1985; [Nash and Forrester, 1986]). Finally, long-term temperature trends derived from SSU need adjustment for increasing atmospheric CO_2 (Shine et al., 2008) as this affects radiation transmission in this band.

Until recently solely one SSU dataset existed (Brownscombe et al., 1985; Scaife et al., 2000; [Nash and Forrester, 1986; Nash and Edge, 1989]), recently updated by Randel et al. (2009). Liu and Weng (2009) have now produced an alternative analysis for Channels 25 and 26 (but not channel 27 for which only a single estimate remains), permitting cursory evaluation of structural uncertainty. Seidel (2011) found substantial differences for Channel 26 (Figure 2.20); Randel et al. [(2009)] show cooling of 0.5K and Liu and Weng [(2009)] slight warming. They noted that the incompleteness of available documentation significantly complicates further investigation. Channel 25 was found to be in broad long-term trend agreement but with substantial differences in behaviour in the 1980s. Trends broadly agree with MSU and radiosonde estimates for the LS layer. Seidel (2011) also noted likely spurious vertical structure in Randel et al. with Channel 26 substantially departing from a weighted mean of Channels 25 and 27 noting that a very distinctive vertical structure would be required to explain this (Figure 2.20).

[INSERT FIGURE 2.20 HERE]
Figure 2.20: Global temperature anomaly time series from SSU data from the three SSU channels, as analysed by Randel et al. (2009) and, for Channels 25 and 26, as analysed by Liu and Weng (2009), and differences between them for Channels 25 and 26. Symbols indicate major volcanic eruptions in 1982 (El Chichón) and 1991 (Pinatubo). Reproduced from Seidel (2011).

2.2.5.6 Indirect Estimates from Changes in Atmospheric Winds

Atmospheric circulation is driven by thermal gradients. Any change in horizontal temperature gradients should be accompanied by a shift in winds, although this potentially breaks down in the deep tropics where the Coriolis effect diminishes to zero. Radiosonde wind records are far less obviously afflicted by time varying biases than their temperature records (Gruber and Haimberger, 2008; Sherwood et al., 2008). Allen and Sherwood (2007) first investigated applicability of using these winds to infer relative temperature gradients to the Tropical West Pacific warm pool region. They then extended to a global analysis (Allen and Sherwood, 2008) which implied a distinct tropical upper tropospheric maximum, but with large uncertainty. This uncertainty largely arose because winds can only tell about relative change and require an anchor point such as the HadAT trends at 62.5N utilized (Allen and Sherwood, 2008). The large uncertainty range was predominantly driven by uncertainty that arises through this choice of anchor point, a finding later confirmed

by Christy (2010), who in addition queried the stability of such an approach given the sparse geographical sampling, particularly in the tropics, and possible systematic wind speed bias sampling effects amongst other potential issues.

2.2.5.7 Synthesis of Free Atmosphere Temperature Estimates

Global-mean lower tropospheric temperatures have increased since the mid-20th century with each decade warmer than all preceding decades in the record (Figure 2.21). Structural uncertainties are larger than for surface datasets over the common period of record (c.f. Figure 2.21) but insufficient to preclude a conclusion that globally the troposphere has warmed. Uncertainty relates to the rate rather than sign of long-term changes, at least at the global — and tropical (not shown) — mean. On top of this long-term trend is super-imposed interannual and multiannual variability. These variations are highly correlated with those at the surface (c.f. Figure 2.2) but of slightly greater amplitude.

[INSERT FIGURE 2.21 HERE]
Figure 2.21: Global average lower tropospheric temperature anomaly time series for the mean of all included radiosonde datasets and offset therefrom the differences from this composite for each dataset (left hand panel). Decadal mean global anomalies for each dataset (right hand panel). All time series have been anomalized to a common 1989–1998 reference period.

Global mean lower stratospheric temperatures have decreased since the mid-20th century punctuated by short-lived warming events associated with explosive volcanic activity (Figure 2.22). Each decade has been cooler than all preceding decades. Uncertainties are larger still than for the troposphere but these uncertainties again impact understanding of rate but not sign of long-term changes. Cooling rates are greater from radiosonde datasets than MSU products. This likely relates to widely recognized cooling biases in radiosondes [(Mears et al., 2006)] which several dataset producers explicitly caveat likely remain in their products (Thorne, 2011a; Haimberger et al., 2008; Sherwood et al., 2008). Stratospheric temperature behaviour is far from linear and since the mid-1990s little net change has occurred.

[INSERT FIGURE 2.22 HERE]
Figure 2.22: Global average lower stratospheric temperature anomaly time series for the mean of all included radiosonde datasets and offset there from the differences from this composite for each dataset (left hand panel). Decadal mean global anomalies for each dataset (right hand panel). All time series have been anomalized to a common 1989–1998 reference period.

Tropospheric warming has not been zonally uniform (Figure 2.23). Warming has been largest in the Northern Hemisphere extra-tropical troposphere with a second, smaller maximum in Southern Hemisphere mid-latitudes. Interannual variability is greatest in tropical and Northern Hemisphere polar latitudes. Tropical interannual variability is dominated by variations in ENSO which it lags by 3–6 months (Christy and McNider, 1994), readily apparent from the peak in 1998 following the very strong 1997/1998 ENSO event. LT and MT channels exhibit very similar temporal behaviour. Stratospheric temperature trends and variability are also far from zonally uniform. The quasi-biennial oscillation signature is apparent in the tropics. Large variations in polar regions are a reflection of variations in the strength of the wintertime vortex in each hemisphere. The two volcanic eruptions (1982 and 1991) yield quasi-global warming for a period of approximately 18 months. Cooling has been greatest in the tropics and mid-latitude Southern Hemisphere. Given the large variability in high latitudes, trends there are very uncertain. The shorter period of record available for TS that straddles the troposphere and stratosphere exhibits elements of both tropospheric and stratospheric behavior.

[INSERT FIGURE 2.23 HERE]
Figure 2.23: Latitude-time variations in temperature anomalies from v.3.3 of the RSS product (Mears and Wentz, 2009a, 2009b) for estimates from the lower troposphere (bottom) to the lower stratosphere (top).

Zonal analyses hide interesting geographical trend variability (Figure 2.24). Over the satellite era the spatially incomplete HadCRUT3 surface record (Brohan et al., 2006) exhibits greater warming over land than oceans globally with substantial geographic trend structure and much of the sampled area exhibiting a cooling trend. In comparison tropospheric channels exhibit much smoother geographic trends with warming

in most locations north of approximately 45°S. Warming is larger for LT than MT, and LT shows more geographical structure reflecting greater sampling of both skin temperature and the boundary layer. Both tropospheric channels exhibit greatest warming in high Northern latitudes. The lower stratosphere is cooling almost everywhere but this cooling also exhibits substantial structure. Cooling is greatest in the highest southern latitudes and smallest in high northern latitudes, with some slight warming over the Northern Pacific Arctic sector. There is also some slight warming apparent in the Southern Ocean at similar longitudes.

[INSERT FIGURE 2.24 HERE]
Figure 2.24: Trend maps from the surface (HadCRUT3, Brohan et al., 2006) and four atmospheric layers from MSU/AMSU (RSS v. 3.3, Mears and Wentz, 2009a, 2009b) over the period 1979–2009 (except for TS which is 1987–2009).

As discussed in section 2.2.5.3 fair trend comparisons between geographically complete satellite estimates and spatio-temporally incomplete radiosonde estimates requires sub-sampling in space and time to ensure a like-for-like comparison. For both global and regional trends, including the tropics, the sign of tropospheric / stratospheric trends is beyond any reasonable doubt – the troposphere is consistently estimated to be warming and the stratosphere is consistently estimated to be cooling (Figure 2.25). Despite this sign agreement there is a substantial spread in the estimated magnitude of trends. The effect of sampling with different radiosonde dataset data availability masks upon the MSU products is as large as for many between radiosonde dataset estimates and often of similar sign and magnitude implying that at least some of the between radiosonde dataset variability is driven by sampling differences alone. For satellite estimates STAR consistently exhibits least cooling / greatest warming and UAH greatest cooling / least warming. RSS internal uncertainty estimates only include remaining estimates much less than 95% of the time reflecting that in many cases differences arise from fundamental methodological assumptions and the importance of characterizing structural uncertainty through the construction of multiple independently produced algorithms. As discussed previously, many radiosonde products are likely to retain an artificial cooling bias at height.

[INSERT FIGURE 2.25 HERE]
Figure 2.25: Trend estimates for MSU datasets sampled as the radiosonde datasets in space and time (hence multiple estimates for each MSU product) and the radiosonde datasets for a quasi-global average excluding the highest latitude and three sub-domains. For the RSS product internal uncertainty estimates as given in Mears (2011) are shown as whiskers (2 standard deviations). RATPAC RW is for a subsampled set of RATPAC following Randel and Wu (2006) who found potential issues for a number of RATPAC records in the stratosphere.

2.2.6 Summary of Temperature Trends

[PLACEHOLDER FOR FIRST ORDER DRAFT: Soil paragraph if soil is retained.]

Based upon several independently analyzed global and regional land surface temperature data products, of substantial heritage in many cases, it can be concluded with high confidence that it is virtually certain that global land surface temperatures have warmed since the late 19th century and that this warming has been particularly rapid since the 1970s. Since AR4 substantial efforts have been undertaken to identify and adjust for data issues and begin to benchmark their performance in a rigorous manner.

Several studies undertaken since AR4 show with high confidence that it is likely that urban heat-islands and land-use changes have not raised the centennial global near-surface temperature trends by more than 10% of the observed trend. Contributions are not globally uniform. They are likely to underlie about a quarter of the observed warming trends in recent decades in limited regions such as China but have little overall impact elsewhere.

[Inclusion of DTR to be considered.]

It can be concluded with very high confidence that it is virtually certain that global average sea surface temperatures have increased since the beginning of the 20th century. Since AR4, digital archives of marine

data have been expanded and improvements to metadata have led to better understanding of data biases. Warming is seen in datasets based on a wide variety of analysis techniques and is corroborated by independent records of marine temperature.

Globally averaged near-surface temperatures, as estimated by several independent analyses since the late nineteenth century, are consistent in exhibiting multi-decadal warming of approximately 0.8K. Super-imposed upon this is high frequency variability so the warming is not monotonic and trends at decadal or shorter timescales tend to be dominated by such effects. The multi-decadal warming rate has accelerated in recent decades. The redundancy in measurement and analysis techniques, maturity of the field, and multiple published sensitivity studies and uncertainty estimates means that although there is an inevitable degree of uncertainty in the precise magnitude the reality of a long-term global-mean near-surface warming since the late 19th century that has accelerated in recent decades is unequivocal.

Based upon multiple independent analyses from weather balloons and satellites it can be concluded with very high confidence that it is virtually certain that globally the troposphere has warmed since the mid-20th century. The rate of change is less certain than the sign. It is also very likely that the tropical troposphere is warming. Confidence in the rate of change and its vertical structure is lower for the tropics. Through construction of several additional innovative datasets, detailed intercomparisons, and a greater elucidation of uncertainties in a subset of pre-existing datasets the likely magnitude of uncertainty in these trends has become much more apparent since AR4. Confidence is somewhat lower prior to 1979 when only weather balloon data exists.

Four independent observing technologies consistently indicate stratospheric cooling since the mid-twentieth century, punctuated by episodic volcanic warming in the low- to mid- stratosphere. Whilst it is virtually certain that the stratosphere has cooled the rate and nature of the cooling as well as its vertical structure is less certain. Cooling of the lower stratosphere is consistently estimated to have levelled off in the past decade. Confidence is low in temperature changes in the mid- and upper stratosphere where only one observing technology exists and datasets from this are both substantially less mature and poorly documented. Confidence is also low before 1979 when estimates rely solely upon weather balloons and exist solely for the lower stratosphere.

[START FAQ 2.1 HERE]

FAQ 2.1: How do We Know the World is Warming?

The clearest and best known indication that global climate is changing is the rise in global average surface temperatures. The world warmed between 1900 and 1940, there followed a period of some thirty years during which temperatures changed little, or declined slightly. Then, from around the mid-1970s there was a second period of warming that brought the net increase in global temperature to around 0.76°C. The IPCC AR4 concluded that this “warming of the climate system is unequivocal”.

Although popular discussion tends to centre on temperature records made at weather stations over the land, these represent only one single, albeit important, line of evidence. The different elements of the climate system are strongly interlinked and though they have been considered separately, the broader evidence for a warming world comes from bringing together a wide range of physically consistent measurements (FAQ 2.1, Figure 1) that have been analyzed and reanalyzed many times in many different ways by very many people.

[INSERT FAQ 2.1, FIGURE 1 HERE]
FAQ 2.1, Figure 1: Schematic of those climate elements that have been measured quasi-globally and on multi-decadal timescales that would be expected to change if the world were indeed warming; and the direction in which they would be expected to change.

The best known of the global average temperature data sets — GISS, NCDC and HadCRUT3 — are based on air temperatures measured by weather stations over the land and on measurements of sea-surface temperature over the oceans. The underlying archives of land and ocean temperatures are completely

independent, but the changes in temperature recorded in them follow one another closely. The rise in sea-surface temperature is slower because it requires more energy to heat the sea than it does the land.

Although sea-surface temperature is most often used to measure temperature change over the oceans, air temperatures taken by ships are also recorded in marine archives. Physically, one would expect that marine air temperatures would be closely linked to the changes in the sea-surface and this is borne out by a number of independent analyses.

The observed warming is not confined to the surface. Measurements made by weather balloons and satellites show that the temperature of the troposphere — the active weather layer of the atmosphere — has increased. The warming also penetrates into the deeper ocean. More than 80% of the energy absorbed by the climate system since the 1960s has been stored in the oceans. This can be seen in estimates of ocean heat content for which global records exist going back to the 1950s. As the oceans warm, the water itself expands. The expansion can be seen in records of rising sea-levels that extend back more than a century.

A warmer world is also a wetter one as warmer air will hold a greater quantity of water. Globally, specific humidity, which measures the amount of moisture in the atmosphere, has also increased over both the land and the oceans.

The icy parts of the planet — known collectively as the cryosphere — affect, and are affected by, local changes in temperature. The mass of water stored in mountain glaciers globally has fallen year on year for the past 20 years. The lost mass contributes to the observed rise in sea-level. Snow cover is sensitive to changes in temperature particularly during the spring when the snow starts to melt. Spring snow cover has fallen across the Northern Hemisphere since the 1950s. The Arctic has warmed at twice the rate of the rest of the world. Surface observations in this region are sparse, but losses in sea-ice in the Arctic Ocean measured by satellites — particularly at the time of the summer minimum in extent — and reductions in the area of frozen land are consistent with the observed increase in temperature. In the Southern Ocean that surrounds Antarctica, temperatures have not increased significantly. This is consistent with the slight increase in sea-ice extent seen in the Southern Hemisphere.

Individually, any single analysis might be unconvincing, but for all of these different indicators and data sets many research groups have come to the same conclusion. From the deep oceans to the edge of the atmosphere, the evidence of warmer airs and oceans, of melting ice and rising seas, all points undeniably to one thing: the world has warmed (FAQ 2.1, Figure 2).

[INSERT FAQ 2.1, FIGURE 2 HERE]
FAQ 2.1, Figure 2: Multiple redundant indicators of a changing global climate. Each line represents an independently derived estimate of change in the climate element. All publically available, documented, datasets known to the authors have been used in their latest version with no further screening criteria applied. Further details are given in Baringer et al. (2010).

[END FAQ 2.1 HERE]

2.3 Changes in Hydrological Cycle

Changes in the hydrological cycle are less easily measured than changes in temperature, however they potentially have large and long-lasting effects on the climate system. Changes in atmospheric water vapour impact both the energy balance, as water vapour is one of the most abundant greenhouse gases, and the hydrologic cycle. Long-term measurements of precipitation are available only for land areas and thus do not provide true global coverage. Satellite estimates of precipitation do provide global coverage since they include both ocean and land areas, but are only available since about 1979. This section covers the main aspects of the hydrologic cycle including large-scale average precipitation, steam flow and runoff, soil moisture and drought, atmospheric water vapour, and clouds. A more detailed discussion of issues with measurements of precipitation, and climate impacts of the hydrological cycle including aerosols and the energy balance and other impacts are contained in Section 3.3 of the AR4 (Trenberth et al., 2007) and are not repeated here.

2.3.1 Large Scale Changes in Precipitation

[PLACEHOLDER FOR FIRST ORDER DRAFT]

2.3.1.1 Global Land Areas

Figure 2.26 shows the century-scale variations and trends on globally averaged annual precipitation using the GHCN data set updated through 2010 (Vose et al., 1992). Also plotted are the smoothed time series from a number of other data sets including the Global Precipitation Climatology Project (GPCP, Adler et al., 2003; [Smith et al., 2010]). The CRU data set (Brohan et al., 2006) has not been updated since the AR4 and is not included here. One new global data set for monthly total precipitation is a reconstructed data set by [Smith et al. (2010)]. This is a statistical reconstruction using Empirical Orthogonal Functions, similar to the NOAA global temperature product (Smith et al., 2008; [Vose et al., 2011]) that does provide coverage for most of the global surface area from 1900–2008. The reconstruction merges several analyses. Monthly reconstructions that interpolate using large-scale spatial covariance information and gauge data were found to be representative of most interannual variations. Over land such reconstructions are also representative of multi-decadal variations. However, because there are no gauges over the oceans to anchor those analyses, their oceanic multi-decadal signal was found to be less stable. An annual reconstruction using correlations between precipitation and combined sea-level pressure and sea-surface temperature was found to be more stable for analysis of multi-decadal variations. The merged reconstruction combines these two by combining the oceanic multi-decadal signal from the correlation-based analysis with the gauge-based analysis.

As discussed above, the land based GHCN, GPCC and Smith data sets provide the longer term perspective, and the satellite-based data sets provide true global coverage, including over the oceans. However, for Figure 2.26, only land areas are included. Both the GHCN and GPCC V5 data sets show a century-scale increase in global precipitation averaged over land areas, with most of the increase occurring in the early to mid 20th century. The land-only time series from the Smith data set is also shown on Figure 2.26, and suggests that when virtually all the land area is filled in using this reconstruction method, the resulting time series shows little change in land-based precipitation since 1900.

[The trends for the various land-only precipitation time series will be shown in Table 2.3.]

[INSERT FIGURE 2.26 HERE]
Figure 2.26: Globally averaged annual precipitation over land areas from GHCN (green bars) with respect to the 1981–2000 base period. Smoothed curves (see Appendix 3.A from Trenberth et al., 2007) for GHCN and other global precipitation data sets as listed.

[INSERT TABLE 2.3 HERE]
Table 2.3: [PLACEHOLDER FOR FIRST ORDER DRAFT]

2.3.1.2 Spatial Variability of Observed Trends

Figure 2.27 shows the spatial variability of long-term trends (%/century, 1901–2010) and more recent trends (1979–2010) in annual precipitation. The trends, only over land, are computed using the GHCN data set and interpolated to a 5^o x 5^o latitude/longitude grid. Increases for the longer period are seen in the mid- and higher-latitudes of both the Northern and Southern hemispheres, although compared to the same figures in the AR4 (Trenberth et al., 2007) there are many fewer statistically significant trends at the grid box level. The decrease in annual precipitation in the Sahel region of Africa continues to be a significant decline, however, over North America there a now no statistically significant grid box values.

[INSERT FIGURE 2.27 HERE]
Figure 2.27: Linear trend, in % per century for annual precipitation from the GHCN data set for 1901–2010 (top) and 1979–2010 (bottom). Grid boxes with statistically significant trends at the 95% level are indicated by +.

The same holds true for the shorter period map (1979–2010) with many fewer statistically significant trends. The Sahel region for this period continues to show a shorter term increase, although not as strong as in the AR4. Other regions that show a shift in sign between the longer term trends and shorter term include the western US, parts of southern South America, southern Africa, northeastern Africa and Spain, and Iceland.

2.3.1.2 Precipitation in the Satellite Era

Precipitation and associated hydrological cycle variations during 1979–2008 have been examined by comparing the effects of ENSO and two large tropical volcanic eruptions (El Chichón, March 1982; Mt. Pinatubo, June 1991) and compared to the trends during the period associated with global warming. The analysis is carried out primarily using global, satellite-based data sets, including that from the Global Precipitation Climatology Project (GPCP; Adler et al., 2003; [Huffman et al., 2009]). Techniques are applied to the satellite data sets to separate out the ENSO, volcano and long-term (trend or inter-decadal) changes using independent indices (Gu et al., 2007; [Gu and Adler, 2011]). Figure 2.28 summarizes the results at the global scale. In the left panel of the diagram the global surface temperature increases significantly, with only a slight decrease in the rate of warming over the 30-year period when the inter-annual signal is removed. There is a significant increase of global surface temperature during El Niños, for example 1983 and 1998, with a perturbation magnitude of about 0.2C, and similar decreases during La Niñas. These variations have the same sign over both ocean and land. For precipitation the global response to ENSO is muted, with amplitudes of 2%/C as compared to about 7%/C (Clausius-Clapyron relation, Trenberth et al., 2003) for water vapour. This relatively small global precipitation response is related to the opposite-sign responses over land and ocean related to the positioning of ENSO temperature anomalies in the central-eastern Pacific Ocean.

[INSERT FIGURE 2.28 HERE]
Figure 2.28: a) and d) are time series of global mean temperature and precipitation anomalies during 1979–2008, respectively. b) and e) are their corresponding ENSO and volcanic effects. c) and f) are time series of global mean temperature and precipitation anomalies with ENSO and volcanic effects removed. Also shown in a), c), d) and f) are estimated linear trends during the time period.

The global temperature and precipitation response to the two volcano events can also be seen in the figure, with decreases in both variables. This signal is derived using a stratospheric aerosol index as an independent parameter after removing the ENSO signal. The volcano-related temperature signal is comparable in magnitude to that of ENSO, with decreases occurring over both land and ocean. Associated precipitation decreases occur (also over both land and ocean) with a global decrease up to about 3%, or about 4%/C. The global trends in temperature and precipitation over the same period show a near zero trend in precipitation to go along with increasing temperatures. These characteristics are similar to those associated with ENSO inter-annual variations and both indicate the effect of energy constraints on these variations.

The trends or linear changes over the past 30 years are not uniform over the globe (Figure 2.29), with positive temperature changes concentrated in the high latitudes of the northern hemisphere, whereas trends in precipitation are focused in the tropics, where increases are located over parts of the ITCZ and the SPCZ over the Pacific Ocean and in the Indian and Atlantic Oceans, with a marked decrease over the Equator in the Pacific, between the ITCZ and SPCZ mean annual positions ([Adler et al., 2008]). Overall the tropics have an increase over 5-15 N, with compensating decreases over northern hemisphere middle latitudes.

[INSERT FIGURE 2.29 HERE]
Figure 2.29: Linear changes of annual-mean a) surface temperature and b) precipitation during 1979–2008.

The differences between ENSO and volcanic effects can be further characterized by examining various lag responses of precipitation, temperature and tropospheric water vapour to these two phenomena [(Gu and Adler, 2011)]. The ENSO responses of oceanic precipitation and sea surface temperature (SST) have the same time lags (two months for the Tropics). Tropical and global mean tropospheric water vapour over both land and ocean generally follows surface temperature variations, resulting in a closely coupled relation among precipitation, surface temperature and tropospheric water vapour during ENSO. Land precipitation responds to ENSO much faster than temperature, indicating a relatively slower temperature adjustment

process over land following ENSO-related circulation and precipitation anomalies. ENSO is also shown to be ineffective in affecting the tropical and global mean mid-lower tropospheric atmospheric (dry) static stability. For volcanic eruptions, tropical and global mean precipitation over either ocean or land responds faster than (surface and atmospheric) temperature and tropospheric water vapour over the same areas. This faster precipitation response indicates the lack of the water vapour associated feedback during the early stage of volcanic eruptions as compared to ENSO. The volcanic-related precipitation variations are mostly related to the changes in the mid-lower tropospheric atmospheric static instability and the microphysical properties of precipitating clouds caused by volcanic aerosols.

2.3.2 Streamflow and Runoff

The recent widespread drying trend and the effect of surface warming are qualitatively consistent with the observed decreases in streamflow over many low and midlatitude river basins (Dai et al., 2009). The PDSI trends are broadly comparable with those in the soil moisture simulated by another land surface model (Sheffield and Wood, 2008b). The results are also consistent with the model-predicted 21st century climate, which shows severe drought conditions by the middle of this century over most low and midlatitude land areas (Wang, 2005; Sheffield and Wood, 2008a; [Dai, 2010]). Thus, it is very likely that recent warming has caused widespread drying over land, and this drying may become more severe in the coming decades [(Dai, 2010)].

Streamflow records for world's major rivers show large decadal to multi-decadal variations, with small trends for most rivers (Cluis and Laberge, 2001; Lammers et al., 2001; Pekarova et al., 2003; [Mauget, 2003]; Milliman et al., 2008; Dai et al., 2009; Xu et al., 2010). Increased streamflow during the later half of the 20th century has been reported over regions with increased precipitation, such as many parts of the United States ([Lins and Slack, 1999]; Groisman et al., 2004) and southeastern South America [(Genta et al., 1998)]. Decreased streamflow was reported over many Canadian river basins during the last 30–50 years (Zhang et al., 2001) where precipitation has decreased during the period. Because large dams and reservoirs were built along many of world's major rivers during the last 100 years and they can dramatically change the seasonal flow rates (e.g., by increasing winter low flow and reducing spring/summer peak flow; Cowell and Stoudt, 2002; Ye et al., 2003; Yang et al., 2004), trends in seasonal streamflow rates (e. g., Lammers et al., 2001) should be interpreted cautiously. Nevertheless, there is evidence that the rapid warming since the 1970s has caused an earlier onset of spring that induces earlier snowmelt and associated peak streamflow in the western United States (Cayan et al., 2001) and New England, USA (Hodgkins et al., 2003) and earlier breakup of river-ice in Russian Arctic rivers [(Smith, 2000)] and many Canadian rivers (Zhang et al., 2001).

River discharge is unique among water cycle components in that it both spatially and temporally integrates surplus waters upstream within a catchment (Shiklomanov et al., 2010), which makes it well suited for in-situ monitoring [(Fekete et al., 2011)]. Due to its integrated nature, relatively few discharge gauges placed near the mouth of large watersheds can capture a large portion of the continental river fluxes to oceans (Fekete et al., 2002). Dai et al. (2009) assembled a data set of 925 most downstream stations on the largest rivers monitoring 80 % of the global ocean draining land areas and capturing 73 % of the continental runoff. Dai et al. (2009) found that only about one-third of the top 200 rivers (including the Congo, Mississippi, Yenisey, Paraná, Ganges, Columbia, Uruguay, and Niger) show statistically significant trends during 1948–2004, with the rivers having downward trends (45) outnumbering those with upward trends (19). The interannual variations [(Figure 4)] are correlated with the El Niño–Southern Oscillation (ENSO) events for discharge into the Atlantic, Pacific, Indian, and global ocean as a whole. For ocean basins other than the Arctic, and for the global ocean as a whole, the discharge data show small or downward trends, which are statistically significant for the Pacific (-9.4 km^3 yr^{-1}). Precipitation is a major driver for the discharge trends and large interannual-to-decadal variations. For the Arctic drainage areas, upward trends in streamflow are not accompanied by increasing precipitation, especially over Siberia, based on available data, although recent surface warming and associated downward trends in snow cover and soil ice content, as well as changes in evaporation, over the northern high latitudes may have contributed to increased runoff in these regions (Adam and Lettenmaier, 2008). The most recent and most comprehensive analyses (Milliman et al., 2008; Dai et al., 2009) do not support the previous notion (Labat et al., 2004) that there have been an increasing trend in global runoff associated with global warming during the 20th century, based on which many attribution studies (e.g., Gedney et al., 2006) have been carried out.

2.3.3 Soil Moisture and Drought Indices

Historical records from in-situ measurements of soil moisture content are available only for limited regions in Eurasia and the U.S., and they often are short in length (10-30 years) ([Robock et al., 2000]; Li et al., 2005; [Nie et al., 2008]; [Zhang et al., 2008]; Zuo and Zhang, 2009). A rare, 45-year record of soil moisture over Ukraine agricultural lands show little change over the last three decades (Robock et al., 2005). Because of this, other proxy data of soil moisture, such as the Palmer Drought Severity Index (PDSI) derived from observed precipitation, temperature and other surface data (e.g., [Dai et al., 2004; Dai, 2010, 2011; van der Schrier et al., 2006a,2006b, 2007, 2010]; Zou et al., 2005; Zhai et al., 2010), have been used to study changes and variations in surface moisture conditions.

[Consider par from section 2.7]

In general, the PDSI is significantly correlated ($r = 0.4 \sim 0.8$) with available monthly soil moisture data over Eurasia and North America, and with observed yearly streamflow over most of the larger river basins ($r = 0.4 \sim 0.9$) [(Dai, 2011)]. The soil moisture simulated by land surface models forced with observed precipitation, temperature and other atmospheric forcing can generally capture most of the observed seasonal and year-to-year variations of soil moisture (e.g., Qian et al., 2006), but they often contain large mean biases and the long-term changes may be contaminated by spurious changes in the forcing data. Nevertheless, these model-simulated soil moisture data, which often cover a whole continent or the global land and extends back to 1950 or 1900, have been increasingly used to document spatial and temporal variations and long-term changes in soil moisture and drought (e.g., Nijssen et al., 2001; Maurer et al., 2002; Andreadis and Lettenmaier, 2006; Sheffield and Wood, 2007; Sheffield and Wood, 2008b).

A recent review by [Dai (2010)] summarizes the main findings on aridity changes since around 1950 and the underlying factors, including the contribution of global warming. [Figure 1] compares the trend patterns since around 1950 (as data for earlier years are sparse and less reliable) in observed annual precipitation, streamflow, the calculated PDSI and soil moisture. The use of the Penman-Monteith evapotranspiration (PE_pm), instead of the Thornthwaite evapotranspiration (PE_th) as in the original PDSI (e.g., Dai et al., 2004), as well as the self-calibration of the PDSI (Wells et al., 2004), only slightly reduces the long-term PDSI trends [(van der Schrier et al., 2010; Dai 2010, 2011)] because of PDSI's low sensitivity to evapotranspiration (PE). This resolves an earlier suspicion (Trenberth et al., 2007; Hobbins et al., 2008) that the PDSI might overestimate the drying from global warming due to its use of the Thornthwaite PE.

2.3.4 Evapotranspiration Including Pan Evaporation

Direct measurements of evapotranspiration over global land areas are scarce. Evaporation fields from the ERA-40 and NRA are not considered reliable because they are not well constrained by precipitation and radiation (Betts et al., 2003). Numerous gridded datasets have been developed that estimate actual evapotranspiration from either atmospheric forcing and thermal remote sensing, sometimes in combination with direct measurements (e.g., from FLUXNET, a global network of flux towers), or interpolation of FLUXNET data using regression techniques, providing an unprecedented look on global evapotranspiration [(Müller et al., 2011)].

Most gridded datasets cover only a limited time period, while pan evaporation records can span decades. These records provide valuable information on trends in the drying power of the atmosphere, but the link between pan evaporation and actual evapotranspiration from the pan environment is ambiguous. The AR4 reported on widespread decreasing trends in observed pan evaporation, but such decreasing trends can indicate either an increase or decrease in actual evapotranspiration depending on the combined effect of changes in radiation, vapour pressure deficit, temperature, and wind speed in a region (Roderick et al., 2007; Fu et al., 2009a; [van Heerwaarden et al., 2010]).

Different processes can control regional evapotranspiration trends depending on whether evapotranspiration is limited by water or energy. Measurements of actual evapotranspiration from FLUXNET reveal a large North-South gradient over Europe in their response to interannual variations in available energy and precipitation (Teuling et al., 2009). Thus, the recent increase in incoming shortwave radiation in regions with decreasing aerosol concentrations (Wild et al., 2005) can explain positive evapotranspiration trends only in

the humid part of Europe. A continuous decrease in reference and pan evaporation for the period 1960–2000 was reported by Xu et al. (2006a) for a humid region in China, consistent with reported continuous increase in aerosol levels over China (Qian et al., 2006). In (semi-)arid regions, trends in evapotranspiration largely follow trends in precipitation (Jung et al., 2010). Trends in surface winds (Vautard et al., 2010) and CO_2 also alter the partitioning of available energy into evapotranspiration and sensible heat. While surface wind trends largely explain pan evaporation trends over Australia (Roderick et al., 2007; Rayner, 2007), their impact on actual evapotranspiration is likely limited due to the compensating effect of boundary-layer feedbacks [(van Heerwaarden et al., 2010)]. In vegetated regions where a large part of evapotranspiration comes from transpiration through plants' stomata, rising CO_2 concentrations lead to reduced stomatal opening and evapotranspiration ([Idso and Brazel, 1984]; Leakey et al., 2006). Additional regional effects that impact evapotranspiration trends are lengthening of the growing season and land use change.

On a global scale, evapotranspiration increased from the early 1980s up to the late 1990s (Wild et al., 2008; [Wang et al., 2010]; Jung et al., 2010) at a rate of 0.6 W m−2 per decade for the period 1982–2002 [(Wang et al., 2010)]. After 1998, an increase in moisture limitation in the Southern Hemisphere has acted as a constraint to further increase of global evapotranspiration (Jung et al., 2010).

2.3.5 Surface Humidity

Surface water vapour is routinely measured synoptically both over land and ocean with some records dating back to the 1800s. However, it has received far less attention than temperature and precipitation. This is largely because additional complexities associated with its monitoring have made quality assurance difficult and partly because it has been considered of lesser importance to society. Water vapour is the most prolific and therefore one of the most significant of the greenhouse gases thereby affecting the radiation budget. Its properties of evaporation, condensation and consequent latent heating make it fundamental to the Earth energy budget and hydrological cycle. Absolute humidity governs precipitation amounts in intense rainfall events, when most of the water may be rained out of an air parcel. Furthermore, it has significant implications for both human, livestock and crop health where high humidity restricts the cooling mechanisms of the body and may also promote some pests and diseases.

AR4 reported widespread increases in surface air moisture content, alongside near-constant relative humidity over large scales though with some significant changes specific to region, time of day or season. However, this was mostly based on regional studies mainly without homogeneity testing or adjustment: detection and removal/adjustment of biases is essential for any surface air moisture dataset to be considered robust. Most of the conclusions of AR4 still stand, but since AR4 there have been advances in our knowledge and understanding of surface humidity through observations, reanalyses and models.

In good agreement with previous analyses from Dai (2006), Willett et al. (2008) show widespread increasing specific humidity across the globe from the homogenised gridded monthly mean anomaly product HadCRUH. There are some small isolated but coherent areas of drying over the more arid regions (Figure 2.30a). The globally averaged moistening trend from 1973–2003 is 0.07 g kg^{-1} $decade^{-1}$, with very high confidence and comparable with Dai (2006)'s 0.06 g kg^{-1} $decade^{-1}$ for 1976–2004. Moistening is largest in the Tropics (Table 2.4) and summer hemisphere over both land and ocean. There remains large uncertainty over the southern hemisphere where data are sparse. Global specific humidity is sensitive to large scale phenomena such as ENSO (Figure 2.30b-e) and strongly correlated with surface temperature – land only averages over the 23 [Giorgi and Francisco (2000)] regions for the period 1973–2003 show mostly increases at or above Clausius-Clapeyron scaling (about 7% K^{-1}) with very high confidence (Willett et al., 2010).

There is good agreement with ERA reanalyses over land, where ERA-interim shows improvement over ERA-40 as a surface humidity monitoring product for large scale averages (Simmons et al., 2010) (Figure 2.30b, c). Notably, the extended series from ERA-interim shows a flattening of the global land specific humidity series since 2000. While HadCRUH concluded negligible change in surface RH over land in 1973–2003, the more up to date 1989–2008 record from ERA-interim reveals a reduction in RH since 2000, compatible with the plateau in specific humidity. A 'quick-look' extension of HadCRUH to 2007 supports this (Simmons et al., 2010) (Figure 2.30c). This may be linked to the recent divergence of warming between land and oceans (Joshi et al., 2008).

There have been advances in marine humidity analysis since AR4. The specific humidity series of (Berry and Kent, 2009; [Berry and Kent, 2009a]) include uncertainty estimates and adjustments for ship height and data from screens, which are often poorly ventilated, as opposed to handheld psychrometers. The specific humidity and relative humidity dataset HadCRUH (Willett et al., 2008) excludes data failing neighbour consistency checks. Both show good agreement with Dai (2006) (Figure 2.30d, e, Table 2.4). All originate from various releases of the ICOADS database. However, whereas Berry and Kent and Dai use only data from Voluntary Observing Ships, Willett et al. use all data from ships, buoys and marine platforms and shift to operationally telecommunicated data made available by NOAA NCEP from 1998–2003. The marine specific humidity, like that over land, shows widespread increases, that correlate strongly with sea surface temperature. However, there is a marked decline in marine relative humidity around 1982 (Figure 2.30e). This is reported in both Willett et al. (2008) and [Berry (2009)] where its origin, respectively, is variously concluded to be a non-climatic data issue and a response to the shift to a very positive North Atlantic Oscillation at that time.

To conclude, absolute moistening has been widespread across the globe since the 1970s, with very high confidence. However, over recent years this has abated over land, coincident with greater warming over land relative to the oceans [cross-section reference needed]. This has resulted in fairly widespread decreases in relative humidity over land. Whether this is part of a longer term trend or merely a short lived feature remains to be seen.

Table 2.4: Summary of global surface humidity datasets and large scale trends.

Dataset, Reference, source data, period of record and regional delimitations	Global	Northern Hemisphere	Tropics	Southern Hemisphere	Global	Northern Hemisphere	Tropics	Southern Hemisphere
	Specific Humidity (g kg^{-1} decade^{-1})				Relative Humidity (% decade^{-1})			
LAND								
Dai (2006) NCAR DS464.0 GTS weather station reports December 1975 to April 2005 Globe (60 ^{o}S–75 ^{o}N), N. Hem (0-75 ^{o}N), S. Hem (60-0^{o}S)	---	---	---	---	0.05	0.12	---	-0.12
HadCRUH, Willett et al. (2008) NCDC ISD weather station reports January 1973 to December 2003 Globe (60 ^{o}S–60 ^{o}N), N. Hem (20-60 ^{o}N), Tropics (20 ^{o}S-20 ^{o}N), S. Hem (60-20 ^{o}S)	**0.11**	**0.12**	**0.16**	0.01	-0.03	0.07	-0.10	**-0.34**
OCEAN								
Dai (2006) NCAR DS464.0 GTS marine ship reports and ICOADS data December 1975 to May 2005 (boundaries – as above)	**---**	**---**	---	---	**-0.16**	**-0.11**	---	**-0.22**
HadCRUH, Willett et al. (2008) ICOADS v2.1 marine ship, buoy and platform data January 1973 to December 1997, NCEP GTS marine data January 1998 to December 2003 (boundaries - as above)	**0.07**	**0.08**	**0.10**	0.01	**-0.10**	**-0.10**	-0.11	**-0.11**
Berry & Kent (2009a, b) ICOADS v2.4 marine ship data 1970 to 2006 Atlantic Trends only 40 ^{o}S-70 ^{o}N	**0.13**	---	---	---	---	---	---	---
LAND & OCEAN COMBINED								
Dai (2006)	**0.06**	**0.08**	---	0.02	**-0.09**	-0.02	---	**-0.20**

(as above combined) December 1975 to May 2005 (boundaries - as above)								
HadCRUH, Willett et al. (2008) (as above combined) January 1973 to December 2003 (boundaries - as above)	**0.07**	**0.08**	**0.10**	0.02	-0.06	0.00	**-0.10**	-0.10

[INSERT FIGURE 2.30 HERE]

Figure 2.30: Trends and variability in surface humidity. a) Decadal trends in surface specific humidity in g kg^{-1} per decade from HadCRUH over 1973–2003. b) Globally averaged monthly mean anomaly time series of land surface specific humidity. c) Globally averaged monthly mean anomaly time series of land surface relative humidity. d) Globally averaged monthly mean anomaly time series of marine surface specific humidity. e) Globally averaged monthly mean anomaly time series of marine surface relative humidity. Time series show data from HadCRUH (solid thick black), HadCRUHext (solid thick grey), Dai (dotted red), ERA 40 (long dashed light blue), ERA interim (dot dashed royal blue) and Berry and Kent (solid thick orange).

2.3.6 Tropospheric Humidity

Tropospheric water vapour plays an important role in regulating the energy balance of the surface and top-of-atmosphere, and is essential to the formation of clouds and precipitation.

2.3.6.1 Radiosonde

Radiosonde humidity data for the troposphere were used sparingly in AR4, noting a renewed appreciation for biases with the operational radiosonde data that had been highlighted by several major field campaigns and intercomparisons. Since the AR4 there have been three distinct efforts to homogenize the tropospheric humidity records from operational radiosonde measurements (Durre et al., 2009; McCarthy et al., 2009; [Dai et al., 2011]) (Table 2.5). All agree that there are significant issues with the raw data that preclude its use for climate analysis. Each study takes a unique methodological approach to data selection and homogenization. Over the common period of record from 1973 onwards, the resulting estimates are in substantive agreement regarding specific humidity trends at the largest geographical scales. All remove an artificial temporal trend towards drying in the raw data and indicate a positive trend in free tropospheric specific humidity over the period of record. In each analysis, the rate of increase is concluded to be grossly consistent with the increase in equilibrium vapour pressure from the Clausius-Clapeyron relation (about 7% per Kelvin increase in temperature). There is no evidence for a significant change in tropospheric relative humidity. McCarthy et al. (2009) show close agreement between their radiosonde product at the lowest levels and independent surface relative humidity data (Willett et al., 2008) both in low frequency and high frequency behavior.

Table 2.5: Methodologically distinct aspects of the three approaches to homogenizing tropospheric humidity records from radiosondes.

Dataset	Region Considered	Time Resolution and Reporting Levels	Neighbours	First guess	Statistical test	Automated	Variables homogenized
Durre et al.	Northern Hemisphere	Monthly, mandatory and significant levels to 500hPa	Pair-wise homogeni-zation	No	SNHT	Yes	PW (inferred from T, P and DPD)
McCarthy et al.	Northern Hemisphere	Monthly, mandatory levels to 300hPa	All neighbour average, iterative	Yes	KS-test	Yes	T, q, RH
Dai et al.	Globe	Observation resolution, mandatory levels to	None	Yes	KS-test and PMF test	Yes	DPD

	100hPa

2.3.6.2 GPS

Since the early 1990s, estimates of column integrated water vapour have been obtained from ground-based Global Position System (GPS) receivers. An international network started with about 100 stations in 1997 and has currently been expanded to over 400 (primarily land-based) stations. Several studies have complied long-term GPS water vapour datasets for climate studies (Jin et al., 2007; Wang et al., 2007; Wang and Zhang, 2008; Wang and Zhang, 2009). Using such data, Mears (2011) demonstrated general agreement of the interannual anomalies between ocean-based SSM/I and land-based GPS column integrated water vapor data. The interannual water vapour anomalies are closely tied to the atmospheric temperature changes in a manner consistent with that expected from the Clausius-Clapeyron relation. Jin et al. (2007) found an average column integrated water vapour trend of about 2 mm per decade during 1994–2006 for 150 (primarily land-based) stations over the globe, with positive trends at most of Northern Hemispheric stations and negative trends in the Southern Hemisphere. However, given the short length (about 10 years) of the GPS PW records, the estimated trends are sensitive to the start and end years and the analyzed time period, and thus they should not be interpreted as long-term trends.

2.3.6.3 Satellite

The AR4 reported positive decadal trends in lower and upper tropospheric water vapour based upon satellite observations. Since AR4, there has been continued strong evidence for widespread increases in lower tropospheric water vapour from microwave satellite measurements of column integrated water vapour (Santer et al., 2007; Wentz et al., 2007) and globally from satellite measurements of spectrally-resolved reflected solar radiation (Mieruch et al., 2008). Consistent with surface and radiosonde measurements, the rate of moistening at large spatial scales is close to that expected from the Clausius Clapeyron relation with invariant relative humidity.

Upper tropospheric relative humidity (UTH) in the tropics is strongly related to the convective activity and SST of the wet regimes [(Huang et al., 2010)]. Interannual co-variation in temperature and upper tropospheric water vapour have been diagnosed from spectrally-resolved infrared satellite data (Gettelman and Fu, 2008; Dessler et al., 2008) and inferred from increases in broadband clear-sky outgoing longwave radiation (OLR) satellite data (Chung et al., 2010b) and are consistent with invariant RH at large spatial scales. On decadal time-scales, increased greenhouse gas concentrations reduce clear-sky OLR (Allan, 2009; Chung and Soden, 2010), thereby influencing inferred relationships between moisture and temperature. Using Meteosat infrared radiances, Brogniez et al. (2009) demonstrated that interannual variations in free tropospheric humidity over subtropical dry regions are heavily influenced by lateral mixing between the deep tropics and the extra tropics. Regionally, UTH changes in the tropics were shown to relate strongly to the movement of the ITCZ based upon microwave satellite data (Xavier et al., 2010). While microwave satellite measurements have become increasingly relied upon for studies of UTH, the absence of a homogenized data set across multiple satellite platforms presents some difficulty in documenting coherent trends from these records [(John et al., 2011)].

Using NCEP reanalyses for the period 1973–2007, [Paltridge et al., (2008)] found negative trends in specific humidity above 850 mb over both the tropics and southern midlatitudes, and above 600 mb in the northern midlatitudes. However, as noted in AR4, reanalysis products suffer from time dependent biases and have been shown to simulate unrealistic trends and variability over the ocean (John et al., 2009; Mears et al., 2007). As a result, different reanalysis products yield opposing trends in free tropospheric specific humidity (Chen et al., 2008). Furthermore, the main source of observations for reanalyses, radiosondes (Section 2.3.6.1) and infrared satellite measurements (Soden et al., 2005), indicate positive trends in tropospheric specific humidity. Consequently, reanalysis products are still considered to be unsuitable for the analysis of water vapour trends [(Sherwood et al., 2009)].

To summarize, observations of tropospheric water vapour indicate positive trends at large spatial scales occurring at a rate that is generally consistent with the Clausius-Clapeyron relation and the observed increase in atmospheric temperature. Significant trends in tropospheric relative humidity at large spatial scales have

not been observed. It is [very/highly likely] that tropospheric specific humidity has increased since the 1970s.

2.3.7 Stratospheric Humidity

Variations in stratospheric water vapour are important for the radiative balance of the stratosphere, and can also be a significant radiative forcing for surface climate (Solomon et al., 2010a). Based on a few limited long-term data sets, the AR4 concluded that there was significant long-term variability and an apparent upward trend in stratospheric water vapour over the last half of the 20th century. These changes were not well understood and were not linked to known climate change.

New information available since AR4 includes continuing characterization of measurement uncertainties (Vomel et al., 2007a; Vomel et al., 2007b; Weinstock et al., 2009), improved understanding of regional variability from balloon and aircraft observations (Schiller et al., 2009; Fujiwara et al., 2010), and longer time series to evaluate variability and trends. These data sets include frost point hygrometer balloon measurements made at Boulder, Colorado since 1980 [(Hurst et al., 2011)] and global high vertical resolution satellite observations from HALOE (1992–2005) and recently extended using Aura MLS (2004–2010) (Read et al., 2007; Rosenlof and Reid, 2008; [Randel, 2010]). Interannual anomalies in this almost 20-year record include effects linked to the stratospheric quasi-biennial oscillation (QBO), plus a step-like drop after 2001 (noted in AR4), along with more recent increases. The net changes over 1992–2010 show a water vapour decrease of about 0.2 ppmv (about -5%) in the lower stratosphere. These interannual water vapour variations for the satellite record are closely linked to observed changes in tropical tropopause temperatures (Fueglistaler and Haynes, 2005; Randel et al., 2006; Rosenlof and Reid, 2008; [Randel, 2010]), providing reasonable understanding of observed changes.

The longer record of Boulder balloon measurements (1980–2010) has been updated and revised (Scherer et al., 2008; Hurst, 2011), showing decadal-scale variability and long-term increases of up to 1 ppmv for 1980–2010. Significant differences in trends between the Boulder data and satellite observations for the period of overlap are not well understood. Only a small fraction of the Boulder changes are attributable to observed methane trends (Rohs et al., 2006), and there is not good agreement with long-term tropical tropopause temperature trends, so that there is currently poor understanding of the long-term increases inferred from the Boulder data. Observations of water isotopes suggest stratospheric water vapour trends are not linked to ice transported in overshooting deep convection (Notholt et al., 2010).

In summary, observations demonstrate that stratospheric water vapour is closely linked to the coldest tropical tropopause temperatures, and there is good understanding of the tropical seasonal cycle and local, short-term variability. There are limited data sets for evaluating long-term variability and trends in stratospheric water vapour. Global satellite data for 1992–2010 highlight a net decrease of 0.2 ppmv over this period, primarily related to a step-like decrease after 2001, with some increases in recent years. These observed variations are closely linked to interannual changes in tropical tropopause temperatures, although mechanisms for the tropopause changes themselves are not well understood. Long-term balloon observations from Boulder, Colorado suggest increases for 1980–2010 (up to 1 ppmv), however such trends are far from linear. Moreover, the balloon observations show significant differences from satellite observations for the overlap period, and cannot currently be explained by tropical tropopause temperatures or methane oxidation.

2.3.8 Clouds

Clouds are important regulators of solar and infrared radiation and can provide potentially-important feedbacks on changes in surface temperature.

2.3.8.1 Surface Observations

The AR4 reported that surface-observed total cloud cover may have increased over many land areas since the middle of the 20th century, including the USA, the former USSR, Western Europe, midlatitude Canada, and Australia. A few regions exhibited decreases, including China and central Europe. Trends were less globally consistent since the early 1970s, and regional reductions in cloud cover were reported for western Asia and Europe but increases over the USA.

Work done since the AR4 has largely confirmed and extended the preceding research. In agreement with prior results, [Milewska (2006)] reported a significant increase in the frequency of mostly cloudy conditions at most stations in Canada from 1953 to 2002. Wibig (2008) found that total cloud cover over Poland decreased during 1971–2000, with stratiform cloud types becoming less frequent and convective cloud types becoming more frequent. Xia (2010b) reported that total cloud cover declined over most of China since 1954 but then levelled off or slightly increased from the 1990s to 2005. Clear-sky frequency increased over China during the 1971–1996 time period (Endo and Yasunari, 2006). Duan and Wu (2006) documented a diurnal mean reduction in total cloud cover and a night time enhancement of low-level cloud cover over Tibet during 1961–2003, and they attributed part of the observed local warming to these cloud trends. Warren et al. (2007) noted that the cloud cover decrease previously documented for China extended into neighbouring countries as well and was primarily attributable to a decrease in higher-level clouds.

Some new developments for surface-observed cloud cover over land since the AR4 include the report of a large decrease in total cloud cover between 1971 and 1996 over South America (Warren et al., 2007). Warren et al. also found small decreases in total cloud cover over Eurasia and Africa and no trend for North America during 1971–1996. In general, low- and mid-level convective cloud types increased, stratiform cloud types decreased, and cirrus cloud cover declined over all continents (Warren et al., 2007).

Warren et al. (2007) found no evidence that interannual anomalies in cloud cover were related to anomalies in smoke aerosol in land regions of biomass burning. They did find a positive correlation between cloud base and surface temperature at middle latitudes. This result is consistent with the finding of Sun et al. (2007), who reported that surface temperature and the ceiling height of clouds with bases below 3.6 km increased between the 1950s and 1990s over most of the USA.

The AR4 documented decreasing trends in upper-level cloud cover over mid- and low-latitude oceans between 1952 and 1997. These appeared generally consistent with satellite observations of upper-level cloud during the period of overlap. In contrast, surface observers reported increasing trends in low-level cloud cover and total cloud cover between 1952 and 1997 whereas satellites reported decreasing trends in these quantities since 1983. The reasons for this discrepancy have not yet been resolved. Updates to the surface ocean cloud record since the AR4 indicate that the positive trends in low-level and total cloud cover during the second half of the 20th century changed sign around 2000, and both quantities decreased until the end of the record in 2008 [(Eastman et al., 2010)]. The cause of the trend reversal is unknown. Further evidence that global decadal variations in surface-observed low-level and total cloud cover are spurious is the finding that interannual anomalies in ship observations of cloud cover agree with nearby island observations of cloud cover only after the removal of globally coherent long-term variations from the ship data [(Eastman et al., 2010)].

Regional variability in surface-observed cloudiness over the ocean appeared more credible than zonal and global mean variations in the AR4. Multidecadal changes in upper-level cloud cover and total cloud cover over particular areas of the tropical Indo-Pacific Ocean were consistent with island precipitation records and SST variability. This has been extended more recently by Deser et al. (2010a), who found that an eastward shift in tropical convection and total cloud cover from the western to central equatorial Pacific occurred over the 20th century and attributed it to a long-term weakening of the Walker circulation. [Eastman et al. (2010)] report that, after the removal of apparently spurious globally coherent variability, cloud cover decreased in all subtropical stratocumulus regions from 1954 to 2008.

2.3.8.2 Satellite Observations

Satellite cloud observations offer the advantage of much better spatial and temporal coverage compared to surface observations. However they require careful efforts to identify and correct for temporal discontinuities in the data sets associated with orbital drift, sensor degradation, and inter-satellite calibration differences.

The AR4 noted that there were substantial uncertainties in decadal trends of cloud cover in all data sets available at the time and concluded that there was no clear consensus regarding the decadal changes in total cloud cover. Since AR4 there has been continued effort to assess the quality of and develop improvements to multi-decadal cloud products from operational satellite platforms (Evan et al., 2007; O'Dell et al., 2008;

Heidinger and Pavolonis, 2009). New cloud climatologies have also recently become available from improved sensors on the Earth Observation System (EOS) adding to our knowledge of the distribution and characterization of cloud properties (Ackerman et al., 2008; [Di Girolamo et al., 2010]).

There are two primary satellite data sets which offer multi-decadal records of cloud cover: the International Satellite Cloud Climatology Project (ISCCP; [Rossow and Schiffer, 1999]) and the Pathfinder Atmospheres Extended dataset (PATMOS-x; Jacobowitz et al., 2003) both of which begin in the early 1980s. As reported in AR4, there are discrepancies in global cloud cover trends between ISCCP and other data products. Most notable is the large downward trend of global cloudiness in ISCCP since the late 1980s, which is inconsistent with PATMOS-x and surface observations [(Foster et al., 2010)]. Recent work has confirmed the conclusion of AR4, that much of the downward trend is spurious and an artefact of changes in satellite viewing geometry [(Evan et al., 2010)]. Cermak et al. (2010) has further documented inconsistencies in the spatial patterns of cloud cover trends between PATMOS-x and ISCCP. However, comparisons of PATMOS-x data with new satellite cloud observations from EOS available since 2000 suggest better agreement on interannual anomalies of global cloud cover [(Foster et al., 2010)]. Satellite observations of low level marine clouds suggest no long term trends in cloud liquid water path or optical properties (O'Dell et al., 2008; Rausch et al., 2010).

Using surface and satellite data, Clement et al. (2009) documented multidecadal variations in total cloud cover and low-level cloud cover over the northeast subtropical Pacific that were consistent with SST and SLP variations associated with the Pacific Decadal Oscillation. Their analysis applied an adjustment to the ISCCP data to correct for artefacts which result from changes in viewing angle geometry (Evan et al., 2007) and other inhomogeneities (Loeb et al., 2007). They found that reductions in low cloud were associated with an increase in SST and symptomatic of positive cloud shortwave radiative feedback.

The responses of water vapour and cloud inferred from the top of atmosphere radiation were noted to be time-scale dependent (Harries and Futyan, 2006) and highly sensitive to the time-periods and regions chosen for analysis (Murphy, 2010; Lindzen and Choi, 2009; Spencer and Braswell, 2010; Chung et al., 2010b; Trenberth et al., 2010). Using recently updated radiation data from the CERES satellite, Dessler (2010) found evidence for a weak interannual global relationship between cloud impacts on net top-of-atmosphere radiation and surface temperature, primarily explained by a positive cloud longwave radiative feedback.

To summarize, while there is consistency in trends of cloud cover between independent data sets in certain regions, substantial ambiguity remains in the observations of global-scale cloud variability and trends. What trends do exist are likely to be within the range of uncertainties for both satellite and observational cloud data sets.

[INSERT FIGURE 2.31 HERE]
Figure 2.31: Global Anomalies in Water Vapour (from State of Climate Report).

[INSERT FIGURE 2.32 HERE]
Figure 2.32: Global Anomalies in Cloud Cover (from State of Climate Report).

2.4 Atmospheric Composition

[PLACEHOLDER FOR FIRST ORDER DRAFT]

2.4.1 Long-Lived Greenhouse Gases

In this section we update observations (see Table 2.6) of the abundances of long-lived greenhouse gases (LLGHG) that have significant radiative forcing since the IPCC WGI Fourth Assessment Report (AR4; IPCC, 2007a). The abundances reported here are used to calculate radiative forcing, which total about 2.8 W m^{-2}, in Chapter 8. These observations are also used to constrain the budgets of LLGHGs. A global GHG budget consists of the total atmospheric burden, total global rate of production or emission (i.e., sources), and the total global rate of destruction or removal (i.e., sinks). Precise, accurate systematic observations from globally distributed measurement networks are used to estimate global means for LLGHGs, and these allow estimates of the global burden. The observed rate of increase (trend) results from the imbalance between

emissions and sinks. When the trend is zero, emissions and sinks are equal, the burden is at steady state, and the atmospheric lifetime is equal to the global burden divided by the global rate of emission or of removal. Emissions are predominantly from surface sources, which are described in Chapter 6. Direct use of observations of LLGHGs to model their regional budgets can also play an important role in emissions verification (Nisbet and Weiss, 2010).

Methods to estimate GHG emissions are described as "bottom-up" and "top-down". Bottom-up methods are inventory-based and rely on estimates of emission factors and activities (e.g., CH_4 emissions per cow multiplies by the number of cows). Top-down methods use observations of atmospheric GHG trends and spatial gradients with a chemical transport model to estimate emissions over various spatial scales.

LLGHGs are removed from the atmosphere by physical, chemical and biological processes. The concept of lifetime is relatively straightforward when the sink processes result in the destruction of the LLGHG, but for processes involving exchange between the atmosphere and other reservoirs the concept is more complicated. Atmospheric CO_2 exchanges on comparatively short time scales with the terrestrial biosphere and with the upper layers of the oceans, but more slowly with the deep oceans, which are isolated from atmospheric exchange (see Chapter 6) and play a major role in the long-term uptake of CO_2 emitted by fossil fuel combustion. For most other LLGHGs, the major sinks are photolysis and/or reaction with the hydroxyl radical (OH). OH concentrations depend, in turn, on the abundances of CH_4, VOCs, CO, NOx, H_2O, and flux of solar UV radiation in the troposphere (IPCC, 2001). As a result, the impacts of LLGHGs on climate strongly depend on atmospheric chemistry.

Systematic time series of atmospheric measurements of LLGHGs in ambient air began at various times during the last six decades, with earlier atmospheric histories being reconstructed from measurements of air trapped in polar ice cores or in firn. Measurements of LLGHGs are reported as dry-air mole fractions, an SI unit that is conserved with changes in temperature and pressure. This eliminates dilution effects from variable amounts of H_2O vapour, which range up to 4% of the total atmospheric composition. Here we use the following abbreviations: ppm = μmol mol^{-1}; ppb = nmol mol^{-1}; and ppt = pmol mol^{-1}.

Table 2.6: Comparison of globally annually averaged dry air mole fractions for LLGHGs from three measurement networks with those reported in AR4 (2005). Units are ppt (parts per trillion) except where noted (ppm = parts per million; ppb = parts per billion). [Note: Prior to publication of AR5, values for 2009 will be updated to 2010 or 2011, and uncertainties will be added.]

		IPCC	UCI	AGAGE	NOAA	MEAN	Std Dev
Chemical species	**Formula**	**2005**	**2009**	**2009**	**2009**	**2009**	**2009**
Carbon dioxide	CO_2 (ppm)	379	---	---	386.27	386.27	N/A
Methane	CH_4 (ppb)	1774	1787.6	1792.31	1793.93	1791.28	3.29
Nitrous oxide	N_2O (ppb)	319	---	322.27	322.5	322.4064	0.19
Sulphur hexafluoride	SF_6	5.6	---	6.7	6.76	6.73	0.04
Perfluoromethane	CF_4	74	---	77.66	---	77.66	N/A
Perfluoroethane	C_2F_6	2.9	---	4.01	---	4.01	N/A
HFC-125	CHF_2CF_3	3.7	---	7.09	7.3	7.20	0.15
HFC-134a	CH_2FCF_3	35	51.7	52.71	52.4	52.28	0.52
HFC-152a	CH_3CHF_2	3.9	---	6.03	5.9	5.96	0.09
HFC-23	CHF_3	18	---	22.57	22.6	22.59	0.02
CFC-11	$CFCl_3$	251	242.1	241.47	243.2	242.25	0.87
CFC-12	CF_2Cl_2	538	530.1	535.16	532.5	532.58	2.53
CFC-113	$CF_2ClCFCl_2$	79	76.4	75.86	75.9	76.04	0.31

HCFC-22	CHF_2Cl	169	196	199.18	198.4	197.86	1.66
HCFC-141b	CH_3CFCl_2	18	19.4	19.9	19.8	19.70	0.27
HCFC-142b	CH_3CF_2Cl	15	19.1	19.95	19.4	19.48	0.43
Carbon tetrachloride	CCl_4	93	90.4	87.1	89.4	88.97	1.69
Methyl chloroform	CH_3CCl_3	19	9.4	8.88	9.1	9.13	0.26

Notes:
AGAGE = Advanced global atmospheric gases experiment
NOAA = National Oceanic and Atmospheric Administration, Earth System Research Laboratory, Global Monitoring Division
UCI = University of California, Irvine, Department of Chemistry

2.4.1.1 Kyoto Protocol Gases (CO_2, CH_4, N_2O, HFCs, PFCs, and SF_6)

[PLACEHOLDER FOR FIRST ORDER DRAFT]

2.4.1.1.1 Carbon dioxide (CO_2)

Although atmospheric CO_2 contributes only 20% of total GHG radiative forcing, and non-CO_2 GHGs supply an additional 5%, together they sustain the terrestrial greenhouse effect, with water vapour (50%) and clouds (25%) providing the remaining 75% of the effect as fast feedbacks (Lacis et al., 2010). An increasing atmospheric burden of CO_2 also affects the ocean food chain through acidification.

Precise, accurate systematic measurements of atmospheric CO_2 were begun by C. D. Keeling in 1957, and estimates of CO_2 atmospheric abundance prior to that date have since been reconstructed from measurements of air extracted from ice cores and from firn. The pre-industrial (1750) globally averaged abundance of atmospheric CO_2 was 278 ppm, and, in 1860, it was 286 ppm (Etheridge et al., 1996). The following discussion is based on the NOAA CO_2 trends web page (ftp://ftp.cmdl.noaa.gov/ccg/co2/trends/co2_annmean_gl.txt). In 2009, globally averaged CO_2 was 386.27 ± 0.10 ppm, and the increase in 2009 was 1.62 ± 0.14 ppm. Since the AR4 (2005), CO_2 has increased by 7.5 ppm (see Figure 2.33). From 1980 to 2009, the average rate of increase in globally averaged CO_2 has been 1.64 ± 0.28 ppm yr^{-1}. The CO_2 growth rate varies significantly from year to year; since 1980, the range in annual increase is 0.67 ± 0.14 ppm in 1992 to 2.90 ± 0.14 ppm in 1998. Most of this interannual variability in growth rate is driven by small changes in the balance between photosynthesis and respiration on land, each having global fluxes of about 100 Pg C yr^{-1}.

The main contributors to increasing atmospheric CO_2 abundance are fossil fuel combustion and land use change. During the past few decades, most of the increasing atmospheric burden of CO_2 is from fossil fuel combustion. This is known from multiple lines of observational evidence (Tans, 2009). The current rate of increase in atmospheric CO_2 is exceptional when compared to changes on geological time scales as assessed from measurements of air trapped in ice cores. Measurements of atmospheric CO_2 at Mauna Loa, Hawaii and South Pole show that the north to south difference is increasing, consistent with increasing CO_2 emissions from fossil fuel combustion, predominantly in the northern hemisphere. Strong evidence also comes from measurements of other tracers such as ^{14}C in CO_2, which is decreasing as a result of adding CO_2 with no ^{14}C from fossil fuel combustion, ^{13}C in CO_2, which shows that the added CO_2 is of organic origin, and measurements of a decrease in O_2/N_2, which is also consistent with O_2 consumption by fossil fuel combustion after correction for land biosphere changes and ocean outgassing (IPCC, 2001).

Approximately half the CO_2 emitted from fossil fuel combustion and cement production from 1751 to 2007 (337 Pg C; ±5 to 10%) (Boden et al., 2010) has been taken up by the ocean and terrestrial biosphere. Several recent studies have suggested that the airborne fraction (AF), that is the fraction of CO_2 emitted from anthropogenic activities (fossil fuel combustion, cement production, and land use change) that remains in the atmosphere, has been increasing (Canadell et al., 2007; Le Quere et al., 2009; Raupach et al., 2008). This would mean the oceans and terrestrial biosphere are becoming less effective as sinks for anthropogenic CO_2. However, Gloor et al. (2010) show that likely omissions in reported emissions from land use change and external forcing events (e.g., volcanic eruptions) are sufficient to explain the observed long-term trend in

airborne fraction, while Knorr (2009) found that the trend in the AF since 1850 has been 0.7 ± 1.4% per decade, i.e., not significantly different from zero.

2.4.1.1.2 Methane (CH_4)

Globally averaged CH_4 in 1750 was about 715 ppb, and by 1860, it had increased to about 815 ppb (Etheridge et al., 1998). Evidence suggests that human influences on the global CH_4 budget began much earlier than the industrial era (Ferretti et al., 2005; Ruddiman, 2003, 2007). By 2009, globally averaged CH_4 at Earth's surface was 1793.9 ± 1.4 ppb (see Figure 2.34). This makes methane the second most abundant LLGHG, and it is the second largest contributor to radiative forcing among LLGHGs. Since AR4, which reported values for 2005, the globally averaged abundance of CH_4 has increased by 19.3 ppb. This increase began in 2007 after a period of near constant atmospheric burden from 1999 to 2006 (Dlugokencky et al., 2009; Rigby et al., 2008). This increase was also observed in CH_4 column averages retrieved from irradiances measured by the satellite sensor SCIAMACHY on board ENVISAT (Frankenberg, 2011). Causes for the increase in atmospheric CH_4 since 2007 are unclear.

Rigby et al. (2008) used CH_4 data from the CSIRO and AGAGE networks, and estimates of [OH] based on AGAGE measurements of 1,1,1-trichloroethane to assess causes of the increase. They concluded that an increase in emissions was necessary to explain the CH_4 observations. The magnitude and distribution of the emissions change depended on assumptions about changes in [OH]. Assuming inter-annually repeating [OH] required a substantial increase in emissions from both hemispheres in 2007 compared to 2006. If an [OH] decrease of 4 ± 14% determined from the 1,1,1-trichloroethane measurements was used, then a smaller increase in emissions, predominantly in the northern hemisphere, was required. Changes in [OH] of more than a few percent are unlikely based on our understanding of atmospheric chemistry and the analysis of Montzka et al. (2011).

Dlugokencky et al. (2009) analyzed surface and vertical profiles of CH_4 mole fraction and measurements of ^{13}C in CH_4. They suggested that the most likely drivers of increased atmospheric CH_4 were anomalously high temperatures in the Arctic in 2007 and greater than average precipitation in the tropics during 2007 and 2008. These drivers increased emissions from wetlands in both regions, where CH_4 production is strongly influenced by water table height and temperature. They also suggested that contributions to the increased CH_4 from biomass burning and changes in [OH] were small.

Bousquet et al. (2011) used observations from multiple independent measurement programs to assess changes in emissions and sinks during 2006–2008 and found that global CH_4 emissions increased by 19 Tg CH_4 (16 to 21 Tg) in 2007 and 13 Tg CH_4 in 2008 (6 to 20 Tg) relative to the average of emissions for 1999–2006. Changes in tropical wetland emissions were the dominant driver in 2007, with a minor contribution from Arctic wetlands. For 2008, the two inversions were not consistent. Neither suggested a strong increase in emissions from wetlands in the tropics nor the Arctic. They found that changes in [OH] were less than 1%, and had only a small impact on observed CH_4 changes.

The atmospheric CH_4 budget is very nearly in balance. Observed increases in CH_4 abundance are the result of small differences between emissions and sinks, both of which are currently on the order of 550 Tg CH_4 yr^{-1}. So small relative changes in emissions from any large source can result in significant changes to methane's rate of increase. The Arctic holds extensive stores of carbon in permafrost and clathrates; both reservoirs are sensitive to changing climate and could provide strong positive feedbacks to temperature as climate warms. Near-zero growth in atmospheric CH_4 in the Arctic during 2008 suggests that we have not yet activated those feedbacks, but even small increases in natural emissions there as the Arctic responds to changing climate would cause the atmospheric CH_4 burden to begin increasing again.

2.4.1.1.3 Nitrous oxide (N_2O)

Globally averaged N_2O in 2009 was 322.5 ppb, an increase of 3.5 ppb over the value reported for 2005 in AR4 (see Figure 2.35). This is an increase of 19% over the value estimated for 1750 from ice cores of 270 ± 7 ppb. Measurements of N_2O and its isotopic composition in firn air suggest the increase, at least since the early 1950s, is dominated by emissions from soils (Ishijima et al., 2007). Since systematic measurements began in the late 1970s, N_2O has increased at an average rate of about 0.8 ppb yr^{-1} (see Figure 2.35); this, combined with a decreasing atmospheric burden of CFC-12 makes it the third most important LLGHG contributing to radiative forcing. NO produced by reaction of $O(^1D)$ with N_2O also depletes stratospheric O_3.

Its emissions weighted by ozone depletion potential (ODP) now dominate emissions of all O_3 depleting substances (Ravishankara et al., 2009).

Approximately 70% of N_2O emissions are from natural sources with the remainder, mostly from use of nitrogen fertilizers, from anthropogenic sources. Emissions may increase if nitrogen fertilizer use increases to produce biofuels (Crutzen et al., 2008). Its main loss process is photochemical destruction in the stratosphere with a lifetime of 114 years.

Observations of N_2O show latitudinal gradients in annual mean values, with maxima in the northern subtropics, values about 1.7 ppb lower in the Antarctic, and values about 0.4 ppb lower in the Arctic. These persistent gradients contain information about anthropogenic emissions from fertilizer use at northern mid-latitudes and natural ocean emissions in upwelling regions of the tropics. N_2O time series also contain seasonal variations with peak to peak amplitudes of about 1 ppb in high latitudes of the northern hemisphere and about 0.4 ppb at high southern and tropical latitudes. In the Northern Hemisphere, exchange of air between the stratosphere and troposphere is the dominant contributor to observed seasonal cycles (Jiang et al., 2007). Nevison et al. (2011) found correlations between the magnitude of detrended N_2O seasonal minima and lower stratospheric temperature providing evidence for a stratospheric influence on the timing and amplitude of the seasonal cycle at surface monitoring sites. In the Southern Hemisphere, observed seasonal cycles are also affected by stratospheric influx, but there are contributions to the seasonal cycle from ventilation and thermal out-gassing of N_2O from the oceans.

Since AR4, one new study has estimated N_2O emissions from surface observations. Huang et al. (2008) used N_2O measurements from AGAGE, NOAA ESRL GMD, and CSIRO, being careful to account for small calibration differences, and estimated $16.3^{+1.5}_{-1.2}$ Tg N (N_2O) yr^{-1} for 1997–2001 and $15.4^{+1.7}_{-1.3}$ Tg N (N_2O) yr^{-1} for 2001–2005 (uncertainties are 66% confidence limits). Results from Huang et al. (2008) are in good agreement with those from Hirsch et al. (2006), reported in AR4, despite different sets of observations and a different analysis framework. Both recent studies put significantly more emissions in the region 0 to 30°N and less in 30°S to 90°S than the GEIA inventory (Bouwman et al., 1995) and an earlier model study (Prinn et al., 1990). They also conclude that uncertainties in air mass exchange between the stratosphere and troposphere (STE) results in a significant portion of the uncertainty in estimated fluxes, particularly on regional scales. Nevison et al. (2007) have used complementary stratospheric tracers with strong sinks in the stratosphere (e.g., CFC-12) to assess the contribution of STE to the observed N_2O seasonal cycle. New observations of N_2O from aircraft are also being used to determine the influence of STE as a function of latitude (Ishijima et al., 2010).

2.4.1.1.4 HFCs, PFCs, and SF_6

Current atmospheric abundances and radiative forcing for HFCs are small. However, as they replace CFCs and HCFCs in many applications, their contribution to future climate forcing is projected to grow considerably in the absence of controls on global production (Velders et al., 2009). HFC-134a is a replacement for CFC-12 in automobile air conditioners and is also used in foam blowing applications. In 2009, it reached 52.4 ppt, an increase of 18 ppt since 2005. Based on analysis of high-frequency measurements, significant emissions occur in N. America, Europe, and East Asia (Stohl et al., 2009).

HFC-23 is a byproduct of HCFC-22 production. Atmospheric HFC-23 mole fractions increased from about 19 ppt in 2005 to 22 ppt in 2009. Atmospheric observations agree, within uncertainties, with bottom-up inventories. Based on an inverse model analysis of current atmospheric observations and measurements of a Southern Hemisphere air archive, Miller et al. (2010) show that CFC-23 emissions increased from the late 1970s, peaked in 2006 at 15 (+1.3/-1.2) Gg yr^{-1}, then decreased to 8.6 (+0.9/-1.0) Gg yr^{-1} in 2009. Factors contributing to these changes since the late 1990s are decreased emissions from developed countries because of voluntary destruction followed by increased emissions from developing countries. They find that most of the decrease in HFC-23 emissions since 2006 is consistent with abatement efforts under the Clean Development Mechanism (CDM) of the UNFCCC. Montzka et al. (2010), using measurements of HFC-23 in firn and modern air, infer that HFC-23 emissions from developing countries averaged 11 ± 2 Gg yr^{-1} during 2006–2008 which is about double the about 6 Gg yr^{-1} destroyed under the CDM during 2007 and 2008. The lifetime of HFC-23 has been revised from 270 to 222 yr (WMO, 2011) based on new laboratory studies.

HFC-125 increased from about 3.7 ppt in 2005 to 7.3 ppt in 2009. The relative rate of increase at the beginning of 2008 was 16% yr^{-1}, and global emissions were 21 Gg in 2007, having increased by 15% yr^{-1} since 2000 (O'Doherty et al., 2009). These estimated emissions are within about 20% of emissions reported to the UNFCCC when estimates of emissions from East Asia are included. HFC-152a, which is used as a foam-blowing agent and as an aerosol propellant, increased from 3.6 ppt in 2005 to 5.9 ppt in 2009. New measurements of several HFCs have been reported since AR4: HFC-365mfc, HFC-245fa, and HFC-227ea. All were ≤2 ppt in recent years, but their abundances are increasing.

PFCs, CF_4 and C_2F_6, strongly absorb thermal IR radiation and have lifetimes of 50 kyr and 10 kyr, respectively. CF_4 and C_2F_6 are emitted as a byproduct of aluminum production and used in plasma etching of electronics. Because of their physical properties they are difficult to measure, but new instrumental developments that can pre-concentrate trace species from ambient air at -165°C now allow precise measurements of both species (Miller et al., 2008). CF_4 has a natural lithospheric source (Deeds et al., 2008) with a preindustrial level (about 1750) determined from Greenland and Antarctic firn air of 34.7 ± 0.2 ppt (Muhle et al., 2010) in good agreement with Worton et al. (2007). The sum of emissions of CF_4 reported by aluminum producers and for non-aluminum production in EDGAR v4 only accounts for about half of global emissions estimated from atmospheric observations (Muhle et al., 2010). For C_2F_6, emissions reported to the UNFCCC are also substantially lower than those estimated from atmospheric observations (Muhle et al., 2010).

Global annual mean SF_6 in 2009 was 6.8 ppt, increasing from 5.7 ppt in 2005. SF_6 has a lifetime of about 3200 years, so its emissions accumulate in the atmosphere and can be estimated directly from its observed rate of increase. Levin et al. (2010) and Rigby et al. (2010) showed that SF_6 emissions decreased after 1995, most likely because of emissions reductions in developed countries, but then increased after 1998. During the past decade, they found that actual SF_6 emissions from developed countries are at least twice the reported values.

Since AR4, atmospheric observations of two new species that are not covered by the Kyoto Protocol were reported. Prather and Hsu (2008) suggested that NF_3 is a missing greenhouse gas with a potential large impact on radiative forcing. It is a substitute for PFCs as a plasma source in the semiconductor industry, has a lifetime of 500 years, and a GWP_{100} = 17,500 (WMO, 2011). Weiss et al. (2008) determined 0.45 ppt for its global annual mean mole fraction in 2008, increasing at 0.05 ppt yr^{-1}. Initial bottom-up inventories underestimated its emissions; based on the atmospheric observations, NF_3 emissions were 0.62 Gg in 2008. SO_2F_2 replaces CH_3Br, an ODS, as a fumigant. Its $GWP_{100} \approx 4740$, is comparable to CFC-11. A new estimate of its lifetime, 36 ± 11 yr (Muhle et al., 2009), is significantly longer than previous estimates. Its global annual mean mole fraction in 2008 was 1.51 ppt and increased by 0.04 ppt from 2007 to 2008.

2.4.1.2 Montreal Protocol Gases (CFCs, Chlorocarbons, HCFCs, and Halons)

CFC atmospheric abundances are decreasing because of the successful reduction in emissions resulting from the Montreal Protocol on Substances that Deplete the Ozone Layer. By 2010, the Montreal Protocol had reduced emissions from ODSs by an amount equivalent to about 11 Pg CO_2 yr^{-1} (including offsets) ; this is 5 to 6 times the reduction target of the first commitment period (2008–2012) of the Kyoto Protocol (2 Pg CO_2 eq yr^{-1}) (Velders et al., 2007). Recent observations in Arctic and Antarctic firn air further confirm that emissions of CFCs are predominantly anthropogenic (Martinerie et al., 2009). CFC-12 has the largest atmospheric abundance and GWP-weighted emissions of the CFCs. Its tropospheric abundance peaked during 2000–2004. Since AR4, its global annual mean mole fraction declined from 541.5 ppt in 2005 to 532.5 ppt in 2009. CFC-11 continued to decrease from 252.2 ppt in 2005 to 243.2 ppt in 2009. CFC-113 decreased from 78.2 ppt in 2005 to 75.9 ppt in 2009. A discrepancy exists between top-down and bottom-up methods for calculating CFC-11 emissions. Emissions calculated using top-down methods come into agreement with bottom-up estimates when a lifetime of 64 yr is used for CFC-11 in place of the accepted value of 45 yr; this longer lifetime (64 yr) is at the upper end of the range estimated by Douglass et al. (2008a) in a study of the CFC-11 lifetime with models that more accurately simulate stratospheric circulation. Future emissions of CFCs will largely come from “banks” (i.e., material residing in existing equipment or stores) rather than current production.

The CCl_4 global annual mean decreased from 94.6 to 89.4 ppt from 2005 to 2009. The observed rate of decrease and interhemispheric difference of CCl_4 suggest that emissions determined from the observations are on average greater and less variable than bottom-up emission estimates, although large uncertainties in the CCl_4 lifetime result in large uncertainties in the top-down estimates of emissions. CH_3CCl_3 has declined exponentially for about a decade, decreasing from 18.8 ppt in 2005 to 9.1 ppt in 2009. Because its atmospheric loss is dominated by reaction with hydroxyl radical (OH), CH_3CCl_3 has been used extensively to estimate globally averaged OH concentrations (e.g., Prinn et al., 2005). Montzka et al. (2011) exploited the exponential decrease and small emissions in CH_3CCl_3 to show that interannual variations in OH concentration from 1998 to 2007 are 2.3 ± 1.5%, which is consistent with the interannual variability in OH estimated from other species including CH_4, C_2Cl_4, CH_2Cl_2, CH_3Cl, and CH_3Br.

HCFCs are classified as "transitional substitutes" by the Montreal Protocol, so their global production and use will ultimately be phased out. But global HCFC production is not currently capped and has increased in recent years. As a result, global levels of the three most abundant HCFCs in the atmosphere continue to increase. HCFC-22 increased from 168.3 ppt in 2005 to 198.4 ppt in 2009. HCFC-141b increased from 17.6 ppt in 2005 to 19.8 ppt in 2009, and for HCFC-142b, the increase was from 15.2 ppt to 19.4 ppt. The rates of increase in these 3 HCFCs increased since 2004, but the change in HCFC-141b growth rate was smaller and less persistent than for the others, which approximately doubled from 2004 to 2007 (Montzka et al., 2009). Based on changes in observed spatial gradients, there has likely been a shift in emissions within the Northern Hemisphere from regions north of about 30°N to regions south of 30°N.

Atmospheric abundances of halons, except for halon-1301, have been decreasing. All have relatively small atmospheric burdens, ≤ 5 ppt, and are unlikely to accumulate to levels that can significantly affect radiative forcing, if current projections are followed (WMO, 2011).

[INSERT FIGURE 2.33 HERE]
Figure 2.33: a) Solid line shows globally averaged CO_2 dry air moles fractions; dashed line is a deseasonalized trend curve fitted to the global averages. b) Instantaneous growth rate for globally averaged atmospheric CO_2 (solid line; dashed lines are ±68% confidence limits). The growth rate is the time-derivative of the dashed line in a). Symbols are annual increases from January 1 in one year to January 1 in the next year, plotted in the middle of the year.

[INSERT FIGURE 2.34 HERE]
Figure 2.34: a) Solid line shows globally averaged CH_4 dry air moles fractions; dashed line is a deseasonalized trend curve fitted to the global averages. b) Instantaneous growth rate for globally averaged atmospheric CH_4 (solid line; dashed lines are ±68% confidence limits). The growth rate is the time-derivative of the dashed line in a). Symbols are annual increases from January 1 in one year to January 1 in the next year, plotted in the middle of the year.

[INSERT FIGURE 2.35 HERE]
Figure 2.35: a) Solid line shows globally averaged N_2O dry air moles fractions; dashed line is a deseasonalized trend curve fitted to the global averages. b) Instantaneous growth rate for globally averaged atmospheric N_2O. The growth rate is the time-derivative of the dashed line in a).

2.4.2 Trends in Short-Lived Greenhouse Gases

[PLACEHOLDER FOR FIRST ORDER DRAFT]

2.4.2.1 Tropospheric Ozone

The AR4 reported a best estimate for the RF by tropospheric ozone of 0.35 W m-2 [0.25–0.65 Wm-2]. The two main factors that contributed to the large uncertainty range were model uncertainties, and the apparent discrepancy between observed pre-industrial levels of tropospheric ozone (10–15 ppbv) and the corresponding higher model calculations (20–25 ppbv). Recent model analysis (Parrella et al., 2011) suggest that tropospheric bromine chemistry, previously not included in models, could explain much of the discrepancies. In perspective, current background tropospheric ozone, is around 35–40 ppbv (HTAP, 2010).

Assessment of trends in tropospheric ozone remains difficult due to the paucity of high quality long-term datasets, representative for larger regions.

O_3 measurements in ambient air were collected at the Montsouris Observatory close to Paris from 1876–1912, showing low O_3 (10–15 ppbv) in the planetary boundary layer (Volz and Kley, 1988). Compared to AR4, there is no new information regarding the levels of pre-industrial ozone, however more analysis has been performed regarding the consistency of these pre-industrial O_3 values with more recent O_3 time series starting at the 1960s. Measurements using similar techniques were conducted from 1956–1983 at Arkona, a coastal site on the Baltic Sea (Feister and Warmbt, 1987), and the series was continued at the nearby Zingst site (Figure 2.36). Consistent with the Montsouris time series, the earliest springtime measurements at Arkona show O_3 concentrations around 15 ppbv followed by an increase (amounting to about 20 ppbv) to the present Zingst concentrations (Figure 2.36). Measured trends at European background stations (Mace Head, Hohenpeissenberg and Zugspitze) are between 0.2 and 0.6 ppbv/year and are generally somewhat higher in winter and spring than in summer (HTAP, 2010). We note here that O_3 trends close to pollution sources may be rather different, for example an analysis of EMEP station data by (Jonson et al., 2006; Pozzoli et al., 2011) shows partly opposing positive winter and negative summer O_3 trends, in response to emission reductions.

In the Eastern Parts of the US, Hidy and Pennell (2010) report decreasing 8-hr average ozone trends for 1997–2006 in the order of -0.1 to -0.4 ppbv/yr. The declines are stronger for the higher ozone concentrations, reflecting local pollution controls [reference needed]. In view of the dominating westerly circulation, O_3 trends at North America's West Coast may be indicative for large scale ozone changes in the Asian pacific region. The magnitude and reason for these trends are somewhat debated. Oltmans et al. (2008) report trends covering 20 years of data amounting to 0.53 and 0.82 % yr^{-1} for two remote Californian surface stations, however other factors than long-range transport could have contributed to these trends. Oltmans et al. (2008) do not find significant changes in ozone derived from a 10 years dataset of vertical soundings at Trinidad Head.

Parrish et al. (2009) analyse data from 8 Pacific stations with time series between 8–25 years, to derive a trend of 0.34 ± 0.09 ppbv yr^{-1} (Figure 2.36). These trends are very similar to the trends measured at Mace Head (west coast Ireland), although the North American trends continue after 2000, and flatten in Europe. Cooper at al. (2010) derive a trend of 0.63 ± 0.34 ppbv yr^{-1} in springtime free tropospheric ozone over western North America between 1984–2008, in approximate accord with the trends derived from the surface measurements by Parrish et al. (2009), and the trends were stronger in air with strong influence from the South and East Asian boundary layer. Jaffe et al. (2007) report that average O_3 concentrations generally increased from 1987–2004 at 7 rural sites in the western and Northern US, with significant increase rates of 0.19–0.51 ppbv yr^{-1} at 7 sites, while no significant trends were detected at two others sites.

The few long-term continuous O_3 measurements in Asia indicate increasing O_3 concentrations. In Japan, continuous measurements at Mt. Happo Observatory (1.9 km asl) show a springtime O_3 increase of 1.30 ± 0.28 ppbv yr^{-1} from 1991 to 2007 (Tanimoto, 2009) and also in other seasons the trends are larger than anywhere else in the world. Six Pacific Rim island sites (Tanimoto, 2009; Tanimoto et al., 2009), e.g., Rishiri Island, indicate an increasing springtime trend of on average 0.62 ± 0.36 ppbv yr^{-1} [possibly include more recent analysis from MOZAIC (contacted V. Thouret)].

[INSERT FIGURE 2.36 HERE]

Figure 2.36: Springtime trends in O_3 concentrations measured in a) Europe and b) western North America and Japan. The lines (in colour) indicate the linear regressions to the data, and the curves (in black) indicate quadratic polynomial fits to the three central European sites over the time span of the lines. Arkona and Zingst are two sites located close to the Baltic Sea. Mace Head is located at the west coast of Ireland. Hohenpiessenberg (1.0 km asl) and Zugspitze (3.0 km asl) are in southern Germany, and Jungfraujoch (3.6 km asl) is in Switzerland. The North American data are from several sea level Pacific coastal sites and Lassen National Park (1.8 km asl) near the west coast, and from the free troposphere over the western part of the continent. The Japanese data are from Mt. Happo (1.9 km asl) on the Japanese mainland and Rishiri, a northern (45N) sea level island site (HTAP, 2010).

These measurements at surface background stations and mountain tops are further corroborated by new analysis of ozone sounding data by [S. Tilmes et al. (2011, in preparation)]. Figure 2.37 shows a regional and seasonal analysis of boundary layer ozone (950–850 hPa). The consistency of surface observations obtained at Hohenpeissenberg and the average of soundings in Western Europe suggests that there are no experimental biases in the early period. Between 1970 and 1990 ozone in West Europe has increased by about 15 ppb in summer, 12 ppb in spring and about 10 ppb in winter and less than 10 ppb in fall. Since 1990 a slight increase of ozone (about 6–8 ppb) is observed in winter and spring and less than 3 ppb in summer and fall in the NH polar region. For the other regions and seasons ozone changes, if any, are very small (less than 3 ppb between 1990–2009). The limited amount of sonde-derived boundary layer observations in Japan and North America does not suggest a significant difference with the trend in West Europe. Statistical significance of trends was not assessed by [Tilmes et al. (2011)].

[INSERT FIGURE 2.37 HERE]

Figure 2.37: Seasonal and regional ozone from soundings at 850–950 hPa pressure levels between 1968 and 2009. Each seasonal data point represents the median statistics of >10 soundings. Winter refers to NH December-January-February and SH, July-August-September, etc.

In the Southern Hemisphere Oltmans et al. (2006) report increases of surface ozone in the order of 0.3–0.5% yr^{-1}, based on three time series covering 20 years. They point out that long-term ozone trends are varied in sign and magnitude among various regions, but broadly consistent with the expected behaviour of precursor emissions. HTAP (2010) states that qualitatively but not quantitatively models reproduce the observed trends of baseline ozone.

Relatively little progress has been made in the use of satellite for deriving trends of tropospheric ozone columns. Thompson et al. (2001b) report strong El Niño signals, but no trends using Nimbus 7/TOMS data. Using a different technique, but the same instrument, Ziemke et al. (2005) show a statistically significant upward trend in the midlatitudes of both hemispheres but not in the tropics. Model analysis by de Laat et al. (2005) suggests serious instrumental limitations for retrieving extratropical trends. Beig and Singh (2007) report TOMS derived tropospheric ozone trends (1979–2005) of 0.4–0.9% yr^{-1} for some parts of South Asia. A newer generation of satellites, TES (Tropospheric Emission Spectrometer), OMI (Ozone Monitoring Instrument), operational since 2004, and IASI, operational since 2007, may in the near future more robust information on tropospheric ozone trends (Keim et al., 2009; Liu et al., 2010; Zhang et al., 2010).

The level of scientific understanding of tropospheric ozone trends is medium (unchanged from AR4), with most recent measurements of background tropospheric ozone at the coasts of Europe and North America suggesting upward trends between 0.3–0.5% yr^{-1}.

2.4.2.2 Stratospheric Ozone

AR4 reported the radiative forcing from stratospheric ozone to be -0.05 ± 0.10 W m^{-2}. The recent Scientific Assessment of Ozone Depletion report (Ajavon et al., 2010), using various measurements, shows a rather consistent picture for changes of stratospheric ozone at mid-latitudes as well as polar ozone (Figure 2.38, adapted from Chapter 2 in Ajavon et al. (2010). In summary, average total ozone columns have remained at the same level for the past decade, about 3.5% below the 1964–1980 averages for the entire globe, and 2.5% for the latitudes 60°S–60°N. These results are consistent with the AR4 report, and the level of understanding of changes in stratospheric ozone is medium. For further discussion regarding changes in stratospheric dynamics see [Section xxx?].

[INSERT FIGURE 2.38 HERE]

Figure 2.38: Trends in midlatitude a) and polar b) stratospheric ozone. Total ozone average of 63°–90° latitude in March (NH) and October (SH). Symbols indicate the satellite data that have been used in different years. The horizontal grey lines represent the average total ozone for the years prior to 1983 in March for the NH and in October in the SH.

2.4.2.3 Stratospheric H_2O Vapour

Stratospheric H_2O vapour has important roles in Earth's radiative balance and in stratospheric chemistry. Increased H_2O vapour causes the troposphere to warm and the stratosphere to cool, and, when halogen-containing compounds are present, it increases rates of O_3 loss.

The longest continuous time series of stratospheric H_2O vapour abundance is from in situ measurements made with frost point hydrometers starting in 1980 over Boulder, CO, USA (40°N, 105°W) (Oltmans et al., 2000). These observations have been complemented by satellite observations by from SAGE II (1984–2005; Stratospheric Aerosol and Gas Experiment II), HALOE (1991–2005; HALogen Occultation Experiment), and Aura MLS (2004–present; Microwave Limb Sounder). H_2O vapour mixing ratios obtained using these different methods do not always agree, even in their trends.

AR4 reported that stratospheric H_2O vapour increased from 1980 to 2000 by 0.05 ppm yr^{-1}, but then decreased after that. Hurst (2011) analyzed the Boulder record for trends. They divided the record into 4 multi-year periods (1980–1989: period 1, 1990–2000: period 2, 2001–2005: period 3, and 2006–2010: period 4) and 6,2 km thick altitude layers from 16 to 28 km. Statistically significant non-zero trends were found for all four periods in the lowest 5 layers up to 26 km. Positive trends were found for periods 1, 2, and 4, and a negative trend was found for period 3. Averaged over the entire 30 year period and the lowest 5 layers (16–26 km), the average increase was 1.0 ± 0.2 ppm, with a vertical gradient of 0.07 ± 0.04 ppm km^{-1}. The pattern of increased growth with increasing altitude obtained for the entire period did not hold for each period. Growth during period 1 ranged from 0.07 to 0.51 ppm among the altitude layers, but diminished with altitude by -0.06 ± 0.02 ppm km^{-1}. Positive growth increased with increasing altitude for period 2 (range 0.29–0.89 ppm at 0.08 ± 0.02 ppm km^{-1}) and period 4 (range 0.21–0.64 ppm at 0.03 ppm km^{-1}). Growth in period 3 averaged -0.35 ± 0.04 ppm with no significant dependence on altitude (range -0.29 to -0.39 ppm). Solomon et al. (2010b) showed that decreased stratospheric H_2O vapour in this period slowed the rate of increase in global surface temperature by 25% compared to that which would have occurred due only to CO_2 and other GHGs. Data and trends reported by Hurst (2011) for H_2O vapour over Boulder are in qualitative agreement with those reported by Fujiwara et al. (2010) for the tropical stratosphere based on based on data from balloon-borne frost point hydrometers and satellite sensors for 1993–2009.

The major sources of H_2O vapour to the stratosphere are transport through the tropical troposphere and oxidation of CH_4 and H_2. These processes alone cannot explain the observed trends in H_2O vapour and their dependence on altitude. Hurst (2011) concluded that there must be at least one other mechanism that preferentially increases mid-latitude stratospheric H_2O vapour at higher altitudes than lower ones. Improving our ability to attribute H_2O vapour changes to specific processes will require an expanded in situ observation network, particularly in the tropics.

2.4.3 Trends in Aerosols

[PLACEHOLDER FOR FIRST ORDER DRAFT]

2.4.3.1 Global and Regional Trends of AOD from Remote Sensing

Aerosol properties can be determined in-situ as well as using active and passive remote sensing from satellites or the ground. An extensive discussion on various optical properties derived from passive remote sensing data, which address aerosol amount, size and composition is given in Chapter 7. In this section we discuss trends derived from remote sensing.

The aerosol amount over the entire atmospheric column is usually expressed by aerosol optical depth (AOD) data in the mid-visible region of the solar spectrum. The AOD is either measured by sun's direct intensity from the ground (e.g., sun-photometry) or estimated from changes in reflected sun-light to space by satellite sensors. Satellite data offer information on spatial distributions, as illustrated for seasonal AOD data in Figure 2.39 (Kinne, 2009).

[INSERT FIGURE 2.39 HERE]
Figure 2.39: Global seasonal maps for aerosol optical depth (AOD) distributions at 550nm based a multi-annual satellite sensor retrievals by MODIS, MISR and AVHRR (after validations against ground-based sun-photometry). Strongest aerosol loads are caused by a) biomass burning during DJF in western Africa and

during SON in southern America, southern Africa and Indonesia, b) by dust during MAM and JJA in northern Africa and during MAM also over the mid-east and eastern Asia and c) by pollution in MAM and especially during JJA over the industrial centres of the Northern Hemisphere.

However, the AOD retrievals from satellite data are uncertain, because inaccurate assumptions on aerosol absorption and solar surface reflectance. If the retrieval model does not account for multi-annual changes in these properties (e.g., changes in aerosol mixture or changes to vegetation characteristics), erroneous trends may be derived. Trends from ground-based sun-photometry are more reliable, but it is often uncertain if detected local trends are characteristic for the surrounding region.

Even now, with more than 10 year data-records by aerosol dedicated satellite sensors (e.g., MODIS, MISR) or local monitoring by sun-photometer networks (e.g., AERONET, SkyNET, GAW) the identification of large scale multi-annual anthropogenic trends remains difficult. Since about half of today's atmospheric global AOD can be linked to super-micrometer dust and sea-salt with natural origin, atmospheric load is strongly linked to meteorological conditions which often have strong inter-annual variations. In addition, in certain years violent volcanic eruptions (e.g., Mt. Pinatubo in 1991) can add stratospheric AOD values comparable to those of the troposphere. We note, however, that volcanic contributions of such magnitude have not occurred during the last 10 years. Therefore, retrieval of anthropogenic aerosol in the troposphere may be limited to regions and seasons of extraordinary anthropogenic change or where anthropogenic AOD levels are high, such as over industrial regions over eastern Asia, Europe or the US.

There is a host of satellite instruments providing long-term information on aerosol, however, in all cases an extremely careful evaluation of noise, bias, calibration within and among sensors, etc, is needed, while also retrieval issues such as the assumptions on surface characterization, sampling issues, cloud contamination and the aerosol models used in the inversion procedure, may also influence the retrieval of trends (Zhang and Reid, 2010).

Older studies include the use of the TOMS (1979–1993) the absorbing aerosol index product for determining the variability of dust sources (Prospero et al., 2002), and biomass burning (Thompson et al., 2001a).

Of particular interest are trends in regions with higher anthropogenic AOD levels, such as the regions over eastern Asia and over the eastern US. During the 1980s and 1990s TOMS data indicate continued AOD increases during the dry fall/winter season over East Asia (Torres et al., 2002). And from the mid-1980s on AVHRR data indicate continued AOD decreases and slightly decreasing aerosol sizes over coastal waters of the Eastern US (Mishchenko et al., 2003). These suggested reductions to the fine-mode AOD over time are consistent with reductions for sulfate emissions over the eastern US.

[INSERT FIGURE 2.40 HERE]
Figure 2.40: Comparison of AVHRR based trends between 1984 and 2000 for mid-visible AOD (amount) and Angstrom parameter (size) based on data off the US east coast. The data show continued decreases for AOD over the entire annual cycle and also reduction to particles size in winter (smaller Angstrom coefficient), suggesting temporal trends for the reduction of fine-mode aerosol particles over the eastern US.

Mishchenko et al. (2007) used 23 years of Advanced High Resolution Radiometer (AVHRR) data over oceans, and reported a significant decreasing trend in global AOD (Aerosol Optical Depth) over the oceans. While the data on a hemispheric basis showed no trend before 1995, between 1995 and 2005 a decrease of AOD by 0.02 over oceans was reported. A qualitative analysis of PATMOSx and AVHRR/GAPC data (Cermak et al., 2010) suggest negative AOD trends over most ocean regions, starting from the beginning of 1990s, in support of the global brightening hypothesis [(see Section xxx)].

This view is contested by more recent analyses of mid-visible bias-corrected MODIS (Moderate Resolution Imaging Spectroradiometer) and MISR (Multi-angle Imaging Spectroradiometer) level 2 time series (Zhang and Reid, 2010). Operating since 2001, MODIS and MISR provide new opportunities to measure aerosol from satellites, using wavelengths more suitable for aerosol retrieval. No significant global AOD trends are found for the 2000–2009 period. However, regionally, over the Arabian Sea and the Bay of Bengal and Coastal China positive AOD trends of 0.03–0.06 per decade are found. Less certain, negative trends were reported downwind of the North American East Coast and West Africa, as well as near Central America.

Differences between MODIS and MISR derived trends can amount to a factor of two. These differences may be related to calibration drift in the MODIS data, and limited spatial sampling of the MISR data (Levy et al., 2010).

A regional analysis of trends over populated regions of the northern hemisphere with stronger anthropogenic signatures (de Meij et al., 2010) suggest for MISR and MODIS retrieval statistics, in agreement with ground-based observations by sun-photometry, decreasing AOD trends over Europe and North America and increasing AOD trends over Asia, as illustrated in Figure 2.41.

[INSERT FIGURE 2.41 HERE]
Figure 2.41: Average AOD temporal profiles from MODIS (Level 3), MISR (level 3) and AERONET (Level 2) for the 2000–2009 time period in Europe, North America and Asia. Level 2 and 3 refer to the amount of temporal, spatial, or spectral aggregration/processing of the data.

AERONET (AErosol RObotic NETwork) is a network of ground-based sun-/sky- photometers which provides multi-annual statistics on aerosol column properties at more than 200 sites (Holben et al., 1998). The first instruments were deployed in the mid-1990s with a rapidly increasing density over the last 10 years. However, there are only very few stations that provide continuous time series for decade or longer. An unpublished analysis of AOD in 2006 [reference needed / B. Holben, xxxx] indicated, that at sites with longer data records, tropospheric aerosol amounts in the 2000–2005 period were declining at sites influenced by urban pollution over the central and eastern US and Europe, whereas no significant trends were found over background sites, and sites strongly influenced by natural aerosol (e.g., biomass burning or dust) no clear trends could be identified. In Japan, a recent study using ground-based broadband radiometers suggest an increase of optical thickness until the mid-1980s, followed by a decrease until the late 1990s and almost constant in the 2000s (Kudo et al., 2011).

In summary, since AR4, new long-term remote sensed datasets of aerosol are becoming available. These datasets indicate a continuing decrease of AOD in the US and Europe, and Japan and continuing increase over Eastern and Southern Asia since the 1980s, which is consistent with anthropogenic emission temporal trends. Some studies report negative trends over the global oceans, but these trends may less certain, due instrumental issues, the length of the data-record, the influence of the natural variability. Our knowledge on trends from remote sensing satellite is globally low, and in some regions medium.

2.4.3.2 Regional Surface Aerosol Trends

Regional aerosol and aerosol precursor emissions have changed and will continue to change due to economic developments and implementation of air pollution controls, and are drivers of variability and trends of aerosol surface concentrations as well as columns in polluted regions. Since at many continental locations a large fraction of the aerosol mass resides in the atmospheric boundary layer (Jaenicke, 1993), long term measurements at the Earth surface may also provide information on the aerosol columns, and the resulting radiative perturbations driving climate change, provided that these measurements are representative for a larger region. However, under marine outflow conditions, aircraft observations often show elevated aerosol levels above the boundary layer (Clarke and Kapustin, 2002; Osborne and Haywood, 2005), and surface measurements may not always accurately represent column changes. This section summarizes reported trends of PM2.5 (particulate matter with diameter <2.5 um) and two of the most widely measured climate relevant anthropogenic aerosol components, sulphate and equivalent black carbon or elemental carbon. Although more and longer time series of PM10 (d <10 um) are available, PM10 trends are less relevant for climate impacts than those of PM2.5, due to the influence of PM10 from local sources. For a detailed discussion on observations and the role of other aerosol components and their properties we refer to Chapter 7, while Chapter 8 evaluates the radiative forcing of aerosol.

Unfortunately, there are no true global networks of in-situ aerosol observations, and, to our knowledge an overview and critical evaluation of worldwide, quality assured, aerosol trend measurement presently does not exist. A few long-term background measurements of aerosol properties are performed in the frame of the WMO GAW (Global Atmospheric Watch) program (WMO GAW, John Ogren, a paper on trends in aerosol scattering, absorption, single-scattering albedo, and asymmetry parameter at a number of background

stations). Surface based remote sensing of aerosol is performed within the AERONET and other networks, and are discussed in Section 2.4.3.1.

In Asia, the Acid Deposition Network East Asia (EANET, 2011), measures since 2001 particulate matter and deposition, but thus far no trend studies have been published. Whereas in some Asian regions (China, India) some long-term measurements from individual research groups are becoming available, there are no nationwide networks [verify] and it is often difficult to assess the significance of these measurements for larger regions. Air quality networks in North America and Europe are the most reliable source of information on long-term surface aerosol trends in these parts of the world.

In Europe, the EMEP network (European Monitoring and Evaluation Programme) provides regionally representative measurements of aerosol composition since the 1980s; these measurements are described in annual reports, and available via www.emep.int. In North America, the U.S. Clean Air Status and Trends Network (CASTNET) and the Canadian Air and Precipitation Monitoring Network (CAPMoN) provide regionally-representative long term measurements of major ions in aerosols, including sulfate, but not PM2.5 mass. The U.S. Interagency Monitoring of Protected Visual Environments (IMPROVE) Network measures regionally PM2.5 mass, total aerosol composition, and visibility.

2.4.3.2.1 PM2.5

In Europe, for PM2.5 only a few time series longer than a decade are available, with the earliest measurements starting in 1997. Figure 2.42 (EMEP, 2010) shows downward trends in PM2.5 in some parts of Europe (e.g., Southern and Central Europe), and no trend in Germany and Norway.

[INSERT FIGURE 2.42 HERE]

Figure 2.42: Time series of annual average PM2.5 (ug/m^3) in Europe (IT Italy; AT Austria; CH Switzerland; DE Germany; ES Spain; NO Norway).

For Canada, annual mean of PM2.5 for all urban measurement sites combined decreased by roughly 40% between 1985 and 2006 (Canada, 2011), corresponding to –3.6 %/yr. This decline was to a large degree attributable to decreases in precursor emissions (SO_2 and NO_x) in Eastern Canada and the Eastern United States (Canada, 2011). Need reference for US PM2.5, did not find trend analysis from IMPROVE.

2.4.3.2.2 Sulfate

Sulfate (SO_4) aerosol is an important mass fraction of PM2.5 (see Chapter 7). Currently, important sources are power generation, industry, and certain transport sectors (international shipping). SO_2 (the precursor gas of SO_4) emissions from industry and the energy sector, have been increasingly mitigated in response to acidification problems, and to reduce the impact of particulate matter on human health.

In Figure 2.43, we show SO_4 trends (Pozzoli et al., 2011) for 1990–2005 of selected stations with long-time series for Europe (EMEP) and North America (CASTNET). Before 1990, the number of measurements was substantially less. Significant negative trends of SO_4 are found in Eastern and Northern Europe (–0.05 to –0.15 ug S/m^3 yr^{-1}; or ca –2 to –6% yr^{-1}), and less (0 to –0.05 ug S/m^3 yr^{-1}) in Scandinavia and Southern Europe. Pozzoli et al. (2011) attribute the trends for a large part to emission changes and not to natural processes. Precipitation scavenging of aerosol provides another view of changes in aerosol column amounts. Consistently with the SO_4 aerosol trends Fowler et al. (2007) report declines in sulfate rainwater concentrations between 1980–2000 of about –3% yr^{-1} in Eastern and Southern Europe, and about –2 % yr^{-1} elsewhere in Europe.

[INSERT FIGURE 2.43 HERE]

Figure 2.43: Observed SO_4 trends 1990–2005 (ug S/m^3 yr^{-1}) in Europe and the US. Not significant trends are denoted with red circle (Pozzoli et al., 2011).

In the US, Figure 2.43 shows non-urban trends (Pozzoli et al., 2011) derived from the CASTNET network. SO_4 aerosol declines in the Eastern United States ranging from 0 to –0.05 ug S/m^3 yr^{-1} (0 to –3% yr^{-1}), and no significant trends in the Western US. These trends are consistent with average trends reported by CASTNET (2010) of -0.045 ugS/m^3 yr^{-1} for the period 1990–2008 in the Eastern US, and a decrease of CASTNET aerosol sulphate concentrations by -21% in the east and northeast, -22% in the Midwest, and -20% in the

south between the two periods 1990–1994 and 2000–2004 (Sickles and Shadwick, 2007b). Indirect evidence for declining sulfate particulate concentrations is found in an analysis of SO_4 wet deposition by 20–30% over a time period of 15 years (Sickles and Shadwick, 2007a), corresponding to a trend of about –1.4% to –2.1% yr^{-1}. In Canada, aerosol sulphate concentrations declined by –30 to –45% from 1991–1993 to 2004–2006 at non-urban CAPMoN sites in the eastern half of the country.

These declines are consistent with the trends of inorganic aerosol components reported by Quinn et al. (2009) at Barrow, Alaska, ranging between –2.3% yr^{-1} for SO_4 to –6.4% for NH_4. Hidy and Pennell (2010) show a remarkable agreement of PM2.5 and SO_4 declines in Canada, pointing to common emission sources of PM2.5 and SO_4.

2.4.3.2.3 Black and elemental carbon trends

The terms black carbon and elemental carbon refer to the operational analysis methods: optical methods (aerosol light absorption) or filter measurements using thermal methods, respectively. The measurements are associated with large uncertainties, intercomparisons showed differences of a factor 2–3 for optical methods, and 4 for thermal methods (Vignati et al., 2010), which renders quantitative comparison of BC time series also uncertain. In addition, while there is a general lack of BC/EC measurements, long-term time series are even scarcer.

In Europe long term EC/BC are available at 2 stations (Norway, Italy) starting at the year 2001 (EMEP, 2010); but thus far these time series have not been published [for Europe: contact Jungfraujoch / Baltensberger].

In North America, the IMPROVE network is measuring black carbon with optical techniques, but data are publicly available until 2003, and to our knowledge to date no trend analysis has been published. Sharma et al. (2006) published long term measurements of equivalent BC at Alert and Barrow, Canada. Downward trends were 54% at Alert and 27% at Barrow for the period 1989–2003; part of the trend differences was associated with changes in circulation patterns.

[PLACEHOLDER FOR FIRST ORDER DRAFT: India: Data may be provided by S.K. Sateesh/Krishnamurty (Lead Author Chapter 7). Paper in preparation by Krishnamoorthy K. (2011). Needs further elaboration of significance of trends, data quality assurance etc.]

In conclusion, in situ ground based measurements of aerosol indicate with large certainty downward trend inorganic (mainly SO_4) aerosol in parts of North America and Europe in the order of –3% yr^{-1} of the last 2–3 decades. The long-term data availability for PM2.5 and black carbon is much less , and prevents to draw firm conclusions. In other parts of the world, coordinated surface aerosol measurements started at best early 2000s, and thus far no clear measurements do not provide a clear picture regarding trends of PM2.5 or aerosol components.

2.5 Radiation Budgets

The radiation budget of the Earth is a key determinant for the genesis and evolution of climate on our planet. Anthropogenic interference with climate occurs first of all through a perturbation of the components of the Earth radiation budget.

2.5.1 Top of Atmosphere Radiation Budget

The radiation budget at the top of atmosphere (TOA) defines the energy flows in and out of the global climate system. It includes the absorption of solar radiation by the Earth, determined as difference between the solar irradiance incident at the TOA and its reflected fraction, and the thermal radiation emitted from the Earth back to space.

2.5.1.1 TOA Solar Irradiance

Since AR4, much progress has been made in understanding the reasons for inconsistencies in total solar irradiance between the more recent measurements from the Total Irradiance Monitor (TIM) on NASA's

Solar Radiation and Climate Experiment (SORCE) (Kopp and Lawrence, 2005) and from earlier missions. For the 2008 solar minimum, the solar irradiance from SORCE/TIM is 1360.8 ± 0.5 W m^{-2} compared to 1365.5 ± 1.3 W m^{-2} from earlier missions. The latter value is commonly adopted in climate models and has widely been assumed in satellite datasets providing estimates of net incoming radiation at the top-of-atmosphere from reflected solar and emitted thermal radiation. The discrepancy is a factor of three greater than the stated uncertainties of the individual measurements and corresponds to an equivalent climate forcing of –0.8 W m^{-2} [(Kopp and Lean, 2011, in press)]. Following extensive comparisons (e.g., Butler et al., 2008) between ground-based versions of the instruments and laboratory references, validation of aperture area calibrations using flight spares from each instrument, and corrections for diffraction from view-limiting aperture (a correction not applied by all instrument teams), it was concluded that uncorrected scattering and diffraction in the earlier instruments produces erroneously high values of total solar irradiance. [Kopp and Lean (2010, in press)] conclude that the SORCE/TIM value of total solar irradiance is the most probable value because it is validated by both a NISR-calibrated cryogenic radiometer and a new state-of-the-art total solar irradiance radiometer facility.

Variations in total solar irradiance since 1978 are shown in Figure 2.44. Figure 2.44a shows values on the native scale of each measurement and illustrates differences in absolute calibration between the instruments. A composite solar irradiance record (Figure 2.44b) constructed by placing three records on the same radiometric scale as SORCE/TIM clearly shows the 11-year solar cycle. The variation from solar minimum to maximum is 1.6 W m^{-2} (0.12%). Superimposed on the 11-year cycle are higher-frequency variations with time scales of days to weeks that can reach 4.6 W m^{-2} (0.34%). The 11-year solar cycle shows high correlation with sunspot number (Figure 2.44d), although there is a difference in peak solar activity between cycles 22 and 23 yet little difference in peak TSI between these cycles. When contributions from both dark sunspots and bright faculae are included in an empirical model (Lean et al., 2005) (Figure 2.44c), the observed variations in solar irradiance in Figure 2.44b are well reproduced, confirming that both dark sunspots and bright faculae are important contributors to solar irradiance variations.

[INSERT FIGURE 2.44 HERE]

Figure 2.44: Space-borne total solar irradiance (TSI) measurements are shown in a) in "native" scales with offsets attributable to calibration errors. Instrument overlap allows corrections for offsets and the creation of a composite TSI record. Plot b) shows the average of three different reported composites [ACRIM, PMOD, and RMIB] adjusted to match the SORCE/TIM absolute scale. The grey shading indicates the standard deviation of the three composites. Shown in c) are irradiance variations estimated from an empirical model that combines the two primary influences of facular brightening and sunspot darkening with their relative proportions determined via regression from direct observations made by SORCE/TIM. The daily sunspot numbers shown in d) indicate fluctuating levels of solar activity for the duration of the database [(from Kopp and Lean, 2010, in press)].

Harder et al. (2009) provide further insight on how different parts of the solar irradiance spectrum vary with time using data from the SORCE Spectral Irradiance Monitor (SIM) instrument. They show that during periods of decreasing solar activity, TSI and irradiance measurements in the UV between 200-400 nm decrease while solar irradiances at longer wavelengths (400-691 nm and greater than 1630 nm) are out-of-phase with TSI. The results suggest that during periods of decreasing solar activity temperature profile changes in the upper photospheric and lower chromospheric layers lead to decreases in solar irradiance and temperature changes in deep photospheric layers lead to increases in solar irradiance.

2.5.1.2 TOA Reflected Solar and Emitted Thermal Radiation

The AR4 reported that large changes in tropical top-of-atmosphere (TOA) radiation occurred between the 1980s to the 1990s. The results were based upon observations from the Earth Radiation Budget Experiment (ERBE, Barkstrom, 1984) Earth Radiation Budget Satellite (ERBS) Nonscanner Wide Field of View (WFOV) instrument (Wong et al., 2006). Net radiation increased by 1.4 W m^{-2}, reflected shortwave (SW) radiation decreased by 2.1 W m^{-2} and emitted longwave (LW) radiation increased by 0.7 W m^{-2} over the period 1985–1998. Since the AR4, Andronova et al. (2009) extended the Wong et al. (2006) ERBS/WFOV record with observations from the Clouds and the Earth's Radiant Energy System (CERES) (Wielicki et al., 1996) on the Terra satellite. The longer record shows a continuation of these trends with tropical net TOA flux increasing by 2 W m^{-2} between 1985–2005 (Figure 2.45). By comparison, when LW data based upon

HIRS and ISCCP-FD are used in place of the ERBS/CERES LW record; the net radiation increase is more pronounced, reaching 6 W m^{-2} for ISCCP-FD. The change in net radiation for ERBS/CERES is associated with a 3 W m^{-2} decrease in SW radiation and an increase of 1 W m^{-2} in LW radiation. Comparisons between ERBS/CERES LW radiation and that derived from the NOAA High Resolution Infrared Radiation Sounder (HIRS) Lee et al. (2004; 2007) show good agreement until approximately 1998, corroborating the reported rise of 0.7 W m^{-2}, after which HIRS LW fluxes show much higher values. The discrepancy is likely due to changes in the channels used for HIRS/3 instruments launched after October 1998 compared to earlier HIRS instruments (Lee et al., 2007). While the underlying causes for the large decadal changes in tropical radiation remain uncertain, several studies have examined plausible reasons for the changes (Allan and Slingo, 2002; Chen et al., 2002; Clement and Soden, 2005).

On a global annual scale, interannual variations in net TOA radiation and ocean heat storage should be correlated, since oceans have a much larger heat capacity compared to land and the atmosphere and therefore serve as the main reservoir for heat added to the Earth-atmosphere system. Wong et al. (2006) showed that these two data sources are in good agreement for 1992–2003. In the ensuing 5 years, however, Trenberth and Fasullo (2010) note that the two diverge from one another. The satellite observations show an increase of about 1 W m^{-2} in the rate of absorbed net radiation at the TOA while the ocean in-situ measurements show a slowing of the increase in global ocean heat content. [Loeb et al. (2011, in press)] point out that the lack of closure between satellite-based net TOA flux changes and in-situ ocean heat content measurements is due to heterogeneous calibration and algorithm approaches in the merged satellite dataset used in Trenberth and Fasullo (2010). A new official version of the CERES climate data record using consistent algorithms and recalibrations throughout showed no significant increase in net TOA flux between 2000–2008, and explained most of the about 1 W m^{-2} discrepancy seen in Trenberth and Fasullo (2010) between the satellite and in-situ observations.

[INSERT FIGURE 2.45 HERE]

Figure 2.45: Net TOA flux anomaly from 1985–2005 for 20S–20N from merged ERBS and CERES Terra (thick solid line). The thin solid and dotted lines are derived using SW measurements from ERBS/CERES and LW observations from ISCCP-FD (Zhang et al., 2004b) and HIRS (Lee et al., 2004; Lee et al., 2007). Anomalies are relative to the average over 1985–1989. From Andronova et al., (2009).

2.5.1.3 Relation to Observed Changes in Aerosol, Humidity and Clouds

Changes in cloud, humidity and aerosol may also be diagnosed from broadband Earth radiation budget measurements. Interannual co-variation in temperature and upper tropospheric water vapour are diagnosed from AIRS infra red satellite data (Dessler et al., 2008; Gettelman and Fu, 2008) and inferred from increases in broadband clear-sky LW satellite data (Chung and Soden, 2010; Chung et al., 2010a), consistent with invariant RH at the largest scales. On decadal time-scales, increased greenhouse gas concentrations reduce clear-sky LW (Allan, 2009; Chung and Soden, 2010), thereby influencing inferred relationships between moisture and temperature. Combining recently updated CERES satellite data and reanalysis fields, Dessler (2010) provides evidence for a weak interannual global relationship between cloud related changes in net radiation and surface temperature, primarily explained by a positive cloud longwave radiative feedback, consistent with theoretical expectations (Zelinka and Hartmann, 2010). Clement et al. (2009) find reductions in low cloud fraction from ship observations and satellite data with decadal increases in SST over the north east Pacific, symptomatic of positive cloud shortwave radiative feedback. Their analysis applied an adjustment to the ISCCP satellite data which suffers from changes in viewing angle geometry (Evan et al., 2007) and inhomogeneity (Loeb et al., 2007). The responses of water vapour and cloud inferred from the top of atmosphere radiation are time-scale dependent (Harries and Futyan, 2006) and highly sensitive to the time-periods and regions chosen for analysis (Lindzen and Choi, 2009; Murphy et al., 2009; Spencer and Braswell, 2010; Trenberth et al., 2010).

2.5.2 Surface Radiation Budget

The surface radiation budget provides the energy for a variety of surface processes and largely determines the thermal and hydrological conditions at the Earth surface. The surface radiation budget takes into account the solar fluxes absorbed at the Earth surface, as well as the upwelling and downwelling thermal fluxes emitted by the surface and atmosphere, respectively.

2.5.2.1 Surface Solar Radiation

Monitoring of radiative fluxes from surface stations began on a widespread basis in the mid-20th century, predominantly measuring the downwelling solar component (also known as global radiation or surface solar radiation, hereafter referred to as SSR).

The first indications for substantial decadal variations in the observational SSR records have been reported in AR4. Specifically, a decline of surface solar radiation from the beginning of widespread measurements in the 1950s until the mid-1980s has been observed at many land-based sites (popularly known as “global dimming”, Stanhill and Cohen, 2001), and a partial recovery from the 1980s onward ("brightening", Wild et al., 2005). Since AR4, numerous studies substantiated the findings of significant decadal SSR changes observed at globally distributed sites (e.g., Dutton et al., 2006; Gilgen et al., 2009; Ohmura, 2009; Wild, 2009 and references therein) as well as in specific regions. Wild et al. (2008) estimated the brightening over land surfaces at 2 W m^{-2} per decade for the period 1986–2000. In Europe, Norris and Wild (2007) noted a dimming until the mid-1980s and subsequent brightening in a pan European time series. Similar changes were found at sites in Northern Europe (Stjern et al., 2009), Estonia (Russak, 2009) and Moscow (Abakumova et al., 2008). Chiacchio and Wild (2010) pointed out that dimming and subsequent brightening in Europe are mainly seen in spring and summer seasons. The brightening phase in Europe from the 1980s onward was further documented at sites in Switzerland and Germany (Ruckstuhl et al., 2008), as well as in Greece (Thessaloniki) (Zerefos et al., 2009). At continental US sites, Long et al. (2009) noted a significant brightening of SSR as well, of 10 W m^{-2} per decade between 1995 and 2007, and Riihimaki et al. (2009) found brightening at sites in Oregon over the extended period 1980–2007. The general pattern of dimming until the 1980s and brightening thereafter was also found at numerous sites in Japan (Norris and Wild, 2009; Ohmura, 2009; Wild et al., 2005). Analyses of sites in China confirmed strong declines in SSR from the 1960s to 1980s, which also did not persist in the 1990s (Che et al., 2005; Liang and Xia, 2005; Norris and Wild, 2009; Qian et al., 2006; Shi et al., 2008; Xia, 2010a). Dimming and subsequent brightening was not only found on the Northern Hemisphere, but also at sites in New Zealand (Liley, 2009). On the other hand, persistent dimming since the mid-20th century with no evidence for a trend reversal was noted at sites in India (Kumari and Goswami, 2010; Kumari et al., 2007; Wild et al., 2005), and in the Canadian Prairie (Cutforth and Judiesch, 2007).

The longest observational SSR records, extending back to the 1920s and 1930s at a few sites in Europe, further indicate some brightening during the first half of the 20th century, known as “early brightening” (Figure 2.46) (Ohmura, 2009; Wild, 2009). This suggests that dimming, at least in Europe, was confined to a period between the 1950s and 1980s.

Updates on SSR changes observed at the surface beyond the year 2000 suggest a continuation of the brightening at sites in Europe, U.S., and parts of Asia. Brightening seems to level off at sites in Japan and Antarctica after 2000, while indications for a renewed dimming are seen in China (Wild et al., 2009).

Alpert et al. (2005) and Alpert and Kishcha (2008) pointed out that the observed decline in surface solar radiation between 1960 and 1990 is larger in areas with dense population than in rural areas. The magnitude of this “urbanization effect” in the radiation data is not yet well quantified. Dimming and brightening is, however, also notable at remote and rural sites (Dutton et al., 2006; Karnieli et al., 2009; Liley, 2009; Russak, 2009; Wild, 2009).

While extended areas of the globe are not covered by surface measurements, satellite-derived fluxes can provide a near global picture. Such estimates are available since the early 1980s (Hatzianastassiou et al., 2005; Hinkelman et al., 2009; Pinker et al., 2005). Satellites do not directly measure the surface fluxes, but have to infer them from measurable top-of-atmosphere signals using in addition empirical or physical models to remove atmospheric perturbations. Satellite-inferred SSR records may also suffer from potential inhomogeneities due to changes in satellites, viewing geometries, inaccurate positioning, or sensor degradation, particularly in the earlier records (Evan et al., 2007). Available satellite-derived products qualitatively agree on a brightening from the mid-1980s to 2000 globally as well as over oceans (Hatzianastassiou et al., 2005; Hinkelman et al., 2009; Pinker et al., 2005). Over land, however, trends are positive or negative depending on the respective satellite product (Wild, 2009). Variations in aerosol

attenuation, considered relevant for the decadal SSR changes particularly over land, are difficult to infer from satellites.

Reconstructions of SSR changes from more widely measured meteorological variables can help to increase their spatial and temporal coverage. Decadal SSR changes have been related to observed changes in sunshine duration, diurnal temperature range (DTR), and evaporation. Overall, these proxies provide independent evidence for the existence of large-scale decadal variations in SSR. Specifically, the dimming of SSR from the 1950s to the 1980s obtained additional support from widespread observations of concurrent declines in pan evaporation (Roderick and Farquhar, 2002). The decline of DTR over global land surfaces and its trend reversal during the 1980s is in line with the transition from dimming to brightening (Wild et al., 2007). Over Europe, the dimming of SSR from the 1950s to the 1980s and brightening thereafter is consistent with concurrent declines and subsequent inclines in sunshine duration (Sanchez-Lorenzo et al., 2008a), evaporation in energy limited environments (Teuling et al., 2009) and DTR (Makowski et al., 2009). The early brightening in the 1930s and 1940s seen in the European records gets support from corresponding changes in DTR and sunshine duration (Makowski et al., 2009; Sanchez-Lorenzo et al., 2008a). In China, the levelling off in SSR in the 1990s after decades of decline is in line with similar tendencies in the pan evaporation records and DTR (Liu et al., 2004a; Liu et al., 2004b; Qian et al., 2006). Dimming up to the 1980s and brightening in the 1990s is also indicated in a set of 237 sunshine duration records in South America [(Raichijk, 2011, in press)].

[INSERT FIGURE 2.46 HERE]

Figure 2.46: Annual mean surface solar radiation (in W m^{-2}) as observed at Potsdam, Germany, from 1937 to 2006. Five year moving average in blue. Distinct phases of inclines (1930s–1940s, “early brightening”), declines (1950s–1980s, ”dimming”) and renewed inclines (since 1980s, “brightening”) can be seen. From Wild (2009).

2.5.2.2 Surface Thermal Exchanges and Net Radiation

Long-term measurements of the thermal surface components as well as surface net radiation are available at many fewer sites than SSR. Downward thermal radiation observations started to become available during the early 1990s with the setup of the Baseline Surface Radiation Network (BSRN) (Ohmura et al., 1998). From these records, Wild et al. (2008) determined an overall increase of 2.6 W m^{-2} per decade over the 1990s, in line with model projections and the expectations of an increasing greenhouse effect. Wang and Liang (2009) inferred an increase in downward thermal radiation of 2.2 W m^{-2} per decade over the period 1973–2008 from observations of temperature, humidity and cloud fraction at 3200 sites. Prata (2008) estimated a slightly lower increase of 1.7 W m^{-2} per decade for clear sky conditions over the earlier period 1964–1990, based on radiative transfer calculations using observed temperature and humidity profiles from radiosondes. Philipona et al. (2009; 2004) measured increasing downward thermal fluxes since the mid-1990s at stations in the Swiss Alps, corroborating an increasing greenhouse effect. There is growing evidence that the absolute magnitude of the global mean downward thermal radiation has been underestimated in previous assessments and climate models, and that the value should be around 345–350 W m^{-2} (Stephens et al., in preparation; Wild, 2008).

The changes in the upward thermal radiation emitted by the Earth surface closely follow the changes in the surface temperature according to the Stefan-Boltzmann law and needs no additional discussion.

Little is known about decadal changes in the surface net radiation. Wild et al. (2008; 2004) inferred a decline in the land surface net radiation from the 1960s to the 1980s, and an incline from the 1980s to 2000, from estimated changes of the individual surface radiative components.

2.5.2.3 Relation to Observed Changes in Aerosol, Humidity and Clouds

The observed decadal variations in SSR cannot be explained by changes in the luminosity of the Sun, which are an order of magnitude smaller (Willson and Mordvinov, 2003). They therefore have to originate from alterations in the transparency of the atmosphere, which depends on the presence of clouds, aerosols, and radiatively active gases (Kim and Ramanathan, 2008; Kvalevag and Myhre, 2007). Cloud cover changes effectively modulate SSR on an interannual basis, but their contribution to the detected longer-term SSR

trends is not always obvious. While cloud cover changes were found to explain the trends in some areas (e.g., Liley, 2009), this is not the case particularly in relatively polluted regions such as Europe and China (Norris and Wild, 2007, 2009; Qian et al., 2006; Wild, 2009). SSR dimming and brightening has also been observed under cloudless atmospheres at various locations, pointing to a prominent role of atmospheric aerosols (Norris and Wild, 2007, 2009; Ohvril et al., 2009; Russak, 2009; Wild, 2009; Wild et al., 2005; Zerefos et al., 2009). Aerosols can directly attenuate SSR by scattering and absorbing solar radiation (direct effect), or indirectly, through their ability to act as Cloud Condensation Nuclei (CCNs), thereby increasing cloud reflectivity and lifetime (first and second indirect effects) (Lohmann and Feichter, 2005; Ramanathan et al., 2001).

The trend reversal from SSR dimming to brightening in the 1980s is reconcilable with trends in aerosol emission and aerosol optical depth, which also indicate a distinct reversal during the 1980s (Mishchenko et al., 2007; Ohvril et al., 2009; Stern, 2006; Streets et al., 2006; Streets et al., 2009; Wild et al., 2005).

Observed changes in atmospheric water vapour and other radiatively active gases are considered to be major contributors to the observed increases in downwelling thermal radiation (Allan, 2009; Philipona et al., 2009; Prata, 2008; Stephens et al., in preparation).

2.5.2.4 Relation to the Hydrological Cycle

The Earth radiation balance is the key driver of the global hydrological cycle (Ramanathan et al., 2001; Wild and Liepert, 2010). Global precipitation changes are constrained by the atmospheric and surface radiative energy balance to rise at around 2–3%/K (Allen and Ingram, 2002). Increased atmospheric moisture with warming (Willett et al., 2008) has been shown, using reanalyses and observationally-based methods, to enhance the LW radiative cooling of the atmosphere to the surface (Allan, 2009; Philipona et al., 2009; Prata, 2008; Wang and Liang, 2009; Wild et al., 2008). The rises in atmospheric radiative cooling rate with warming over interannual time-scales (John et al., 2009) are predominantly controlled by changes in the clear-sky atmosphere (Allan, 2009) and are consistent with enhanced precipitation with warming as part of radiative convective balance (Lambert and Webb, 2008; Stephens and Ellis, 2008). Links between global precipitation over land and the surface radiation balance are demonstrated by Wild et al. (2008) who argue that decreases in scattering aerosol, also detected by satellite measurements at the global scale (Mishchenko et al., 2007), and enhanced surface shortwave radiation provide the causal link. While scattering aerosol may influence global precipitation indirectly through surface temperature dependent responses, absorbing aerosols have the potential to directly influence changes in clouds and precipitation through radiative/convective adjustment (Andrews et al., 2009). Liepert and Previdi (2009) argue that large observed increases in global precipitation and ocean evaporation (Wentz et al., 2007) with warming of around 7%/K over the period 1987–2006 require an increase in net atmospheric radiative cooling of 0.7 W m^{-2} per decade to balance the global energy balance. While some evidence suggests enhanced radiative cooling to space over this period (Section 2.5.1.2; Wong et al., 2006; Zhang et al., 2007a) and a reversal of the weakening of the Walker circulation strength (Sohn and Park, 2010) statistical uncertainty is substantial and currently precludes definitive connection between these decadal changes.

2.6 Changes in Atmospheric Circulation and Patterns of Variability

Climatic changes at any given location depend not only on changes in the local radiative forcing, but also on changes in atmospheric circulation which themselves are partly radiatively driven. Changes in atmospheric circulation and patterns of variability were assessed in AR4 (2007). Substantial multi-decadal variability was found in the large-scale atmospheric circulation over the Atlantic and the Pacific. A decrease was found in tropospheric geopotential height (GPH) over high latitudes of both hemispheres and an increase over the mid-latitudes in boreal winter for the period 1979–2001. These changes were found to be associated with an intensification and poleward displacement of Atlantic and southern polar front jet streams and enhanced storm track activity in the NH from the 1960s to at least the 1990s. Changes in the North Atlantic Oscillation (NAO) and the Southern Annular Mode (SAM) towards their positive phases were observed, but it was noted that both returned their long term mean states in the early 2000s.

In AR4, many studies based on reanalysis data were assessed. Since AR4, reanalyses have gained even more weight in the scientific literature (see Box 2.2). Also, more and improved observational data sets have been

published (encompassing ground based, radiosonde, and space-borne data sets), and inaccuracies in all data sets are better understood. Finally, the time elapsed since AR4 extends the period for trend calculation, in particular since several data sets start only in (or are considered most reliable only after) 1979, when satellite information was included in many reanalyses data sets.

In this section we assess the observational evidence for changes in atmospheric circulation in fields of sea level pressure (SLP), GPH, and wind, in circulation features (such as the Hadley circulation or the jet streams), as well as in regional circulation variability modes. Monsoons are assessed in Chapter 14.

[START BOX 2.2 HERE]

Box 2.2: Global Dynamical Reanalyses

[INSERT BOX 2.2, FIGURE 1 HERE]
Box 2.2, Figure 1: Top: Linear trends in SLP from HadSLP2 (Allan and Ansell, 2006) between 1970 and 2010 (top) and 500 hPa GPH from 20CR (Compo et al., 2011) between 1970 and 2008 (bottom) for May-October season (left) and November-April (right). Only trends that are significant at the 10% level are shown.
[THIS IS A SIMPLE KNMI CLIMATE EXPLORER STRAWMAN; NEEDS TO BE REDONE WITH TREND ESTIMATE.]

Dynamical reanalyses constitute an ever increasingly valuable and utilized resource for assessing weather and climate phenomena. Applications span a very broad range of disciplines including all three IPCC Working Groups and beyond. The highest cited paper in all of geosciences (Kalnay et al., 1996) describes the first multi-decadal reanalysis that was produced (NCEP/NCAR reanalysis or NNR). Although used in previous assessments their characteristics have never been clearly outlined. Given their more abundant use in this assessment it is necessary to outline their characteristics more explicitly to aid interpretation.

Reanalyses are distinct from and complement more ‘traditional’ statistical approaches to assessing the raw data. They do not produce gridded fields of observations. At the most basic level they use a modern day data assimilation scheme and weather forecasting model to integrate all historically available observations from multiple disparate sources and create a dynamically consistent estimate of the past atmospheric states. Unlike real-world observations reanalyses are complete in space and time and also provide variables that are not directly observable. These aspects make them intuitively appealing for climate applications, particularly for some aspects of climate model validation where traditional observations simply are not available.

Several groups are actively pursuing reanalysis development and many of these have several generations of reanalyses products available (Box 2.2, Table 1). Since the first generation of reanalyses produced in the 1990s, substantial development has taken place. The reanalyses MERRA and ERA-Interim use satellite information in a very sophisticated way, aiming at a better representation of the hydrological cycle. The NCEP/CFSR reanalysis uses a coupled ocean-atmosphere assimilation system (Saha et al., 2010). The 20th century Reanalyses (20CR, Compo et al., 2011) provides information on uncertainty and covers 140 years by assimilating only surface and sea-level pressure in addition to monthly sea-surface temperatures. This proliferation of groups and approaches enables an improved handle on uncertainties for any given application.

Reanalyses products provide invaluable information on process understanding and interannual variability. For their ability to characterize long-term trends there exist a range of views within the climate research community. Although reanalyses projects by definition use a “frozen” assimilation system, there are many other sources of potential errors. Changes in the observational systems (e.g., the introduction of satellite data) and errors in the underlying observations or in the boundary conditions can lead to inhomogeneities. Reanalysis projects are extremely complex and processing errors cannot be avoided completely.

Early generation reanalyses contained ubiquitous shifts that rendered them of limited value for trend characterization (Thorne and Vose, 2010 and references therein). As subsequent products have learnt from these pioneering efforts the ability to determine trends and quantify the uncertainties has improved. This has

led to a more nuanced position whereby adequacy depends upon the variable under consideration, the time period and region of interest. For example, the latest generation reanalyses from ECMWF have been shown to perform well for land surface temperature and humidity - variables not directly assimilated and therefore quasi-independent (Simmons et al., 2010) but caused controversy when applied to polar tropospheric temperature trends (Bitz and Fu, 2008; Grant et al., 2008; Graversen et al., 2008; Thorne, 2008).

Box 2.2, Table 1: Overview of global dynamical reanalysis data sets. In addition to the global reanalyses listed here, several regional reanalyses exist or are currently being produced.

Institution	Reanalysis	Period	Resolution at equator	Reference
National Centers for Environmental Prediction (NCEP) and National Center for Atmospheric Research (NCAR), USA	NCEP/NCAR R1	1948–	320 km	Kistler et al. (2001)
NCEP, US Department of Energy, USA	NCEP/DOE R2	1978–	320 km	Kanamitsu et al. (2002)
European Centre for Medium Range Weather Forecasts (ECMWF)	ERA-40	1957–2002	125 km	Uppala et al. (2005)
Japanese Meteorological Agency (JMA)	JRA-25	1978–	190 km	Onogi et al. (2007)
National Aeronautics and Space Administration (NASA), USA	MERRA	1978–	75 km	Bosilovich (2008)
European Centre for Medium Range Weather Forecasts (ECMWF)	ERA-Interim	1989–	80 km	-
National Centers for Environmental Prediction (NCEP), USA	CFSR	1979–	50 km	Saha et al. (2010)
Japanese Meteorological Agency (JMA)	JRA-55	1958–	60 km	-
Cooperative Institute for Research in Environmental Sciences (CIRES), USA	20th century Reanalysis Vers. 1	1908–1958	320 km	-
Cooperative Institute for Research in Environmental Sciences (CIRES), USA	20th century Reanalysis, Vers. 2	1871–	320 km	Compo et al. (2011)

[END BOX 2.2 HERE]

2.6.1 Sea Level Pressure

The spatial distribution of SLP represents the distribution of atmospheric mass, which is the surface imprint of the atmospheric circulation. Barometric measurements in weather stations or onboard ships are relatively simple and local effects are comparably small. Fields are produced from the observations by interpolation or using data assimilation. One of the most widely used observational data sets is HadSLP2 (Allan and Ansell, 2006), which integrates 2228 historical global terrestrial stations with marine observations from the International Comprehensive Ocean-Atmosphere Data Set (ICOADS) on a 5°x5°grid. Although the quality of SLP data is generally considered good, there are discrepancies between gridded SLP data sets, in particular away from observations sites, e.g., over Antarctica (Jones and Lister, 2007).

For the period 1949–2009, Gillett and Stott (2009) find decreasing SLP in HadSLP2 in the high latitudes of both hemispheres in all seasons and increasing SLP in the tropics and subtropics most of the year, similar as in the earlier studies summarized in AR4. Vecchi et al. (2006) find a weakening of the annual mean equatorial Pacific zonal SLP gradient based on marine data over the period 1861–1992. An increase in SLP over the Indian Ocean was found by Copsey et al. (2006) in two data sets over the period 1950–1996. However, trends in SLP strongly depend on the time period. In fact, some of the trends that appeared from the 1950s to 1990s vanish or reverse when analyzing more recent periods (e.g., 1970s to 2010).

Box 2.2, Figure 1 shows trends from 1970 to 2010 for May-October (left) and November-April (right). The most prominent feature is the SLP decrease in southern mid-to-high latitudes. Trends in other regions are less consistent over this time period; no trends at all are found in boreal winter. However, relatively large changes in SLP have been reported for individual pressure centres on multidecadal scales. The Siberian High

is strengthening again after decades of weakening (Panagiotopoulos et al., 2005), although trend magnitudes are data set dependent (Huang et al., 2010). The Western Pacific subtropical high has been extending westward from 1980 to 1999 (Zhou et al., 2009b). Favre and Gershunov (2006) find an eastward shift and intensification of the Aleutian low from the mid-1970s to 2001. The Icelandic low has been weakening since the late 1980s, culminating in the recent extreme winter 2009/2010 (Osborn, 2011) (see also Section 2.6.6). The large multidecadal variability in SLP makes the detection of trends difficult.

On interannual time scales, variations in SLP have specific spatial characteristics known as "modes", some of which are thought to be atmospheric phenomena while others represent the atmospheric part of intrinsically coupled modes in the atmosphere-ocean system. Trends in the indices that capture the strength of these modes are reported in Section 2.6.9.

2.6.2 Surface Winds

Surface wind is measured in-situ with anemometers or from space using the microwave band. Marine wind observations have been extracted from ship logbooks and are collected in ICOADS (currently version 2.5; Woodruff et al., 2011). Early observations were made using the Beaufort scale. Anemometer measurements were introduced starting in the 1950s. Growth in ship size is thought to be responsible for an upward trend in the (largely unreported) anemometer measurement heights and to cause a spurious increasing trend in wind speed estimates based on ICOADS data (Cardone et al., 1990; Gulev et al., 2007; Tokinaga and Xie, 2011a). This trend, being non-uniform in space and time because of varying proportion and unknown characteristics of anemometer measurements, has stymied most of research efforts to study long-term variability in winds from observations. The WASWind data set by Tokinaga and Xie (2011a), covering the period 1950–2008, uses ICOADS surface wave information to correct biases in the ICOADS wind speed.

Surface winds can also be measured from space. However, quality scatterometer-based satellite observations of marine surface winds only span a decade. Recent efforts on homogenization of available SSM/I observations from satellites produced a wind data set that starts in July 1987 (Wentz et al., 2007).

Satellite products cover only the oceans. Over land, surface winds have been measured with anemometers since the 1960s, but until recently the data have been rarely used for trend analysis due to suspect quality. Winds near the surface can be derived from reanalysis products (see Box 2.2), but discrepancies are found when comparing trends therein with trends on land stations (McVicar et al., 2008; Smits et al., 2005). 20CR (Compo et al., 2011) might be more promising in this respect, having restricted their observational stream to surface pressure only and thus avoiding artefacts due to changes in the observing system.

Figure 2.47 shows linear trends in surface wind speeds over the oceans estimated from 19 years of SSM/I wind data (Wentz et al., 2007). The trend pattern is largely consistent with that obtained from ICOADS, wherever the latter observations were abundant, and with the corresponding trend in 20CR. Decreasing wind speeds are found over certain areas in the North Atlantic, tropical and North Pacific, and increasing winds south of 40° S and over the Bering Sea.

Over land, a weakening of seasonal and annual winds is reported for many regions, including China (Guo et al., 2010; Xu et al., 2006b) and the Tibetan region (Zhang et al., 2007b) from the 1960s to the early 2000s, the Netherlands from 1962 to 2002 (Smits et al., 2005), much of the USA from 1973 to 2005 (Pryor et al., 2007), Australia from 1975 to 2006 (McVicar et al., 2008), and southern and western Canada from 1953 to 2006 (Wan et al., 2010). Increasing wind speeds were found at high latitudes in both hemispheres, namely in Alaska from 1921 to 2001 (Lynch et al., 2004), in parts of the Canadian Arctic from 1953 to 2006, and in Antarctica over the second half of the 20th century (Turner et al., 2005).

Vautard et al. (2010) analysed a global land surface wind data sets from 1979 to 2008 after rigorous quality screening. They found decreasing trends on the order of -0.1m/s per decade (termed "atmospheric stilling"), over large portions of Northern Hemispheric land areas which they could not find in geostrophic wind calculated from SLP fields and which they attributed to an increased surface roughness.

[INSERT FIGURE 2.47 HERE]

Figure 2.47: Surface wind trends for the period July 1986 to August 2006 computed at a spatial resolution of 2.5°. a) SSM/I wind trends, b) ICOADS wind trends (Wentz et al., 2007), c) 0.995 sigma level wind trend from 20CR.
[THIS IS A STRAWMAN FIGURE: PANELS B AND C COULD BE COMPLEMENTED WITH LAND SURFACE WINDS FROM ANEMOMETERS AND 20CR, RESPECTIVELY, BUT NEEDS FURTHER EFFORT.]

2.6.3 Upper-Air Winds

In contrast to surface winds, which were discussed in previous assessment reports, upper level winds got little attention. Radiosondes and pilot balloon observations are available on a global scale from around the 1930s onwards (Stickler et al., 2010). While radiosonde wind records contain temporal inhomogeneities, they are far less common and also less systematic than those in temperature records (Gruber and Haimberger, 2008), at least from about 960 onwards.

In the past few years, interest in an accurate depiction of upper air winds has grown since they are essential for estimating the state and changes of the general atmospheric circulation and for explaining changes in the surface winds (Vautard et al., 2010). In contrast to the wind stilling at the surface, no or much weaker trends were found for lower tropospheric winds from balloon data or reanalyses. Allen and Sherwood (2008) diagnosed significantly increasing vertical wind shear of up to 1 m/s per decade in the subtropics for the period 1979–2005, which has implications for upper tropical tropospheric temperature trends (see Section 2.2.5.6). However, systematic trend analyses of radiosonde winds are lacking.

Trends in upper-air winds in the extratropics from reanalysis data sets are studied mostly in the context of trends in the jet streams and storms. These studies are discussed in Sections 2.6.6. and 2.7, respectively.

2.6.4 Tropospheric Geopotential Height and Tropopause

Changes in GPH, which can be addressed using radiosonde data or reanalysis data, are an integral picture of SLP and temperature changes in the atmospheric levels below. At the same time the spatial gradients of the trend reflects changes in the upper-level circulation. Box 2.2, Figure 1 shows trends in 500 hPa GPH from 1970 to 2008 for May-October (left) and November-April (right). It shows the decrease in tropospheric GPH at southern high latitudes that was noted in AR4 and is also found in radiosonde data (Forster et al., 2011), whereas increasing GPHs are found over the subtropics (especially the Mediterranean region), the tropics and in some areas of the northern extratropics. The high-latitude trends indicate changes in the polar vortices. Neff et al. (2008), analysing radiosonde data over the period 1957–2007, find asymmetric 500 hPa GPH trends over Antarctica, with falling GPH at East Antarctic stations in December-May, rising GPH over West Antarctica in May-December, and increasing GPH at the South Pole in all months. Over the Arctic (60°–90°N) from 1979 to 2003, tropospheric GPHs from radiosonde data decreased in winter and increased in fall (Forster et al., 2011). Angell (2006) found similar trends in NNR from 1963 to 2001.

Changes in the tropopause affect trace gas transport, chemistry, and radiative processes. Specifically, changes in the cold point temperatures near the tropical tropopause largely control stratospheric humidity (see Fueglistaler et al., 2009). Based on radiosonde data, Randel et al. (2006) found a decrease of tropical tropopause temperatures between the periods 1994–2000 and 2001–2004, which is consistent with changes in tropical upwelling (see Section 2.6.8.). However, trends in tropopause temperature are generally considered uncertain (Fueglistaler et al., 2009). Trends in tropopause altitude are discussed in the next subsection.

2.6.5 The Tropical Circulation

In this section we assess evidence for changes in the strength of the Hadley and Walker circulations as well as the width of the tropical belt. Evidence for changes in the tropical circulation is based on radiosonde and reanalyses data. Additionally, the tropical circulation imprints on other fields that are observed from space (e.g., total ozone, outgoing long-wave radiation). To a limited extent, changes in the water cycle provide constraints for changes in the tropical circulation (Schneider et al., 2010).

As reported in AR4, Mitas and Clement (2005) found a strengthening of the northern Hadley circulation in boreal winter in some, but not all data set. The two most widely used reanalysis data sets — NNR and ERA-40 — both have demonstrated shortcomings with respect to tropical circulation, hence their long-term changes in the Hadley circulation might be artificial (Hu et al., 2011; Mitas and Clement, 2005; Song and Zhang, 2007). However, Broennimann et al. (2009) extended the study to additional reanalysis data sets (20CR, JRA-25, ERA-Interim) and found a strengthening from the mid 1970s to 2008 (following a weakening between the 1920s and 1970s). Sohn and Park (2010) found a strengthening of the Hadley circulation in reanalyses and satellite-based humidity data from 1979 to the 2000s. Overall, the confidence in trends in the strength of the Hadley circulation is low.

Vecchi et al. (2006) suggest a weakening of the Pacific Walker circulation based on changes of SLP gradients across the Pacific from 1861 to 1992. Boreal spring and summer contribute most strongly to the trend (Karnauskas et al., 2009). Nicholls (2008), over the period 1958–2007, finds an increasing trend in SLP at Darwin, Australia, in March-September, but not November-February, when the Walker circulation is strongest. Based on the vertical velocity at 500 hPa over the Pacific from various reanalysis data sets, Broennimann et al. (2009) and Compo et al. (2011) find no change in the strength of the Walker circulation in boreal winter over the past 100 to 140 years. Deser et al.(2010a), based on marine air temperature and cloud cover over the Pacific, find a weakening of the Walker circulation during most of the 20th century to be consistent with observations (see also Yu and Zwiers, 2010). However, since around 1980 the trend has reversed (cf. equatorial SOI linear trends and evolution in Table 2.7 and Box 2.3 Figure 1). Sohn and Park (2010) analysing water vapour flux from satellite and reanalysis data, find a strengthening of the Walker circulation over the period 1979–2006 (see also Seager and Naik, 2011).

A suite of observed changes in atmospheric parameters suggest that the width of the tropical belt increased from 1979 to the early 2000s (Forster et al., 2011; Hu et al., 2011; Seidel et al., 2008). Various surface, upper-tropospheric, and stratospheric features have been used to distinguish the tropics from the extratropics, and independent sources of evidence indicate an increase in the latitudinal extent of the tropics (see Figure 2.47). Evidence is strongest for the respective summer hemisphere.

Since 1979 the region of low column ozone values typical of the tropics has expanded in the NH (Hudson et al., 2006). In parallel, the region of high tropical tropopause expanded poleward in both hemispheres (Birner, 2010; Seidel and Randel, 2007). Tropopause height trends suggest widening over a longer period (since 1960), but observational evidence is scantier (Birner, 2010; Seidel and Randel, 2007). Even during the period since 1979, the magnitude of the tropopause-based estimate of widening depends on methodological and data choices (Birner, 2010; Seidel and Randel, 2007).

The downward, outer branches of the Hadley cell, where deep clouds are relatively rare, have expanded polewards, as seen in outgoing longwave radiation, a surrogate for cloudiness (Hu and Fu, 2007), as have the associated regions of low precipitation and high surface pressure (Hu et al., 2011). Changes in the north-south atmospheric mass flow independently support this finding (Hu and Fu, 2007; Hu et al., 2011).

The findings of tropical belt widening have uncertainties that have been only partially explored (Birner, 2010). However, the qualitative consistency of these observed changes in independent datasets suggests that it is likely that the tropical belt has been widening. The widening amounts to about 2 and 5 degrees latitude between 1979 and 2005 (Seidel et al., 2008).

[INSERT FIGURE 2.48 HERE]
Figure 2.48: Width of the tropical belt as seen in various observation-based data sets (Seidel et al., 2008). [THIS IS A STRAWMAN FIGURE; I SUGGEST UPDATING IT AND ADDING INDICES ON STORM TRACKS.]

2.6.6 Jets, Storm Tracks and Weather Types

[PLACEHOLDER FOR FIRST ORDER DRAFT]

2.6.6.1 Midlatitude and Subtropical Jets

Subtropical and midlatitude (eddy-driven) jet streams are three-dimensional entities that vary meridionally and vertically and hence are difficult to capture. GPH can be accurately determined from radiosonde measurements, hence wind speed estimates using quasi-geostrophic flow assumptions are considered reliable. However, a high vertical resolution is required. Using reanalysis data sets, it is possible to track 3-dimensional jet variations by identifying a surface of maximum wind (SMW).

Prior to AR4, no global or hemispheric-scale studies of jet stream variability had been conducted; most work was regional or dealt with overall vortex changes or large-scale patterns of trends in GPH. In NH summer, subtropical jets have lowered significantly over most of the tropics and subtropics from 1958 to 2004, particularly in the Eastern Hemisphere (Strong and Davis, 2006). Similar long-term trends in the SMW are not evident in boreal winter, where interannual jet variability is linked to monthly variations in the Arctic Oscillation or ENSO (Strong and Davis, 2008a).

Various analyses (from different reanalysis data sets that both include and exclude data from the pre-satellite era) indicate that the jet streams (midlatitude and subtropical) have been moving poleward in most regions (on both hemispheres) over the last three decades (Archer and Caldeira, 2008b; Fu et al., 2009b; Fu et al., 2006; Strong and Davis, 2007). There is inconsistency with respect to speed trends based upon whether one uses an SMW-based or isobaric-based approach (Archer and Caldeira, 2008a, 2008b; Strong and Davis, 2007, 2008b). In general, eddy-driven jets have become more common (and jet speeds have increased) over Canada, the North Atlantic, and Europe (Barton and Ellis, 2009; Strong and Davis, 2007) — trends that are coupled with regional increases in GPH gradients and circumpolar vortex contraction (Angell, 2006; Frauenfeld and Davis, 2003). From a climate dynamics perspective, these trends are driven by regional patterns of tropospheric and lower stratospheric warming or cooling and thus are coupled to large-scale circulation variability. While jet speed trends are uncertain, it is likely that, at least in the NH, the jet core has been contracting towards the pole since the 1970s.

2.6.6.2. Storm Tracks and Frequency of Cyclones

Storm tracks are regions of enhanced synoptic activity due to the passage of cyclones. The main storm tracks stretch across the North Pacific, North Atlantic, and Southern Ocean. They are defined by applying band pass filtering or cyclone tracking to daily or sub-daily SLP data (station data, gridded data, or reanalyses) or to upper level fields from reanalyses. Trends have shown to be sensitive to the method (Raible et al., 2008).

In AR4 changes in storm tracks were assessed. A poleward shift of the NH storm track was found, however, it was also noted that uncertainties are significant and that NNR and ERA-40 disagree in important aspects. For the North Atlantic, studies based on reanalysis data (Schneidereit et al., 2007), SLP measurements from ships (Chang, 2007a) and sea level time series (Vilibic and Sepic, 2010) further support a poleward shift of the cyclone tracks from the 1950s to the early 2000s, with more wintertime high-latitude cyclones (see also Sorteberg and Walsh, 2008) but fewer at mid-latitudes. This is consistent with changes in the NAO to which the Atlantic storm track is associated (Schneidereit et al., 2007). However, storminess derived from SLP station triangles in Europe from the 1870s to 2005 shows large decadal variations (Matulla et al., 2008). No trend was found in North Atlantic polar lows based on a downscaling of NNR data (Zahn and von Storch, 2008) and in the North Pacific storm track based on reanalysis data (Mesquita et al., 2010) and ship-based observations (Chang, 2007a). Simmonds et al. (2008) find no trend in Arctic cyclones in reanalyses in 1979–2006.

Pezza et al. (2007a), using ERA-40 data, found a trend towards fewer but more intense storms in the southern extratropics (40°–70°S) from 1957 to 2002 and an intensification of anticyclones. However, ERA-40 and NNR differ with respect to SH storm tracks (Wang et al., 2006). A southward shift of the SH storm track has been reported based on NNR data (Hope et al., 2006). A decrease in storminess at Cape Otway (AUS) based on a 130-year long SLP time series is consistent with this interpretation (Alexander and Power, 2009).

2.6.6.3. Weather Types and Blocking

Changes in climate lead to or are driven by changes in weather. Changes in the frequency of weather types are of interest since weather extremes can be associated to specific weather types. For instance, persistent

blocking is held responsible for the 2010 heat wave in Russia .[(Dole et al., 2011)]. In practice, synoptic classifications or statistical clustering (Philipp et al., 2007) are used to attribute the weather on a given day to a weather type. In addition, feature-based methods (Croci-Maspoli et al., 2007a) are used to obtain measures of the synoptic feature of interest. These methods require daily SLP fields or upper-level fields from reanalyses.

In AR4, weather types were not assessed as such, but an increase in blocking frequency in the Western Pacific and a decrease in North Atlantic was noted. Comparing synoptic weather classifications for Central Europe for the two 30-year periods 1951–1980 and 1974–2003, Werner et al. (2008) found an increase of anticyclonic weather types in summer and cyclonic weather types in winter. Trnka et al. (2009) also found an increase by more than 80% of the frequency of drought-conducive weather types in central Europe from 1940–2005, with strongest changes during April to June. Applying a statistical clustering approach to daily SLP fields for Europe from 1850 to 2003, Philipp et al. (2007) found trends towards more frequent westerly circulation types and less frequent continental highs in winter, more frequent blocking over Great Britain in spring, and a retreated Azores high in summer. The circulation types explain a significant amount of temperature variability over Europe including trends. However, low-frequency variability in extreme indices is governed by within-type variability rather than changes in frequency (Jacobeit et al., 2009).

Using a feature-based approach, Croci-Maspoli et al. (2007a) found negative trends of blocking in winter over Greenland and in spring over the North Pacific during the period 1957–2001. Long-lasting blocking is closely associated with circulation modes such as the NAO or the PNA (Croci-Maspoli et al., 2007b), which is discussed in Section 2.6.9. For the SH, Dong et al. (2008) found a decrease in number but increase in intensity of blocking days over the period 1948 to 1999.

2.6.7 Stratospheric Circulation

The stratosphere is coupled with the troposphere through fluxes of radiation, momentum, and mass. The most relevant characteristics of stratospheric circulation for climate and for trace gas distribution are the winter polar vortices, the Quasi-Biennial Oscillation, and the Brewer-Dobson circulation (BDC). Radiosonde observations (GPH and wind) and circulation diagnostics from reanalysis data sets are used to assess stratospheric circulation. Indirect evidence comes from space-borne trace gas observations.

Changes in the stratospheric circulation have been assessed in AR4 and more recently in the WMO assessment of ozone depletion (Forster et al., 2011). It was noted that detection of long-term changes is difficult because wind observations are sparse and not homogenised and indirect evidence for changes in the stratospheric circulation carry large uncertainties. A significant decrease in lower-stratospheric GPH in summer over Antarctica was found in AR4 and further corroborated in Forster et al. (2011), whereas trends in the Northern Polar vortex were considered uncertain due to its large variability.

This assessment has not changed since. Cohen et al. (2009) report an increase in number of stratospheric sudden warmings (rapid warmings of the middle stratosphere accompanied by a collapse of the polar vortex and reversal of the flow) during the last two decades. However, interannual variability in the Arctic polar vortex is large and the uncertainties in the data products high (Tegtmeier et al., 2008). Langematz and Kunze (2008) find a strong dependence of stratospheric GPH trends over the Arctic on the time period, while the deepening of the Antarctic vortex was found to be more robust.

2.6.8 Brewer-Dobson Circulation

The BDC or stratospheric overturning circulation transports air upward in the tropics, poleward in the extratropics, and downward at middle and high latitudes. The BDC is relevant for the transport of trace gases and water vapour and affects their chemical and transport lifetime. However, the BDC is only indirectly observable via wave activity fluxes (which according to the current understanding are a major driver of the BDC), via the distribution of trace gases, or via determination of the “age of air” (i.e., the time an air parcel has resided in the stratosphere after its entry from the troposphere). All of these methods are subject to considerable uncertainties, and they might shed light only on some aspects of the BDC. For instance, wave activity fluxes can be estimated from reanalysis data, however it is not clear whether long term trends are accurate. Randel et al. (2006), using observational data, found a sudden change in lower stratospheric water

vapour and ozone around 2001 that is consistent with an increase in the mean tropical upwelling [(see also Rosenlof and Reid, 2008)]. Engel et al. (2009) found no change in the age of air from measurements of chemically inert trace gases from 1975–2005, which however does not rule out trends in the lower stratospheric branch of the BDC (Bonisch et al., 2009). Hence, while an acceleration of the ascent in the tropical lower stratosphere to date is a robust feature of chemistry-climate models (Li et al., 2009), this has not been confirmed by observations and the responsible mechanisms remain unclear (Forster et al., 2011).

[START BOX 2.3 HERE]

Box 2.3: Patterns and Indices of Climate Variability

Some traditional and some newer indices of climate variability are defined in the Box 2.3, Table 1 and are illustrated by the figures embedded therein. Only those indices are included, which (1) have been used by a variety of authors, (2) are defined relatively simply from raw or statistically analyzed observations of a *single* climate variable, (3) are based on a surface variable, so that observational data sets longer than a century exist (with an exception of PNA and AAO that are defined on the basis of 500 and 850 hPa GPH, respectively). Multiplicity of indices used for the same climate phenomenon is due to the fact that in the real climate system and with the observational record of limited length and quality, no index can perfectly separate a target phenomenon from all other effects. As a result, each index is affected by many climate phenomena; their relative contributions to the index variance change with time periods and data used. Researchers are choosing indices that they hope are most appropriate for the goals of their projects.

[INSERT BOX 2.3, TABLE 1 HERE]

Box 2.3, Table 1: Established indices of climate variability with global or regional influence. Columns are: (1) name of a general climate phenomenon, (2) name of a specific index intended to describe it, (3) index definition, (4) primary reference, (5) Figures in this Box, if any, illustrating this index and/or corresponding spatial pattern, (6) Sections of the report using this index, (7) characterization of the index or its corresponding spatial pattern as an optimal or dominant pattern of variability, and (8) Comments.

[INSERT BOX 2.3, FIGURE 1 HERE]

Box 2.3, Figure 1: Selected indices of ENSO as defined in Box 2.3, Table 1. To ease visual comparison, sign is inverted for all SOI versions; 13-month-running-means filter is applied to all indices. SOIs are standardized over 1971–2000 period by construction; temperature-based indices NINO3.4 and ENSO Modoki Index (EMI) are standardized here over the same period. Their standardization factors (in units of $1/^{o}C$) are specified in the legend.

[INSERT BOX 2.3, FIGURE 2 HERE]

Box 2.3, Figure 2: ENSO-related variability patterns in SST, MSLP, and rainfall corresponding to the three of ENSO indices shown in Box 2.3, Figure 1: NINO3.4, Troup SOI, and EMI. Patterns are obtained by regressing monthly mean fields of these variables on each of the indices. HadISST1 and HadSLP2r for 1901–2010 period are used for SST and MSLP data respectively, and Xie and Arkin's CMAP precipitation data set is used for the rainfall fields (January 1979 – August 2009). Units of regression patterns for SST, MSLP, and rainfall, on either of temperature indices (NINO3.4 and EMI) are unitless, $mb/^{o}C$, and $mm/day/^{o}C$, respectively, and ^{o}C, mb, and mm/day per one standard deviation for SOI. Regression patterns on NINO3.4 and SOI are very similar: these are viewed as traditional ENSO impact patterns. Patterns corresponding to EMI are somewhat different, since the EMI indexes a non-canonical type of El Niño: Modoki, or Central Pacific El Niño.

[INSERT BOX 2.3, FIGURE 3 HERE]

Box 2.3, Figure 3: Selected indices of NAO and AO (a.k.a. NAM) as defined in Box 2.3, Table 1. Station-based (Lisbon/Ponta Delgada minus Stykkisholmur/Reykjavik) and PC-based NAO indices are according to Hurrell (1995a), and AO index is computed by CPC on the basis of NCEP/NCAR Atmospheric Reanalysis. All indices are standardized for the 1971–2000 period. The last value in the plot corresponds to the 2009–2010 DJFM average is formally a record low in the data interval 1865 to present that is shown here (although it is very close to the previous record, set in 1880–1881 winter). The 2010–2011 DJFM value (not shown) is expected to be similarly low.

[INSERT BOX 2.3 FIGURE 4 HERE]

Box 2.3, Figure 4: NAO- and AO-related variability patterns in the SST and MSLP. The patterns are obtained by regressing monthly mean fields of these variables on the NAO station-based index from Hurrell (1995a) and the AO index from the CPC. Regressions are performed for the DJFM averages. HadISST1 and HadSLP2r for 1901–2010 period are used for the SST and MSLP data, respectively. Units in the regression patterns for SST and MSLP are ^{o}C/s.d and mb/s.d., respectively.

[PLACEHOLDER FOR FIRST ORDER DRAFT: INSERT A FEW MORE FIGURES HERE, CURRENTLY IN PREPARATION, TO ILLUSTRATE OTHER MODES.]

[END BOX 2.3 HERE]

2.6.9 Changes in Indices of Climate Variability

Traditional indices of climate variability index natural modes of climate variability. While it is expected that significant amounts of anthropogenic warming might cause systematic changes in index values or in the character of their variability, definite inferences about such occurrences in observational data sets are not easy to make, especially when the records are relatively short, prone to error, and when indices are subject to the natural multidecadal variability. In AR4 patterns of atmospheric circulation variability were assessed in detail. Multidecadal variability was found in patterns referring to Pacific and Atlantic SSTs. The NAO and SAM were found to exhibit increasing trends (strengthened midlatitude westerlies) from the 1960s to 1990s, but have returned to near their long-term mean state thereafter.

Table 2.7 summarizes observed changes in the most prominent indices of climate variability. Bunge and Clarke (2009) find an increase in the NINO3.4 index since about 1870s. However, the sign of trends in east-west SST gradient across the Pacific remains ambiguous (Bunge and Clarke, 2009; Deser et al., 2010a; Karnauskas et al., 2009; Vecchi and Soden, 2007) and SST data sets differ with respect to trends in the tropical equatorial Pacific (Deser et al., 2010a; Karnauskas et al., 2009; Vecchi et al., 2008). Indeed, NINO3.4 computed on the basis of a well-established ERSSTv3b analysis of SST shows significant increasing trends in the periods from 1876 to 1990 and further, while NINO3.4 computed from HadISST1, another well-established analyzed SST data set, does not show significant trends of any sign in multidecadal periods (Table 2.7). Power and Smith (2007) found that the period 1977–2006 showed the lowest SOI, the highest recorded value in mean sea-level pressure at Darwin, the weakest equatorial surface wind-stresses and the highest tropical sea-surface temperatures on record. The formal veracity of this statement is supported by visual inspection of Box 2.3, Figure 1, however, high level of variability obvious in this plot suggest caution in interpreting such observed changes as secular variability.

In addition to possible changes in the mean values of climate indices, changes in the nature of variability are also possible. In particular, attempts to identify changes in the character of ENSO variability were always getting a lot of attention but resulting in a limited success. In the recent years, however, starting from the work by Larkin and Harrison (2005) and Ashok et al. (2007), a different type of El Niño events (dateline El Niño, Central Pacific El Niño, or Modoki) has been identified that appeared more frequently from the mid-20th century on (Lee and McPhaden, 2010). The influence of this type of SST anomaly on the atmosphere appears to be different from that of the canonical ENSO SST (Ashok and Yamagata, 2009; Kim et al., 2009; Weng et al., 2009).

PDO and IPO indices show changes since 1980s that are consistent with the discussion in Section 2.6.1. This change, and the teleconnection between the Equator and midlatitudes is likely responsible for reverting the trends in the Walker Circulation (Section 2.6.5), which was reported to have slowed down before 1992, but now seems to have sped up again. Specifically, in the period 1876–1990 equatorial SOI was decreasing with a linear trend of -0.047 ± 0.016 s.d. per decade, i.e. was significant at 0.3% level (Table 2.7) in a standard two-sided Student's *t* test. Since this decrease was reverted after 1990 (Box 2.3, Figure 1), the trend for the entire period 1876–2010 reduced to -0.026 ± 0.016 s.d. per decade, which is not significant even at the 5% level.

The observed detrended multidecadal SST anomaly averaged over the North Atlantic is often called Atlantic Multidecadal Oscillation (AMO, see Box 2.3, Table 1) and has significant regional and hemispheric climate impacts. Warm AMO phases occurred during in the late 19th century, in 1925–1965 and since 1995, cold phases occurred during 1900–1925 and 1965–1995. The Atlantic "Niño" mode reflects the east-intensified warming, related to the weakening of the Atlantic equatorial cold tongue over the last 60 years that [Tokinaga and Xie (2011b)] identified and interpreted.

The NAO is the most important variability mode for large parts of the northern extratropics (Hurrell et al., 2003). An increasing trend in the NAO index from the 1960s to the 1990s that has stimulated NAO-related research (Stephenson et al., 2003) has reversed since (Osborn, 2011) so that no trend appears over the past 40 years. In contrast, the SAM has continued its upward trend that was noted in AR4, peaking in a record high SAM index in austral winter 2010. Fogt et al. (2009) find a positive trend in the SAM index from 1957 to 2005, Visbeck (2009), in a station-based index, finds an increase in recent decades (1970s to 2000s).

Table 2.7, Part 1: [Other three parts of this table, as listed below, for (2) NAO, PNA, annular modes; (3) decadal and longer variability, and (4) tropical Atlantic and Indian Ocean variability are under calculation] Trends in different periods for ENSO-related indices from Box 2.3, Table 1. Trends are computed by ordinary least squares regression of annual means of indices on the time axis; one standard deviation uncertainty is reported as well. Provisions to account for sequential correlations by reducing estimated number of degrees of freedom were not made. Trend values that are formally significantly different from zero at 5% and 1% level are underlined and shown in bold, respectively.

Climate Phenomenon	Index name	Data set used for calculating the index	Lin trends for annual averages of index in different time intervals, using OLS, no DF reduction: reported as a slope of index units per decade ± 1 error s.d.					
			1876--2010	1876--1950	1876--1970	1876--1990	1950--2010	1970--2010
El Niño – Southern Oscillation (ENSO) - canonical, Eastern Pacific ENSO	NINO3	HadISST1	0.009± 0.013	-0.005± 0.029	-0.008± 0.021	0.001± 0.016	0.056± 0.046	0.030± 0.088
	NINO3.4	HadISST1	0.006± 0.012	-0.001± 0.029	0.003± 0.020	-0.001± 0.016	0.038± 0.043	0.045± 0.084
		ERSSTv3b	**0.046**± 0.013	-0.012± 0.030	0.030± 0.021	0.034± 0.016	0.072± 0.045	0.106± 0.084
	Cold Tongue Index (CTI)	HadISST1	**-0.030**± 0.011	-0.025± 0.026	0.031± 0.018	-0.030± 0.014	-0.011± 0.038	-0.043± 0.073
	Troup SOI *(-1)	BOM-computed	0.009± 0.013	-0.010± 0.032	-0.007± 0.021	0.002± 0.016	0.056± 0.044	0.026± 0.084
	SOI *(-1)	BOM Darwin and Tahiti records	0.008± 0.013	0.010± 0.031	-0.006± 0.021	0.003± 0.016	0.048± 0.042	0.013± 0.081
	Darwin SOI *(-1)	BOM Darwin record	0.011± 0.012	-0.024± 0.028	0.020± 0.019	-0.006± 0.015	**0.102**± 0.038	0.102± 0.073
	Equatorial SOI (EQSOI) *(-1)	HadSLP2r	0.026± 0.014	0.056± 0.028	0.040± 0.020	**0.047**± 0.016	-0.022± 0.051	-0.176± 0.099
Central Pacific El Niño (Modoki)	El Niño Modoki Index (EMI)	HadISST1	-0.006± 0.007	0.015± 0.013	0.021± 0.009	-0.003± 0.008	-0.034± 0.027	0.016 ±0.054

Table 2.7. Part 2: [PLACEHOLDER FOR FIRST ORDER DRAFT] Trends in different periods for NAO, PNA, and annular mode indices from Box 2.3, Table 1.

Table 2.7. Part 3: [PLACEHOLDER FOR FIRST ORDER DRAFT] Trends in different periods for indices of decadal, interdecadal, and multidecadal variability (PDO, IPO, and AMO) from Box 2.3, Table 1.

Table 2.7. Part 4: [PLACEHOLDER FOR FIRST ORDER DRAFT] Trends in tropical Atlantic and Indian ocean variability indices from Box 2.3, Table 1.

2.6.10 Synthesis

Changes in atmospheric circulation are relevant for local climate change. Although new and improved data sets (e.g., reanalyses) are now available, changes in the large-scale atmospheric circulation remain difficult to detect. Apart from remaining problems in the data sets, this is due to a large variability on decadal time scales. In fact, many trends features that appeared from the 1950s to 1990s (e.g., an increase in the NAO

index or a weakening of the Pacific Walker circulation) have reversed in more recent periods. This is important as many studies are based on ERA-40 over the period 1957–2001 and thus represent the former period. The trend in the winter NAO index, estimated from Hurrell (1995a) Lisbon—Stykkisholmur station data record, for instance, was 0.041 ± 0.012 s.d. per decade during the 1957–2001 period, i.e. was highly significant with $p<0.001$, whereas in the last two decades (1989–2011, i.e., the period currently covered by ERA-Interim) it reversed to -0.086 ± 0.039 s.d. per decade, which incidentally, can be viewed as "significant," with 2.7% significance level, despite the shortness of the time period (Box 2.3, Figure 3, Table 2.7 Part 2).

Several changes could nevertheless be found, including a poleward motion of zonal mean circulation features (widening of the tropical belt, poleward shift of storm tracks and jet streams, contraction of the polar vortex) since the 1960s or 1970s and a strengthening of the SAM since the 1970s.

2.7 Changes in Extreme Events

The AR4 (Trenberth et al., 2007) highlighted the importance of understanding changes in extreme climatic events given their disproportionate impact on society and ecosystems compared to changes in mean climate (see also WGII AR4). More recently a comprehensive review of observed changes in extreme events was undertaken by the IPCC SREX report [(Nicholls et al., 2011)]. The SREX defines extreme weather and climate events as those which occur above (or below) a threshold value near the upper (or lower) ends ("tails") of the range of observed values of a given climate variable. Definitions of thresholds vary, but values with less than a 5% or 1% or even lower chance of occurrence during a specified reference period (generally 1961–1990) are often used. Absolute thresholds (rather than relative thresholds based on the range of observed values of a variable) can also be used to identify extreme events. The definition of an extreme climate event will vary from place to place in an absolute sense (e.g., a hot day in the tropics will be a different temperature than a hot day in mid latitudes). Extremes in some climate variables (e.g., drought or flood) may not necessarily be induced by extremes in meteorological variables (precipitation, temperature), but may be the result of an accumulation of moderate weather or climate events.

Since errors in long-term climate data are likely to show up as "extreme" and some variables are particularly sensitive to changing measurement practices over time, data availability, quality and consistency are of particular importance for the analysis of extreme events. For example, the historical tropical cyclone records are known to be heterogeneous due to changing observing technology and reporting protocols (e.g., Landsea et al., 2004). Further heterogeneity is introduced when records from multiple ocean basins are combined to explore global trends because data quality and reporting protocols vary substantially between regions (Knapp and Kruk, 2010). In addition, it has been difficult to provide a precise definition of an extreme (e.g., Stephenson et al., 2008) because events can vary between locations and can depend on the application for which analysis is required. For example, it has been difficult to define a universally valid critical threshold globally for defining a heat wave and differences exist between impact-dictated definitions (e.g., mortality rates) and physical definitions (e.g., temperature threshold and duration-driven definitions). Generally definitions have consisted of a certain number of consecutive days with temperatures exceeding percentile-based or fixed temperature thresholds (see Box 2.4). However these definitions can be complicated by the changing nature of the statistical properties of the probability distributions of a given climate variable particularly as might occur under non-stationary climate conditions. Many studies have shown that changes in probability distribution functions associated with changes in variance or skewness can be as or more important than changes in the mean. Subsequently, in the following sections we assess the conclusions from both AR4 and SREX and comment on studies subsequent to that assessment.

[START BOX 2.4 HERE]

Box 2.4: Extremes Indices

A large amount of the available scientific literature on climate extremes is based on the use of so-called "extreme indices", which can either be based on the probability of occurrence of given quantities or on threshold exceedances. Typical indices that are seen in the scientific literature include the number, percentage or fraction of cold/warm days/nights (days with maximum temperature, Tmax or minimum

temperature, Tmin, below or above the 10th percentile, or the 90th percentile, generally defined with respect to the 1961–1990 reference time period). Other definitions relate to e.g., the number of days above specific absolute temperature or precipitation thresholds, or more complex definitions related to the length or persistence of climate extremes. Some advantages of using predefined extreme indices are that they allow some comparability across modelling and observational studies and across regions. Moreover, in the case of observations, derived indices may be easier to obtain than is the case with daily temperature and precipitation data, which are not always distributed by meteorological services. Peterson and Manton (2008) discuss collaborative international efforts to monitor extremes by employing extreme indices. Typically, although not exclusively, extreme indices used in the scientific literature reflect "moderate" extremes, e.g., events occurring as often as 5% or 10% of the time. More extreme "extremes" can be better investigated using Extreme Value Theory. Extreme indices are more generally defined for (daily) temperature and precipitation characteristics, and are rarely applied to other weather and climate variables, such as wind speed, humidity, or physical impacts and phenomena. Some examples are available in the literature for wind-based (Della-Marta et al., 2009) and pressure-based (Beniston, 2009) indices, for health-relevant indices combining temperature and relative humidity characteristics (e.g., Diffenbaugh et al., 2007; Fischer and Schar, 2010), and for a range of dryness indices.

[END BOX 2.4 HERE]

2.7.1 Temperature

The AR4 (Trenberth et al., 2007) concluded that it was very likely that over 70% of the global land area had seen a decrease in cold extremes including frosts and an increase in warm extremes since 1951. Globally warm spells and heat waves were likely to have exhibited an increase over a similar period with some changes in inter-seasonal variability of cool and warm seasons in Central Europe. Subsequently the SREX [(Nicholls et al., 2011)] came to similar conclusions based on more recent available evidence and the level of confidence in these statements remains high.

Globally, significant increases in warm nights and significant decreases in cold nights have been detected since about 1950. Alexander et al. (2006) found that over 70% of the global land area sampled showed a significant decrease in the annual occurrence of cold nights and a significant increase in the annual occurrence of warm nights. While this could imply a positive shift in the location of the distribution of daily minimum temperature (Tmin) throughout the globe, changes in variance and skewness also play an important role in these changes (e.g., Ballester et al., 2010; Brown et al., 2008; Caesar et al., 2006; Della-Marta et al., 2007b; Orlowksy and Seneviratne, submitted). Changes in the occurrence of cold and warm days also show warming, but generally less marked except in some regions where the El Niño Southern Oscillation tends to dominate maximum temperature variability (e.g.,[Alexander et al., in preparation]). This is consistent with Tmin increasing more than maximum temperature (Tmax), leading to a reduction in diurnal temperature range (DTR) since 1951 in many regions (see Section 2.2.1.1). Some regions have experienced close to a doubling (or halving) of the occurrence of warm and cold nights e.g., parts of the Asia-Pacific region (e.g., Choi et al., 2009), parts of Eurasia (e.g., Klein Tank et al., 2006) although this is not the case across all regions. Recent studies covering central and eastern Europe (Bartholy and Pongracz, 2007; Kurbis et al., 2009), the Tibetan Plateau (You et al., 2008) and China (You et al., 2010), and North America (Peterson and Manton, 2008), show significant increases in unusually warm nights and days and a reduction in unusually cold nights and days. Parts South America indicate similar trends in these indices (e.g., Marengo et al., 2009) although a study for Uruguay (Rusticucci and Renom, 2008) suggests more complex trends in the region, with a reduction of cold nights, a positive but not significant trend in warm nights, non-significant decreases in cold days, and inconsistent trends in warm days. Changes in both local and global sea surface temperature patterns and large scale circulation patterns have been shown to be associated with regional changes in temperature extremes (e.g., Alexander and Arblaster, 2009; Barrucand et al., 2008) particularly in regions around the Pacific Rim (Kenyon and Hegerl, 2008). Record daily maximum temperatures averaged across the USA now outnumber record daily minimum temperatures by a ratio of 2:1 in recent decades compared to preceding decades (Meehl et al., 2009) while in Australia, Trewin and Vermont (2010) found a marked tendency for low temperature records to outnumber high temperature records in the 1957–66 decade, and for high temperature records to outnumber low temperature records in the 1997–2009 period. While SREX did not assess the occurrences of frosts, globally the annual occurrence

of frost days and ice days are likely to have decreased since 1951 over those parts of the globe where this index can be defined (Alexander et al., 2006) with century long decreases observed in some mid-latitude regions of the Northern Hemisphere (Qian et al., 2010). Globally, there are likely to have been large-scale warming trends in the extremes of temperature, especially minimum temperature, since the beginning of the 20th century (Horton et al., 2001); [CLIMDEX reference needed]. There are still however large data sparse areas on the globe e.g., central Africa. Collaborative international efforts have been established to fill in some of this regional detail (Peterson and Manton, 2008) which generally indicate trends consistent with global analyses e.g., Aguilar et al. (2009) showed that in western central Africa there had been a decrease in cold extremes and an increase in warm extremes since the mid-1950s.

Warm spells or heat waves containing a series of consecutive extremely hot days or nights, have substantially larger impacts than individual hot days (Trenberth et al., 2007), although fewer studies have investigated heat wave characteristics compared to changes in warm days or nights. Heat waves are often associated with quasi-stationary anticyclonic circulation anomalies that produce subsidence, light winds, clear skies, warm-air advection, and prolonged hot conditions at the surface [Black, 2004, Factors contributing to the Summer 2003 European heat wave]. Long-term changes in the persistence of anticyclonic summer circulation, which potentially have large effects on the duration of heat waves, are still relatively poorly understood. Heat waves can also be amplified by pre-existing dry soil conditions in transitional climate zones (Ferranti and Viterbo, 2006; Fischer et al., 2007b) resulting from a precipitation deficit (Della-Marta et al., 2007b; Vautard et al., 2010; Vautard et al., 2007), low-cloudiness producing a higher evaporative demand [Black, 2004, Factors contributing to the Summer 2003 European heat wave]; Fischer et al., 2007a), and earlier vegetation onset (Zaitchik et al., 2006). This amplification of soil moisture-temperature feedbacks is likely to have enhanced the duration of extreme summer heat waves in southeastern Europe during the latter half of the 20th century (Hirschi et al., 2011).

Since AR4 many studies have analysed local to regional changes in more detail, specifically addressing different heat wave aspects such as frequency, intensity, duration and spatial extent. Several studies suggest that the increase in the temperature mean accounts for most of the changes in heat wave frequency and duration (Ballester et al., 2010; Barnett et al., 2006). However, heat wave intensity/amplitude is highly sensitive to changes in temperature variability and shape (Clark et al., 2006; Della-Marta et al., 2007a; Della-Marta et al., 2007b; Fischer and Schar, 2010; Schar et al., 2004). Regional studies have generally found statistically significant increasing trends in heat waves and decreasing trends in cold spells e.g., over USA (Kunkel et al., 2008), China (Ding et al., 2010), Iran (Rahimzadeh et al., 2009), and Australia (Tryhorn and Risbey, 2006). Over western Europe the length of summer heat waves has doubled in the period 1880 to 2005 (Della-Marta et al., 2007a). Across the eastern Mediterranean region pronounced changes have been reported particularly after the 1960s, with average heat wave length increased by +0.85 ± 0.02 days per decade, heat wave intensity by +1.33 ± 0.06°C per decade, and heat wave number by +0.17 ± 0.01 per decade, respectively (Kuglitsch et al., 2010). Over the Iberian Peninsula warm spells increased throughout the 20th century, a trend that intensified during recent decades at rates higher than those of cold spells [Brunet, 2007, Long-term changes in extreme temperatures and precipitation in Spain]. Alexander and Arblaster (2009) showed a substantial increase in warm spell duration over southeastern Australia between 1957 and 1999 while Choi et al. (2009) find an increase over much of the rest of Australia particularly in Queensland. Over the United States there is a significant upward trend in heat wave occurrence since the 1960s (Karl et al., 2008). Over the 20th century as a whole however no significant trend is detected, as the 1930s remain the decade with the highest heat wave occurrence in the United States. However, while daytime temperatures were extremely high in the 1930s, night-time temperatures were not as unusual (Karl et al., 2008). Local increases in heat wave occurrence have also been reported for central America (Cueto et al., 2010). Over Asia spatially consistent patterns of changes in warm spell duration were apparent over roughly the past five decades (Choi et al., 2009), increasing by 1-6 days/decade in numerous homogenized station series in Japan, Republic of Korea, China, Mongolia, Vietnam, Thailand, and Malaysia with only one analyzed station in Asia showed a decrease in heat wave duration (Choi et al., 2009). A long station series for Hong Kong showed a trend towards longer heat waves over the period 1885–2008 (Lee et al., 2011). Significant increases in warm spell duration have further been identified at several weather stations in Iran (Rahimzadeh et al., 2009). For Africa there is insufficient evidence regarding changes in heat waves.

In summary, analyses continue to support the AR4 and IPCC SREX conclusions that since 1950 it is *very likely* that there has been an overall decrease in the number of unusually cold days and nights and an overall

increase in the number of unusually warm days and nights on the global scale, i.e., for land areas with data. It is *likely* that such changes have also occurred at the continental scale in North America and Europe, and *very likely* in Australia. There is *medium confidence* of a warming trend in temperature extremes in much of Asia. There is *low confidence* in trends for Africa, because of *lack of dat*a and studies. In South America, lack of data, and some inconsistencies between reported trends imply *low confidence* in some of the trends at the continental scale. It is *likely* that the number of warm spells, including heat waves, have increased since the middle of the 20th century in many (but not all) regions.

2.7.2 Hydrological Cycle

The Hydrological cycle refers to the continuous movement of water around the Earth. In Section 2.3 mean state changes in all aspects of the hydrological cycle were discussed. In this section we focus on the more extreme aspects of the cycle including extreme rainfall, snowfall and flooding. Droughts are discussed in more detail in Section 2.3, and extreme events associated with tropical and extratropical storms are discussed in Sections 2.7.3 and 2.7.4 respectively. The AR4 (Trenberth et al., 2007) concluded that it was likely that annual heavy precipitation events had disproportionately increased compared to mean changes between 1951 and 2003 over many mid-latitude regions even where there had been a reduction in annual total precipitation. Rare precipitation events were likely to have increased over regions with sufficient data since the late 19th century. The SREX assessment supported this view as have subsequent analyses.

Given the diverse climates across the globe it has been difficult to provide a universally valid definition of "extreme precipitation". However, in general statistical tests indicate changes in precipitation extremes are consistent with a wetter climate although with a less spatially coherent pattern of change than temperature change, i.e., large areas showing both increasing and decreasing trends and a lower level of statistical significance (e.g., Alexander et al., 2006).

Recent studies of heavy precipitation extremes in North America, indicate an increasing trend over the last half century (DeGaetano, 2009; Gleason et al., 2008; Kunkel et al., 2008; Pryor et al., 2009) while results for Central and South America indicate both positive and negative trends over a similar period. In more detail, Peterson et al. (2008) reported that heavy precipitation has been increasing over 1950–2004 in Canada, the U.S., and Mexico as well as the average amount of precipitation falling on days with precipitation. (DeGaetano, 2009) showed a 20% reduction in the return period for extreme precipitation over 1950 to 2007 while Gleason et al. (2008) reported an increasing trend in the area experiencing a much above-normal proportion of heavy daily precipitation from 1950 to 2006. Pryor et al. (2009) provided evidence of increases in rainfall intensity above the 95th percentile during the 20th century, particularly at the end of the century. The central plains/northwestern Midwest regions showed the largest trends towards increased annual total precipitation, number of rainy days and intense precipitation (e.g., fraction of precipitation derived from events in excess of the 90th percentile value). In northwest Mexico, statistically significant positive trends were found in daily precipitation intensity and the seasonal contribution of daily precipitation greater than its 95th percentile in mountain sites for the period 1961–1998. However, no statistically significant changes were found in coastal stations (Cavazos et al., 2008). Positive trends in extreme rainfall events were detected in southeastern South America, north central Argentina, northwest Peru and Ecuador and Sao Paulo, Brazil (Dufek and Ambrizzi, 2008; Marengo et al., 2009; Re and Barros, 2009) however negative trends were observed in winter extreme precipitation in some regions (Penalba and Robledo, 2010).

Studies for European countries indicate general increases in the intensity and frequency of extreme precipitation during the last four decades however with some inconsistencies between studies and regions. For example, winter extreme precipitation has increased in Central-Western Europe and European Russia (Zolina et al., 2008), but the trend in summer precipitation has been weak or not spatially coherent (Bartholy and Pongracz, 2007; Costa and Soares, 2009; Durao et al., 2010; Kysely, 2009; Maraun et al., 2008; Moberg et al., 2006; Pavan et al., 2008; Rodda et al., 2010; Zolina et al., 2008). Zolina et al. (2010) indicated that there has been a 15–20% increase in the persistence of wet spells over most of Europe over the last 60 years not associated with an increase of the total number of wet days. Increasing trends were found between 1901 and 2000 in 90th, 95th and 98th percentiles of daily winter precipitation (Moberg et al., 2006), which has been confirmed by more detailed country-based studies for the United Kingdom (Maraun et al., 2008), Germany (Zolina et al., 2008), Belgium (Ntegeka and Willems, 2008), Central and Eastern Europe (Bartholy and Pongracz, 2007; Kysely, 2009), while decreasing trends have been found in some regions such as

northern Italy (Pavan et al., 2008), Poland (Lupikasza, 2010) and some Mediterranean coastal sites (Toreti et al., 2010). Uncertainties are overall larger in Southern Europe and the Mediterranean, where there is low confidence in the trends.

Several recent studies focused on Africa, in general, have not found significant trends in extreme precipitation (Aguilar et al., 2009; Kruger, 2006; New et al., 2006; Seleshi and Camberlin, 2006). Observations at 143 weather stations in ten Asia-Pacific Network countries during 1955–2007 did not indicate systematic, regional trends in the frequency and duration of extreme precipitation events (Choi et al., 2009). However, other studies have suggested significant trends in extreme precipitation at sub-regional scales in the Asia-Pacific region and during monsoon seasons over Indian subcontinent (Krishnamurthy et al., 2009; Pattanaik and Rajeevan, 2010; Rajeevan et al., 2008; Sen Roy, 2009). Zhai et al. (2005) found significant increases over the period 1951–2000 in extreme precipitation in western China, and in parts of the southwest and south China coastal area, but a significant decrease in extremes is observed in north China and the Sichuan Basin.

Fewer studies have focussed on heavy snowfall events although throughout the temperate and sub-polar Northern Hemisphere, statistically significant decreases have generally been found during the latter part of the 20th century with indications that an increasing proportion of heavy winter precipitation falls in the form of rain instead of snow (e.g., Laternser and Schneebeli, 2003). However there are regional variations and in China for instance, [Sun et al. (2010)] found intense snowfall events decreased over the latter part of the 20th century in eastern China but increased in northern Xinjiang and the eastern Tibetan plateau. Averaged across the United States, there does not appear to have been a statistically significant trend in the occurrence of either high or low snowfall years based on over a century of record but there have been regional changes (Kunkel et al., 2009). Most notable are large decreases in the frequency of low-extreme snowfall years in the west north-central and east north-central US and large increases in the frequency of low-extreme snowfall years in the Northeast, Southeast, and Northwest. These trends have been much more consistent during the latter part of the 20th century.

Changes in droughts and drought-related variables such as soil moisture are covered in Section 2.3. IPCC AR4 noted that while flood damage was increasing (Kundzewicz et al., 2007), there was not a general global trend in the incidence of floods. There is however an abundance of evidence that there has been an earlier occurrence of spring peak river flows in snow-dominated regions (Rosenzweig et al., 2007). For example, Cunderlik and Ouarda (2009), find that snow-melt spring floods are coming significantly earlier in southern Canada. While the most evident flood trends appear to be in northern high latitudes, where warming trends have been largest in the observational record, there are regions where no evidence of a trend in extreme flooding has been found (e.g., Shiklomanov et al., 2007) over Russia based on daily river discharge. Other studies for Europe (e.g., Benito et al., 2005; Petrow and Merz, 2009) and Asia (e.g., Delgado et al., 2010; Jiang et al., 2008) show evidence for upward, downward or no trend in the magnitude and frequency of floods so we conclude that there is currently no clear and widespread evidence for observed changes in flooding (except for the earlier spring flow in snow-dominated regions).

In summary, analyses continue to support the AR4 and IPCC SREX conclusions that it is *likely* that there has been statistically significant increases in the number of heavy precipitation events (e.g., 95th percentile) in more regions than there has been statistically significant decreases, but there are strong regional and subregional variations in the trends. There is *medium confidence* that some regions have experienced more intense and longer droughts since the 1950s (e.g., Southern Europe, West Africa, East Africa) but also opposite trends exist in other regions (e.g., Central North America, Northwestern Australia). There continues to be a *lack of evidence* regarding the sign of trend in the magnitude and/or frequency of floods on a global scale although there is *high confidence* for earlier spring flow in snow-dominated regions.

2.7.3 Tropical Storms

The AR4 concluded that it was likely that a trend had occurred in intense tropical cyclone activity since 1970 in some regions (IPCC, 2007b). In more detail it was stated that “there is observational evidence for an increase in intense tropical cyclone activity in the North Atlantic since about 1970, correlated with increases of tropical SSTs. There are also suggestions of increased intense tropical cyclone activity in some other regions where concerns over data quality are greater. Multi-decadal variability and the quality of the tropical

cyclone records prior to routine satellite observations in about 1970 complicate the detection of long-term trends in tropical cyclone activity. There is no clear trend in the annual numbers of tropical cyclones". Subsequent assessments, including SREX, have somewhat revised these confidence estimates as follows.

There have been no significant trends observed in global tropical cyclone frequency records, including over the present 40-year period of satellite observations (e.g., Webster et al., 2005). Regional trends in tropical cyclone frequency have been identified in the North Atlantic, but the fidelity of these trends is debated (Holland and Webster, 2007; Landsea, 2007; Landsea et al., 2006; Mann et al., 2007b). Different methods for estimating undercounts in the earlier part of the North Atlantic tropical cyclone record provide mixed conclusions (Chang and Guo, 2007; Kunkel et al., 2008; Mann et al., 2007a; Vecchi and Knutson, 2008). Regional trends have not been detected in other oceans (Chan and Xu, 2009; Kubota and Chan, 2009). It thus remains uncertain whether any reported long-term increases in tropical cyclone frequency are robust, after accounting for past changes in observing capabilities (Knutson et al., 2010).

Whereas frequency estimation requires only that a tropical cyclone be identified and reported at some point in its lifetime, intensity estimation requires a series of specifically targeted measurements over the entire duration of the tropical cyclone (e.g., Landsea et al., 2006). Consequently, intensity values in the historical records are especially sensitive to changing technology and improving methodology, which heightens the challenge of detecting trends within the backdrop of natural variability. Global reanalyses of tropical cyclone intensity using a homogenous satellite record have suggested that changing technology has introduced a non-stationary bias that inflates trends in measures of intensity (Kossin et al., 2007), but a significant upward trend in the intensity of the strongest tropical cyclones remains after this bias is accounted for (Elsner et al., 2008). While these analyses are suggestive of a link between observed tropical cyclone intensity and climate change, they are necessarily confined to a 30+ year period of satellite observations, and cannot provide clear evidence for a longer-term trend.

Time series of power dissipation, an aggregate compound of tropical cyclone frequency, duration, and intensity that measures total energy consumption by tropical cyclones, show upward trends in the North Atlantic and weaker upward trends in the western North Pacific over the past 25 years (Emanuel, 2007), but interpretation of longer-term trends is again constrained by data quality concerns. Since 2005, accumulated cyclone energy, which is an integrated metric analogous to power dissipation, has been declining globally and is presently at a 40-year low point (Maue, 2009). The present period of quiescence, as well as the period of heightened activity leading up to a high point in 2005, do not clearly represent substantial departures from past variability (Maue, 2009).

Based on research subsequent to the IPCC AR4, which further elucidated the scope of uncertainties in the historical tropical cyclone data, the most recent assessment by the World Meteorological Organization Expert Team on Climate Change Impacts on Tropical Cyclones (Knutson et al., 2010) does not conclude that it is likely that annual numbers of tropical storms, hurricanes and major hurricanes counts have increased over the past 100 years in the North Atlantic basin, nor does it conclude that the Atlantic Power Dissipation Index increase is "likely substantial" since the 1950s and 1960s. The subsequent SREX forms a similar assessment, which remains unchanged in the present assessment i.e. there is *low confidence* that any reported long-term increases in tropical cyclone activity are robust, after accounting for past changes in observing capabilities.

2.7.4 Extratropical Storms

The AR4 noted a likely net increase in frequency/intensity of Northern Hemisphere extreme extratropical cyclones and a poleward shift in the tracks since the 1950s (Trenberth et al., 2007, Table 3.8), and report on several papers showing increases in the number or strength of intense extratropical cyclone both over the North Pacific and the North Atlantic storm track (Trenberth et al., 2007, p. 312), during the last 50 years. SREX and subsequent studies appear to build evidence for these assertions.

Many studies on extratropical storms have necessarily been limited to the period covered by reanalysis data. These have indicated a northward and eastward shift in North Atlantic cyclone activity during the last 60 years with both more frequent and more intense wintertime cyclones in the high-latitude North Atlantic (Raible et al., 2008; Schneidereit et al., 2007; Vilibic and Sepic, 2010; Wang et al., 2006; Weisse et al.,

2005) and fewer (Raible et al., 2008; Wang et al., 2006) in the mid-latitude North Atlantic. The increase in high-latitude cyclone activity was also reported in several studies of Arctic cyclone activity (Sorteberg and Walsh, 2008; Zhang et al., 2004a). There are inconsistencies among studies of extreme cyclones in reanalyses, since some studies show an increase in intensity and number of extreme Atlantic cyclones (Geng and Sugi, 2001; Paciorek et al., 2002) while others show a reduction (Gulev et al., 2001). Problems with reanalyses are particularly pronounced in the Southern Hemisphere (Hodges et al., 2003; Wang et al., 2006).

Studies using long homogenous historical records of European storminess proxies show no clear trends over the last century (Allan et al., 2009; Barring and Fortuniak, 2009; Hanna et al., 2008; Matulla et al., 2008) or the period for which reanalysis data exist (Della-Marta et al., 2009; Raible, 2007). Studies using wind proxies in the North Atlantic and Europe indicate that there is a tendency for increased storminess around 1900 and in the 1990s, while the 1960s and 1970s were periods of low storm activity (Allan et al., 2009; Wang et al., 2009). Links identified between positive (negative) NAM/NAO to stronger (weaker) Atlantic/European cyclone activity (e.g., Chang, 2009; Pinto et al., 2009) have proved to be somewhat intermittent in a long historical context due to interdecadal shifts in the location of the positions of the NAO pressure centres (Vicente-Serrano and Lopez-Moreno, 2008; Zhang et al., 2008).

In the North Pacific wintertime intense extratropical cyclone systems have increased in number and intensity since the 1950s (Graham and Diaz, 2001; Raible et al., 2008; Simmonds and Keay, 2002) with increased cyclone activity (Zhang et al., 2004a), but signs of some of the trends appeared dependent on the tracking algorithms or reanalysis products used (Raible et al., 2008). A slight positive trend has been found in North Pacific extreme cyclones (Geng and Sugi, 2001; Gulev et al., 2001; Paciorek et al., 2002). Using ship measurements, Chang (2007b) found intensity related wintertime trends in the Pacific to be about 20–60% of that found in the reanalysis. Using hourly tide gauge records at the western coast of the U.S. as a proxy for storminess, an increasing trend was observed in the extreme winter non-tide residuals over the last decades (Bromirski et al., 2003; Menendez et al., 2008). North Pacific cyclonic activity has been linked to tropical SST anomalies (NINO3.4) and PNA (Eichler and Higgins, 2006; Favre and Gershunov, 2006; Seierstad et al., 2007), showing that the PNA and NINO3.4 influence storminess, in particular over the eastern north Pacific with an equatorward shift in storm tracks in the North Pacific basin, as well as an increase of storm track activity along the U.S. East Coast during El Niño events.

Based on reanalyses North American cyclone numbers have increased over the last 50 years, with no statistically significant change in cyclone intensity (Zhang et al., 2004a). Hourly MSLP data from Canadian stations showed that winter cyclones have become significantly more frequent, longer lasting, and stronger in the lower Canadian Arctic over the last 50 years (1953–2002), but less frequent and weaker in the south, especially along the southeast and southwest Canadian coasts (Wang et al., 2006). Further south, a tendency toward weaker low-pressure systems over the past few decades was found for U.S. east coast winter cyclones using reanalyses, but no statistically significant trends in the frequency of occurrence of systems (Hirsch et al., 2001).

There are fewer studies of extratropical cyclone activity in Asia. Using ERA-40 reanalysis Wang et al., (2009) improved an algorithm by Geng and Sugi (2001) to show that the number of extratropical cyclones has significantly decreased in lower latitude regions but has increased in the higher latitudes of northern East Asia during 1958–2001. Other studies in this region using reanalyses indicate a decrease in extratropical cyclone activity (Wang et al., 2009; Zhang et al., 2004a) over the same period with a possible northward shift with increased cyclone frequency in the higher latitudes (50–45°N) and decrease in the lower latitudes (south of 45°N). The lower latitude decrease was also noted by Zou et al. (2006b) who reported a decrease in the number of severe storms for mainland China based on an analysis of extremes of observed 6-hourly pressure tendencies over the last 50 years. Variation of the annual number of cyclones in northern East Asia is associated with the mean intensity of baroclinic frontal zone, which is dominated by climate warming in the higher latitudes. Moreover, the dipole structure of extratopical cyclone change, with increases in the north and decreases in the south in northern East Asia, is related to the northward movement of a baroclinic frontal zone at either side of 110E.

In the Southern Hemisphere, studies using in situ pressure observations indicate a significant decline in storminess since the mid-19th century (Alexander and Power, 2009; [Alexander et al., 2011]), strengthening the evidence of a southward shift in storm tracks previously noted using reanalyses (Fyfe, 2003; Hope et al.,

2006). Frederiksen and Frederiksen (2007) linked the reduction in cyclogenesis at 30°S and southward shift to a decrease in the vertical mean meridional temperature gradient. Pezza et al. (2007a) confirmed previous studies using reanalysis showing a trend towards fewer and more intense low pressure systems. A study (Lim and Simmonds, 2009) using the ERA-40 reanalysis instead of the NCEP reanalysis used in previous studies, confirmed the trend towards more intense systems, but did not support the decrease in the number of cyclones seen in previous studies, emphasising the weaker consistency among reanalysis products for the Southern Hemisphere extratropical cyclones. Recent studies support the notion of more cyclones around Antarctica when the Southern Annular Mode (SAM) is in its positive phase and a shift of cyclones toward midlatitudes when the SAM is in its negative phase (Pezza and Simmonds, 2008). Additionally, more intense (and fewer) cyclones seem to occur when the Pacific Decadal Oscillation (PDO) is strongly positive and vice versa (Pezza et al., 2007b).

In summary, research subsequent to the AR4 and SREX continues to support a *likely* poleward shift of extratropical cyclones in addition to their intensification at high latitudes since the 1950s.

2.7.5 Severe Local Weather Events

Severe local weather events such as thunderstorms, tornadoes and hail storms are not well observed in many parts of the world. Evidence for changes in the number or intensity of tornadoes is more likely to reflect enhanced detection and reporting efficiency than any real trend [(Nicholls et al., 2011)]. In the light of the very strong spatial variability of small-scale severe weather phenomena, the density of surface meteorological observing stations connected to severe thunderstorm detection is too coarse to measure all such events. Moreover, homogeneity of existing station series is questionable (Doswell et al., 2005). While remote sensing techniques allow detection of thunderstorms even in remote areas, they do not always uniquely identify severe weather events from these storms.

Alternatively, measures of severe thunderstorms or hailstorms can be derived by assessing the environmental conditions that are favourable for their formation. Using this technique, [Brooks and Dotzek (2008)] found significant variability but no clear trend in the past 50 years in severe thunderstorms in a region east of the Rocky Mountains in the U.S. A decreasing trend was detected in number of thunderstorm days in China between 1970 and 2006, especially in the Tibetan Plateau and southern China (Lin and Ou, 2008). Using direct measurement of hail, Cao (2008) suggests an increasing frequency of severe hail events in Ontario, Canada during 1979–2002. Kunz et al. (2009) found that hail days significantly increased during 1974–2003 in southwest Germany. In China between 1961 and 2005, the number of hail days was found to generally decrease, with the highest occurrence in 1960s–1980s but with a sharp drop since the mid-1980s [(CMA, 2007)].

Extreme wind events, which are often associated with tropical and extratropical cyclones, thunderstorm downbursts and tornadoes, are regularly considered in this context. Wind speed thresholds are used to characterize the severity of those phenomena (e.g., the Saffir Simpson scale for tropical cyclones). Changes in wind extremes may occur from changes in the intensity or location of their associated phenomena or from others changes in the climate system (e.g., a change in local convective activity). Recent studies that have examined trends in wind extremes from observations tend to point to declining trends in extremes in mid-latitudes (Pirazzoli and Tomasin, 2003; Pryor et al., 2007; Smits et al., 2005; Zhang et al., 2007b) and increasing trends in high latitudes (Hundecha et al., 2008; Lynch et al., 2004; Turner et al., 2005). Other recent studies have compared the trends from observations with reanalysis data and reported differing or even opposite trends in the reanalysis products (e.g., McVicar et al., 2008; Smits et al., 2005). On the other hand, declining trends reported by Xu et al. (2006b) over China were generally consistent with trends in NCEP reanalysis. The accuracy of trends extracted from reanalysis products however remains a source of debate since data assimilation methods can induce artificial trends (e.g., Bengtsson et al., 2004).

These differing conclusions from the study of small scale severe weather events indicate that there is still *insufficient evidence* to determine whether robust global trends exist in these phenomena.

[START FAQ 2.2 HERE]

FAQ 2.2: Is the Climate Becoming More Extreme?

While there is evidence that increases in greenhouse gases have likely caused changes in some types of extremes, there is no simple answer to the question of whether the climate, in general, has become more or less extreme. Both the terms "more extreme" and "less extreme" can be defined in different ways, resulting in different characterizations of observed changes in extremes. Additionally, from a physical climate science perspective it is difficult to devise a comprehensive metric that encompasses all aspects of extreme behaviour in the climate.

One approach for evaluating whether the climate is becoming more extreme would be to determine whether there have been changes in the typical range of variation of specific climate variables. For example, if there was evidence that temperature variations in a given region had become significantly larger than in the past, then it would be reasonable to conclude that temperatures in that region had become more extreme. More simply, temperature variations might be considered to be becoming more extreme if the difference between the highest and the lowest temperature observed in a year is increasing. According to this approach, daily temperature over the globe may have become less extreme because there have generally been greater increases in annual minimum temperatures globally than in annual maximum temperatures, over the second half of the 20th century. On the other hand, one might conclude that daily precipitation has become more extreme because observations suggest that the magnitude of the heaviest precipitation events has increased in many parts of the world. Another approach would be to ask whether there have been significant changes in the frequency with which climate variables cross fixed thresholds that have been associated with human or other impacts. For example, an increase in the mean temperature usually results in an increase in hot extremes and a decrease in cold extremes. Such a shift in the temperature distribution would not increase the "extremeness" of day-to-day variations in temperature, but would be perceived as resulting in a more extreme warm temperature climate, and a less extreme cold temperature climate. So the answer to the question posed here would depend on the variable of interest, and on which specific measure of the extremeness of that variable is examined. As well, to provide a complete answer to the above question, one would also have to collate not just trends in single variables, but also indicators of change in complex extreme events resulting from a sequence of individual events, or the simultaneous occurrence of different types of extremes. So it would be difficult to comprehensively describe the full suite of phenomena of concern, or to find a way to synthesize all such indicators into a single extremeness metric that could be used to comprehensively assess whether the climate as a whole has become more extreme from a physical perspective. And to make such a metric useful to more than a specific location, one would have to combine the results at many locations, each with a different perspective on what is "extreme".

Three types of metrics have been considered to avoid these problems, and thereby allow an answer to this question. One approach is to count the number of record-breaking events in a variable and to examine such a count for any trend. However, one would still face the problem of what to do if, for instance, hot extremes are setting new records, while cold extremes were not occurring as frequently as in the past. In such a case counting the number of records might not indicate whether the climate was becoming more or less extreme, rather just whether there was a shift in the mean climate. Also, the question of how to combine the numbers of record-breaking events in various extremes (e.g., daily precipitation and hot temperatures) would need to be considered. Another approach is to combine indicators of a selection of important extremes into a single index, such as the Climate Extremes Index (CEI) which measures the fraction of the area of a region or country experiencing extremes in monthly mean surface temperature, daily precipitation, and drought. The CEI, however, omits many important extremes such as tropical cyclones and tornadoes, and could, therefore, not be considered a complete index of "extremeness". Nor does it take into account complex or multiple extremes, nor the varying thresholds that relate extremes to impacts in various sectors.

A third approach to solving this dilemma arises from the fact that extremes often have deleterious economic consequences. It may therefore be possible to measure the integrated economic effects of the occurrence of different types of extremes into a common instrument such as insurance payout to determine if there has been an increase or decrease in that instrument. This approach would have the value that it clearly takes into account those extremes with economic consequences. But trends in such an instrument will be dominated by changes in vulnerability and exposure and it will be difficult, if not impossible, to disentangle changes in the instrument caused by non-climatic changes in vulnerability or exposure in order to leave a residual that reflects only changes in climate extremes. For example, coastal development can increase the exposure of

populations to hurricanes; therefore, an increase in damage in coastal regions caused by hurricane landfalls will largely reflect changes in exposure and may not be indicative of increased hurricane activity. Moreover, it may not always be possible to associate impacts such as the loss of human life or damage to an ecosystem due to climate extremes to a measurable instrument.

None of the above instruments has yet been developed sufficiently as to allow us to confidently answer the question posed here. Thus we are restricted to questions about whether specific extremes are becoming more or less common, and our confidence in the answers to such questions, including the direction and magnitude of changes in specific extremes, depends on the type of extreme, as well as on the region and season, linked 1 with the level of understanding of the underlying processes and the reliability of their simulation in models.

[END FAQ 2.2 HERE]

2.8 Consistency Across Observations

[Note: consistency between sections to be discussed]

Three independently analyzed data products of the global mean surface temperature indicate that it is *virtually certain* that the world has warmed since the mid-19th century. The best estimate for the warming between 1860 and 2010 is […°C ± …°C per decade]. The rate of warming in recent decades was significantly higher [(…°C ± …°C per decade after 1980)]. In each dataset, the decade 2001–2010 was the warmest decade on record. Although far from completed, substantial efforts have been undertaken to expand and improve digital archives and to identify and adjust for data biases since the AR4.

Surface air temperatures over land have risen at about double the rate for sea surface temperature (SST) after 1979 [(…°C per decade vs. …°C per decade)], with the greatest warming during winter (December to February) and spring (March to May) in the Northern Hemisphere. Changes in extremes of temperature are consistent with the warming, showing decreases in cold extremes and increases in warm extremes.

Urban heat island effects and land use change effects are *likely* to underlie about a quarter of the observed warming trends in recent decades in areas with strong urbanization, including some regions of China. However, the available evidence (which has substantially increased since the AR4) suggests with high confidence that it is *likely* that the global land-based surface temperature trends are not biased more than about 10% by urban heat effects or land use change effects.

Based upon multiple independent analyses from weather balloons, satellites and reanalyses it can be concluded with very high confidence that it is *virtually certain* that globally the troposphere has warmed since the mid-20th century. Lower-tropospheric temperatures have slightly greater warming rates than those at the surface over the period 1958 to 2010. The satellite tropospheric temperature record is broadly consistent with surface temperature trends. The likely magnitude of uncertainty in these trends has become much more apparent since the AR4.

Four independent observing technologies consistently indicate stratospheric cooling since the mid-20th century, punctuated by episodic volcanic warmings in the low- to mid- stratosphere. Cooling of the lower stratosphere is consistently estimated to have levelled off in the past decade.

Since the AR4 more spatially complete precipitation datasets have become available, which indicate that, rather than the precipitation increase over land north of 30°N since the early 20th century and decrease in the tropics since the 1970s reported in the AR4, the land data suggest little change in precipitation since 1900. This is consistent with the most recent and comprehensive analyses of streamflow which do not support the previous notion that there has been an increasing trend in global runoff associated with global warming during the 20th century. The patterns of precipitation change are more spatially and seasonally variable than temperature change. The decrease in annual precipitation in the Sahel region of Africa continues to be significant.

On a global scale, evapotranspiration increased from the early 1980s up to the late 1990s (at a rate of 0.6 W m^{-2} per decade for the period 1982–2002). After 1998, an increase in moisture limitation in the Southern Hemisphere has acted as a constraint to further increase of global evapotranspiration.

Absolute moistening has been widespread across the globe since the 1970s, with very high confidence. However, over recent years this has abated over land, coincident with greater warming over land relative to the oceans. This has resulted in fairly widespread decreases in relative humidity over land. Note that the AR4 reported a constant relative humidity instead. Whether the decrease reported here is part of a longer term trend or merely a short lived feature remains to be seen.

Global satellite data for 1992–2010 highlight a net decrease in stratospheric water vapour, primarily related to a step-like decrease after 2001, with some increases in recent years. These observed variations are closely linked to interannual changes in tropical tropopause temperatures. The available balloon observations show significant differences from satellite observations for the overlap period, and cannot currently be explained by tropical tropopause temperatures or methane oxidation.

While there is consistency in trends of cloud cover between independent data sets in certain regions, substantial ambiguity remains in the observations of global-scale cloud variability and trends. What trends do exist are likely to be within the range of uncertainties for both satellite and observational cloud data sets.

The globally averaged atmospheric abundance of CO_2 in 2009 was 386.3 ± 0.1 ppm. From 1980 to 2009 the average rate of increase of CO_2 was 1.64 ± 0.28 ppm yr^{-1}, or about 0.43% yr^{-1}. During the past few decades most of this increase is *very likely* from fossil fuel combustion.

The globally averaged atmospheric abundance of CH_4 was 1791.3 ± 3.0 ppb in 2009. After 8 years of near-constant atmospheric burden, CH_4 began increasing again in 2007, and this increase continues through 2009. The causes of the increase are *likely* increased emissions from natural wetlands in the tropics and the Arctic because of natural variations in temperature and precipitation and increased anthropogenic emissions.

The globally averaged atmospheric abundance of N_2O in 2009 was 322.4 ± 0.2 ppb. N_2O continues to increase at an average rate of about 0.8 ppb yr^{-1}.

Kyoto Protocol gases that contain fluorine (HFCs, PFCs, and SF_6) are increasing at relatively large rates, although their contribution to total radiative forcing from LLGHGs is still small.

Atmospheric burdens of some gases whose emissions are controlled by the Montreal Protocol are decreasing (CFCs), while others (HCFCs) are increasing at relative rates from 3 to 6% yr^{-1}.

After decreasing during 2000–2005, stratospheric H_2O began increasing again in 2005, with increasingly larger rates of increase at higher altitudes.

Ground based measurements of aerosol in North America and Europe indicate with high confidence downward trends of inorganic (mainly SO_4) aerosol, in the order of -3% yr^{-1} over the last 2–3 decades. In other parts of the world, coordinated surface aerosol measurements, which started at best early 2000s, do not yet provide a clear picture regarding trends of PM2.5 or aerosol components. Long-term remote remote-sensed datasets of aerosol indicate a decrease of AOD in the US and Europe, and Japan and continuing increase over Eastern and Southern Asia since the 1980s, which is consistent with anthropogenic emission temporal trends. Our knowledge on trends from remote sensing satellite is globally low, and in some regions medium.

Several datasets in North America, Europe and Japan provide evidence that baseline surface ozone levels are increasing with about 0.3-0.5% yr^{-1} over the past decades. These increases are likely associated with changes in pre-cursor emissions on the hemispheric scale, but the drivers behind ozone trends and variability on various spatial and temporal scales are not completely understood.

New measurements suggest that the total solar irradiance, averaged over a solar cycle is roughly 5 W m^{-2} smaller than previously thought, but estimates of the magnitude of the variation in total solar irradiance associated with the solar cycle remains the same at about 1.6 W m^{-2}.

Measurements of radiation at the surface show variations in solar radiation with predominant declines from the 1950s to 1980s and partial recovery thereafter. Similar decadal variations are observed in the related climate variables sunshine duration, diurnal temperature range, and pan evaporation. These changes appear to be consistent with increasing and decreasing aerosol loading.

Evidence is emerging of increases in downward longwave radiation consistent with a warming climate. A growing body of evidence suggests that average downward longwave is 345-350 W m^{-2}, which is larger than previously thought.

Changes in the large-scale atmospheric circulation remain difficult to detect, in part because of the large variability on decadal time scales. In fact, many trend features that appeared from the 1950s to 1990s (e.g., an increase in the NAO index or a weakening of the Pacific Walker circulation) have reversed in the more recent period. The trend in the winter NAO index was 0.041 ± 0.012 s.d. per decade during the 1957–2001 period (Hurrell, 1995a) but reversed to -0.086 ± 0.039 s.d. per decade in the last two decades (1989–2011).

Several other systematic changes in large-scale atmospheric circulation could nevertheless be found, including a poleward motion of zonal mean circulation features (widening of the tropical belt, poleward shift of storm tracks and jet streams, contraction of the polar vortex) since the 1960s or 1970s and a strengthening of the SAM since the 1970s.

With respect to extremes, it is *very likely* that there has been an overall decrease in the number of unusually cold days and nights and an overall increase in the number of unusually warm days and nights on the global scale since 1950. It is *likely* that such changes have also occurred at the continental scale in North America and Europe, and *very likely* in Australia. There is *medium confidence* of a warming trend in temperature extremes in much of Asia. There is *low confidence* in trends for Africa, because of *lack of data* and studies. In South America, lack of data, and some inconsistencies between reported trends imply *low confidence* in the trends at the continental scale. It is *likely* that the number of warm spells, including heat waves, have increased since the middle of the 20th century in many (but not all) regions.

Substantial increases are found in heavy precipitation events. It is *likely* that there have been increases in the number of heavy precipitation events (e.g., 95th percentile) within many land regions, even in those where total precipitation amount has decreased, consistent with a warming climate and observed significant increasing amounts of water vapour in the atmosphere.

It is *very likely* that droughts have become more common, especially in the tropics and subtropics, since the 1970s. There is *medium confidence* that some regions have experienced more intense and longer droughts since the 1950s (e.g., Southern Europe, West Africa, East Africa) but also opposite trends exist in other regions (e.g., Central North America, Northwestern Australia). There continues to be a *lack of evidence* regarding the sign of trend in the magnitude and/or frequency of floods on a global scale although there is *high confidence* for earlier spring flow in snow-dominated regions.

There is *low confidence* that any reported long-term increases in tropical cyclone activity are robust, after accounting for past changes in observing capabilities. Research subsequent to the AR4 and SREX continues to support a *likely* poleward shift of extratropical cyclones in addition to their intensification at high latitudes since the 1950s. These differing conclusions from the study of small scale severe weather events indicate that there is still *insufficient evidence* to determine whether robust global trends exist in these phenomena.

References

Abakumova, G. M., E. V. Gorbarenko, E. I. Nezval, and O. A. Shilovtseva, 2008: Fifty years of actinometrical measurements in Moscow. *International Journal of Remote Sensing*, **29,** 2629-2665.

Ackerman, S. A., R. E. Holz, R. Frey, E. W. Eloranta, B. C. Maddux, and M. McGill, 2008: Cloud detection with MODIS. Part II: Validation. *Journal of Atmospheric and Oceanic Technology*, **25,** 1073-1086.

Adam, J. C., and D. P. Lettenmaier, 2008: Application of new precipitation and reconstructed streamflow products to streamflow trend attribution in northern Eurasia. *Journal of Climate*, **21,** 1807-1828.

Adler, R. F., et al., 2003: The version-2 global precipitation climatology project (GPCP) monthly precipitation analysis (1979-present). *Journal of Hydrometeorology*, **4,** 1147-1167.

Aguilar, E., et al., 2009: Changes in temperature and precipitation extremes in western central Africa, Guinea Conakry, and Zimbabwe, 1955-2006. *Journal of Geophysical Research-Atmospheres*, **114**.

Ajavon, A. L., P. A. Newman, J. Pyle, and A. R. Ravishankara, 2010: Scientific Assessment of ozone depletion: 2010.

Alexander, L. V., and J. M. Arblaster, 2009: Assessing trends in observed and modelled climate extremes over Australia in relation to future projections. *International Journal of Climatology*, **29,** 417-435.

Alexander, L. V., and S. Power, 2009: Severe storms inferred from 150 years of sub-daily pressure observations along Victoria's "Shipwreck Coast". *Australian Meteorological and Oceanographic Journal*, **58,** 129-133.

Alexander, L. V., et al., 2006: Global observed changes in daily climate extremes of temperature and precipitation. *Journal of Geophysical Research-Atmospheres*, **111**.

Allan, R., and T. Ansell, 2006: A new globally complete monthly historical gridded mean sea level pressure dataset (HadSLP2): 1850-2004. *Journal of Climate*, **19,** 5816-5842.

Allan, R., S. Tett, and L. Alexander, 2009: Fluctuations in autumn-winter severe storms over the British Isles: 1920 to present. *International Journal of Climatology*, **29,** 357-371.

Allan, R. P., 2009: Examination of Relationships between Clear-Sky Longwave Radiation and Aspects of the Atmospheric Hydrological Cycle in Climate Models, Reanalyses, and Observations. *Journal of Climate*, **22,** 3127-3145.

Allan, R. P., and A. Slingo, 2002: Can current climate model forcings explain the spatial and temporal signatures of decadal OLR variations? *Geophysical Research Letters*, **29,** 1141.

Allen, M. R., and W. J. Ingram, 2002: Constraints on future changes in climate and the hydrologic cycle. *Nature*, **419,** 224-+.

Allen, R. J., and S. C. Sherwood, 2007: Utility of radiosonde wind data in representing climatological variations of tropospheric temperature and baroclinicity in the western tropical Pacific. *Journal of Climate*, **20,** 5229-5243.

——, 2008: Warming maximum in the tropical upper troposphere deduced from thermal winds. *Nature Geoscience*, **1,** 399-403.

Alpert, P., and P. Kishcha, 2008: Quantification of the effect of urbanization on solar dimming. *Geophysical Research Letters*, **35,** L08801.

Alpert, P., P. Kishcha, Y. J. Kaufman, and R. Schwarzbard, 2005: Global dimming or local dimming?: Effect of urbanization on sunlight availability. *Geophysical Research Letters*, **32,** L17802.

Andreadis, K. M., and D. P. Lettenmaier, 2006: Trends in 20th century drought over the continental United States. *Geophysical Research Letters*, **33**.

Andrews, T., P. M. Forster, and J. M. Gregory, 2009: A Surface Energy Perspective on Climate Change. *Journal of Climate*, **22,** 2557-2570.

Andronova, N., J. E. Penner, and T. Wong, 2009: Observed and modeled evolution of the tropical mean radiation budget at the top of the atmosphere since 1985. *Journal of Geophysical Research-Atmospheres*, **114,** -.

Angell, J. K., 2006: Changes in the 300-mb North Circumpolar Vortex, 1963-2001. *Journal of Climate*, **19,** 2984-2994.

Anthes, R. A., et al., 2008: The COSMOC/FORMOSAT-3 - Mission early results. *Bulletin of the American Meteorological Society*, **89,** 313-+.

Archer, C. L., and K. Caldeira, 2008a: Historical trends in the jet streams. *Geophysical Research Letters*, **35**.

——, 2008b: Reply to comment by Courtenay Strong and Robert E. Davis on "Historical trends in the jet streams". *Geophysical Research Letters*, **35**.

Ashok, K., and T. Yamagata, 2009: CLIMATE CHANGE The El Nino with a difference. *Nature*, **461,** 481-+.

Ashok, K., S. K. Behera, S. A. Rao, H. Y. Weng, and T. Yamagata, 2007: El Nino Modoki and its possible teleconnection. *Journal of Geophysical Research-Oceans*, **112**.

Ballester, J., F. Giorgi, and X. Rodo, 2010: Changes in European temperature extremes can be predicted from changes in PDF central statistics. *Climatic Change*, **98,** 277-284.

Baringer, M. O., D. S. Arndt, and M. R. Johnson, 2010: STATE OF THE CLIMATE IN 2009. *Bulletin of the American Meteorological Society*, **91,** S1-+.

Barkstrom, B. R., 1984: The Earth Radiation Budget Experiment (Erbe). *Bulletin of the American Meteorological Society*, **65,** 1170-1185.

Barnett, D. N., S. J. Brown, J. M. Murphy, D. M. H. Sexton, and M. J. Webb, 2006: Quantifying uncertainty in changes in extreme event frequency in response to doubled CO_2 using a large ensemble of GCM simulations. *Climate Dynamics*, **26,** 489-511.

Barnston, A. G., and R. E. Livezey, 1987: Classification, seasonality and persistence of low-frequency atmospheric circulation patterns. *Monthly Weather Review*, **115,** 1083-1126.

Barring, L., and K. Fortuniak, 2009: Multi-indices analysis of southern Scandinavian storminess 1780-2005 and links to interdecadal variations in the NW Europe-North Sea region. *International Journal of Climatology*, **29,** 373-384.
Barrucand, M., M. Rusticucci, and W. Vargas, 2008: Temperature extremes in the south of South America in relation to Atlantic Ocean surface temperature and Southern Hemisphere circulation. *Journal of Geophysical Research-Atmospheres*, **113**.
Bartholy, J., and R. Pongracz, 2007: Regional analysis of extreme temperature and precipitation indices for the Carpathian Basin from 1946 to 2001. *Global and Planetary Change*, **57,** 83-95.
Barton, N. P., and A. W. Ellis, 2009: Variability in wintertime position and strength of the North Pacific jet stream as represented by re-analysis data. *International Journal of Climatology*, **29,** 851-862.
Baumer, D., and B. Vogel, 2007: An unexpected pattern of distinct weekly periodicities in climatological variables in Germany. *Geophysical Research Letters*, **34**.
Beig, G., and V. Singh, 2007: Trends in tropical tropospheric column ozone from satellite data and MOZART model. *Geophys. Res. Lett.*, **34,** L17801.
Bell, G. D., and M. S. Halpert, 1998: Climate assessment for 1997. *Bulletin of the American Meteorological Society*, **79,** S1-S50.
Bengtsson, L., and K. I. Hodges, 2011: On the evaluation of temperature trends in the tropical troposphere. *Climate Dynamics*, **36,** 419-430.
Bengtsson, L., S. Hagemann, and K. I. Hodges, 2004: Can climate trends be calculated from reanalysis data? *Journal of Geophysical Research-Atmospheres*, **109**.
Beniston, M., 2009: Decadal-scale changes in the tails of probability distribution functions of climate variables in Switzerland. *International Journal of Climatology*, **29,** 1362-1368.
Benito, G., T. Ouarda, and A. Bardossy, 2005: Applications of palaeoflood hydrology and historical data in flood risk analysis. *Journal of Hydrology*, **313,** 1-2.
Berry, D. I., and E. C. Kent, 2009: A NEW AIR-SEA INTERACTION GRIDDED DATASET FROM ICOADS WITH UNCERTAINTY ESTIMATES. *Bulletin of the American Meteorological Society*, **90,** 645-+.
Berry, D. I., E. C. Kent, and P. K. Taylor, 2004: An analytical model of heating errors in marine air temperatures from ships. *Journal of Atmospheric and Oceanic Technology*, **21,** 1198-1215.
Betts, A. K., J. H. Ball, and P. Viterbo, 2003: Evaluation of the ERA-40 surface water budget and surface temperature for the Mackenzie River basin. *Journal of Hydrometeorology*, **4,** 1194-1211.
Birner, T., 2010: Recent widening of the tropical belt from global tropopause statistics: Sensitivities. *Journal of Geophysical Research-Atmospheres*, **115**.
Bitz, C. M., and Q. Fu, 2008: Arctic warming aloft is data set dependent. *Nature*, **455,** E3-E4.
Boden, T. A., G. Marland, and R. J. Andres: Global, Regional, and National Fossil-Fuel CO_2 Emissions.
Bonisch, H., A. Engel, J. Curtius, T. Birner, and P. Hoor, 2009: Quantifying transport into the lowermost stratosphere using simultaneous in-situ measurements of SF6 and CO_2. *Atmospheric Chemistry and Physics*, **9,** 5905-5919.
Bosilovich, M., 2008: NASA's Modern Era Retrospective-analysis for Research and Applications: Integrating Earth Observations. Earthzine, http://www.earthzine.org/2008/2009/2026/nasas-modern-era-retrospective-analysis/.
Bousquet, P., 2011: Source attribution of the changes in atmospheric methane for 2006–2008. *Atmos. Chem. Phys. Discuss.*, **10,** 27603-27630.
Bouwman, A. F., K. W. VanderHoek, and J. G. J. Olivier, 1995: Uncertainties in the global source distribution of nitrous-oxide. *Journal of Geophysical Research-Atmospheres***,** 2785-2800.
Brogniez, H., R. Roca, and L. Picon, 2009: Study of the Free Tropospheric Humidity Interannual Variability Using Meteosat Data and an Advection-Condensation Transport Model. *Journal of Climate*, **22,** 6773-6787.
Brohan, P., J. J. Kennedy, I. Harris, S. F. B. Tett, and P. D. Jones, 2006: Uncertainty estimates in regional and global observed temperature changes: A new data set from 1850. *Journal of Geophysical Research-Atmospheres*, **111**.
Brohan, P., R. Allan, J. E. Freeman, A. M. Waple, D. Wheeler, C. Wilkinson, and S. Woodruff, 2009: MARINE OBSERVATIONS OF OLD WEATHER. *Bulletin of the American Meteorological Society*, **90,** 219-+.
Bromirski, P. D., R. E. Flick, and D. R. Cayan, 2003: Storminess variability along the California coast: 1858-2000. *Journal of Climate*, **16,** 982-993.
Bronnimann, S., et al., 2009: Variability of large-scale atmospheric circulation indices for the northern hemisphere during the past 100 years. *Meteorologische Zeitschrift*, **18,** 379-396.
Brown, S. J., J. Caesar, and C. A. T. Ferro, 2008: Global changes in extreme daily temperature since 1950. *Journal of Geophysical Research-Atmospheres*, **113**.
Brownscombe, J. L., J. Nash, G. Vaughan, and C. F. Rogers, 1985: SOLAR TIDES IN THE MIDDLE ATMOSPHERE .1. DESCRIPTION OF SATELLITE-OBSERVATIONS AND COMPARISON WITH THEORETICAL CALCULATIONS AT EQUINOX. *Quarterly Journal of the Royal Meteorological Society*, **111,** 677-689.
Bunge, L., and A. J. Clarke, 2009: A Verified Estimation of the El Nino Index Nino-3.4 since 1877. *Journal of Climate*, **22,** 3979-3992.
Butler, J. J., B. C. Johnson, J. P. Rice, E. L. Shirley, and R. A. Barnes, 2008: Sources of Differences in On-Orbital Total Solar Irradiance Measurements and Description of a Proposed Laboratory Intercomparison. *Journal of Research of the National Institute of Standards and Technology*, **113,** 187-203.

Caesar, J., L. Alexander, and R. Vose, 2006: Large-scale changes in observed daily maximum and minimum temperatures: Creation and analysis of a new gridded data set. *Journal of Geophysical Research-Atmospheres*, **111**.

Canada, 2011: Canadian Smog Science Assessment - Highlights and Key Messages., tbd pp.

Canadell, J., et al., 2007: Contributions to accelerating atmospheric CO_2 growth from economic activity, carbon intensity, and efficiency of natural sinks. *Proceedings of the National Academy of Sciences of the United States of America*, 18866-18870.

Cane, M. A., S. E. Zebiak, and S. C. Dolan, 1986: Experimental forecasts of El Nino. *Nature*, **321,** 827-832.

Cao, Z. H., 2008: Severe hail frequency over Ontario, Canada: Recent trend and variability. *Geophysical Research Letters*, **35**.

Cardone, V. J., J. G. Greenwood, and M. A. Cane, 1990: ON TRENDS IN HISTORICAL MARINE WIND DATA. *Journal of Climate*, **3,** 113-127.

CASTNET, 2010: Clean Air Status and Trends Network (CASTNET) 2008 Annual Report, 80 pp.

Cavazos, T., C. Turrent, and D. P. Lettenmaier, 2008: Extreme precipitation trends associated with tropical cyclones in the core of the North American monsoon. *Geophysical Research Letters*, **35**.

Cayan, D. R., S. A. Kammerdiener, M. D. Dettinger, J. M. Caprio, and D. H. Peterson, 2001: Changes in the onset of spring in the western United States. *Bulletin of the American Meteorological Society*, **82,** 399-415.

Cermak, J., M. Wild, R. Knutti, M. I. Mishchenko, and A. K. Heidinger, 2010: Consistency of global satellite-derived aerosol and cloud data sets with recent brightening observations. *Geophys. Res. Lett.*, **37,** L21704.

Chan, J. C. L., and M. Xu, 2009: Inter-annual and inter-decadal variations of landfalling tropical cyclones in East Asia. Part I: time series analysis. *International Journal of Climatology*, **29,** 1285-1293.

Chang, E. K. M., 2007a: Assessing the increasing trend in Northern Hemisphere winter storm track activity using surface ship observations and a statistical storm track model. *Journal of Climate*, **20,** 5607-5628.

——, 2007b: Assessing the increasing trend in Northern Hemisphere winter storm track activity using surface ship observations and a statistical storm track model. *Journal of Climate*, **20,** 5607-5628.

——, 2009: Are band-pass variance statistics useful measures of storm track activity? Re-examining storm track variability associated with the NAO using multiple storm track measures. *Climate Dynamics*, **33,** 277-296.

Chang, E. K. M., and Y. J. Guo, 2007: Is the number of North Atlantic tropical cyclones significantly underestimated prior to the availability of satellite observations? *Geophysical Research Letters*, **34**.

Che, H. Z., et al., 2005: Analysis of 40 years of solar radiation data from China, 1961-2000. *Geophysical Research Letters*, **32,** L06803.

Chen, J. Y., B. E. Carlson, and A. D. Del Genio, 2002: Evidence for strengthening of the tropical general circulation in the 1990s. *Science*, **295,** 838-841.

Chen, J. Y., A. D. Del Genio, B. E. Carlson, and M. G. Bosilovich, 2008: The spatiotemporal structure of twentieth-century climate variations in observations and reanalyses. Part I: Long-term trend. *Journal of Climate*, **21,** 2611-2633.

Chiacchio, M., and M. Wild, 2010: Influence of NAO and clouds on long-term seasonal variations of surface solar radiation in Europe. *Journal of Geophysical Research-Atmospheres*, **115,** D00d22.

Choi, G., et al., 2009: Changes in means and extreme events of temperature and precipitation in the Asia-Pacific Network region, 1955-2007. *International Journal of Climatology*, **29,** 1906-1925.

Christy, J. R., and R. T. McNider, 1994: SATELLITE GREENHOUSE SIGNAL. *Nature*, **367,** 325-325.

Christy, J. R., and W. B. Norris, 2006: Satellite and VIZ-radiosonde intercomparisons for diagnosis of nonclimatic influences. *Journal of Atmospheric and Oceanic Technology*, **23,** 1181-1194.

——, 2009: Discontinuity Issues with Radiosonde and Satellite Temperatures in the Australian Region 1979-2006. *Journal of Atmospheric and Oceanic Technology*, **26,** 508-522.

Christy, J. R., R. W. Spencer, and W. B. Norris, 2011: The role of remote sensing in monitoring global bulk tropospheric temperatures. *International Journal of Remote Sensing*, **32,** 671-685.

Christy, J. R., W. B. Norris, R. W. Spencer, and J. J. Hnilo, 2007: Tropospheric temperature change since 1979 from tropical radiosonde and satellite measurements. *Journal of Geophysical Research-Atmospheres*, **112**.

Christy, J. R., R. W. Spencer, W. B. Norris, W. D. Braswell, and D. E. Parker, 2003: Error estimates of version 5.0 of MSU-AMSU bulk atmospheric temperatures. *Journal of Atmospheric and Oceanic Technology*, **20,** 613-629.

Christy, J. R., Herman, B, Pielke, R., Klotzbach, P., McNider, R. T., Hnilo, J. J., Spencer, R. W., Chase, T., Douglass, D., 2010: What do observational datasets say about modeled tropospheric temperature trends since 1979? , 2148-2169.

Chung, E. S., and B. J. Soden, 2010: Investigating the Influence of Carbon Dioxide and the Stratosphere on the Long-Term Tropospheric Temperature Monitoring from HIRS. *Journal of Applied Meteorology and Climatology*, **49,** 1927-1937.

Chung, E. S., B. J. Soden, and B. J. Sohn, 2010a: Revisiting the determination of climate sensitivity from relationships between surface temperature and radiative fluxes. *Geophysical Research Letters*, **37**.

Chung, E. S., D. Yeomans, and B. J. Soden, 2010b: An assessment of climate feedback processes using satellite observations of clear-sky OLR. *Geophysical Research Letters*, **37**.

Clark, R. T., S. J. Brown, and J. M. Murphy, 2006: Modeling northern hemisphere summer heat extreme changes and their uncertainties using a physics ensemble of climate sensitivity experiments. *Journal of Climate*, **19,** 4418-4435.
Clarke, A. D., and V. N. Kapustin, 2002: A Pacific Aerosol Survey. Part I: A Decade of Data on Particle Production, Transport, Evolution, and Mixing in the Troposphere*. *Journal of the Atmospheric Sciences*, **59,** 363-382.
Clement, A. C., and B. Soden, 2005: The sensitivity of the tropical-mean radiation budget. *Journal of Climate*, **18,** 3189-3203.
Clement, A. C., R. Burgman, and J. R. Norris, 2009: Observational and Model Evidence for Positive Low-Level Cloud Feedback. *Science*, **325,** 460-464.
Cluis, D., and C. Laberge, 2001: Climate change and trend detection in selected rivers within the Asia-Pacific region. *Water International*, **26,** 411-424.
CMA, 2007: Atlas of China disastrous weather and climate.
Cohen, J., M. Barlow, and K. Saito, 2009: Decadal Fluctuations in Planetary Wave Forcing Modulate Global Warming in Late Boreal Winter. *Journal of Climate*, **22,** 4418-4426.
Compo, G. P., et al., 2011: The Twentieth Century Reanalysis Project. *Q. J. Roy. Meteorol. Soc.*, **137,** 1-28.
Cooper, O. R., et al., 2010: Increasing springtime ozone mixing ratios in the free troposphere over western North America. *Nature*, **463,** 344-348.
Copsey, D., R. Sutton, and J. R. Knight, 2006: Recent trends in sea level pressure in the Indian Ocean region. *Geophysical Research Letters*, **33**.
Costa, A. C., and A. Soares, 2009: Trends in extreme precipitation indices derived from a daily rainfall database for the South of Portugal. *International Journal of Climatology*, **29,** 1956-1975.
Cowell, C. M., and R. T. Stoudt, 2002: Dam-induced modifications to upper Allegheny River streamflow patterns and their biodiversity implications. *Journal of the American Water Resources Association*, **38,** 187-196.
Croci-Maspoli, M., C. Schwierz, and H. C. Davies, 2007a: A multifaceted climatology of atmospheric blocking and its recent linear trend. *Journal of Climate*, **20,** 633-649.
——, 2007b: Atmospheric blocking: space-time links to the NAO and PNA. *Climate Dynamics*, **29,** 713-725.
Crutzen, P., A. Mosier, K. Smith, and W. Winiwarter, 2008: N2O release from agro-biofuel production negates global warming reduction by replacing fossil fuels. *Atmospheric Chemistry and Physics***,** 389-395.
Cueto, R. O. G., A. T. Martinez, and E. J. Ostos, 2010: Heat waves and heat days in an arid city in the northwest of M,xico: current trends and in climate change scenarios. *International Journal of Biometeorology*, **54,** 335-345.
Cunderlik, J. M., and T. Ouarda, 2009: Trends in the timing and magnitude of floods in Canada. *Journal of Hydrology*, **375,** 471-480.
Cutforth, H. W., and D. Judiesch, 2007: Long-term changes to incoming solar energy on the Canadian Prairie. *Agricultural and Forest Meteorology*, **145,** 167-175.
Dai, A., 2006: Recent climatology, variability, and trends in global surface humidity. *Journal of Climate*, **19,** 3589-3606.
Dai, A., K. E. Trenberth, and T. T. Qian, 2004: A global dataset of Palmer Drought Severity Index for 1870-2002: Relationship with soil moisture and effects of surface warming. *Journal of Hydrometeorology*, **5,** 1117-1130.
Dai, A., T. T. Qian, K. E. Trenberth, and J. D. Milliman, 2009: Changes in Continental Freshwater Discharge from 1948 to 2004. *Journal of Climate*, **22,** 2773-2792.
de Laat, A. T. J., I. Aben, and G. J. Roelofs, 2005: A model perspective on total tropospheric O3 column variability and implications for satellite observations. *J. Geophys. Res.*, **110,** D13303.
de Meij, A., A. Pozzer, and J. Lelieveld, 2010: Global and regional trends in aerosol optical depth based on remote sensing products and pollutant emission estimates between 2000 and 2009. *Atmos. Chem. Phys. Discuss.*, **10,** 30731-30776.
Deeds, D., et al., 2008: Evidence for crustal degassing of CF4 and SF6 in Mojave Desert groundwaters. *Geochimica Et Cosmochimica Acta***,** 999-1013.
DeGaetano, A. T., 2009: Time-Dependent Changes in Extreme-Precipitation Return-Period Amounts in the Continental United States. *Journal of Applied Meteorology and Climatology*, **48,** 2086-2099.
Delgado, J. M., H. Apel, and B. Merz, 2010: Flood trends and variability in the Mekong river. *Hydrology and Earth System Sciences*, **14,** 407-418.
Della-Marta, P. M., M. R. Haylock, J. Luterbacher, and H. Wanner, 2007a: Doubled length of western European summer heat waves since 1880. *Journal of Geophysical Research-Atmospheres*, **112**.
Della-Marta, P. M., J. Luterbacher, H. von Weissenfluh, E. Xoplaki, M. Brunet, and H. Wanner, 2007b: Summer heat waves over western Europe 1880-2003, their relationship to large-scale forcings and predictability. *Climate Dynamics*, **29,** 251-275.
Della-Marta, P. M., H. Mathis, C. Frei, M. A. Liniger, J. Kleinn, and C. Appenzeller, 2009: The return period of wind storms over Europe. *International Journal of Climatology*, **29,** 437-459.
Deser, C., and J. M. Wallace, 1990: Large-scale atmospheric circulation features of warm and cold episodes in the tropical Pacific. *Journal of Climate*, **3,** 1254-1281.
Deser, C., A. S. Phillips, and M. A. Alexander, 2010a: Twentieth century tropical sea surface temperature trends revisited. *Geophysical Research Letters*, **37**.

Deser, C., M. A. Alexander, S. P. Xie, and A. S. Phillips, 2010b: Sea Surface Temperature Variability: Patterns and Mechanisms. *Annual Review of Marine Science*, **2,** 115-143.
Dessler, A. E., 2010: A Determination of the Cloud Feedback from Climate Variations over the Past Decade. *Science*, **330,** 1523-1527.
Dessler, A. E., Z. Zhang, and P. Yang, 2008: Water-vapor climate feedback inferred from climate fluctuations, 2003-2008. *Geophysical Research Letters*, **35**.
Diffenbaugh, N. S., J. S. Pal, F. Giorgi, and X. J. Gao, 2007: Heat stress intensification in the Mediterranean climate change hotspot. *Geophysical Research Letters*, **34**.
Ding, T., W. H. Qian, and Z. W. Yan, 2010: Changes in hot days and heat waves in China during 1961-2007. *International Journal of Climatology*, **30,** 1452-1462.
Dlugokencky, E., et al., 2009: Observational constraints on recent increases in the atmospheric CH4 burden. *Geophysical Research Letters***,** -.
Dong, L., T. J. Vogelsang, and S. J. Colucci, 2008: Interdecadal trend and ENSO-related interannual variability in Southern Hemisphere blocking. *Journal of Climate*, **21,** 3068-3077.
Donlon, C., et al., 2007: The global ocean data assimilation experiment high-resolution sea surface temperature pilot project. *Bulletin of the American Meteorological Society*, **88,** 1197-1213.
Doswell, C. A., H. E. Brooks, and M. P. Kay, 2005: Climatological estimates of daily local nontornadic severe thunderstorm probability for the United States. *Weather and Forecasting*, **20,** 577-595.
Douglass, A., et al., 2008a: Relationship of loss, mean age of air and the distribution of CFCs to stratospheric circulation and implications for atmospheric lifetimes. *Journal of Geophysical Research-Atmospheres***,** -.
Douglass, D. H., J. R. Christy, B. D. Pearson, and S. F. Singer, 2008b: A comparison of tropical temperature trends with model predictions. *International Journal of Climatology*, **28,** 1693-1701.
Duan, A. M., and G. X. Wu, 2006: Change of cloud amount and the climate warming on the Tibetan Plateau. *Geophysical Research Letters*, **33**.
Dufek, A. S., and T. Ambrizzi, 2008: Precipitation variability in Sao Paulo State, Brazil. *Theoretical and Applied Climatology*, **93,** 167-178.
Durao, R. M., M. J. Pereira, A. C. Costa, J. Delgado, G. del Barrio, and A. Soares, 2010: Spatial-temporal dynamics of precipitation extremes in southern Portugal: a geostatistical assessment study. *International Journal of Climatology*, **30,** 1526-1537.
Durre, I., C. N. Williams, X. G. Yin, and R. S. Vose, 2009: Radiosonde-based trends in precipitable water over the Northern Hemisphere: An update. *Journal of Geophysical Research-Atmospheres*, **114**.
Durre, I., M. J. Menne, B. E. Gleason, T. G. Houston, and R. S. Vose, 2010: Comprehensive Automated Quality Assurance of Daily Surface Observations. *Journal of Applied Meteorology and Climatology*, **49,** 1615-1633.
Dutton, E. G., D. W. Nelson, R. S. Stone, D. Longenecker, G. Carbaugh, J. M. Harris, and J. Wendell, 2006: Decadal variations in surface solar irradiance as observed in a globally remote network. *Journal of Geophysical Research-Atmospheres*, **111,** D19101.
EANET, 2011: EANET Data Report on the Acid Deposition in the East Asian Region 2009.
Eichler, T., and W. Higgins, 2006: Climatology and ENSO-related variability of North American extratropical cyclone activity. *Journal of Climate*, **19,** 2076-2093.
Elsner, J. B., J. P. Kossin, and T. H. Jagger, 2008: The increasing intensity of the strongest tropical cyclones. *Nature*, **455,** 92-95.
Emanuel, K., 2007: Environmental factors affecting tropical cyclone power dissipation. *Journal of Climate*, **20,** 5497-5509.
EMEP, 2010: EMEP Status report 4/2010, Transboundary Particulate Matter in Europe.
Endo, N., and T. Yasunari, 2006: Changes in low cloudiness over China between 1971 and 1996. *Journal of Climate*, **19,** 1204-1213.
Enfield, D. B., A. M. Mestas-Nunez, and P. J. Trimble, 2001: The Atlantic multidecadal oscillation and its relation to rainfall and river flows in the continental US. *Geophysical Research Letters*, **28,** 2077-2080.
Engel, A., et al., 2009: Age of stratospheric air unchanged within uncertainties over the past 30 years. *Nature Geoscience*, **2,** 28-31.
Etheridge, D., L. Steele, R. Francey, and R. Langenfelds, 1998: Atmospheric methane between 1000 AD and present: Evidence of anthropogenic emissions and climatic variability. *Journal of Geophysical Research-Atmospheres***,** 15979-15993.
Etheridge, D. M., L. P. Steele, R. L. Langenfelds, R. J. Francey, J. M. Barnola, and V. I. Morgan, 1996: Natural and anthropogenic changes in atmospheric CO_2 over the last 1000 years from air in Antarctic ice and firn. *Journal of Geophysical Research-Atmospheres***,** 4115-4128.
Evan, A. T., A. K. Heidinger, and D. J. Vimont, 2007: Arguments against a physical long-term trend in global ISCCP cloud amounts. *Geophysical Research Letters*, **34,** L04701.
Fall, S., D. Niyogi, A. Gluhovsky, R. A. Pielke, E. Kalnay, and G. Rochon, 2010: Impacts of land use land cover on temperature trends over the continental United States: assessment using the North American Regional Reanalysis. *International Journal of Climatology*, **30,** 1980-1993.
Favre, A., and A. Gershunov, 2006: Extra-tropical cyclonic/anticyclonic activity in North-Eastern Pacific and air temperature extremes in Western North America. *Climate Dynamics*, **26,** 617-629.

Feister, W., and W. Warmbt, 1987: Long-term measurements of surface ozone in the German Democratic Republic. *Journal of Atmospheric Chemistry*, **5,** 1-21.
Fekete, B. M., C. J. Vorosmarty, and W. Grabs, 2002: High-resolution fields of global runoff combining observed river discharge and simulated water balances. *Global Biogeochemical Cycles*, **16**.
Ferranti, L., and P. Viterbo, 2006: The European summer of 2003: Sensitivity to soil water initial conditions. *Journal of Climate***,** 3659-3680.
Ferretti, D., et al., 2005: Unexpected changes to the global methane budget over the past 2000 years. *Science***,** 1714-1717.
Fischer, E. M., and C. Schar, 2010: Consistent geographical patterns of changes in high-impact European heatwaves. *Nature Geoscience*, **3,** 398-403.
Fischer, E. M., S. I. Seneviratne, D. Luthi, and C. Schar, 2007a: Contribution of land-atmosphere coupling to recent European summer heat waves. *Geophysical Research Letters*, **34**.
Fischer, E. M., S. I. Seneviratne, P. L. Vidale, D. Luthi, and C. Schar, 2007b: Soil moisture - Atmosphere interactions during the 2003 European summer heat wave. *Journal of Climate*, **20,** 5081-5099.
Foelsche, U., B. Pirscher, M. Borsche, G. Kirchengast, and J. Wickert, 2009: Assessing the Climate Monitoring Utility of Radio Occultation Data: From CHAMP to FORMOSAT-3/COSMIC. *Terrestrial Atmospheric and Oceanic Sciences*, **20,** 155-170.
Fogt, R. L., J. Perlwitz, A. J. Monaghan, D. H. Bromwich, J. M. Jones, and G. J. Marshall, 2009: Historical SAM Variability. Part II: Twentieth-Century Variability and Trends from Reconstructions, Observations, and the IPCC AR4 Models. *Journal of Climate*, **22,** 5346-5365.
Folland, C. K., and D. E. Parker, 1995: CORRECTION OF INSTRUMENTAL BIASES IN HISTORICAL SEA-SURFACE TEMPERATURE DATA. *Quarterly Journal of the Royal Meteorological Society*, **121,** 319-367.
Folland, C. K., D. E. Parker, A. Colman, and W. R., 1999: Large scale modes of ocean surface temperature since the late nineteenth century. *Beyond El Nino: Decadal and Interdecadal Climate Variability*, A. Navarra, Ed., Springer-Verlag, 73-102.
Forster, P. M., et al., 2011: Stratospheric changes and climate, Chapter 4 in Scientific Assessment of Ozone Depletion: 2010, Global Ozone Research and Monitoring Project–Report No. 52 (in press).
Fowler, D., R. Smith, J. Muller, N. Cape, M. Sutton, J. W. Erisman, and H. Fagerli, 2007: Long Term Trends in Sulphur and Nitrogen Deposition in Europe and the Cause of Non-linearities. *Water Air Soil Pollution*, **7,** 41–47.
Frankenberg, C., 2011: Global column-averaged methane mixing ratios from 2003 to 2009 as derived from SCIAMACHY: Trends and variability. *J. Geophys. Res.*, **116**.
Frauenfeld, O. W., and R. E. Davis, 2003: Northern Hemisphere circumpolar vortex trends and climate change implications. *Journal of Geophysical Research-Atmospheres*, **108**.
Frederiksen, J. S., and C. S. Frederiksen, 2007: Interdecadal changes in southern hemisphere winter storm track modes. *Tellus Series a-Dynamic Meteorology and Oceanography*, **59,** 599-617.
Free, M., and D. J. Seidel, 2005: Causes of differing temperature trends in radiosonde upper air data sets. *Journal of Geophysical Research-Atmospheres*, **110**.
Free, M., D. J. Seidel, J. K. Angell, J. Lanzante, I. Durre, and T. C. Peterson, 2005: Radiosonde Atmospheric Temperature Products for Assessing Climate (RATPAC): A new data set of large-area anomaly time series. *Journal of Geophysical Research-Atmospheres*, **110**.
Fu, G. B., S. P. Charles, and J. J. Yu, 2009a: A critical overview of pan evaporation trends over the last 50 years. *Climatic Change*, **97,** 193-214.
Fu, G. B., S. P. Charles, J. J. Yu, and C. M. Liu, 2009b: Decadal Climatic Variability, Trends, and Future Scenarios for the North China Plain. *Journal of Climate*, **22,** 2111-2123.
Fu, Q., C. M. Johanson, S. G. Warren, and D. J. Seidel, 2004: Contribution of stratospheric cooling to satellite-inferred tropospheric temperature trends. *Nature*, **429,** 55-58.
Fu, Q., C. M. Johanson, J. M. Wallace, and T. Reichler, 2006: Enhanced mid-latitude tropospheric warming in satellite measurements. *Science*, **312,** 1179-1179.
Fueglistaler, S., and P. H. Haynes, 2005: Control of interannual and longer-term variability of stratospheric water vapor. *Journal of Geophysical Research-Atmospheres*, **110**.
Fueglistaler, S., A. E. Dessler, T. J. Dunkerton, I. Folkins, Q. Fu, and P. W. Mote, 2009: TROPICAL TROPOPAUSE LAYER. *Reviews of Geophysics*, **47**.
Fujibe, F., 2009: Detection of urban warming in recent temperature trends in Japan. *International Journal of Climatology*, **29,** 1811-1822.
Fujiwara, M., et al., 2010: Seasonal to decadal variations of water vapor in the tropical lower stratosphere observed with balloon-borne cryogenic frost point hygrometers. *Journal of Geophysical Research-Atmospheres*, **115**.
Fyfe, J. C., 2003: Extratropical southern hemisphere cyclones: Harbingers of climate change? *Journal of Climate*, **16,** 2802-2805.
Gedney, N., P. M. Cox, R. A. Betts, O. Boucher, C. Huntingford, and P. A. Stott, 2006: Detection of a direct carbon dioxide effect in continental river runoff records. *Nature*, **439,** 835-838.
Geng, Q. Z., and M. Sugi, 2001: Variability of the North Atlantic cyclone activity in winter analyzed from NCEP-NCAR reanalysis data. *Journal of Climate*, **14,** 3863-3873.

Gettelman, A., and Q. Fu, 2008: Observed and simulated upper-tropospheric water vapor feedback. *Journal of Climate*, **21,** 3282-3289.
Gilgen, H., A. Roesch, M. Wild, and A. Ohmura, 2009: Decadal changes in shortwave irradiance at the surface in the period from 1960 to 2000 estimated from Global Energy Balance Archive Data. *Journal of Geophysical Research-Atmospheres*, **114,** D00d08.
Gillett, N. P., and P. A. Stott, 2009: Attribution of anthropogenic influence on seasonal sea level pressure. *Geophysical Research Letters*, **36**.
Gleason, K. L., J. H. Lawrimore, D. H. Levinson, T. R. Karl, and D. J. Karoly, 2008: A revised US Climate Extremes Index. *Journal of Climate*, **21,** 2124-2137.
Gloor, M., J. Sarmiento, and N. Gruber, 2010: What can be learned about carbon cycle climate feedbacks from the CO_2 airborne fraction? *Atmospheric Chemistry and Physics***,** 7739-7751.
Gong, D. Y., and S. W. Wang, 1999: Definition of Antarctic Oscillation Index. *Geophysical Research Letters*, **26,** 459-462.
Graham, N. E., and H. F. Diaz, 2001: Evidence for intensification of North Pacific winter cyclones since 1948. *Bulletin of the American Meteorological Society*, **82,** 1869-1893.
Grant, A. N., S. Bronnimann, and L. Haimberger, 2008: Recent Arctic warming vertical structure contested. *Nature*, **455,** E2-E3.
Graversen, R. G., T. Mauritsen, M. Tjernstrom, E. Kallen, and G. Svensson, 2008: Vertical structure of recent Arctic warming. *Nature*, **451,** 53-U54.
Grody, N. C., K. Y. Vinnikov, M. D. Goldberg, J. T. Sullivan, and J. D. Tarpley, 2004: Calibration of multisatellite observations for climatic studies: Microwave Sounding Unit (MSU). *Journal of Geophysical Research-Atmospheres*, **109**.
Groisman, P. Y., R. W. Knight, T. R. Karl, D. R. Easterling, B. M. Sun, and J. H. Lawrimore, 2004: Contemporary changes of the hydrological cycle over the contiguous United States: Trends derived from in situ observations. *Journal of Hydrometeorology*, **5,** 64-85.
Gruber, C., and L. Haimberger, 2008: On the homogeneity of radiosonde wind time series. *Meteorologische Zeitschrift*, **17,** 631-643.
Gu, G. J., R. F. Adler, G. J. Huffman, and S. Curtis, 2007: Tropical rainfall variability on interannual-to-interdecadal and longer time scales derived from the GPCP monthly product. *Journal of Climate*, **20,** 4033-4046.
Gulev, S., T. Jung, and E. Ruprecht, 2007: Estimation of the impact of sampling errors in the VOS observations on air-sea fluxes. Part II: Impact on trends and interannual variability. *Journal of Climate*, **20,** 302-315.
Gulev, S. K., O. Zolina, and S. Grigoriev, 2001: Extratropical cyclone variability in the Northern Hemisphere winter from the NCEP/NCAR reanalysis data. *Climate Dynamics*, **17,** 795-809.
Guo, H., M. Xu, and Q. Hub, 2010: Changes in near-surface wind speed in China: 1969–2005. *Int. J. Climatol.*
Haimberger, L., 2004: Checking the temporal homogeneity of radiosonde data in the Alpine region using ERA-40 analysis feedback data. *Meteorologische Zeitschrift*, **13,** 123-129.
——, 2007: Homogenization of radiosonde temperature time series using innovation statistics. *Journal of Climate*, **20,** 1377-1403.
Haimberger, L., C. Tavolato, and S. Sperka, 2008: Toward elimination of the warm bias in historic radiosonde temperature records - Some new results from a comprehensive intercomparison of upper-air data. *Journal of Climate*, **21,** 4587-4606.
Hajj, G. A., et al., 2004: CHAMP and SAC-C atmospheric occultation results and intercomparisons. *Journal of Geophysical Research-Atmospheres*, **109**.
Hanna, E., J. Cappelen, R. Allan, T. Jonsson, F. Le Blancq, T. Lillington, and K. Hickey, 2008: New Insights into North European and North Atlantic Surface Pressure Variability, Storminess, and Related Climatic Change since 1830. *Journal of Climate*, **21,** 6739-6766.
Hansen, J., R. Ruedy, M. Sato, and K. Lo, 2010: GLOBAL SURFACE TEMPERATURE CHANGE. *Reviews of Geophysics*, **48**.
Hansen, J., et al., 2001: A closer look at United States and global surface temperature change. *Journal of Geophysical Research-Atmospheres*, **106,** 23947-23963.
Harder, J. W., J. M. Fontenla, P. Pilewskie, E. C. Richard, and T. N. Woods, 2009: Trends in solar spectral irradiance variability in the visible and infrared. *Geophysical Research Letters*, **36,** -.
Harries, J. E., and J. M. Futyan, 2006: On the stability of the Earth's radiative energy balance: Response to the Mt. Pinatubo eruption. *Geophysical Research Letters*, **33**.
Hatzianastassiou, N., C. Matsoukas, A. Fotiadi, K. G. Pavlakis, E. Drakakis, D. Hatzidimitriou, and I. Vardavas, 2005: Global distribution of Earth's surface shortwave radiation budget. *Atmospheric Chemistry and Physics*, **5,** 2847-2867.
Heidinger, A. K., and M. J. Pavolonis, 2009: Gazing at Cirrus Clouds for 25 Years through a Split Window. Part I: Methodology. *Journal of Applied Meteorology and Climatology*, **48,** 1100-1116.
Hidy, G. M., and G. T. Pennell, 2010: Multipollutant Air Quality Management: 2010 Critical Review. *J. Air & Waste Management Assocciation*, **60, DOI:10.3155/1047-3289.60.6.645,** 645–674.

Hinkelman, L. M., P. W. Stackhouse, B. A. Wielicki, T. P. Zhang, and S. R. Wilson, 2009: Surface insolation trends from satellite and ground measurements: Comparisons and challenges. *Journal of Geophysical Research-Atmospheres*, **114,** D00d20.

Hirsch, A., A. Michalak, L. Bruhwiler, W. Peters, E. Dlugokencky, and P. Tans, 2006: Inverse modeling estimates of the global nitrous oxide surface flux from 1998-2001. *Global Biogeochemical Cycles*, **-**.

Hirsch, M. E., A. T. DeGaetano, and S. J. Colucci, 2001: An East Coast winter storm climatology. *Journal of Climate*, **14,** 882-899.

Hirschi, M., et al., 2011: Observational evidence for soil-moisture impact on hot extremes in southeastern Europe. *Nature Geoscience*, **4,** 17-21.

Ho, C. H., Y. S. Choi, and S. K. Hur, 2009a: Long-term changes in summer weekend effect over northeastern China and the connection with regional warming. *Geophysical Research Letters*, **36**.

Ho, S. P., W. He, and Y. H. Kuo, 2009b: *Construction of Consistent Temperature Records in the Lower Stratosphere Using Global Positioning System Radio Occultation Data and Microwave Sounding Measurements.* 207-217 pp.

Ho, S. P., Y. H. Kuo, Z. Zeng, and T. C. Peterson, 2007: A comparison of lower stratosphere temperature from microwave measurements with CHAMP GPS RO data. *Geophysical Research Letters*, **34**.

Ho, S. P., M. Goldberg, Y. H. Kuo, C. Z. Zou, and W. Schreiner, 2009c: Calibration of Temperature in the Lower Stratosphere from Microwave Measurements Using COSMIC Radio Occultation Data: Preliminary Results. *Terrestrial Atmospheric and Oceanic Sciences*, **20,** 87-100.

Ho, S. P., et al., 2009d: Estimating the uncertainty of using GPS radio occultation data for climate monitoring: Intercomparison of CHAMP refractivity climate records from 2002 to 2006 from different data centers. *Journal of Geophysical Research-Atmospheres*, **114**.

Hobbins, M. T., A. Dai, M. L. Roderick, and G. D. Farquhar, 2008: Revisiting the parameterization of potential evaporation as a driver of long-term water balance trends. *Geophysical Research Letters*, **35**.

Hodges, K. I., B. J. Hoskins, J. Boyle, and C. Thorncroft, 2003: A comparison of recent reanalysis datasets using objective feature tracking: Storm tracks and tropical easterly waves. *Monthly Weather Review*, **131,** 2012-2037.

Hodgkins, G. A., R. W. Dudley, and T. G. Huntington, 2003: Changes in the timing of high river flows in New England over the 20th Century. *Journal of Hydrology*, **278,** 244-252.

Holben, B. N., et al., 1998: AERONET--A Federated Instrument Network and Data Archive for Aerosol Characterization. *Remote Sensing of Environment*, **66,** 1-16.

Holland, G. J., and P. J. Webster, 2007: Heightened tropical cyclone activity in the North Atlantic: natural variability or climate trend? *Philosophical Transactions of the Royal Society a-Mathematical Physical and Engineering Sciences*, **365,** 2695-2716.

Hope, P. K., W. Drosdowsky, and N. Nicholls, 2006: Shifts in the synoptic systems influencing southwest Western Australia. *Climate Dynamics*, **26,** 751-764.

Horton, E. B., C. K. Folland, and D. E. Parker, 2001: The changing incidence of extremes in worldwide and Central England temperatures to the end of the twentieth century. *Climatic Change*, **50,** 267-295.

HTAP, 2010: Hemispheric Transport of Airpollution: Final Report, in press pp.

Hu, Y., and Q. Fu, 2007: Observed poleward expansion of the Hadley circulation since 1979. *Atmospheric Chemistry and Physics*, **7,** 5229-5236.

Hu, Y. Y., C. Zhou, and J. P. Liu, 2011: Observational evidence for the poleward expansion of the Hadley circulation. *Adv. Atmos. Sci.*, **28,** 33-44.

Huang, J., et al., 2008: Estimation of regional emissions of nitrous oxide from 1997 to 2005 using multinetwork measurements, a chemical transport model, and an inverse method. *Journal of Geophysical Research-Atmospheres*, **-**.

Huang, W.-R., S.-Y. Wang, and J. C. L. Chan, 2010: Discrepancies between global reanalyses and observations in the interdecadal variations of Southeast Asian cold surge. *Int. J. Climatol.*

Hudson, R. D., M. F. Andrade, M. B. Follette, and A. D. Frolov, 2006: The total ozone field separated into meteorological regimes - Part II: Northern Hemisphere mid-latitude total ozone trends. *Atmospheric Chemistry and Physics*, **6,** 5183-5191.

Hundecha, Y., A. St-Hilaire, T. Ouarda, S. El Adlouni, and P. Gachon, 2008: A Nonstationary Extreme Value Analysis for the Assessment of Changes in Extreme Annual Wind Speed over the Gulf of St. Lawrence, Canada. *Journal of Applied Meteorology and Climatology*, **47,** 2745-2759.

Hurrell, J. W., 1995a: DECADAL TRENDS IN THE NORTH-ATLANTIC OSCILLATION - REGIONAL TEMPERATURES AND PRECIPITATION. *Science*, **269,** 676-679.

——, 1995b: Decadal trends in the North Atlantic Oscillation: Regional temperatures and precipitation. *Science*, **269,** 676-679.

Hurrell, J. W., Y. Kushnir, G. Ottersen, and M. Visbeck, 2003: *An Overview of the North Atlantic Oscillation.* Vol. 134, 1-36 pp.

Hurst, D., 2011: Stratospheric water vapor trends over Boulder, Colorado: Analysis of the 30 year Boulder record. *J. Geophys. Res.*, **116**.

IPCC, 2001: Climate Change 2001: The scientific basis. *Contribution of working group I to the Third assessment report of the Intergovernmental Panel on Climate*, J. T. Houghton, et al., Eds., Cambridge University Press.

——, 2007a: *Climate Change 2007: The Physical Science Basis. Contribution of Working Group I to the Fourth Assessment Report of the Intergovernmental Panel on Climate Change (IPCC).* Cambridge University Press, 996 pp pp.

——, 2007b: *Summary for Policymakers, In: Climate Change 2007: The Physical Science Basis. Contribution of Working Group I to the Fourth Assessment Report of the Intergovernmental Panel on Climate Change.* Cambridge University Press.

Ishijima, K., et al., 2007: Temporal variations of the atmospheric nitrous oxide concentration and its delta N-15 and delta O-18 for the latter half of the 20th century reconstructed from firn air analyses. *Journal of Geophysical Research-Atmospheres***,** -.

——, 2010: Stratospheric influence on the seasonal cycle of nitrous oxide in the troposphere as deduced from aircraft observations and model simulations. *Journal of Geophysical Research-Atmospheres***,** -.

Jackson, L. S., and P. M. Forster, 2010: An Empirical Study of Geographic and Seasonal Variations in Diurnal Temperature Range. *Journal of Climate*, **23,** 3205-3221.

Jacobeit, J., J. Rathmann, A. Philipp, and P. D. Jones, 2009: Central European precipitation and temperature extremes in relation to large-scale atmospheric circulation types. *Meteorologische Zeitschrift*, **18,** 397-410.

Jacobowitz, H., L. L. Stowe, G. Ohring, A. Heidinger, K. Knapp, and N. R. Nalli, 2003: The advanced very high resolution radiometer Pathfinder Atmosphere (PATMOS) climate dataset - A resource for climate research. *Bulletin of the American Meteorological Society*, **84,** 785-+.

Jaenicke, R., 1993: Tropospheric Aerosols. *International Geophysics*, **54,** 1-31.

Jaffe, D., and J. Ray, 2007: Increase in surface ozone at rural sites in the western US. *Atmospheric Environment*, **41,** 5452-5463.

Jiang, T., Z. W. Kundzewicz, and B. Su, 2008: Changes in monthly precipitation and flood hazard in the Yangtze River Basin, China. *International Journal of Climatology*, **28,** 1471-1481.

Jiang, X., W. Ku, R. Shia, Q. Li, J. Elkins, R. Prinn, and Y. Yung, 2007: Seasonal cycle of N2O: Analysis of data. *Global Biogeochemical Cycles***,** -.

Jin, S. G., J. U. Park, J. H. Cho, and P. H. Park, 2007: Seasonal variability of GPS-derived zenith tropospheric delay (1994-2006) and climate implications. *Journal of Geophysical Research-Atmospheres*, **112**.

John, V. O., R. P. Allan, and B. J. Soden, 2009: How robust are observed and simulated precipitation responses to tropical ocean warming? *Geophysical Research Letters*, **36**.

Jones, P. D., and D. H. Lister, 2007: Intercomparison of four different Southern Hemisphere sea level pressure datasets. *Geophysical Research Letters*, **34**.

Jones, P. D., T. Jonsson, and D. Wheeler, 1997: Extension to the North Atlantic Oscillation using early instrumental pressure observations from Gibraltar and south-west Iceland. *International Journal of Climatology*, **17,** 1433-1450.

Jones, P. D., D. H. Lister, and Q. Li, 2008: Urbanization effects in large-scale temperature records, with an emphasis on China. *Journal of Geophysical Research-Atmospheres*, **113**.

Jonson, J. E., D. Simpson, H. Fagerli, and S. Solberg, 2006: Can we explain the trends in European ozone levels? *Atmos. Chem. Phys.*, **6,** 51-66.

Joshi, M. M., J. M. Gregory, M. J. Webb, D. M. H. Sexton, and T. C. Johns, 2008: Mechanisms for the land/sea warming contrast exhibited by simulations of climate change. *Climate Dynamics*, **30,** 455-465.

Jung, M., et al., 2010: Recent decline in the global land evapotranspiration trend due to limited moisture supply. *Nature*, **467,** 951-954.

Kalnay, E., et al., 1996: The NCEP/NCAR 40-year reanalysis project. *Bulletin of the American Meteorological Society*, **77,** 437-471.

Kanamitsu, M., W. Ebisuzaki, J. Woollen, S. K. Yang, J. J. Hnilo, M. Fiorino, and G. L. Potter, 2002: NCEP-DOE AMIP-II reanalysis (R-2). *Bulletin of the American Meteorological Society*, **83,** 1631-1643.

Karl, T. R., G. A. Meehl, D. M. Christopher, S. J. Hassol, A. M. Waple, and W. L. Murray, 2008: *Weather and Climate Extremes in a Changing Climate. Regions of Focus: North America, Hawaii, Caribbean, and U.S. Pacific Islands.* A Report by the U.S. Climate Change Science Program and the Subcommittee on Global Change Research, 164 pp.

Karnauskas, K. B., R. Seager, A. Kaplan, Y. Kushnir, and M. A. Cane, 2009: Observed Strengthening of the Zonal Sea Surface Temperature Gradient across the Equatorial Pacific Ocean. *Journal of Climate*, **22,** 4316-4321.

Karnieli, A., et al., 2009: Temporal trend in anthropogenic sulfur aerosol transport from central and eastern Europe to Israel. *Journal of Geophysical Research-Atmospheres*, **114,** D00d19.

Keeling, C. D., Bacastow, R. B., Bainbridge, A. E., Ekdahl, C. A., Guenther, P. R., Waterman, L. S., 1976: Atmospheric carbon dioxide variations at Mauna Loa Observatory, Hawaii. 538-551.

Keim, C., et al., 2009: Tropospheric ozone from IASI: comparison of different inversion algorithms and validation with ozone sondes in the northern middle latitudes. *Atmos. Chem. Phys.*, **9,** 9329-9347.

Kennedy, J. J., P. Brohan, and S. F. B. Tett, 2007: A global climatology of the diurnal variations in sea-surface temperature and implications for MSU temperature trends. *Geophysical Research Letters*, **34**.

Kent, E. C., and P. G. Challenor, 2006: Toward estimating climatic trends in SST. Part II: Random errors. *Journal of Atmospheric and Oceanic Technology*, **23,** 476-486.

Kent, E. C., S. D. Woodruff, and D. I. Berry, 2007: Metadata from WMO publication no. 47 and an assessment of voluntary observing ship observation heights in ICOADS. *Journal of Atmospheric and Oceanic Technology*, **24,** 214-234.

Kenyon, J., and G. C. Hegerl, 2008: Influence of modes of climate variability on global temperature extremes. *Journal of Climate*, **21,** 3872-3889.

Kim, D. Y., and V. Ramanathan, 2008: Solar radiation budget and radiative forcing due to aerosols and clouds. *Journal of Geophysical Research-Atmospheres*, **113,** D02203.

Kim, H. M., P. J. Webster, and J. A. Curry, 2009: Impact of Shifting Patterns of Pacific Ocean Warming on North Atlantic Tropical Cyclones. *Science*, **325,** 77-80.

Kinne, S., 2009: Remote sensing data combinations-superior global maps for aerosol optical depth. *Satellite Aerosol Remote Sensing Over Land*, A.Kokhanovsky and G. de Leeuw, Ed., Springer, 361-381.

Kistler, R., et al., 2001: The NCEP-NCAR 50-year reanalysis: Monthly means CD-ROM and documentation. *Bulletin of the American Meteorological Society*, **82,** 247-267.

Klein Tank, A. M. G., et al., 2006: Changes in daily temperature and precipitation extremes in central and south Asia. *Journal of Geophysical Research-Atmospheres*, **111**.

Knapp, K. R., and M. C. Kruk, 2010: Quantifying Interagency Differences in Tropical Cyclone Best-Track Wind Speed Estimates. *Monthly Weather Review*, **138,** 1459-1473.

Knorr, W., 2009: Is the airborne fraction of anthropogenic CO_2 emissions increasing? *Geophysical Research Letters*, -.

Knutson, T. R., et al., 2010: Tropical cyclones and climate change. *Nature Geoscience*, **3,** 157-163.

Kobayashi, S., M. Matricardi, D. Dee, and S. Uppala, 2009: Toward a consistent reanalysis of the upper stratosphere based on radiance measurements from SSU and AMSU-A. *Quarterly Journal of the Royal Meteorological Society*, **135,** 2086-2099.

Kopp, G., and G. Lawrence, 2005: The Total Irradiance Monitor (TIM): Instrument design. *Solar Physics*, **230,** 91-109.

Kossin, J. P., K. R. Knapp, D. J. Vimont, R. J. Murnane, and B. A. Harper, 2007: A globally consistent reanalysis of hurricane variability and trends. *Geophysical Research Letters*, **34**.

Krishnamurthy, C. K. B., U. Lall, and H. H. Kwon, 2009: Changing Frequency and Intensity of Rainfall Extremes over India from 1951 to 2003. *Journal of Climate*, **22,** 4737-4746.

Kruger, A. C., 2006: Observed trends in daily precipitation indices in South Africa: 1910-2004. *International Journal of Climatology*, **26,** 2275-2285.

Kubota, H., and J. C. L. Chan, 2009: Interdecadal variability of tropical cyclone landfall in the Philippines from 1902 to 2005. *Geophysical Research Letters*, **36**.

Kudo, R., A. Uchiyama, A. Yamazaki, T. Sakami, and O. Ijima, 2011: Decadal changes in aerosol optical thickness and single scattering albedo estimated from ground-based broadband radiometers: A case study in Japan. *J. Geophys. Res.*, **116,** D03207.

Kuglitsch, F. G., A. Toreti, E. Xoplaki, P. M. Della-Marta, C. S. Zerefos, M. Turkes, and J. Luterbacher, 2010: Heat wave changes in the eastern Mediterranean since 1960. *Geophysical Research Letters*, **37**.

Kumari, B. P., and B. N. Goswami, 2010: Seminal role of clouds on solar dimming over the Indian monsoon region. *Geophysical Research Letters*, **37,** -.

Kumari, B. P., A. L. Londhe, S. Daniel, and D. B. Jadhav, 2007: Observational evidence of solar dimming: Offsetting surface warming over India. *Geophysical Research Letters*, **34,** L21810.

Kundzewicz, Z. W., et al., 2007: Freshwater resources and their management. *Climate Change 2007: Impacts, Adaptation and Vulnerability. Contribution of Working Group II to the Fourth Assessment Report of the Intergovernmental Panel on Climate Change*, Cambridge University Press.

Kunkel, K. E., M. A. Palecki, L. Ensor, D. Easterling, K. G. Hubbard, D. Robinson, and K. Redmond, 2009: Trends in Twentieth-Century US Extreme Snowfall Seasons. *Journal of Climate*, **22,** 6204-6216.

Kunkel, K. E., et al., 2008: Observed Changes in Weather and Climate Extremes. *Weather and Climate Extremes in a Changing Climate. Regions of Focus: North America, Hawaii, Caribbean, and U.S. Pacific Islands.*, T. R. Karl, G. A. Meehl, D. M. Christopher, S. J. Hassol, A. M. Waple, and W. L. Murray, Eds., A Report by the U.S. Climate Change Science Program and the Subcommittee on Global Change Research, 222.

Kunz, M., J. Sander, and C. Kottmeier, 2009: Recent trends of thunderstorm and hailstorm frequency and their relation to atmospheric characteristics in southwest Germany. *International Journal of Climatology*, **29,** 2283-2297.

Kuo, Y. H., W. S. Schreiner, J. Wang, D. L. Rossiter, and Y. Zhang, 2005: Comparison of GPS radio occultation soundings with radiosondes. *Geophysical Research Letters*, **32**.

Kurbis, K., M. Mudelsee, G. Tetzlaff, and R. Brazdil, 2009: Trends in extremes of temperature, dew point, and precipitation from long instrumental series from central Europe. *Theoretical and Applied Climatology*, **98,** 187-195.

Kvalevag, M. M., and G. Myhre, 2007: Human impact on direct and diffuse solar radiation during the industrial era. *Journal of Climate*, **20,** 4874-4883.

Kysely, J., 2009: Trends in heavy precipitation in the Czech Republic over 1961-2005. *International Journal of Climatology*, **29,** 1745-1758.

Labat, D., Y. Godderis, J. L. Probst, and J. L. Guyot, 2004: Evidence for global runoff increase related to climate warming. *Advances in Water Resources*, **27,** 631-642.

Lacis, A., G. Schmidt, D. Rind, and R. Ruedy, 2010: Atmospheric CO_2: Principal Control Knob Governing Earth's Temperature. *Science*, 356-359.
Lambert, F. H., and M. J. Webb, 2008: Dependency of global mean precipitation on surface temperature. *Geophys. Res. Lett.*, **35**.
Lammers, R. B., A. I. Shiklomanov, C. J. Vorosmarty, B. M. Fekete, and B. J. Peterson, 2001: Assessment of contemporary Arctic river runoff based on observational discharge records. *Journal of Geophysical Research-Atmospheres*, **106,** 3321-3334.
Landsea, C. W., 2007: Counting Atlantic tropical cyclones back to 1900. *EOS Transactions (AGU)*, **88,** 197-202.
Landsea, C. W., B. A. Harper, K. Hoarau, and J. A. Knaff, 2006: Can we detect trends in extreme tropical cyclones? *Science*, **313,** 452-454.
Landsea, C. W., et al., 2004: The Atlantic hurricane database re-analysis project: Documentation for the 1851-1910 alterations and additions to the HURDAT database. *Hurricanes and Typhoons: Past, Present and Future*, R. J. Murnane, and K. B. Liu, Eds., Columbia University Press, 177-221.
Langematz, U., and M. Kunze, 2008: Dynamical changes in the Arctic and Antarctic stratosphere during spring. *Climate Variability and Extremes during the Past 100 Years. Advances in Global Change Research*, S. Brönnimann, J. Luterbacher, T. Ewen, H. F. Diaz, R. S. Stolarski, and U. Neu, Eds., 293-301.
Larkin, N. K., and D. E. Harrison, 2005: On the definition of El Nino and associated seasonal average US weather anomalies. *Geophysical Research Letters*, **32**.
Laternser, M., and M. Schneebeli, 2003: Long-term snow climate trends of the Swiss Alps (1931-99). *International Journal of Climatology*, **23,** 733-750.
Laux, P., and H. Kunstmann, 2008: Detection of regional weekly weather cycles across Europe. *Environmental Research Letters*, **3**.
Lawrimore, J. H., Menne, M. J., Gleason, B. E., Williams, C. N., Wuertz, D. B., Vose, R. S., Rennie, J., 2011: An Overview of the Global Historical Climatology Network Monthly Mean Temperature Dataset, Version 3.
Le Quere, C., et al., 2009: Trends in the sources and sinks of carbon dioxide. *Nature Geoscience*, 831-836.
Leakey, A. D. B., M. Uribelarrea, E. A. Ainsworth, S. L. Naidu, A. Rogers, D. R. Ort, and S. P. Long, 2006: Photosynthesis, productivity, and yield of maize are not affected by open-air elevation of CO_2 concentration in the absence of drought. *Plant Physiology*, **140,** 779-790.
Lean, J., G. Rottman, J. Harder, and G. Kopp, 2005: SORCE contributions to new understanding of global change and solar variability. *Solar Physics*, **230,** 27-53.
Lee, H. T., A. Heidinger, A. Gruber, and R. G. Ellingson, 2004: The HIRS outgoing longwave radiation product from hybrid polar and geosynchronous satellite observations. *Climate Change Processes in the Stratosphere, Earth-Atmosphere-Ocean Systems, and Oceanographic Processes from Satellite Data*, **33,** 1120-1124.
Lee, H. T., A. Gruber, R. G. Ellingson, and I. Laszlo, 2007: Development of the HIRS outgoing longwave radiation climate dataset. *Journal of Atmospheric and Oceanic Technology*, **24,** 2029-2047.
Lee, T., and M. J. McPhaden, 2010: Increasing intensity of El Nino in the central-equatorial Pacific. *Geophysical Research Letters*, **37**.
Lee, T. C., H. S. Chan, E. W. L. Ginn, and M. C. Wong, 2011: Long-Term Trends in Extreme Temperatures in Hong Kong and Southern China. *Advances in Atmospheric Sciences*, **28,** 147-157.
Levin, I., et al., 2010: The global SF6 source inferred from long-term high precision atmospheric measurements and its comparison with emission inventories. *Atmospheric Chemistry and Physics*, 2655-2662.
Levy, R. C., L. A. Remer, R. G. Kleidman, S. Mattoo, C. Ichoku, R. Kahn, and T. F. Eck, 2010: Global evaluation of the Collection 5 MODIS dark-target aerosol products over land. *Atmos. Chem. Phys.*, **10,** 10399-10420.
Li, F., R. S. Stolarski, and P. A. Newman, 2009: Stratospheric ozone in the post-CFC era. *Atmospheric Chemistry and Physics*, **9,** 2207-2213.
Li, H. B., A. Robock, S. X. Liu, X. G. Mo, and P. Viterbo, 2005: Evaluation of reanalysis soil moisture simulations using updated Chinese soil moisture observations. *Journal of Hydrometeorology*, **6,** 180-193.
Liang, F., and X. A. Xia, 2005: Long-term trends in solar radiation and the associated climatic factors over China for 1961-2000. *Annales Geophysicae*, **23,** 2425-2432.
Liepert, B. G., and M. Previdi, 2009: Do Models and Observations Disagree on the Rainfall Response to Global Warming? *J. Climate*, **22,** 3156-3166.
Liley, J. B., 2009: New Zealand dimming and brightening. *Journal of Geophysical Research-Atmospheres*, **114,** D00d10.
Lim, E. P., and I. Simmonds, 2009: Effect of tropospheric temperature change on the zonal mean circulation and SH winter extratropical cyclones. *Climate Dynamics*, **33,** 19-32.
Lim, Y. K., M. Cai, E. Kalnay, and L. Zhou, 2008: Impact of vegetation types on surface temperature change. *Journal of Applied Meteorology and Climatology*, **47,** 411-424.
Lin, J., and X. Ou, 2008: Spatial and temporal characteristics of thunderstorm in China. *Meteorological Monthly*, **34,** 22-30.
Lindzen, R. S., and Y. S. Choi, 2009: On the determination of climate feedbacks from ERBE data. *Geophysical Research Letters*, **36**.
Liu, B. H., M. Xu, M. Henderson, and W. G. Gong, 2004a: A spatial analysis of pan evaporation trends in China, 1955-2000. *Journal of Geophysical Research-Atmospheres*, **109,** D15102.

Liu, B. H., M. Xu, M. Henderson, Y. Qi, and Y. Q. Li, 2004b: Taking China's temperature: Daily range, warming trends, and regional variations, 1955-2000. *Journal of Climate*, **17,** 4453-4462.
Liu, Q. H., and F. Z. Weng, 2009: Recent Stratospheric Temperature Observed from Satellite Measurements. *Sola*, **5,** 53-56.
Liu, X., P. K. Bhartia, K. Chance, R. J. D. Spurr, and T. P. Kurosu, 2010: Ozone profile retrievals from the Ozone Monitoring Instrument. *Atmos. Chem. Phys.*, **10,** 2521-2537.
Loeb, N. G., et al., 2007: Multi-instrument comparison of top-of-atmosphere reflected solar radiation. *Journal of Climate*, **20,** 575-591.
Lohmann, U., and J. Feichter, 2005: Global indirect aerosol effects: a review. *Atmospheric Chemistry and Physics*, **5,** 715-737.
Long, C. N., E. G. Dutton, J. A. Augustine, W. Wiscombe, M. Wild, S. A. McFarlane, and C. J. Flynn, 2009: Significant decadal brightening of downwelling shortwave in the continental United States. *Journal of Geophysical Research-Atmospheres*, **114,** D00d06.
Lupikasza, E., 2010: Spatial and temporal variability of extreme precipitation in Poland in the period 1951-2006. *International Journal of Climatology*, **30,** 991-1007.
Lynch, A. H., J. A. Curry, R. D. Brunner, and J. A. Maslanik, 2004: Toward an integrated assessment of the impacts of extreme wind events on Barrow, Alaska. *Bulletin of the American Meteorological Society*, **85,** 209-+.
Makowski, K., E. B. Jaeger, M. Chiacchio, M. Wild, T. Ewen, and A. Ohmura, 2009: On the relationship between diurnal temperature range and surface solar radiation in Europe. *Journal of Geophysical Research-Atmospheres*, **114,** D00d07.
Mann, M. E., T. A. Sabbatelli, and U. Neu, 2007a: Evidence for a modest undercount bias in early historical Atlantic tropical cyclone counts. *Geophysical Research Letters*, **34**.
Mann, M. E., K. A. Emanual, G. J. Holland, and P. J. Webster, 2007b: Atlantic tropical cyclones revisited. *Eos Transactions (AGU)*, **88,** 349-350.
Mantua, N. J., S. R. Hare, Y. Zhang, J. M. Wallace, and R. C. Francis, 1997: A Pacific interdecadal climate oscillation with impacts on salmon production. *Bulletin of the American Meteorological Society*, **78,** 1069-1079.
Maraun, D., T. J. Osborn, and N. P. Gillett, 2008: United Kingdom daily precipitation intensity: improved early data, error estimates and an update from 2000 to 2006. *International Journal of Climatology*, **28,** 833-842.
Marengo, J. A., R. Jones, L. M. Alves, and M. C. Valverde, 2009: Future change of temperature and precipitation extremes in South America as derived from the PRECIS regional climate modeling system. *International Journal of Climatology*, **29,** 2241-2255.
Marshall, G. J., 2003: Trends in the southern annular mode from observations and reanalyses. *Journal of Climate*, **16,** 4134-4143.
Martinerie, P., et al., 2009: Long-lived halocarbon trends and budgets from atmospheric chemistry modelling constrained with measurements in polar firn. *Atmospheric Chemistry and Physics***,** 3911-3934.
Matulla, C., W. Schoner, H. Alexandersson, H. von Storch, and X. L. Wang, 2008: European storminess: late nineteenth century to present. *Climate Dynamics*, **31,** 125-130.
Maue, R. N., 2009: Northern Hemisphere tropical cyclone activity. *Geophysical Research Letters*, **36**.
Maurer, E. P., A. W. Wood, J. C. Adam, D. P. Lettenmaier, and B. Nijssen, 2002: A long-term hydrologically based dataset of land surface fluxes and states for the conterminous United States. *Journal of Climate*, **15,** 3237-3251.
McCarthy, M. P., P. W. Thorne, and H. A. Titchner, 2009: An Analysis of Tropospheric Humidity Trends from Radiosondes. *Journal of Climate*, **22,** 5820-5838.
McCarthy, M. P., H. A. Titchner, P. W. Thorne, S. F. B. Tett, L. Haimberger, and D. E. Parker, 2008: Assessing bias and uncertainty in the HadAT-adjusted radiosonde climate record. *Journal of Climate*, **21,** 817-832.
McKitrick, R. R., and P. J. Michaels, 2007: Quantifying the influence of anthropogenic surface processes and inhomogeneities on gridded global climate data. *Journal of Geophysical Research-Atmospheres*, **112**.
McVicar, T. R., T. G. Van Niel, L. T. Li, M. L. Roderick, D. P. Rayner, L. Ricciardulli, and R. J. Donohue, 2008: Wind speed climatology and trends for Australia, 1975-2006: Capturing the stilling phenomenon and comparison with near-surface reanalysis output. *Geophysical Research Letters*, **35**.
Mears, C. A., and F. J. Wentz, 2009a: Construction of the RSS V3.2 Lower-Tropospheric Temperature Dataset from the MSU and AMSU Microwave Sounders. *Journal of Atmospheric and Oceanic Technology*, **26,** 1493-1509.
——, 2009b: Construction of the Remote Sensing Systems V3.2 Atmospheric Temperature Records from the MSU and AMSU Microwave Sounders. *Journal of Atmospheric and Oceanic Technology*, **26,** 1040-1056.
Mears, C. A., B. D. Santer, F. J. Wentz, K. E. Taylor, and M. F. Wehner, 2007: Relationship between temperature and precipitable water changes over tropical oceans. *Geophysical Research Letters*, **34**.
Mears, C. A., Wentz, F. J., Thorne, P., Bernie, D., 2011: Assessing uncertainty in estimates of atmospheric temperature changes from MSU and AMSU using a monte-carlo estimation technique.
Meehl, G. A., C. Tebaldi, G. Walton, D. Easterling, and L. McDaniel, 2009: Relative increase of record high maximum temperatures compared to record low minimum temperatures in the U. S. *Geophysical Research Letters*, **36**.
Menendez, M., F. J. Mendez, I. J. Losada, and N. E. Graham, 2008: Variability of extreme wave heights in the northeast Pacific Ocean based on buoy measurements. *Geophysical Research Letters*, **35**.
Menne, M. J., and C. N. Williams, 2009: Homogenization of Temperature Series via Pairwise Comparisons. *Journal of Climate*, **22,** 1700-1717.

Merchant, C. J., et al., 2008: Deriving a sea surface temperature record suitable for climate change research from the along-track scanning radiometers. *Advances in Space Research*, **41,** 1-11.
Mesquita, M. D. S., D. E. Atkinson, and K. I. Hodges, 2010: Characteristics and Variability of Storm Tracks in the North Pacific, Bering Sea, and Alaska. *Journal of Climate*, **23,** 294-311.
Mieruch, S., S. Noel, H. Bovensmann, and J. P. Burrows, 2008: Analysis of global water vapour trends from satellite measurements in the visible spectral range. *Atmospheric Chemistry and Physics*, **8,** 491-504.
Miller, B., R. Weiss, P. Salameh, T. Tanhua, B. Greally, J. Muhle, and P. Simmonds, 2008: Medusa: A sample preconcentration and GC/MS detector system for in situ measurements of atmospheric trace halocarbons, hydrocarbons, and sulfur compounds. *Analytical Chemistry***,** 1536-1545.
Miller, B., et al., 2010: HFC-23 (CHF3) emission trend response to HCFC-22 (CHClF2) production and recent HFC-23 emission abatement measures. *Atmospheric Chemistry and Physics***,** 7875-7890.
Milliman, J. D., K. L. Farnsworth, P. D. Jones, K. H. Xu, and L. C. Smith, 2008: Climatic and anthropogenic factors affecting river discharge to the global ocean, 1951-2000. *Global and Planetary Change*, **62,** 187-194.
Mishchenko, M. I., et al., 2007: Long-Term Satellite Record Reveals Likely Recent Aerosol Trend. *Science*, **315,** 1543-1543.
——, 2003: Aerosol retrievals from AVHRR radiances: effects of particle nonsphericity and absorption and an updated long-term global climatology of aerosol properties. *Journal of Quantitative Spectroscopy and Radiative Transfer*, **79-80,** 953-972.
Mitas, C. M., and A. Clement, 2005: Has the Hadley cell been strengthening in recent decades? *Geophysical Research Letters*, **32**.
Mo, T., 2009: A study of the NOAA-15 AMSU-A brightness temperatures from 1998 through 2007. *Journal of Geophysical Research-Atmospheres*, **114**.
Moberg, A., et al., 2006: Indices for daily temperature and precipitation extremes in Europe analyzed for the period 1901-2000. *Journal of Geophysical Research-Atmospheres*, **111**.
Montzka, S., B. Hall, and J. Elkins, 2009: Accelerated increases observed for hydrochlorofluorocarbons since 2004 in the global atmosphere. *Geophysical Research Letters***,** -.
Montzka, S., M. Krol, E. Dlugokencky, B. Hall, P. Jockel, and J. Lelieveld, 2011: Small Interannual Variability of Global Atmospheric Hydroxyl. *Science***,** -.
Montzka, S., L. Kuijpers, M. Battle, M. Aydin, K. Verhulst, E. Saltzman, and D. Fahey, 2010: Recent increases in global HFC-23 emissions. *Geophysical Research Letters***,** -.
Muhle, J., et al., 2009: Sulfuryl fluoride in the global atmosphere. *Journal of Geophysical Research-Atmospheres***,** -.
——, 2010: Perfluorocarbons in the global atmosphere: tetrafluoromethane, hexafluoroethane, and octafluoropropane. *Atmospheric Chemistry and Physics***,** 5145-5164.
Murphy, D. M., 2010: Constraining climate sensitivity with linear fits to outgoing radiation. *Geophysical Research Letters*, **37**.
Murphy, D. M., S. Solomon, R. W. Portmann, K. H. Rosenlof, P. M. Forster, and T. Wong, 2009: An observationally based energy balance for the Earth since 1950. *Journal of Geophysical Research-Atmospheres*, **114**.
Nan, S., and J. P. Li, 2003: The relationship between the summer precipitation in the Yangtze River valley and the boreal spring Southern Hemisphere annular mode. *Geophysical Research Letters*, **30**.
Neff, W., J. Perlwitz, and M. Hoerling, 2008: Observational evidence for asymmetric changes in tropospheric heights over Antarctica on decadal time scales. *Geophysical Research Letters*, **35**.
Nevison, C., 2011: Abiotic and biogeochemical signals derived from the seasonal cycles of tropospheric nitrous oxide. *Atmos. Chem. Phys. Discuss.*, **10,** 25803-25839.
Nevison, C., N. Mahowald, R. Weiss, and R. Prinn, 2007: Interannual and seasonal variability in atmospheric N2O. *Global Biogeochemical Cycles***,** -.
New, M., et al., 2006: Evidence of trends in daily climate extremes over southern and west Africa. *Journal of Geophysical Research-Atmospheres*, **111**.
Nicholls, N., 2008: Recent trends in the seasonal and temporal behaviour of the El Nino-Southern Oscillation. *Geophysical Research Letters*, **35**.
Nijssen, B., R. Schnur, and D. P. Lettenmaier, 2001: Global retrospective estimation of soil moisture using the variable infiltration capacity land surface model, 1980-93. *Journal of Climate*, **14,** 1790-1808.
Nisbet, E., and R. Weiss, 2010: Top-Down Versus Bottom-Up. *Science***,** 1241-1243.
Norris, J. R., and M. Wild, 2007: Trends in aerosol radiative effects over Europe inferred from observed cloud cover, solar dimming and solar brightening. *Journal of Geophysical Research-Atmospheres*, **112**.
——, 2009: Trends in aerosol radiative effects over China and Japan inferred from observed cloud cover, solar dimming, and solar brightening. *Journal of Geophysical Research-Atmospheres*, **114,** D00d15.
Notholt, J., et al., 2010: Trend in ice moistening the stratosphere - constraints from isotope data of water and methane. *Atmospheric Chemistry and Physics*, **10,** 201-207.
Ntegeka, V., and P. Willems, 2008: Trends and multidecadal oscillations in rainfall extremes, based on a more than 100-year time series of 10 min rainfall intensities at Uccle, Belgium. *Water Resources Research*, **44**.
O'Dell, C. W., F. J. Wentz, and R. Bennartz, 2008: Cloud liquid water path from satellite-based passive microwave observations: A new climatology over the global oceans. *Journal of Climate*, **21,** 1721-1739.

O'Doherty, S., et al., 2009: Global and regional emissions of HFC-125 (CHF2CF3) from in situ and air archive atmospheric observations at AGAGE and SOGE observatories. *Journal of Geophysical Research-Atmospheres*, **-**, .

Ohmura, A., 2009: Observed decadal variations in surface solar radiation and their causes. *Journal of Geophysical Research-Atmospheres*, **114,** D00d05.

Ohmura, A., et al., 1998: Baseline Surface Radiation Network (BSRN/WCRP): New precision radiometry for climate research. *Bulletin of the American Meteorological Society*, **79,** 2115-2136.

Ohvril, H., et al., 2009: Global dimming and brightening versus atmospheric column transparency, Europe, 1906-2007. *Journal of Geophysical Research-Atmospheres*, **114,** D00d12.

Oltmans, S., H. Vomel, D. Hofmann, K. Rosenlof, and D. Kley, 2000: The increase in stratospheric water vapor from balloonborne, frostpoint hygrometer measurements at Washington, DC, and Boulder, Colorado. *Geophysical Research Letters*, 3453-3456.

Oltmans, S. J., A. S. Lefohn, J. M. Harris, and D. S. Shadwick, 2008: Background ozone levels of air entering the west coast of the US and assessment of longer-term changes. *Atmospheric Environment*, **42,** 6020-6038.

Oltmans, S. J., et al., 2006: Long-term changes in tropospheric ozone. *Atmospheric Environment*, **40,** 3156-3173.

Onogi, K., et al., 2007: The JRA-25 reanalysis. *Journal of the Meteorological Society of Japan*, **85,** 369-432.

Orlowksy, B., and S. I. Seneviratne, submitted: Global changes in extremes events: Regional and seasonal dimension. *Climatic Change*.

Osborn, T. J., 2011: Winter 2009/2010 temperatures and a record breaking North Atlantic Oscillation index. *Weather*, **66,** 19-21.

Osborne, S. R., and J. M. Haywood, 2005: Aircraft observations of the microphysical and optical properties of major aerosol species. *Atmospheric Research*, **73,** 173-201.

Paciorek, C. J., J. S. Risbey, V. Ventura, and R. D. Rosen, 2002: Multiple indices of Northern Hemisphere cyclone activity, winters 1949-99. *Journal of Climate*, **15,** 1573-1590.

Panagiotopoulos, F., M. Shahgedanova, A. Hannachi, and D. B. Stephenson, 2005: Observed trends and teleconnections of the Siberian high: A recently declining center of action. *Journal of Climate*, **18,** 1411-1422.

Parrella, J. P., et al., 2011: Effect of bromine chemistry on natural tropospheric ozone: improved simulation of observations from the turn of the 20th century. *Atmos Chemistry Physics ???, submitted.*

Parrish, D. D., D. B. Millet, and A. H. Goldstein, 2009: Increasing ozone in marine boundary layer inflow at the west coasts of North America and Europe. *Atmos. Chem. Phys.*, **9,** 1303-1323.

Pattanaik, D. R., and M. Rajeevan, 2010: Variability of extreme rainfall events over India during southwest monsoon season. *Meteorological Applications*, **17,** 88-104.

Pavan, V., R. Tomozeiu, C. Cacciamani, and M. Di Lorenzo, 2008: Daily precipitation observations over Emilia-Romagna: mean values and extremes. *International Journal of Climatology*, **28,** 2065-2079.

Pekarova, P., P. Miklanek, and J. Pekar, 2003: Spatial and temporal runoff oscillation analysis of the main rivers of the world during the l9th-20th centuries. *Journal of Hydrology*, **274,** 62-79.

Penalba, O. C., and F. A. Robledo, 2010: Spatial and temporal variability of the frequency of extreme daily rainfall regime in the La Plata Basin during the 20th century. *Climatic Change*, **98,** 531-550.

Peterson, T. C., and M. J. Manton, 2008: Monitoring changes in climate extremes - A tale of international collaboration. *Bulletin of the American Meteorological Society*, **89,** 1266-1271.

Peterson, T. C., X. B. Zhang, M. Brunet-India, and J. L. Vazquez-Aguirre, 2008: Changes in North American extremes derived from daily weather data. *Journal of Geophysical Research-Atmospheres*, **113**.

Petrow, T., and B. Merz, 2009: Trends in flood magnitude, frequency and seasonality in Germany in the period 1951-2002. *Journal of Hydrology*, **371,** 129-141.

Pezza, A. B., and I. Simmonds, 2008: Large-scale Factors in Tropical. and Extratropical Cyclone Transition and Extreme Weather Events. *Trends and Directions in Climate Research*, L. Gimeno, R. GarciaHerrera, and R. M. Trigo, Eds., 189-211.

Pezza, A. B., I. Simmonds, and J. A. Renwick, 2007a: Southern Hemisphere cyclones and anticyclones: Recent trends and links with decadal variability in the Pacific Ocean. *International Journal of Climatology*, **27,** 1403-1419.

——, 2007b: Southern Hemisphere cyclones and anticyclones: Recent trends and links with decadal variability in the Pacific Ocean. *International Journal of Climatology*, **27,** 1403-1419.

Philipona, R., K. Behrens, and C. Ruckstuhl, 2009: How declining aerosols and rising greenhouse gases forced rapid warming in Europe since the 1980s. *Geophysical Research Letters*, **36,** L02806.

Philipona, R., B. Durr, C. Marty, A. Ohmura, and M. Wild, 2004: Radiative forcing - measured at Earth's surface - corroborate the increasing greenhouse effect. *Geophysical Research Letters*, **31,** L03202.

Philipp, A., P. M. Della-Marta, J. Jacobeit, D. R. Fereday, P. D. Jones, A. Moberg, and H. Wanner, 2007: Long-term variability of daily North Atlantic-European pressure patterns since 1850 classified by simulated annealing clustering. *Journal of Climate*, **20,** 4065-4095.

Pinker, R. T., B. Zhang, and E. G. Dutton, 2005: Do satellites detect trends in surface solar radiation? *Science*, **308,** 850-854.

Pinto, J. G., S. Zacharias, A. H. Fink, G. C. Leckebusch, and U. Ulbrich, 2009: Factors contributing to the development of extreme North Atlantic cyclones and their relationship with the NAO. *Climate Dynamics*, **32,** 711-737.

Pirazzoli, P. A., and A. Tomasin, 2003: Recent near-surface wind changes in the central Mediterranean and Adriatic areas. *International Journal of Climatology*, **23,** 963-973.
Power, S., T. Casey, C. Folland, A. Colman, and V. Mehta, 1999: Inter-decadal modulation of the impact of ENSO on Australia. *Climate Dynamics*, **15,** 319-324.
Power, S. B., and I. N. Smith, 2007: Weakening of the Walker Circulation and apparent dominance of El Nino both reach record levels, but has ENSO really changed? *Geophysical Research Letters*, **34**.
Pozzoli, L., et al., 2011: Reanalysis of tropospheric sulfate aerosol and ozone for the period 1980-2005 using the aerosol-chemistry-climate model ECHAM5-HAMMOZ. *Atmospheric Chemistry and Physics, in preparation*.
Prata, F., 2008: The climatological record of clear-sky longwave radiation at the Earth's surface: evidence for water vapour feedback? *International Journal of Remote Sensing*, **29,** 5247-5263.
Prather, M., and J. Hsu, 2008: NF3, the greenhouse gas missing from Kyoto. *Geophysical Research Letters*, **-**.
Prinn, R., et al., 1990: Atmospheric Emissions and Trends of Nitrous Oxide Deduced From 10 Years of ALE-GAGE Data. *J. Geophys. Res.*, **95,** 18,369-318,385.
——, 2005: Evidence for variability of atmospheric hydroxyl radicals over the past quarter century. *Geophysical Research Letters*, **-**.
Prospero, J. M., P. Ginoux, O. Torres, S. E. Nicholson, and T. E. Gill, 2002: Environmental characterization of global sources of atmospheric soil dust identified with the Nimbus 7 Total Ozone Mapping Spectrometer (TOMS) absorbing aerosol product. *Rev. Geophys*, **40**.
Pryor, S. C., R. J. Barthelmie, and E. S. Riley, 2007: Historical evolution of wind climates in the USA - art. no. 012065. *Science of Making Torque from Wind*, M. O. L. Hansen, and K. S. Hansen, Eds., 12065-12065.
Pryor, S. C., et al., 2009: Wind speed trends over the contiguous United States. *Journal of Geophysical Research-Atmospheres*, **114**.
Qian, B. D., X. B. Zhang, K. Chen, Y. Feng, and T. O'Brien, 2010: Observed Long-Term Trends for Agroclimatic Conditions in Canada. *Journal of Applied Meteorology and Climatology*, **49,** 604-618.
Qian, Y., D. P. Kaiser, L. R. Leung, and M. Xu, 2006: More frequent cloud-free sky and less surface solar radiation in China from 1955 to 2000. *Geophysical Research Letters*, **33,** L01812.
Quinn, P. K., T. S. Bates, K. Schulz, and G. E. Shaw, 2009: Decadal trends in aerosol chemical composition at Barrow, Alaska: 1976-2008. *Atmos. Chem. Phys.*, **9,** 8883-8888.
Rahimzadeh, F., A. Asgari, and E. Fattahi, 2009: Variability of extreme temperature and precipitation in Iran during recent decades. *International Journal of Climatology*, **29,** 329-343.
Raible, C. C., 2007: On the relation between extremes of midlatitude cyclones and the atmospheric circulation using ERA40. *Geophysical Research Letters*, **34**.
Raible, C. C., P. M. Della-Marta, C. Schwierz, H. Wernli, and R. Blender, 2008: Northern hemisphere extratropical cyclones: A comparison of detection and tracking methods and different reanalyses. *Monthly Weather Review*, **136,** 880-897.
Rajeevan, M., J. Bhate, and A. K. Jaswal, 2008: Analysis of variability and trends of extreme rainfall events over India using 104 years of gridded daily rainfall data. *Geophysical Research Letters*, **35**.
Ramanathan, V., P. J. Crutzen, J. T. Kiehl, and D. Rosenfeld, 2001: Atmosphere - Aerosols, climate, and the hydrological cycle. *Science . Dec*, **294,** 2119-2124.
Randall, R. M., and B. M. Herman, 2008: Using limited time period trends as a means to determine attribution of discrepancies in microwave sounding unit-derived tropospheric temperature time series. *Journal of Geophysical Research-Atmospheres*, **113**.
Randel, W. J., and F. Wu, 2006: Biases in stratospheric and tropospheric temperature trends derived from historical radiosonde data. *Journal of Climate*, **19,** 2094-2104.
Randel, W. J., F. Wu, H. Vomel, G. E. Nedoluha, and P. Forster, 2006: Decreases in stratospheric water vapor after 2001: Links to changes in the tropical tropopause and the Brewer-Dobson circulation. *Journal of Geophysical Research-Atmospheres*, **111**.
Randel, W. J., et al., 2009: An update of observed stratospheric temperature trends. *Journal of Geophysical Research-Atmospheres*, **114**.
Rasmusson, E. M., and J. M. Wallace, 1983: Meteorological aspects of the El Nino - Southern Oscillation. *Science*, **222,** 1195-1202.
Raupach, M., J. Canadell, and C. Le Quere, 2008: Anthropogenic and biophysical contributions to increasing atmospheric CO_2 growth rate and airborne fraction. *Biogeosciences*, **5,** 1601-1613.
Rausch, J., A. Heidinger, and R. Bennartz, 2010: Regional assessment of microphysical properties of marine boundary layer cloud using the PATMOS-x dataset. *Journal of Geophysical Research-Atmospheres*, **115**.
Ravishankara, A. R., J. S. Daniel, and R. W. Portmann, 2009: Nitrous Oxide (N2O): The Dominant Ozone-Depleting Substance Emitted in the 21st Century. *Science*, **326,** 123-125.
Rayner, D. P., 2007: Wind run changes: The dominant factor affecting pan evaporation trends in Australia. *Journal of Climate*, **20,** 3379-3394.
Rayner, N. A., et al., 2003: Global analyses of sea surface temperature, sea ice, and night marine air temperature since the late nineteenth century. *Journal of Geophysical Research-Atmospheres*, **108**.
——, 2006: Improved analyses of changes and uncertainties in sea surface temperature measured in situ sice the mid-nineteenth century: The HadSST2 dataset. *Journal of Climate*, **19,** 446-469.

Re, M., and V. R. Barros, 2009: Extreme rainfalls in SE South America. *Climatic Change*, **96,** 119-136.
Read, W. G., et al., 2007: Aura Microwave Limb Sounder upper tropospheric and lower stratospheric H2O and relative humidity with respect to ice validation. *Journal of Geophysical Research-Atmospheres*, **112**.
Ren, G. Y., Y. Q. Zhou, Z. Y. Chu, J. X. Zhou, A. Y. Zhang, J. Guo, and X. F. Liu, 2008: Urbanization effects on observed surface air temperature trends in north China. *Journal of Climate*, **21,** 1333-1348.
Reynolds, R. W., C. L. Gentemann, and G. K. Corlett, 2010: Evaluation of AATSR and TMI Satellite SST Data. *Journal of Climate*, **23,** 152-165.
Reynolds, R. W., N. A. Rayner, T. M. Smith, D. C. Stokes, W. Wang, and A. M. S. Ams, 2002: *An improved in situ and satellite SST analysis.* 146-148 pp.
Reynolds, R. W., T. M. Smith, C. Liu, D. B. Chelton, K. S. Casey, and M. G. Schlax, 2007: Daily high-resolution-blended analyses for sea surface temperature. *Journal of Climate*, **20,** 5473-5496.
Rigby, M., et al., 2008: Renewed growth of atmospheric methane. *Geophysical Research Letters***,** -.
——, 2010: History of atmospheric SF6 from 1973 to 2008. *Atmospheric Chemistry and Physics***,** 10305-10320.
Riihimaki, L. D., F. E. Vignola, and C. N. Long, 2009: Analyzing the contribution of aerosols to an observed increase in direct normal irradiance in Oregon. *Journal of Geophysical Research-Atmospheres*, **114,** D00d02.
Robock, A., M. Q. Mu, K. Vinnikov, I. V. Trofimova, and T. I. Adamenko, 2005: Forty-five years of observed soil moisture in the Ukraine: No summer desiccation (yet). *Geophysical Research Letters*, **32**.
Rodda, J. C., M. A. Little, H. J. E. Rodda, and P. E. McSharry, 2010: A comparative study of the magnitude, frequency and distribution of intense rainfall in the United Kingdom. *International Journal of Climatology*, **30,** 1776-1783.
Roderick, M. L., and G. D. Farquhar, 2002: The cause of decreased pan evaporation over the past 50 years. *Science*, **298,** 1410-1411.
Roderick, M. L., L. D. Rotstayn, G. D. Farquhar, and M. T. Hobbins, 2007: On the attribution of changing pan evaporation. *Geophysical Research Letters*, **34**.
Rohs, S., et al., 2006: Long-term changes of methane and hydrogen in the stratosphere in the period 1978-2003 and their impact on the abundance of stratospheric water vapor. *Journal of Geophysical Research-Atmospheres*, **111**.
Rosenlof, K. H., and G. C. Reid, 2008: Trends in the temperature and water vapor content of the tropical lower stratosphere: Sea surface connection. *Journal of Geophysical Research-Atmospheres*, **113**.
Rosenzweig, C., et al., 2007: Assessment of observed changes and responses in natural and managed systems. *Climate Change 2007: Impacts, Adaptation and Vulnerability. Contribution of Working Group II to the Fourth Assessment Report of the Intergovernmental Panel on Climate Change*, M. L. Parry, O. F. Canziani, J. P. Palutikof, P. J. van der Linden, and C. E. Hanson, Eds., Cambridge University Press.
Ruckstuhl, C., et al., 2008: Aerosol and cloud effects on solar brightening and the recent rapid warming. *Geophysical Research Letters*, **35,** L12708.
Ruddiman, W., 2003: The anthropogenic greenhouse era began thousands of years ago. *Climatic Change***,** 261-293.
——, 2007: The early anthropogenic hypothesis: Challenges and responses. *Reviews of Geophysics***,** -.
Russak, V., 2009: Changes in solar radiation and their influence on temperature trend in Estonia (1955-2007). *Journal of Geophysical Research-Atmospheres*, **114,** D00d01.
Rusticucci, M., and M. Renom, 2008: Variability and trends in indices of quality-controlled daily temperature extremes in Uruguay. *International Journal of Climatology*, **28,** 1083-1095.
Saha, S., et al., 2010: THE NCEP CLIMATE FORECAST SYSTEM REANALYSIS. *Bulletin of the American Meteorological Society*, **91,** 1015-1057.
Saji, N. H., B. N. Goswami, P. N. Vinayachandran, and T. Yamagata, 1999: A dipole mode in the tropical Indian Ocean. *Nature*, **401,** 360-363.
Sanchez-Lorenzo, A., J. Calbo, and J. Martin-Vide, 2008a: Spatial and Temporal Trends in Sunshine Duration over Western Europe (1938-2004). *Journal of Climate*, **21,** 6089-6098.
Sanchez-Lorenzo, A., J. Calbo, J. Martin-Vide, A. Garcia-Manuel, G. Garcia-Soriano, and C. Beck, 2008b: Winter "weekend effect" in southern Europe and its connections with periodicities in atmospheric dynamics. *Geophysical Research Letters*, **35**.
Santer, B. D., et al., 2007: Identification of human-induced changes in atmospheric moisture content. *Proceedings of the National Academy of Sciences of the United States of America*, **104,** 15248-15253.
——, 2008: Consistency of modelled and observed temperature trends in the tropical troposphere. *International Journal of Climatology*, **28,** 1703-1722.
Scaife, A. A., J. Austin, N. Butchart, S. Pawson, M. Keil, J. Nash, and I. N. James, 2000: Seasonal and interannual variability of the stratosphere diagnosed from UKMO TOVS analyses. *Quarterly Journal of the Royal Meteorological Society*, **126,** 2585-2604.
Schar, C., P. L. Vidale, D. Luthi, C. Frei, C. Haberli, M. A. Liniger, and C. Appenzeller, 2004: The role of increasing temperature variability in European summer heatwaves. *Nature*, **427,** 332-336.
Scherer, M., H. Vomel, S. Fueglistaler, S. J. Oltmans, and J. Staehelin, 2008: Trends and variability of midlatitude stratospheric water vapour deduced from the re-evaluated Boulder balloon series and HALOE. *Atmospheric Chemistry and Physics*, **8,** 1391-1402.
Schiller, C., J. U. Grooss, P. Konopka, F. Ploger, F. H. S. dos Santos, and N. Spelten, 2009: Hydration and dehydration at the tropical tropopause. *Atmospheric Chemistry and Physics*, **9,** 9647-9660.

Schneider, T., P. A. O'Gorman, and X. J. Levine, 2010: Water vapour and the dynamics of climate changes. Reviews of Geophysics, RG3001.
Schneidereit, A., R. Blender, K. Fraedrich, and F. Lunkeit, 2007: Icelandic climate and north Atlantic cyclones in ERA-40 reanalyses. *Meteorologische Zeitschrift*, **16,** 17-23.
Seager, R., and N. Naik, 2011: A mechanism-based approach for distinguishing between internal hydroclimate variability and anthropogenic-driven hydroclimate change (submitted). *J. Clim.*
Seidel, D. J., and W. J. Randel, 2007: Recent widening of the tropical belt: Evidence from tropopause observations. *Journal of Geophysical Research-Atmospheres*, **112**.
Seidel, D. J., Q. Fu, W. J. Randel, and T. J. Reichler, 2008: Widening of the tropical belt in a changing climate. *Nature Geoscience*, **1,** 21-24.
Seidel, D. J., Gillett, N. P., Lanzante, J. R., Shine, K. P., Thorne, P. W., 2011: Stratospheric temperature trends: Our evolving understanding.
Seierstad, I. A., D. B. Stephenson, and N. G. Kvamsto, 2007: How useful are teleconnection patterns for explaining variability in extratropical storminess ? *Tellus Series a-Dynamic Meteorology and Oceanography*, **59,** 170-181.
Seleshi, Y., and P. Camberlin, 2006: Recent changes in dry spell and extreme rainfall events in Ethiopia. *Theoretical and Applied Climatology*, **83,** 181-191.
Sen Roy, S., 2009: A spatial analysis of extreme hourly precipitation patterns in India. *International Journal of Climatology*, **29,** 345-355.
Sen Roy, S., and R. C. Balling, 2005: Analysis of trends in maximum and minimum temperature, diurnal temperature range, and cloud cover over India. *Geophysical Research Letters*, **32**.
Sharma, S., E. Andrews, L. A. Barrie, J. A. Ogren, and D. Lavoué, 2006: Variations and sources of the equivalent black carbon in the high Arctic revealed by long-term observations at Alert and Barrow: 1989-2003. *J. Geophys. Res.*, **111,** D14208.
Sheffield, J., and E. F. Wood, 2007: Characteristics of global and regional drought, 1950-2000: Analysis of soil moisture data from off-line simulation of the terrestrial hydrologic cycle. *Journal of Geophysical Research-Atmospheres*, **112**.
——, 2008a: Projected changes in drought occurrence under future global warming from multi-model, multi-scenario, IPCC AR4 simulations. *Climate Dynamics*, **31,** 79-105.
——, 2008b: Global trends and variability in soil moisture and drought characteristics, 1950-2000, from observation-driven Simulations of the terrestrial hydrologic cycle. *Journal of Climate*, **21,** 432-458.
Sherwood, S. C., 2007: Simultaneous detection of climate change and observing biases in a network with incomplete sampling. *Journal of Climate*, **20,** 4047-4062.
Sherwood, S. C., C. L. Meyer, R. J. Allen, and H. A. Titchner, 2008: Robust Tropospheric Warming Revealed by Iteratively Homogenized Radiosonde Data. *Journal of Climate*, **21,** 5336-5350.
Shi, G. Y., et al., 2008: Data quality assessment and the long-term trend of ground solar radiation in China. *Journal of Applied Meteorology and Climatology*, **47,** 1006-1016.
Shiklomanov, A. I., R. B. Lammers, M. A. Rawlins, L. C. Smith, and T. M. Pavelsky, 2007: Temporal and spatial variations in maximum river discharge from a new Russian data set. *Journal of Geophysical Research-Biogeosciences*, **112**.
Shiklomanov, I. A., V. Y. Georgievskii, V. I. Babkin, and Z. A. Balonishnikova, 2010: Research Problems of Formation and Estimation of Water Resources and Water Availability Changes of the Russian Federation. *Russian Meteorology and Hydrology*, **35,** 13-19.
Shine, K. P., J. J. Barnett, and W. J. Randel, 2008: Temperature trends derived from Stratospheric Sounding Unit radiances: The effect of increasing CO_2 on the weighting function. *Geophysical Research Letters*, **35**.
Shiu, C. J., S. C. Liu, and J. P. Chen, 2009: Diurnally Asymmetric Trends of Temperature, Humidity, and Precipitation in Taiwan. *Journal of Climate*, **22,** 5635-5649.
Sickles, J. E., II, and D. S. Shadwick, 2007a: Seasonal and regional air quality and atmospheric deposition in the eastern United States. *J. Geophys. Res.*, **112,** D17302.
——, 2007b: Changes in air quality and atmospheric deposition in the eastern United States: 1990-2004. *J. Geophys. Res.*, **112,** D17301.
Simmonds, I., and K. Keay, 2002: Surface fluxes of momentum and mechanical energy over the North Pacific and North Atlantic Oceans. *Meteorology and Atmospheric Physics*, **80,** 1-18.
Simmonds, I., C. Burke, and K. Keay, 2008: Arctic Climate Change as Manifest in Cyclone Behavior. *Journal of Climate*, **21,** 5777-5796.
Simmons, A. J., K. M. Willett, P. D. Jones, P. W. Thorne, and D. P. Dee, 2010: Low-frequency variations in surface atmospheric humidity, temperature, and precipitation: Inferences from reanalyses and monthly gridded observational data sets. *Journal of Geophysical Research-Atmospheres*, **115**.
Smith, T. M., and R. W. Reynolds, 1998: A high-resolution global sea surface temperature climatology for the 1961-90 base period. *Journal of Climate*, **11,** 3320-3323.
——, 2002: Bias corrections for historical sea surface temperatures based on marine air temperatures. *Journal of Climate*, **15,** 73-87.
Smith, T. M., R. W. Reynolds, T. C. Peterson, and J. Lawrimore, 2008: Improvements to NOAA's historical merged land-ocean surface temperature analysis (1880-2006). *Journal of Climate*, **21,** 2283-2296.

Smits, A., A. Tank, and G. P. Konnen, 2005: Trends in storminess over the Netherlands, 1962-2002. *International Journal of Climatology*, **25,** 1331-1344.
Soden, B. J., D. L. Jackson, V. Ramaswamy, M. D. Schwarzkopf, and X. L. Huang, 2005: The radiative signature of upper tropospheric moistening. *Science*, **310,** 841-844.
Sohn, B. J., and S. C. Park, 2010: Strengthened tropical circulations in past three decades inferred from water vapor transport. *Journal of Geophysical Research-Atmospheres*, **115**.
Solomon, S., K. H. Rosenlof, R. W. Portmann, J. S. Daniel, S. M. Davis, T. J. Sanford, and G. K. Plattner, 2010a: Contributions of Stratospheric Water Vapor to Decadal Changes in the Rate of Global Warming. *Science*, **327,** 1219-1223.
Solomon, S., K. Rosenlof, R. Portmann, J. Daniel, S. Davis, T. Sanford, and G. Plattner, 2010b: Contributions of Stratospheric Water Vapor to Decadal Changes in the Rate of Global Warming. *Science***,** 1219-1223.
Song, H., and M. H. Zhang, 2007: Changes of the boreal winter Hadley circulation in the NCEP-NCAR and ECMWF reanalyses: A comparative study. *Journal of Climate*, **20,** 5191-5200.
Sorteberg, A., and J. E. Walsh, 2008: Seasonal cyclone variability at 70 degrees N and its impact on moisture transport into the Arctic. *Tellus Series a-Dynamic Meteorology and Oceanography*, **60,** 570-586.
Spencer, R. W., and J. R. Christy, 1992: PRECISION AND RADIOSONDE VALIDATION OF SATELLITE GRIDPOINT TEMPERATURE ANOMALIES .2. A TROPOSPHERIC RETRIEVAL AND TRENDS DURING 1979-90. *Journal of Climate*, **5,** 858-866.
Spencer, R. W., and W. D. Braswell, 2010: On the diagnosis of radiative feedback in the presence of unknown radiative forcing. *Journal of Geophysical Research-Atmospheres*, **115**.
Stanhill, G., and S. Cohen, 2001: Global dimming: a review of the evidence for a widespread and significant reduction in global radiation with discussion of its probable causes and possible agricultural consequences. *Agricultural and Forest Meteorology*, **107,** 255-278.
Stephens, G. L., and T. D. Ellis, 2008: Controls of Global-Mean Precipitation Increases in Global Warming GCM Experiments. *Journal of Climate*, **21,** 6141-6155.
Stephens, G. L., M. Wild, P. Stackhouse, T. L'Ecuyer, and S. Kato, in preparation: Th**e global characteristics of the flux of downward longwave radiation**.
Stephenson, D. B., H. F. Diaz, and R. J. Murnane, 2008: Definition, diagnosis, and origin of extreme weather and climate events. *Climate Extremes and Society*, R. J. Murnane, and H. F. Diaz, Eds., Cambridge University Press, 11-23.
Stephenson, D. B., H. Wanner, S. Brönnimann, and J. Luterbacher, 2003: *The history of scientific research on the North Atlantic Oscillation.* Vol. 134, 37-50 pp.
Stern, D. I., 2006: Reversal of the trend in global anthropogenic sulfur emissions. *Global Environmental Change-Human and Policy Dimensions*, **16,** 207-220.
Stickler, A., et al., 2010: THE COMPREHENSIVE HISTORICAL UPPER-AIR NETWORK. *Bulletin of the American Meteorological Society*, **91,** 741-+.
Stjern, C. W., J. E. Kristjansson, and A. W. Hansen, 2009: Global dimming and global brightening - an analysis of surface radiation and cloud cover data in northern Europe. *International Journal of Climatology*, **29,** 643-653.
Stohl, A., et al., 2009: An analytical inversion method for determining regional and global emissions of greenhouse gases: Sensitivity studies and application to halocarbons. *Atmospheric Chemistry and Physics***,** 1597-1620.
Streets, D. G., Y. Wu, and M. Chin, 2006: Two-decadal aerosol trends as a likely explanation of the global dimming/brightening transition. *Geophysical Research Letters*, **33,** L15806.
Streets, D. G., et al., 2009: Anthropogenic and natural contributions to regional trends in aerosol optical depth, 1980-2006. *Journal of Geophysical Research-Atmospheres*, **114**.
Strong, C., and R. E. Davis, 2006: Temperature-related trends in the vertical position of the summer upper tropospheric surface of maximum wind over the Northern Hemisphere. *International Journal of Climatology*, **26,** 1977-1997.
——, 2007: Winter jet stream trends over the Northern Hemisphere. *Quarterly Journal of the Royal Meteorological Society*, **133,** 2109-2115.
——, 2008a: Variability in the position and strength of winter jet stream cores related to northern hemisphere teleconnections. *Journal of Climate*, **21,** 584-592.
——, 2008b: Comment on "Historical trends in the jet streams" by Cristina L. Archer and Ken Caldeira. *Geophysical Research Letters*, **35**.
Sun, B. M., T. R. Karl, and D. J. Seidel, 2007: Changes in cloud-ceiling heights and frequencies over the United States since the early 1950s. *Journal of Climate*, **20,** 3956-3970.
Sun, B. M., A. Reale, D. J. Seidel, and D. C. Hunt, 2010: Comparing radiosonde and COSMIC atmospheric profile data to quantify differences among radiosonde types and the effects of imperfect collocation on comparison statistics. *Journal of Geophysical Research-Atmospheres*, **115**.
Tanimoto, H., 2009: Increase in springtime tropospheric ozone at a mountainous site in Japan for the period 1998-2006. *Atmospheric Environment*, **43,** 1358-1363.
Tanimoto, H., T. Ohara, and I. Uno, 2009: Asian anthropogenic emissions and decadal trends in springtime tropospheric ozone over Japan: 1998-2007. *Geophys. Res. Lett.*, **36,** L23802.
Tans, P., 2009: An Accounting of the Observed Increase in Oceanic and Atmospheric CO_2 and an Outlook for the Future. *Oceanography***,** 26-35.

Tegtmeier, S., K. Kruger, I. Wohltmann, K. Schoellhammer, and M. Rex, 2008: Variations of the residual circulation in the Northern Hemispheric winter. *Journal of Geophysical Research-Atmospheres*, **113**.
Teuling, A. J., et al., 2009: A regional perspective on trends in continental evaporation. *Geophysical Research Letters*, **36,** L02404.
Thompson, A. M., J. C. Witte, R. D. Hudson, H. Guo, J. R. Herman, and M. Fujiwara, 2001a: Tropical tropospheric biomass burning. *Science*, **291,** 2128-2132.
——, 2001b: Tropical Tropospheric Ozone and Biomass Burning. *Science*, **291,** 2128-2132.
Thompson, D. W. J., and J. M. Wallace, 1998: The Arctic Oscillation signature in the wintertime geopotential height and temperature fields. *Geophysical Research Letters*, **25,** 1297-1300.
——, 2000: Annular modes in the extratropical circulation. Part I: Month-to-month variability. *Journal of Climate*, **13,** 1000-1016.
Thompson, D. W. J., J. J. Kennedy, J. M. Wallace, and P. D. Jones, 2008: A large discontinuity in the mid-twentieth century in observed global-mean surface temperature. *Nature*, **453,** 646-U645.
Thorne, P. W., 2008: Arctic tropospheric warming amplification? *Nature*, **455,** E1-E2.
Thorne, P. W., and R. S. Vose, 2010: REANALYSES SUITABLE FOR CHARACTERIZING LONG-TERM TRENDS Are They Really Achievable? *Bulletin of the American Meteorological Society*, **91,** 353-+.
Thorne, P. W., D. E. Parker, J. R. Christy, and C. A. Mears, 2005a: Uncertainties in climate trends - Lessons from upper-air temperature records. *Bulletin of the American Meteorological Society*, **86,** 1437-+.
Thorne, P. W., D. E. Parker, S. F. B. Tett, P. D. Jones, M. McCarthy, H. Coleman, and P. Brohan, 2005b: Revisiting radiosonde upper air temperatures from 1958 to 2002. *Journal of Geophysical Research-Atmospheres*, **110**.
Thorne, P. W., Brohan, P., Titchner, H. A., McCarthy, M. P., Sherwood, S. C., Peterson, T. C., Haimberger, L., Parker, D. E., Tett, S. F. B., Santer, B. D., Fereday, D. R., Kennedy, J. J., 2011a: A quantification of uncertainties in historical tropospheric temperature trends from radiosondes.
Thorne, P. W., Lanzante, J. R., Peterson, T. C., Seidel, D. J., Shine, K. P., 2011b: Tropospheric temperature trends: History of an ongoing controversy. 66-88.
Titchner, H. A., P. W. Thorne, M. P. McCarthy, S. F. B. Tett, L. Haimberger, and D. E. Parker, 2009: Critically Reassessing Tropospheric Temperature Trends from Radiosondes Using Realistic Validation Experiments. *Journal of Climate*, **22,** 465-485.
Tokinaga, H., and S.-P. Xie, 2011a: Wave and anemometer-based sea surface wind (WASWind) for climate change analysis (in press). *J. Clim.*
Toreti, A., E. Xoplaki, D. Maraun, F. G. Kuglitsch, H. Wanner, and J. Luterbacher, 2010: Characterisation of extreme winter precipitation in Mediterranean coastal sites and associated anomalous atmospheric circulation patterns. *Natural Hazards and Earth System Sciences*, **10,** 1037-1050.
Torres, O., P. Barthia, J. Herman, A. Sinyuk, P. Ginoux, and B. Holben, 2002: A long-term record of aerosol optical depth from TOMS observations and comparison to AERONET measurements. *J.Atmos.Science*, **59,** 398-413.
Trenberth, K. E., 1984: Signal versus noise in the Southern Oscillation. *Monthly Weather Review*, **112,** 326-332.
——, 1997: The definition of El Nino. *Bulletin of the American Meteorological Society*, **78,** 2771-2777.
Trenberth, K. E., and J. W. Hurrell, 1994: Decadal atmosphere-ocean variations in the Pacific. *Climate Dynamics*, **9,** 303-319.
Trenberth, K. E., and T. J. Hoar, 1996: The 1990-1995 El Nino Southern Oscillation event: Longest on record. *Geophysical Research Letters*, **23,** 57-60.
Trenberth, K. E., and D. J. Shea, 2006: Atlantic hurricanes and natural variability in 2005. *Geophysical Research Letters*, **33**.
Trenberth, K. E., and J. T. Fasullo, 2010: CLIMATE CHANGE Tracking Earth's Energy. *Science*, **328,** 316-317.
Trenberth, K. E., A. Dai, R. M. Rasmussen, and D. B. Parsons, 2003: The changing character of precipitation. *Bulletin of the American Meteorological Society*, **84,** 1205-+.
Trenberth, K. E., J. T. Fasullo, C. O'Dell, and T. Wong, 2010: Relationships between tropical sea surface temperature and top-of-atmosphere radiation. *Geophysical Research Letters*, **37**.
Trenberth, K. E., et al., 2007: Observations: Surface and Atmospheric Climate Change. *Climate Change 2007: The Physical Science Basis. Contribution of Working Group I to the Fourth Assessment Report of the Intergovernmental Panel on Climate Change*, Cambridge University Press.
Trewin, B., and H. Vermont, 2010: Changes in the frequency of record temperatures in Australia, 1957-2009. *Australian Meteorological and Oceanographic Journal*, **60,** 113-119.
Trnka, M., J. Kysely, M. Mozny, and M. Dubrovsky, 2009: Changes in Central-European soil-moisture availability and circulation patterns in 1881-2005. *International Journal of Climatology*, **29,** 655-672.
Troup, A. J., 1965: Southern Oscillation. *Quarterly Journal of the Royal Meteorological Society*, **91,** 490-&.
Tryhorn, L., and J. Risbey, 2006: On the distribution of heat waves over the Australian region. *Australian Meteorological Magazine*, **55,** 169-182.
Turner, J., et al., 2005: Antarctic climate change during the last 50 years. *International Journal of Climatology*, **25,** 279-294.
Uppala, S. M., et al., 2005: The ERA-40 re-analysis. *Quarterly Journal of the Royal Meteorological Society*, **131,** 2961-3012.

Vautard, R., J. Cattiaux, P. Yiou, J. N. The paut, and P. Ciais, 2010: Northern Hemisphere atmospheric stilling partly attributed to an increase in surface roughness. *Nature Geoscience*, 756-761.
Vautard, R., et al., 2007: Summertime European heat and drought waves induced by wintertime Mediterranean rainfall deficit. *Geophysical Research Letters*, **34**.
Vecchi, G. A., and B. J. Soden, 2007: Global warming and the weakening of the tropical circulation. *Journal of Climate*, **20,** 4316-4340.
Vecchi, G. A., and T. R. Knutson, 2008: On estimates of historical north Atlantic tropical cyclone activity. *Journal of Climate*, **21,** 3580-3600.
Vecchi, G. A., A. Clement, and B. J. Soden, 2008: Examining the tropical Pacific's response to global warming. *Eos, Trans. Amer. Geophys. Union*, 81-83.
Vecchi, G. A., B. J. Soden, A. T. Wittenberg, I. M. Held, A. Leetmaa, and M. J. Harrison, 2006: Weakening of tropical Pacific atmospheric circulation due to anthropogenic forcing. *Nature*, **441,** 73-76.
Velders, G., S. Andersen, J. Daniel, D. Fahey, and M. McFarland, 2007: The importance of the Montreal Protocol in protecting climate. *Proceedings of the National Academy of Sciences of the United States of America*, 4814-4819.
Velders, G., D. Fahey, J. Daniel, M. McFarland, and S. Andersen, 2009: The large contribution of projected HFC emissions to future climate forcing. *Proceedings of the National Academy of Sciences of the United States of America*, 10949-10954.
Vicente-Serrano, S. M., and J. I. Lopez-Moreno, 2008: Nonstationary influence of the North Atlantic Oscillation on European precipitation. *Journal of Geophysical Research-Atmospheres*, **113**.
Vignati, E., M. Karl, M. Krol, J. Wilson, P. Stier, and F. Cavalli, 2010: Sources of uncertainties in modelling black carbon at the global scale. *Atmos. Chem. Phys.*, **10,** 2595-2611.
Vilibic, I., and J. Sepic, 2010: Long-term variability and trends of sea level storminess and extremes in European Seas. *Global and Planetary Change*, **71,** 1-12.
Visbeck, M., 2009: A Station-Based Southern Annular Mode Index from 1884 to 2005. *Journal of Climate*, **22,** 940-950.
Volz, A., and D. Kley, 1988: Evaluation of the Montsouris series of ozone measurements made in the 19th century. *Nature*, **332,** 240-242.
Vomel, H., D. E. David, and K. Smith, 2007a: Accuracy of tropospheric and stratospheric water vapor measurements by the cryogenic frost point hygrometer: Instrumental details and observations. *Journal of Geophysical Research-Atmospheres*, **112**.
Vomel, H., et al., 2007b: Validation of Aura Microwave Limb Sounder water vapor by balloon-borne Cryogenic Frost point Hygrometer measurements. *Journal of Geophysical Research-Atmospheres*, **112**.
Vose, R. S., D. R. Easterling, and B. Gleason, 2005a: Maximum and minimum temperature trends for the globe: An update through 2004. *Geophysical Research Letters*, **32**.
Vose, R. S., D. Wuertz, T. C. Peterson, and P. D. Jones, 2005b: An intercomparison of trends in surface air temperature analyses at the global, hemispheric, and grid-box scale. *Geophysical Research Letters*, **32**.
Vose, R. S., Oak Ridge National Laboratory. Environmental Sciences Division., U.S. Global Change Research Program, United States. Dept. of Energy. Office of Health and Environmental Research., Carbon Dioxide Information Analysis Center (U.S.), and Martin Marietta Energy Systems Inc., 1992: *The Global historical climatology network : long-term monthly temperature, precipitation, sea level pressure, and station pressure data*. Carbon Dioxide Information Analysis Center
Available to the public from N.T.I.S., 1 v. (various pagings) pp.
Wallace, J. M., and D. S. Gutzler, 1981: Teleconnections in the geopotential height field during the Northern Hemisphere winter. *Monthly Weather Review*, **109,** 784-812.
Wallace, J. M., Y. Zhang, and J. A. Renwick, 1995: Dynamic contribution to hemispheric mean temperature trends. *Science*, **270,** 780-783.
Wan, H., X. L. Wang, and V. R. Swail, 2010: Homogenization and Trend Analysis of Canadian Near-Surface Wind Speeds. *Journal of Climate*, **23,** 1209-1225.
Wang, G. L., 2005: Agricultural drought in a future climate: results from 15 global climate models participating in the IPCC 4th assessment. *Climate Dynamics*, **25,** 739-753.
Wang, J. H., and L. Y. Zhang, 2008: Systematic errors in global radiosonde precipitable water data from comparisons with ground-based GPS measurements. *Journal of Climate*, **21,** 2218-2238.
——, 2009: Climate applications of a global, 2-hourly atmospheric precipitable water dataset derived from IGS tropospheric products. *Journal of Geodesy*, **83,** 209-217.
Wang, J. H., L. Y. Zhang, A. Dai, T. Van Hove, and J. Van Baelen, 2007: A near-global, 2-hourly data set of atmospheric precipitable water from ground-based GPS measurements. *Journal of Geophysical Research-Atmospheres*, **112**.
Wang, K. C., and S. L. Liang, 2009: Global atmospheric downward longwave radiation over land surface under all-sky conditions from 1973 to 2008. *Journal of Geophysical Research-Atmospheres*, **114,** -.
Wang, X. L. L., V. R. Swail, and F. W. Zwiers, 2006: Climatology and changes of extratropical cyclone activity: Comparison of ERA-40 with NCEP-NCAR reanalysis for 1958-2001. *Journal of Climate*, **19,** 3145-3166.

Wang, X. L. L., F. W. Zwiers, V. R. Swail, and Y. Feng, 2009: Trends and variability of storminess in the Northeast Atlantic region, 1874-2007. *Climate Dynamics*, **33,** 1179-1195.
Warren, S. G., R. M. Eastman, and C. J. Hahn, 2007: A survey of changes in cloud cover and cloud types over land from surface observations, 1971-96. *Journal of Climate*, **20,** 717-738.
Webster, P. J., G. J. Holland, J. A. Curry, and H. R. Chang, 2005: Changes in tropical cyclone number, duration, and intensity in a warming environment. *Science*, **309,** 1844-1846.
Weinstock, E. M., et al., 2009: Validation of the Harvard Lyman-alpha in situ water vapor instrument: Implications for the mechanisms that control stratospheric water vapor. *Journal of Geophysical Research-Atmospheres*, **114**.
Weiss, R., J. Muhle, P. Salameh, and C. Harth, 2008: Nitrogen trifluoride in the global atmosphere. *Geophysical Research Letters***,** -.
Weisse, R., H. Von Storch, and F. Feser, 2005: Northeast Atlantic and North Sea storminess as simulated by a regional climate model during 1958-2001 and comparison with observations. *Journal of Climate*, **18,** 465-479.
Wells, N., S. Goddard, and M. J. Hayes, 2004: A self-calibrating Palmer Drought Severity Index. *Journal of Climate*, **17,** 2335-2351.
Weng, H. Y., S. K. Behera, and T. Yamagata, 2009: Anomalous winter climate conditions in the Pacific rim during recent El NiA +/- o Modoki and El NiA +/- o events. *Climate Dynamics*, **32,** 663-674.
Wentz, F. J., L. Ricciardulli, K. Hilburn, and C. Mears, 2007: How much more rain will global warming bring? *Science*, **317,** 233-235.
Werner, P. C., F. W. Gerstengarbe, and F. Wechsung, 2008: Grosswetterlagen and precipitation trends in the Elbe river catchment. *Meteorologische Zeitschrift*, **17,** 61-66.
Wibig, J., 2008: Cloudiness variations in Lodz in the second half of the 20th century. *International Journal of Climatology*, **28,** 479-491.
Wielicki, B. A., B. R. Barkstrom, E. F. Harrison, R. B. Lee, G. L. Smith, and J. E. Cooper, 1996: Clouds and the earth's radiant energy system (CERES): An earth observing system experiment. *Bulletin of the American Meteorological Society*, **77,** 853-868.
Wild, M., 2008: Short-wave and long-wave surface radiation budgets in GCMs: a review based on the IPCC-AR4/CMIP3 models. *Tellus Series a-Dynamic Meteorology and Oceanography*, **60,** 932-945.
——, 2009: Global dimming and brightening: A review. *J. Geophys. Res.-Atmos.*, **114**.
Wild, M., and B. Liepert, 2010: The Earth radiation balance as driver of the global hydrological cycle. *Environmental Research Letters*, **5**.
Wild, M., A. Ohmura, and K. Makowski, 2007: Impact of global dimming and brightening on global warming. *Geophysical Research Letters*, **34,** L04702.
Wild, M., J. Grieser, and C. Schaer, 2008: Combined surface solar brightening and increasing greenhouse effect support recent intensification of the global land-based hydrological cycle. *Geophysical Research Letters*, **35,** L17706.
Wild, M., A. Ohmura, H. Gilgen, and D. Rosenfeld, 2004: On the consistency of trends in radiation and temperature records and implications for the global hydrological cycle. *Geophysical Research Letters*, **31,** L11201.
Wild, M., B. Truessel, A. Ohmura, C. N. Long, G. Konig-Langlo, E. G. Dutton, and A. Tsvetkov, 2009: Global dimming and brightening: An update beyond 2000. *Journal of Geophysical Research-Atmospheres*, **114,** D00d13.
Wild, M., et al., 2005: From dimming to brightening: Decadal changes in solar radiation at Earth's surface. *Science*, **308,** 847-850.
Willett, K. M., P. D. Jones, N. P. Gillett, and P. W. Thorne, 2008: Recent Changes in Surface Humidity: Development of the HadCRUH Dataset. *Journal of Climate*, **21,** 5364-5383.
Willett, K. M., P. D. Jones, P. W. Thorne, and N. P. Gillett, 2010: A comparison of large scale changes in surface humidity over land in observations and CMIP3 general circulation models. *Environmental Research Letters*, **5**.
Willson, R. C., and A. V. Mordvinov, 2003: Secular total solar irradiance trend during solar cycles 21-23. *Geophys. Res. Lett.*, **30**.
WMO, 2011: Scientific Assessment of Ozone Depletion: 2010, Global Ozone Research and Monitoring Project–Report No. 52.
Wong, T., B. A. Wielicki, R. B. Lee, ., G. L. Smith, K. A. Bush, and J. K. Willis, 2006: Reexamination of the observed decadal variability of the earth radiation budget using altitude-corrected ERBE/ERBS nonscanner WFOV data. *Journal of Climate*, **19,** 4028-4040.
Woodruff, S. D., et al., 2011: ICOADS Release 2.5: Extensions and Enhancements to the Surface Marine Meteorological Archive (in press). *Int. J. Climatol.*
Worton, D., et al., 2007: Atmospheric trends and radiative forcings of CF4 and C2F6 inferred from firn air. *Environmental Science & Technology***,** 2184-2189.
Xavier, P. K., V. O. John, S. A. Buehler, R. S. Ajayamohan, and S. Sijikumar, 2010: Variability of Indian summer monsoon in a new upper tropospheric humidity data set. *Geophysical Research Letters*, **37**.
Xia, X., 2010a: A closer looking at dimming and brightening in China during 1961-2005. *Annales Geophysicae*, **28,** 1121-1132.
Xia, X. G., 2010b: Spatiotemporal changes in sunshine duration and cloud amount as well as their relationship in China during 1954-2005. *Journal of Geophysical Research-Atmospheres*, **115**.

Xu, C. Y., L. B. Gong, J. Tong, and D. L. Chen, 2006a: Decreasing reference evapotranspiration in a warming climate - A case of Changjiang (Yangtze) River catchment during 1970-2000. *Advances in Atmospheric Sciences*, **23,** 513-520.
Xu, J. J., and A. M. Powell, 2010: Ensemble spread and its implication for the evaluation of temperature trends from multiple radiosondes and reanalyses products. *Geophysical Research Letters*, **37**.
Xu, K. H., J. D. Milliman, and H. Xu, 2010: Temporal trend of precipitation and runoff in major Chinese Rivers since 1951. *Global and Planetary Change*, **73,** 219-232.
Xu, M., C. P. Chang, C. B. Fu, Y. Qi, A. Robock, D. Robinson, and H. M. Zhang, 2006b: Steady decline of east Asian monsoon winds, 1969-2000: Evidence from direct ground measurements of wind speed. *Journal of Geophysical Research-Atmospheres*, **111**.
Yang, D. Q., B. S. Ye, and D. L. Kane, 2004: Streamflow changes over Siberian Yenisei River Basin. *Journal of Hydrology*, **296,** 59-80.
Ye, B. S., D. Q. Yang, and D. L. Kane, 2003: Changes in Lena River streamflow hydrology: Human impacts versus natural variations. *Water Resources Research*, **39**.
You, Q., et al., 2010: Changes in daily climate extremes in China and their connection to the large scale atmospheric circulation during 1961-2003. *Climate Dynamics*.
You, Q. L., S. C. Kang, E. Aguilar, and Y. P. Yan, 2008: Changes in daily climate extremes in the eastern and central Tibetan Plateau during 1961-2005. *Journal of Geophysical Research-Atmospheres*, **113**.
Yu, B., and F. W. Zwiers, 2010: Changes in equatorial atmospheric zonal circulations in recent decades. *Geophysical Research Letters*, **37**.
Zahn, M., and H. von Storch, 2008: A long-term climatology of North Atlantic polar lows. *Geophysical Research Letters*, **35**.
Zaitchik, B. F., A. K. Macalady, L. R. Bonneau, and R. B. Smith, 2006: Europe's 2003 heat wave: A satellite view of impacts and land-atmosphere feedbacks. *International Journal of Climatology*, **26,** 743-769.
Zebiak, S. E., 1993: Air-sea interaction in the equatorial Atlantic region. *Journal of Climate*, **6,** 1567-1568.
Zelinka, M. D., and D. L. Hartmann, 2010: Why is longwave cloud feedback positive? *J. Geophys. Res. Atmos.*, **115**.
Zerefos, C. S., et al., 2009: Solar dimming and brightening over Thessaloniki, Greece, and Beijing, China. *Tellus Series B-Chemical and Physical Meteorology*, **61,** 657-665.
Zhai, J. Q., B. D. Su, V. Krysanova, T. Vetter, C. Gao, and T. Jiang, 2010: Spatial Variation and Trends in PDSI and SPI Indices and Their Relation to Streamflow in 10 Large Regions of China. *Journal of Climate*, **23,** 649-663.
Zhai, P. M., X. B. Zhang, H. Wan, and X. H. Pan, 2005: Trends in total precipitation and frequency of daily precipitation extremes over China. *Journal of Climate*, **18,** 1096-1108.
Zhang, J., and J. S. Reid, 2010: A decadal regional and global trend analysis of the aerosol optical depth using a data-assimilation grade over-water MODIS and Level 2 MISR aerosol products. *Atmos. Chem. Phys.*, **10,** 10949-10963.
Zhang, L., D. J. Jacob, X. Liu, J. A. Logan, K. Chance, A. Eldering, and B. R. Bojkov, 2010: Intercomparison methods for satellite measurements of atmospheric composition: application to tropospheric ozone from TES and OMI. *Atmos. Chem. Phys.*, **10,** 4725-4739.
Zhang, X. B., K. D. Harvey, W. D. Hogg, and T. R. Yuzyk, 2001: Trends in Canadian streamflow. *Water Resources Research*, **37,** 987-998.
Zhang, X. D., J. E. Walsh, J. Zhang, U. S. Bhatt, and M. Ikeda, 2004a: Climatology and interannual variability of arctic cyclone activity: 1948-2002. *Journal of Climate*, **17,** 2300-2317.
Zhang, X. D., A. Sorteberg, J. Zhang, R. Gerdes, and J. C. Comiso, 2008: Recent radical shifts of atmospheric circulations and rapid changes in Arctic climate system. *Geophysical Research Letters*, **35**.
Zhang, Y., J. M. Wallace, and D. S. Battisti, 1997: ENSO-like interdecadal variability: 1900-93. *Journal of Climate*, **10,** 1004-1020.
Zhang, Y. C., W. B. Rossow, A. A. Lacis, V. Oinas, and M. I. Mishchenko, 2004b: Calculation of radiative fluxes from the surface to top of atmosphere based on ISCCP and other global data sets: Refinements of the radiative transfer model and the input data. *J. Geophys. Res. Atmos.*, **109,** doi:10.1029/2004GL019956.
Zhang, Y. C., W. B. Rossow, P. Stackhouse, A. Romanou, and B. A. Wielicki, 2007a: Decadal variations of global energy and ocean heat budget and meridional energy transports inferred from recent global data sets. *Journal of Geophysical Research-Atmospheres*, **112**.
Zhang, Y. Q., C. M. Liu, Y. H. Tang, and Y. H. Yang, 2007b: Trends in pan evaporation and reference and actual evapotranspiration across the Tibetan Plateau. *Journal of Geophysical Research-Atmospheres*, **112**.
Zhou, L. M., A. Dai, Y. J. Dai, R. Vose, C. Z. Zou, Y. H. Tian, and H. S. Chen, 2009a: Spatial dependence of diurnal temperature range trends on precipitation from 1950 to 2004. *Climate Dynamics*, **32,** 429-440.
Zhou, T. J., et al., 2009b: Why the Western Pacific Subtropical High Has Extended Westward since the Late 1970s. *Journal of Climate*, **22,** 2199-2215.
Ziemke, J. R., S. Chandra, and P. K. Bhartia, 2005: A 25-year data record of atmospheric ozone in the Pacific from Total Ozone Mapping Spectrometer (TOMS) cloud slicing: Implications for ozone trends in the stratosphere and troposphere. *J. Geophys. Res.*, **110,** D15105.
Zolina, O., C. Simmer, S. K. Gulev, and S. Kollet, 2010: Changing structure of European precipitation: Longer wet periods leading to more abundant rainfalls. *Geophysical Research Letters*, **37**.

Zolina, O., C. Simmer, A. Kapala, S. Bachner, S. Gulev, and H. Maechel, 2008: Seasonally dependent changes of precipitation extremes over Germany since 1950 from a very dense observational network. *Journal of Geophysical Research-Atmospheres*, **113**.

Zou, C. Z., and W. H. Wang, 2010: Stability of the MSU-Derived Atmospheric Temperature Trend. *Journal of Atmospheric and Oceanic Technology*, **27,** 1960-1971.

Zou, C. Z., M. Gao, and M. D. Goldberg, 2009: Error Structure and Atmospheric Temperature Trends in Observations from the Microwave Sounding Unit. *Journal of Climate*, **22,** 1661-1681.

Zou, C. Z., M. D. Goldberg, Z. H. Cheng, N. C. Grody, J. T. Sullivan, C. Y. Cao, and D. Tarpley, 2006a: Recalibration of microwave sounding unit for climate studies using simultaneous nadir overpasses. *Journal of Geophysical Research-Atmospheres*, **111**.

Zou, X., L. V. Alexander, D. Parker, and J. Caesar, 2006b: Variations in severe storms over China. *Geophysical Research Letters*, **33**.

Zou, X. K., P. M. Zhai, and Q. Zhang, 2005: Variations in droughts over China: 1951-2003. *Geophysical Research Letters*, **32**.

Zuo, Z. Y., and R. H. Zhang, 2009: Temporal and spatial features of the soil moisture in boreal spring in eastern China. *Science in China Series D-Earth Sciences*, **52,** 269-278.

Box 2.3, Table 1: Established indices of climate variability with global or regional influence. Columns are: (1) name of a general climate phenomenon, (2) name of a specific index intended to describe it, (3) index definition, (4) primary reference, (5) Figures in this Box, if any, illustrating this index and/or corresponding spatial pattern, (6) Sections of the report using this index, (7) characterization of the index or its corresponding spatial pattern as an optimal or dominant pattern of variability, and (8) Comments.

Climate Phenomenon	Index name	Index Definition	Primary Refs	Figs	Secs	Characterization	Comments
El Nino – Southern Oscillation (ENSO) - canonical, Eastern Pacific ENSO	NINO3	SST anomaly averaged over [5°S-5°N; 150°W-90°W]	Cane et al. (1986); Rasmusson and Wallace (1983)			Max. amplitude of "a broader scale warming of the equatorial Pacific" during 1982-83 El Nino event	Traditional SST-based ENSO index
	NINO3.4	SST anomaly averaged over [5°S-5°N; 170°W-120°W]	Trenberth (1997)	**Figure 2.6.4**, **Figure 2.6.5**		Detrended form is close to the 1st PC of linearly detrended global field of monthly SST anomalies (1900-2008, HadISST1, 19%, Deser et al., 2010b)	WMO RA IV Consensus Index for El Nino and La Nina events definition: deviations by no less than 0.5°C from 1971—2000 normals in three-month averages.
	Cold Tongue Index (CTI)	SSTA [6°N-6°S, 180°-90°W] – global mean SSTA	Deser and Wallace (1990)	**Figure 2.6.4**			Matches "cold tongue" area, subtracts the effect of the global average change
	Troup SOI	Standardized for each calendar month MSLP difference: Tahiti (17.5°S 149.6°W) minus Darwin (12.4°S 130.9°E), x10	Troup (1965)	**Figure 2.6.4**, **Figure 2.6.5**			Used by Australian Bureau of Meteorology
	SOI	Standardized difference of standardized MSLP anomalies: Tahiti (17.5°S 149.6°W) minus Darwin (12.4°S 130.9°E)	Trenberth (1984)	**Figure 2.6.4**		Maximizes signal to noise ratio among linear combinations of Darwin and Tahiti records	Used by NOAA Climate Prediction Center (U.S.)
	Darwin SOI	Standardized Darwin (12.4°S 130.9°E) MSLP anomaly	Trenberth and Hoar (1996)	**Figure 2.6.4**			Introduced to avoid the use of the Tahiti record, which is considered suspicious before 1935.
	Equatorial SOI (EQSOI)	Standardized difference between standardized averages of MSLP anomalies over eastern equatorial Pacific Ocean [5°S-5°N; 130°W-80°W] and Indonesia [5°S-5°N; 90°E-140°E]	Bell and Halpert (1998)	**Figure 2.6.4**			
Central Pacific El Nino (Modoki)	El Nino Modoki Index (EMI)	SSTA: [165°E–140°W, 10°S–10°N] - 0.5[110°W–70°W, 15°S–5°N]-0.5[125°E–145°E, 10°S-20°N]	Ashok et al. (2007)	**Figure 2.6.4**, **Figure 2.6.5**			Index for a recently identified type of El Nino events: Modoki or Central Pacific El Nino (non-canonical)
Pacific Decadal and Interdecadal Variability	Pacific Decadal Oscillation (PDO)	1st PC of the North Pacific SST anomaly field (20°N-70°N) with subtracted global mean	Mantua et al. (1997); Zhang et al. (1997)			As defined	
	Intedecadal Pacific Oscillation (IPO)	The 3rd EOF3 of the 13-year low-pass filtered global SST, projected onto annual data	Folland et al. (1999); Power et al. (1999)			As defined	
	North Pacific	SLP [30°N-65°N;	Trenberth and				

	Index (NPI)	160°E-140°W]	Hurrell (1994)				
Atlantic Ocean Themohaline circulation	Atlantic Multidecadal Oscillation (AMO) – original index	Ten-year running mean of de-trended Atlantic mean SST anomalies north of the equator [0-70°N]	Enfield et al.(2001)			Called "virtually identical" to the smoothed first rotated (North Atlantic) EOF mode	
	Atlantic Multidecadal Oscillation (AMO) – revised index	Original AMO Index but with global mean anomaly subtraction instead of de-trending	Trenberth and Shea (2006)				
NAO	Lisbon/ Ponta Delgada -- Stykkisholmur/ Reykjavik North Atlantic Oscillation (NAO) Index	Lisbon/ Ponta Delgada minus Stykkisholmur/ Reykjavik standardized MSLP anomalies	Hurrell , 1995b)	**Figure 2.6.6**, **Figure 2.6.7**		A primary NH teleconnection both in MSLP and Z500 anomalies (Wallace and Gutzler, 1981); one of rotated EOFs of NH Z500 (Barnston and Livezey, 1987)	MSLP anomalies in the NAO index definition could be taken as monthly, seasonally or annually averaged, or as NH winter (cold season) averages. Each of these choices carries to the temporal resolution of the NAO index produced that way.
	Gibraltar – Reykjavik NAO Index	Gibraltar minus Reykjavik standardized MSLP anomalies	Jones et al. (1997)				
	PC-based NAO Index	The leading principal component of MSLP anomalies over the Atlantic sector (20°N-80°N, 90°W-40°E)	Hurrell , 1995b)	**Figure 2.6.6**			
Annular modes: Arctic Oscillation (AO), a.k.a. Northern Annular Mode (NAM) Index and Antarctic Oscillation (AAO), a.k.a. Southern Annular Mode (SAM) Index	PC-based AO index	1st PC of the monthly mean MSLP anomalies poleward of 20°N	Thompson and Wallace (1998, 2000)	**Figure 2.6.6**, **Figure 2.6.7**		As defined	Closely related to the NAO
	PC-based AAO index	1st PC of 850 hPa geopotential height anomalies south of 20°S	Thompson and Wallace (2000)			As defined	
	AAO index as 40°S—65°S difference from a gridded SLP analysis	Difference between normalized zonal mean SLP at 40°S and 65°S	Gong and Wang (1999)				
	AAO index as 40°S—70°S difference from a gridded SLP analysis	Same as above but modified to the difference between latitudes 40°S and 70°S	Nan and Li (2003)				
	AAO index as a station-based 40°S—65°S pressure difference	Estimate of 40°S—65°S difference in normalized zonal mean SLP estimated from station data	Marshall et al. (2003)				
Pacific/North America (PNA) atmospheric teleconnection	PNA pattern index	0.25[Z(20°N, 160°W) - Z(45°N, 165°W) + Z(55N, 115°W) - Z(30°N, 85°W)], where Z denotes standardized 500 hPa geopotential height anomalies	Wallace and Gutzler (1981)			A primary NH teleconnection both in MSLP and Z500 anomalies (Wallace and Gutzler, 1981); one of rotated EOFs of NH Z500 (Barnston and Livezey, 1987)	
Tropical Atlantic Ocean non-ENSO variability	Atlantic Nino Index, ATL3	SSTA [3°S–3°N, 20°W–0°]	Zebiak (1993)			Identified by Deser et al. (2010b) as the two leading PCs of detrended tropical Atlantic monthly SSTA (20S-20N): 38% and 25% variance respectively for HadISST1, 1900-2008	
	Tropical Atlantic Meridional Mode (AMM)	The 2nd PC of the detrended tropical Atlantic monthly SSTA (20S-20N)	Deser et al., 2010a (this definition)				
Tropical Indian Ocean non-ENSO variability	Indian Ocean Basin Mode (IOBM) Index	The 1st PC of the IO detrended SST anomalies (40–110E, 20S–20N)	Deser et al. 2010a (this definition)			Identified by Deser et al.(2010b) as the two leading PCs of detrended tropical	

	Indian Ocean Dipole Mode Index (DMI)	SSTA: [50°E-70°E, 10°S-10°N)]-[90°E-110°E, 10°S-0°]	Saji et al. (1999)			Indian Ocean monthly SSTA (20S-20N): 39% and 12% of the variance, respectively, for HadISST1, 1900-2008	
Cold Ocean – Warm Land (COWL) Variability	COWL Index	Found by fitting to the global temperature field the regression pattern of temperature anomalies with subtracted global mean on that mean	Wallace et al. (1995)				Proved useful for removing some effects of natural climate variability from global mean temperature records.

1

Chapter 2: Observations: Atmosphere and Surface

Coordinating Lead Authors: Dennis Hartmann (USA), Albert Klein Tank (Netherlands), Matilde Rusticucci (Argentina)

Lead Authors: Lisa Alexander (Australia), Stefan Broennimann (Switzerland), Yassine Abdul-Rahman Charabi (Oman), Frank Dentener (EU / Netherlands), Ed Dlugokencky (USA), David Easterling (USA), Alexey Kaplan (USA), Nzioka John Muthama (Kenya), Brian Soden (USA), Peter Thorne (USA / UK), Martin Wild (Switzerland), Panmao Zhai (China)

Contributing Authors:

Review Editors: Jim Hurrell (USA), Jose Marengo (Brazil), Fredolin Tangang (Malaysia), Pedro Viterbo (Portugal)

Date of Draft: 15 April 2011

Notes: TSU Compiled Version

Figures

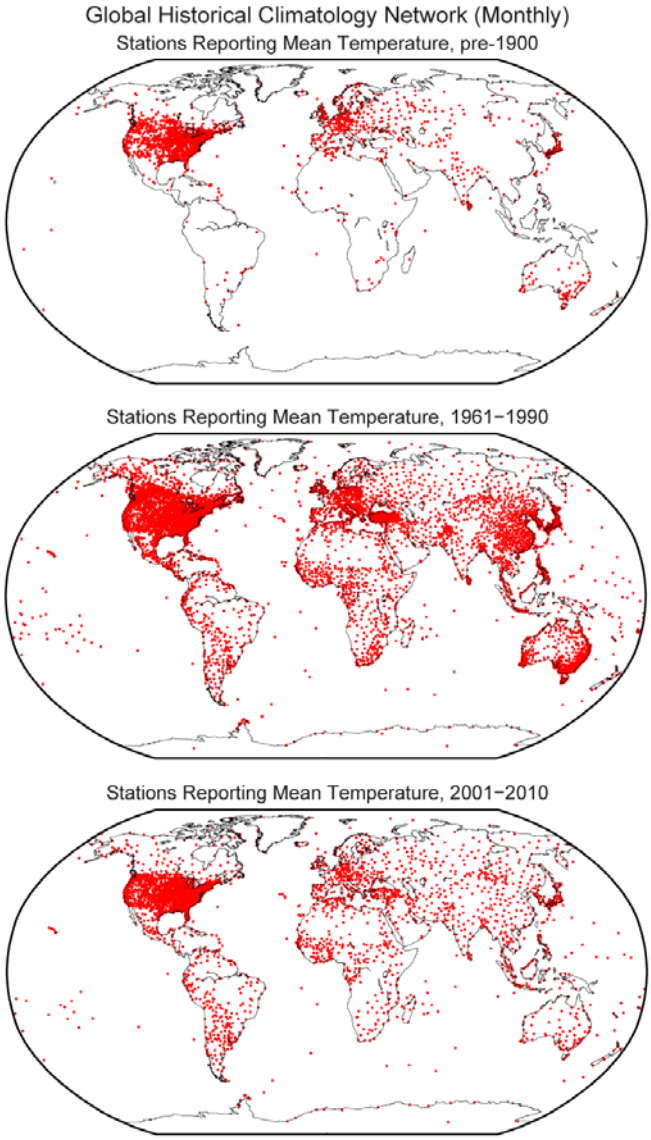

Figure 2.1: Station availability for the GHCN monthly network for the late 19th century, the 1961–1990 period of maximum station density and most recent decade.

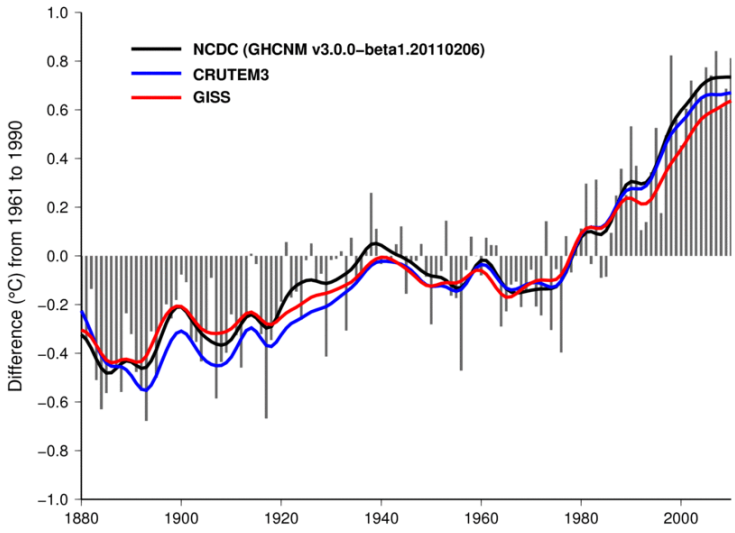

Figure 2.2: Global land surface temperature time series evolution estimates from 1880 to present.

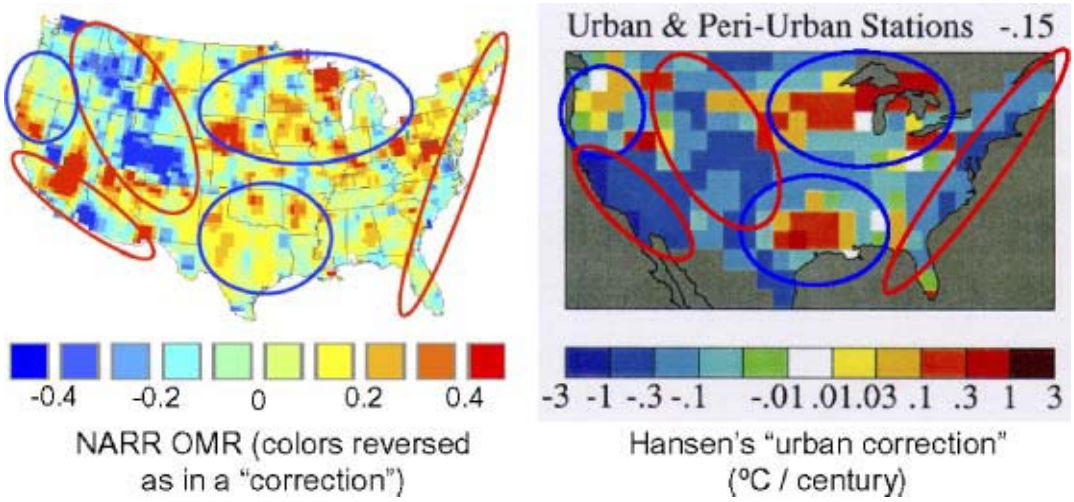

Figure 2.3: Fall et al. (2010)'s Figure 6 comparing (inverted) "Observations minus Reanalysis" temperature trends (°C per decade) over the USA with the Hansen et al. (2001) nightlight-based urban.

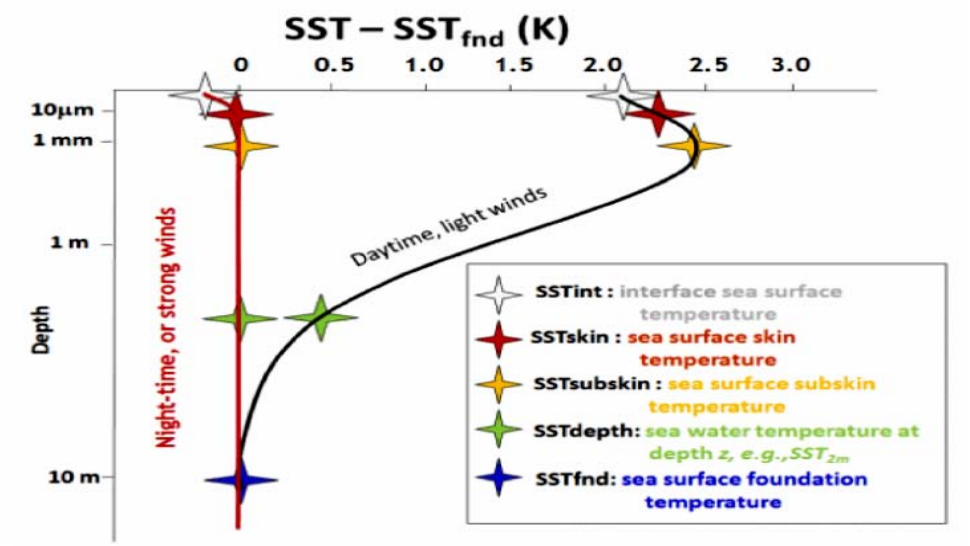

Figure 2.4: Thermal structure of the ocean surface layer (adopted from Donlon et al. (2007) by GHRSST participants; https://www.ghrsst.org/SST-Definitions.html; [precise attribution needs to be].

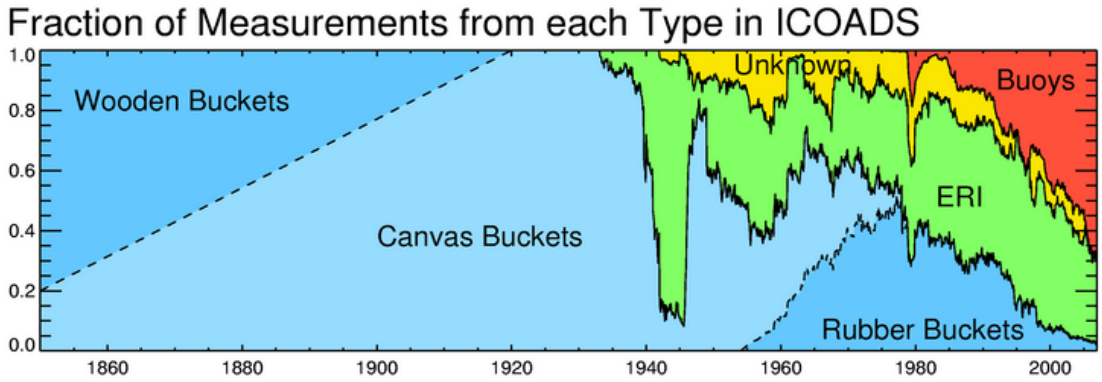

Figure 2.5: Fractional contribution to the global average SST from different measurement methods. The blue area represents bucket observations. The green area, engine inlet and hull contact sensor observations. The red area shows the contribution of moored and drifting buoys and the yellow area represents those observations that cannot be identified.

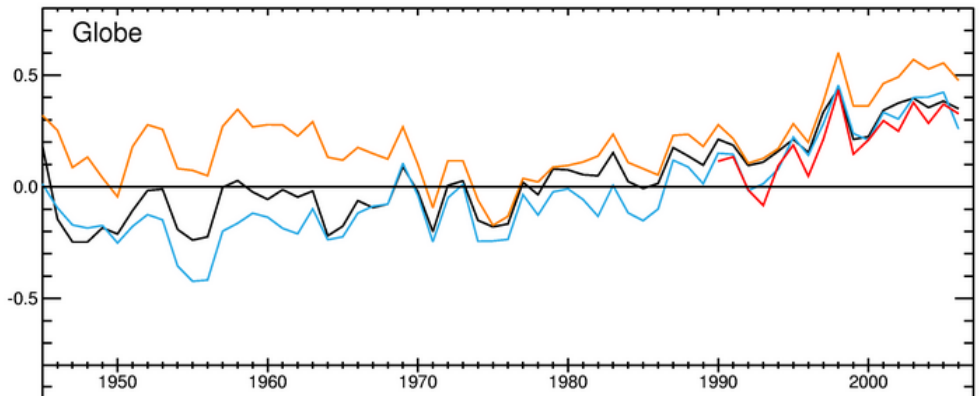

Figure 2.6: Effect of observational platform biases on global mean SST [(from Kennedy et al., 2011c)].

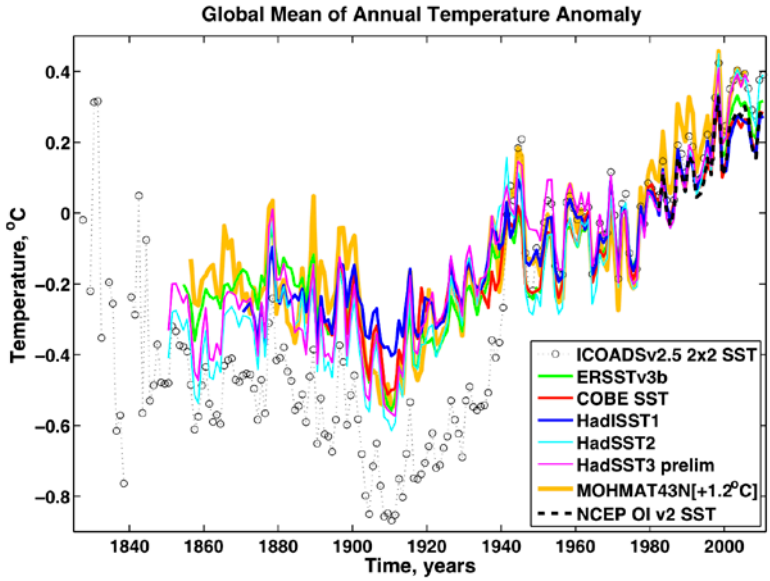

Figure 2.7: Global means of annually averaged anomalies from marine surface temperature data sets. See Table SST1 for descriptions of the data sets. Anomalies for all data sets are computed with regards to a common estimate of 1961–1990 climatological normals for SST (Table 2.2, Smith and Reynolds, 1998). To aid visual comparison, the results for the night marine air temperature data set (MOHMAT4.3N) have been shifted up by 1.2°C.

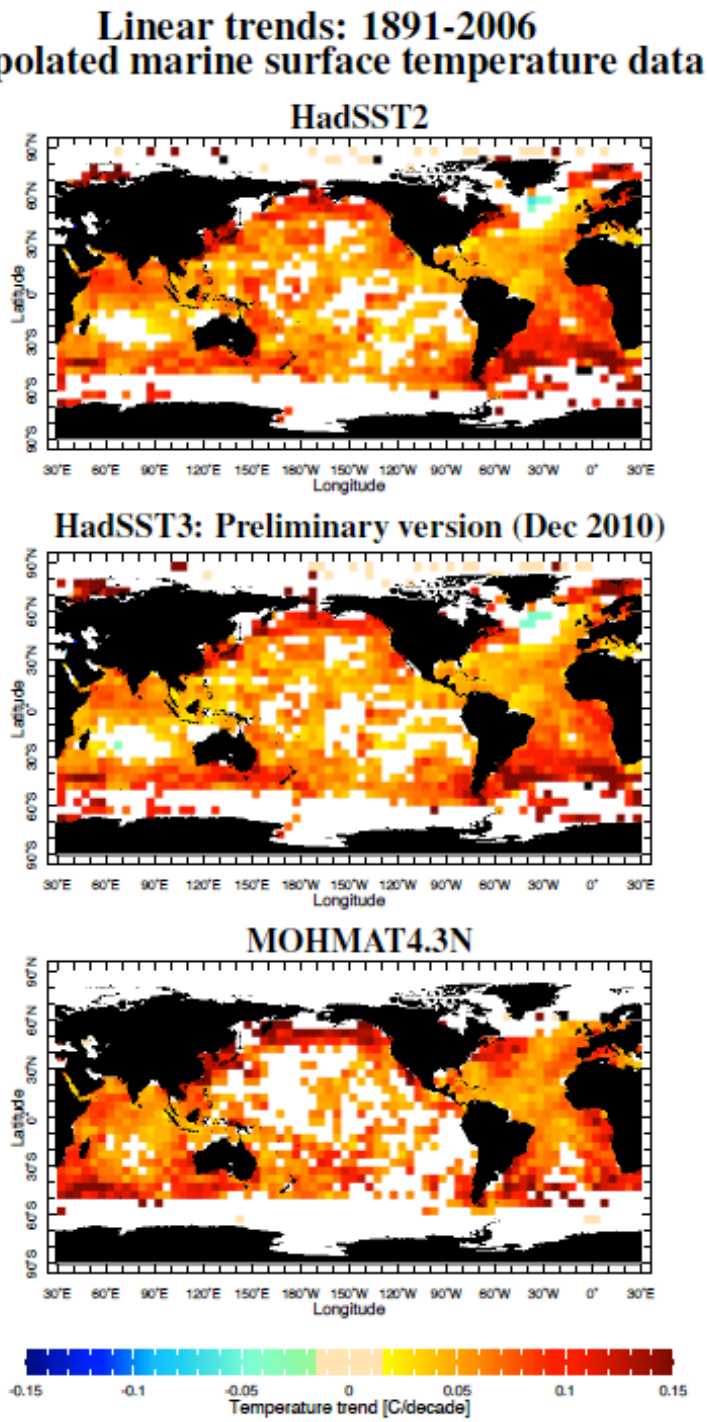

Figure 2.8: Linear trends for 1891–2006 period in the annual means of uninterpolated gridded data sets of marine surface temperature observations. MOHMAT4.3N trend is through 2005. See Table 2.2.1 and references therein for data set details. Trends are computed by ordinary least squares (OLS). In white areas computed trends were not different from zero at 5% significance level.

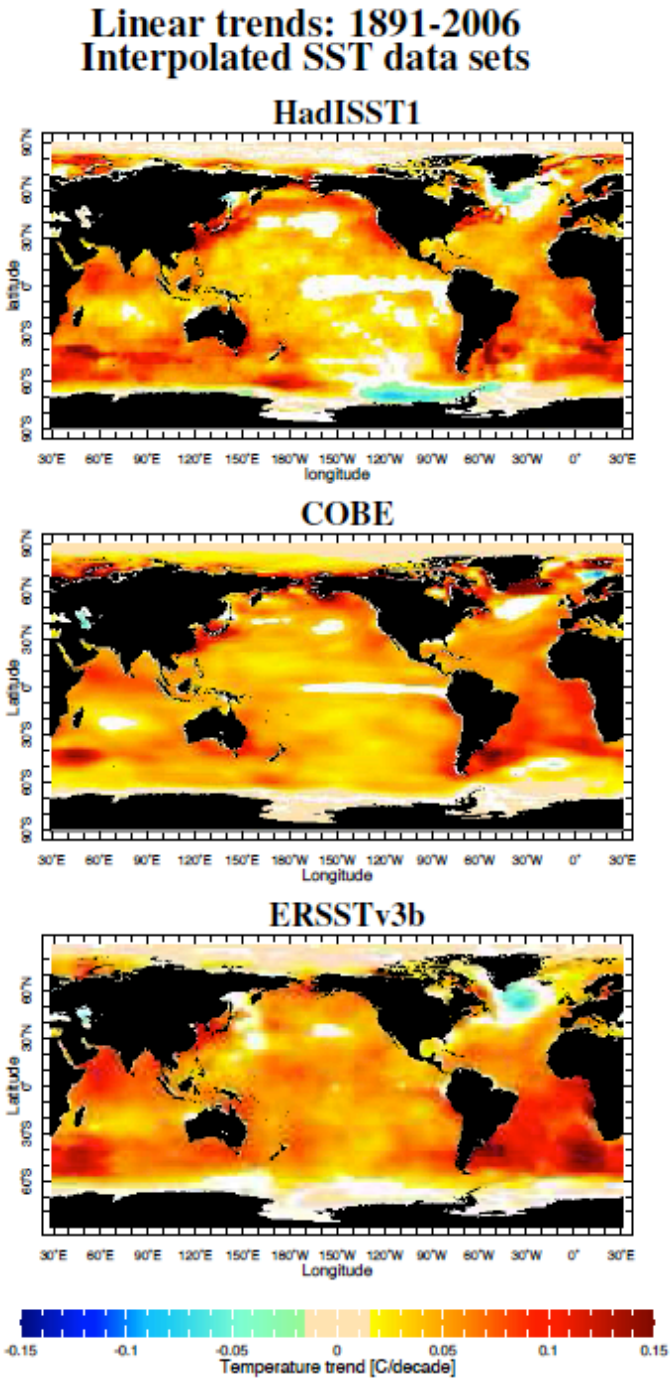

Figure 2.9: Linear trends for 1891–2006 period in the annual means of interpolated globally complete ("analyzed") SST data sets. See Table 2.2.1 and references therein for data set details. Trends are computed by OLS. In white areas computed trends were not different from zero at 5% significance level.

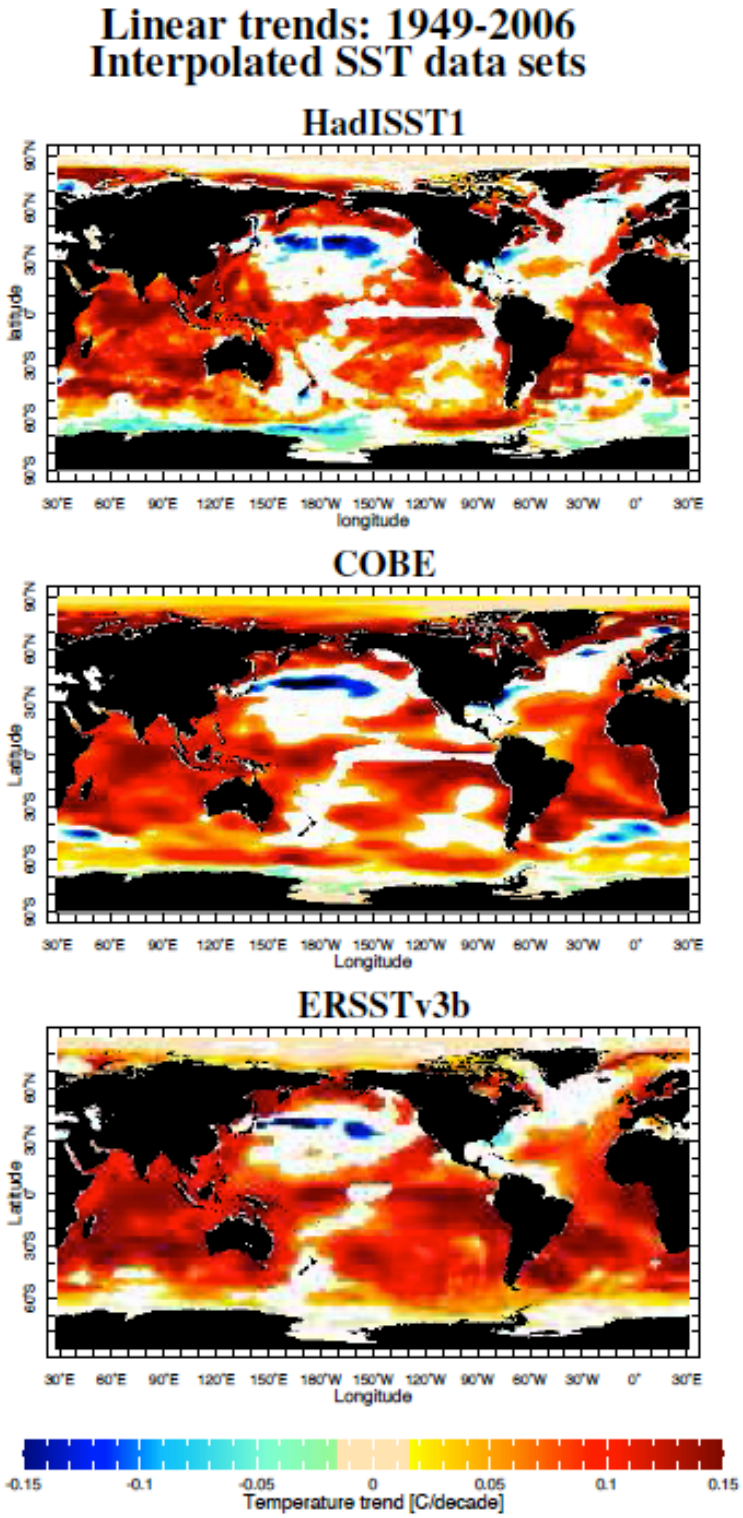

Figure 2.10: Linear trends for 1949–2006 period in the annual means of interpolated globally complete ("analyzed") SST data sets. See Table 2.2.1 and references therein for data set details. Trends are computed by OLS. In white areas computed trends were not different from zero at 5% significance level.

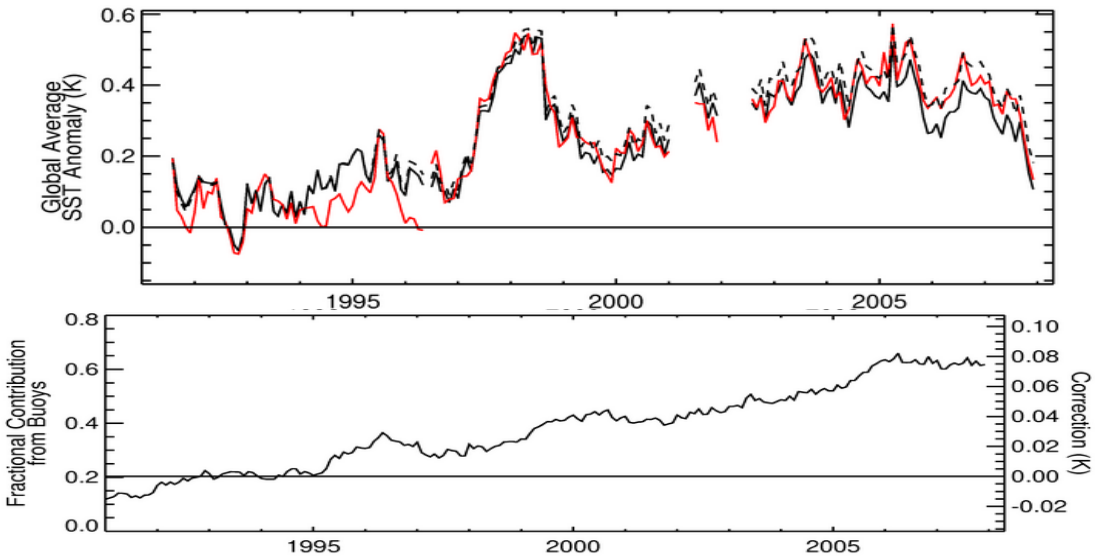

Figure 2.11: Consistency of bias corrections to the in situ SST data with independent satellite observations: (top) Co-located monthly, 5º area global average SST anomalies August 1991 to December 2007 (relative to 1961-1990) for the ATSR instruments (red) and HadSST2 (black, Rayner et al. 2006). D3 retrievals were used where they were available, but between 1992 and 1996 D2 retrievals from the ATSR-1 instrument were used. The dashed black line is an estimate of the HadSST2 time series corrected for the bias between drifting buoys and ships. (bottom) Fractional contribution of drifting buoy observations to the global average calculated by taking the area weighted average of the fraction of drifting buoy observations in each grid box. The correction is shown on the right-hand axis.

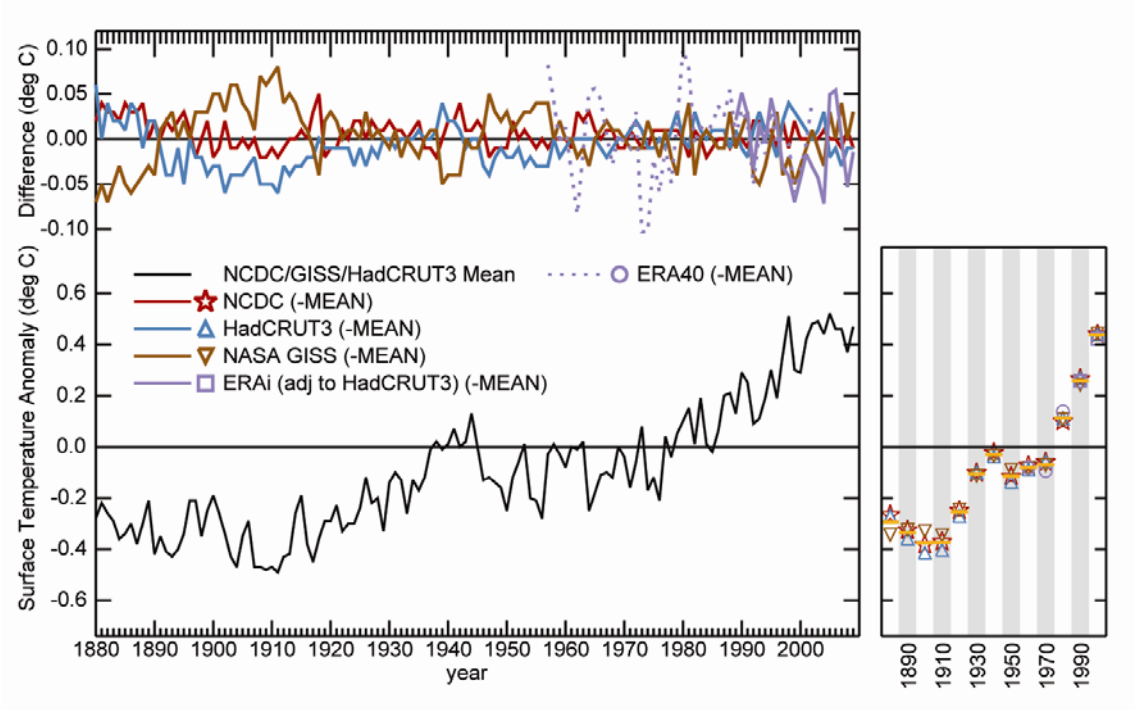

Figure 2.12: Global mean time series at annual resolution from a straight average of the three data products, plus offset from this differences between products. Right hand panel shows decadally averaged values.

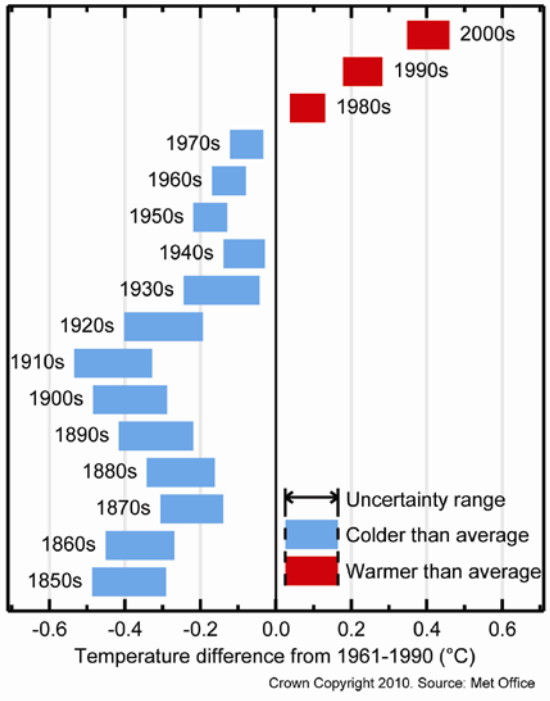

Figure 2.13: Decadal mean anomalies and associated uncertainties based upon Brohan et al. (2006) uncertainty model for HadCRUT3. Anomalies are relative to a 1961–1990 climatology period. Use of NCDC or GISS plus their uncertainties would yield grossly similar results and a similar conclusion that each of the last three decades in turn has been significantly warmer than all preceding decades in the record.

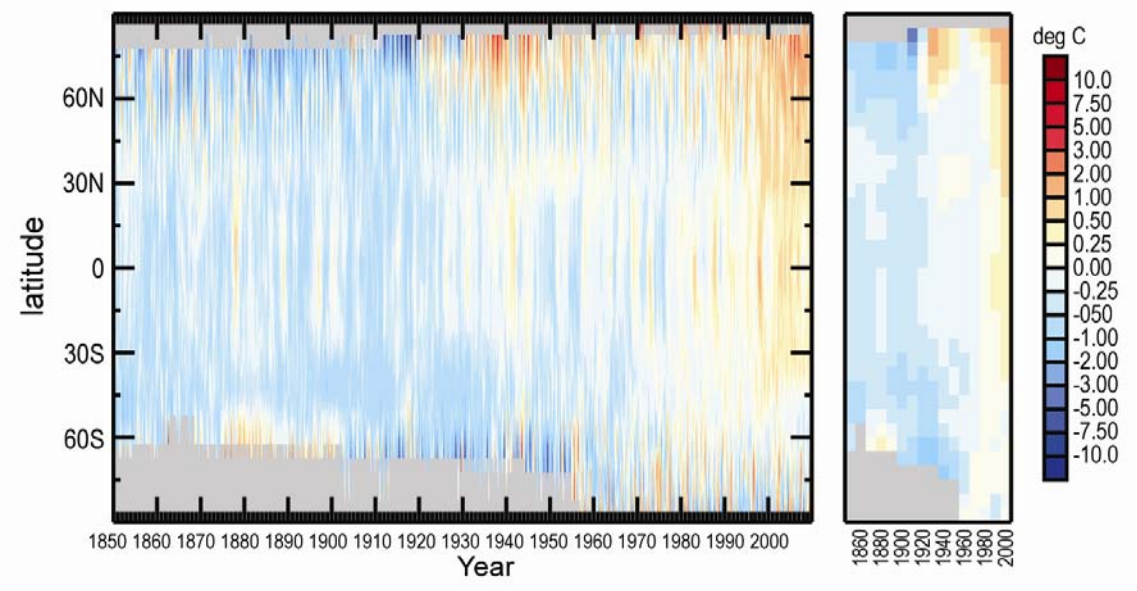

Figure 2.14: Hovmuller plot of surface anomalies from HadCRUT3 on an annual basis (left hand panel) and decadally averaged (right hand panel). Anomalies are relative to a 1961–1990 climatology.

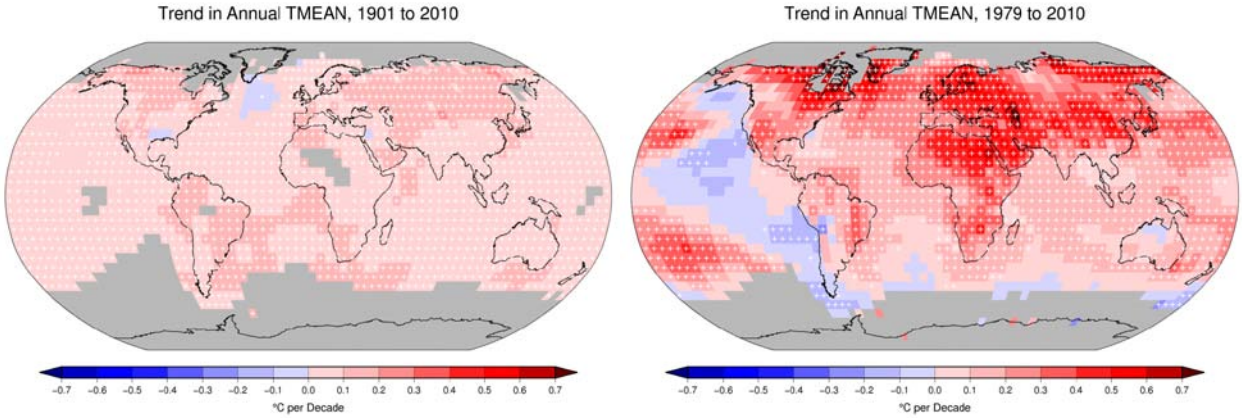

Figure 2.15: Global mean trend maps from NCDC surface record for 1901– 2010 (left hand panel) and 1979–2010.

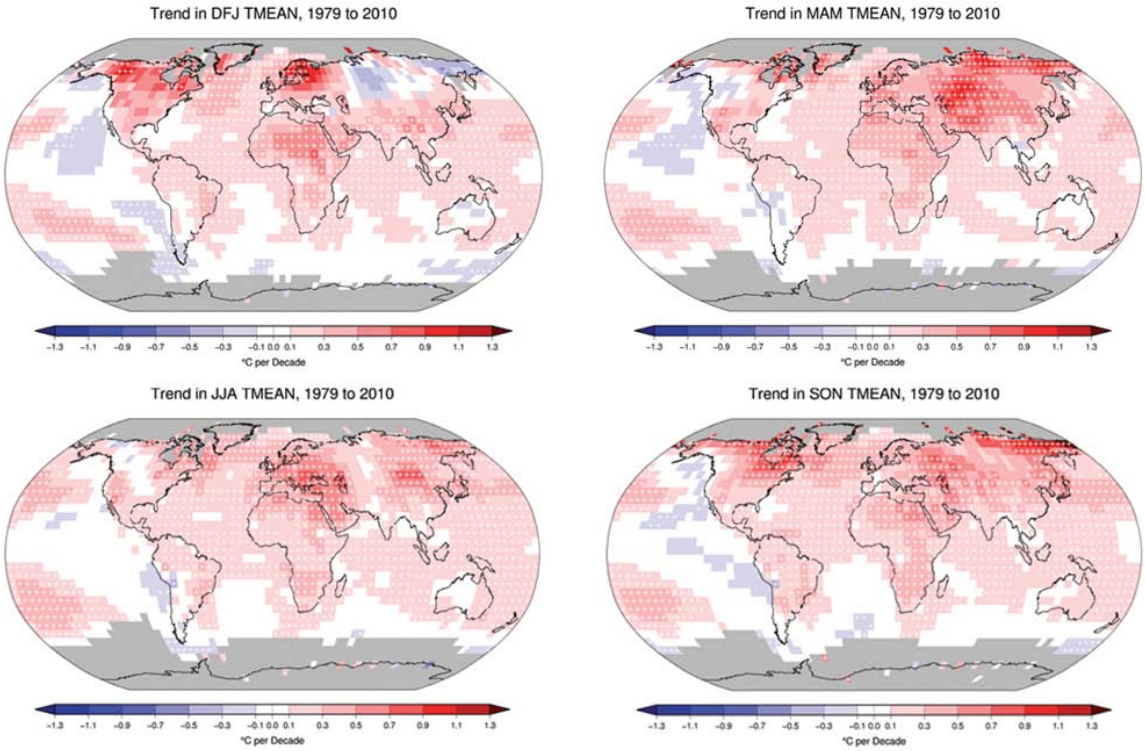

Figure 2.16: Seasonality of trends from the NCDC surface temperature analysis over the period since 1979.

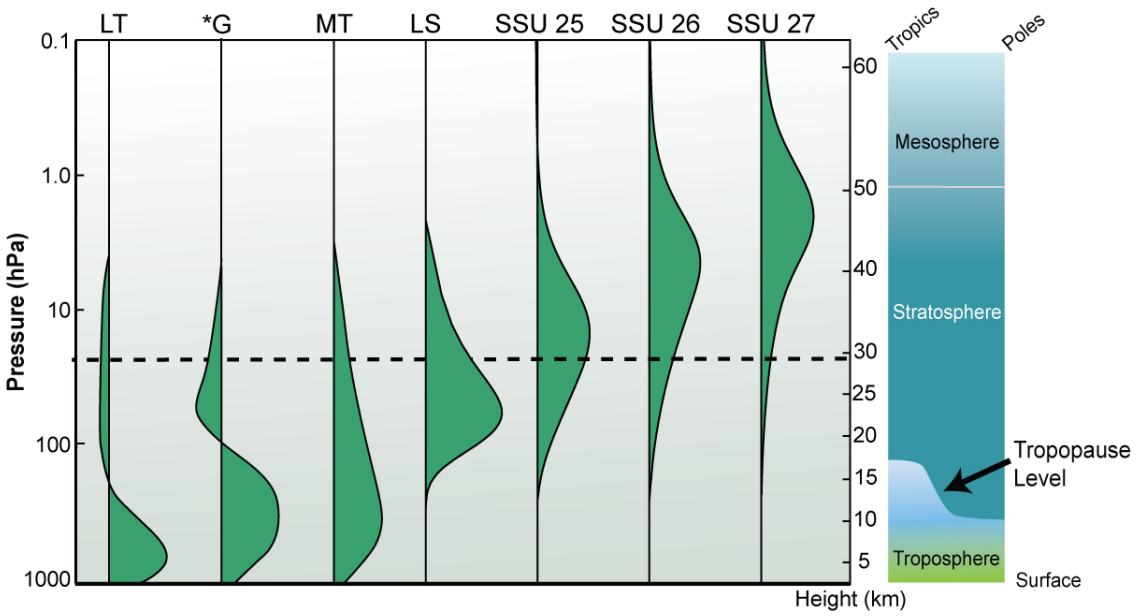

Figure 2.17: Vertical weighting functions for satellite temperature retrievals discussed in this chapter. The dashed line indicates the typical maximum altitude achieved in the historical radiosonde record.

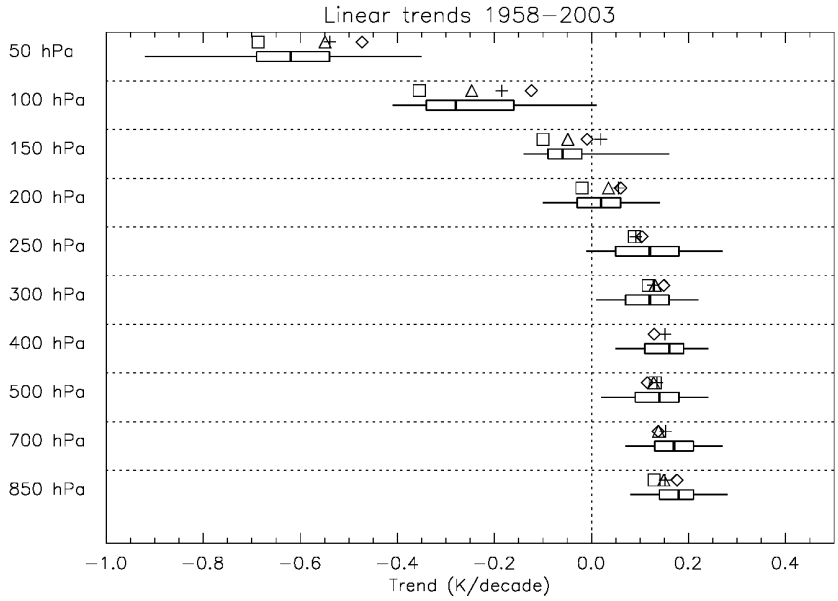

Figure 2.18: Radiosonde product global temperature trend estimates from four datasets (symbols) and the estimated structural uncertainty in the HadAT product from Thorne et al. (2011a) (Box whiskers denote median estimator, 25-75th percentile and range) over the common period of record 1958–2003. All trend estimates are from median of pairwise slopes technique. Global averages were created by calculating zonal means and then weighting zonal anomalies by cos(lat). The four best estimates used are HadAT2 (Δ), IUK (□), RICH (+) and RAOBCORE (◊).

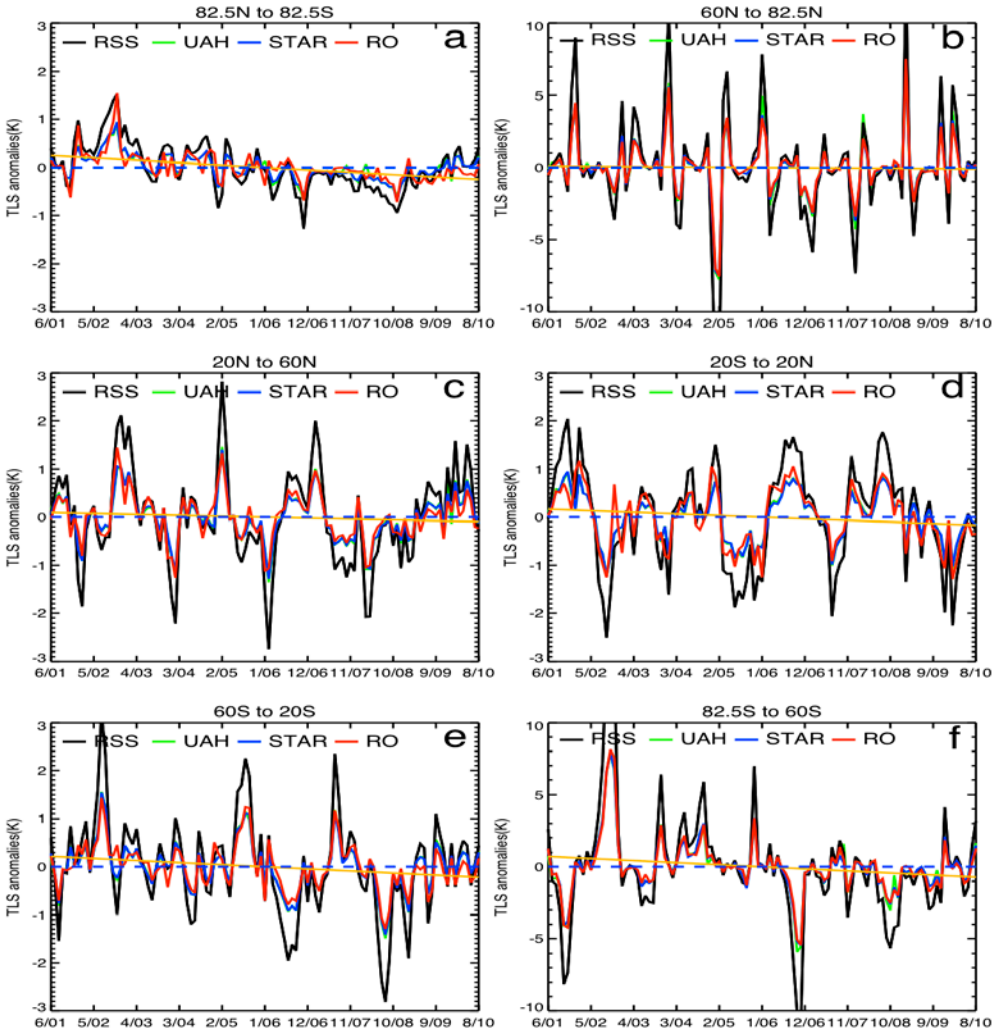

Figure 2.19: LS anomalies of RSS, UAH, STAR, and RO_AMSU for a) the entire globe (82.5ºN–82.5ºS), b) 82.5ºN–60ºN, c) 60ºN–20ºN, d) 20ºN–20ºS, e) 20ºS–60ºS, and f) 60ºS–82.5ºS. The orange line indicates the mean trend for RO_AMSU.

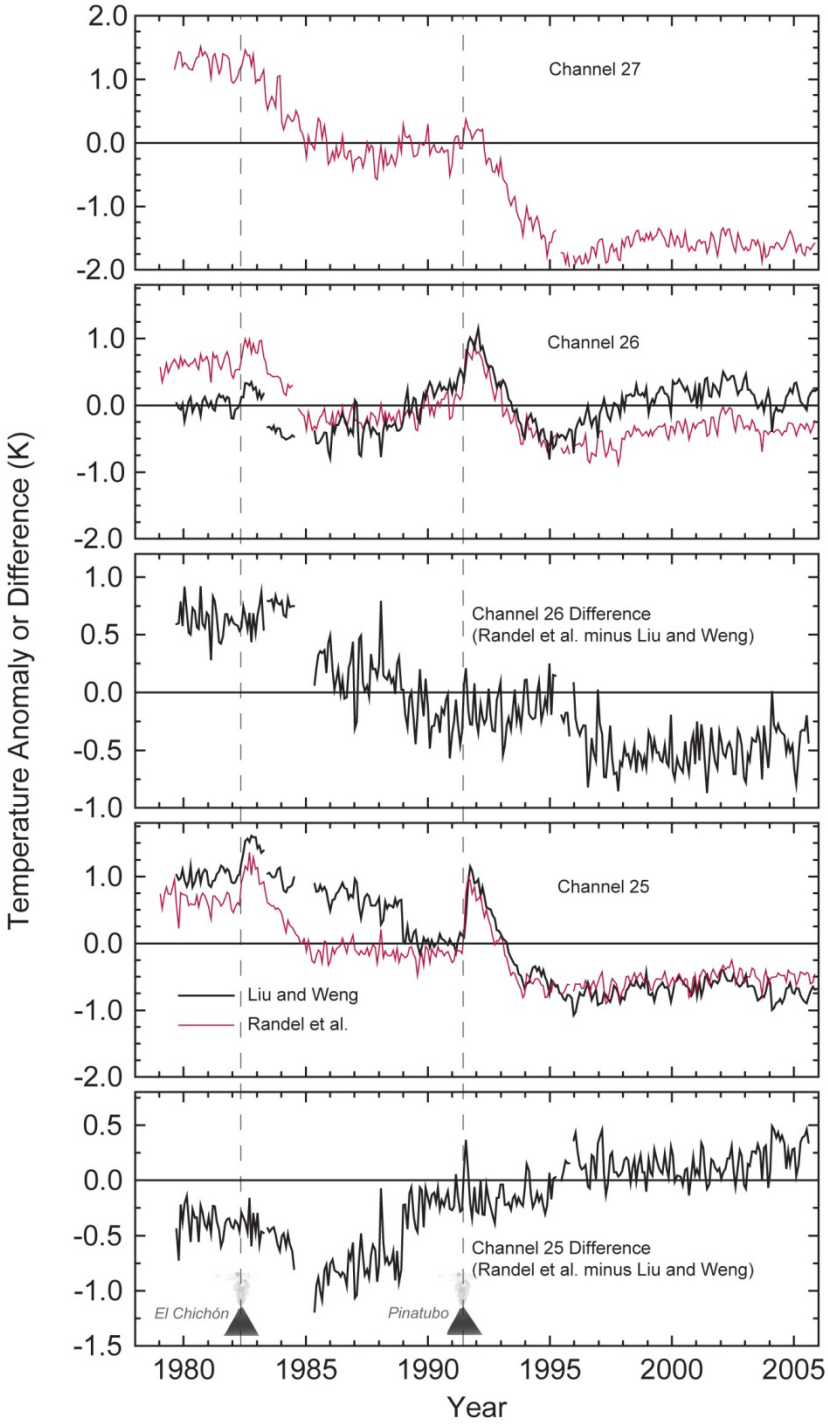

Figure 2.20: Global temperature anomaly time series from SSU data from the three SSU channels, as analysed by Randel et al. (2009) and, for Channels 25 and 26, as analysed by Liu and Weng (2009), and differences between them for Channels 25 and 26. Symbols indicate major volcanic eruptions in 1982 (El Chichón) and 1991 (Pinatubo). Reproduced from Seidel (2011).

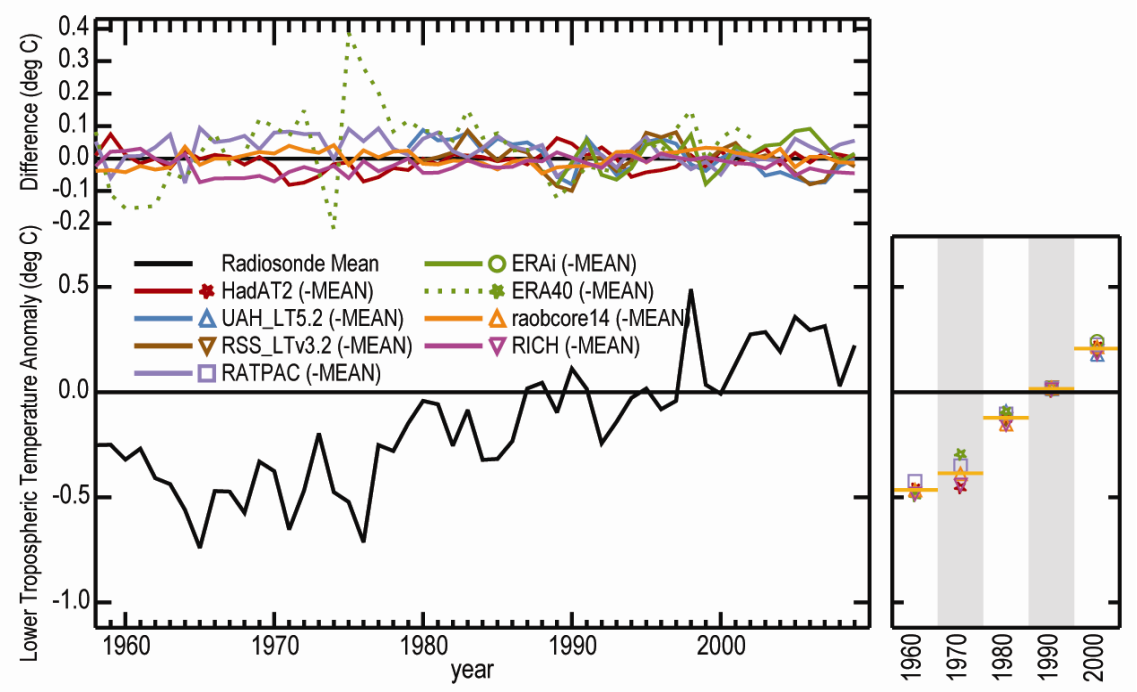

Figure 2.21: Global average lower tropospheric temperature anomaly time series for the mean of all included radiosonde datasets and offset therefrom the differences from this composite for each dataset (left hand panel). Decadal mean global anomalies for each dataset (right hand panel). All time series have been anomalized to a common 1989–1998 reference period.

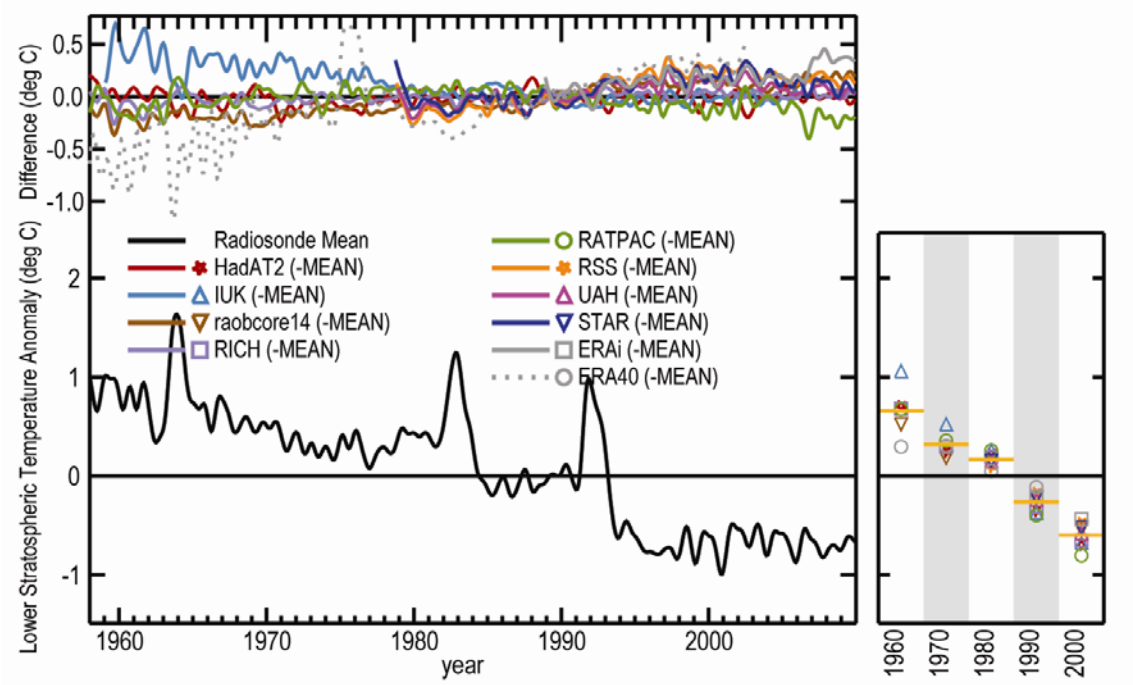

Figure 2.22: Global average lower stratospheric temperature anomaly time series for the mean of all included radiosonde datasets and offset therefrom the differences from this composite for each dataset (left hand panel). Decadal mean global anomalies for each dataset (right hand panel). All timeseries have been anomalized to a common 1989–1998 reference period.

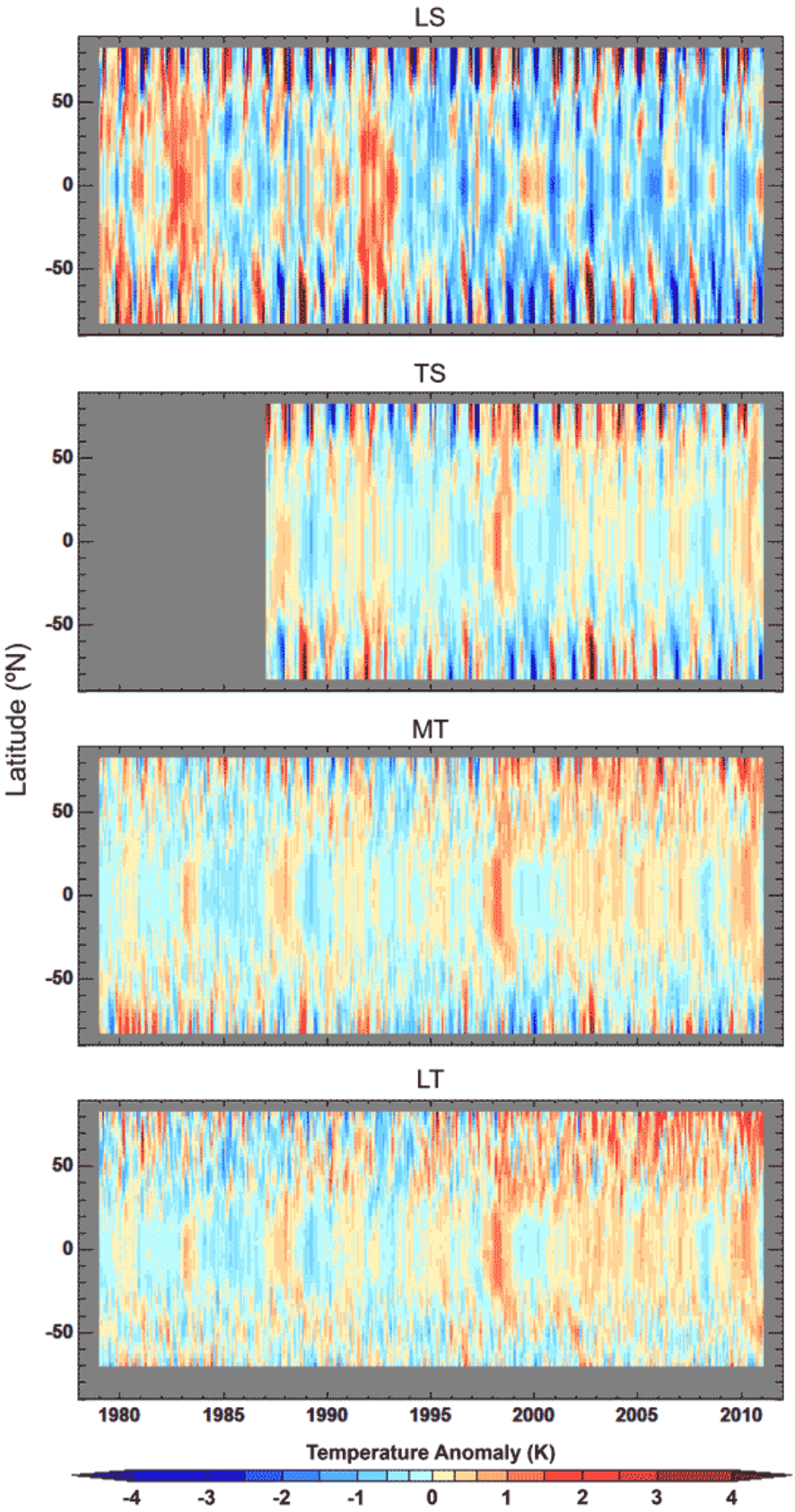

Figure 2.23: Latitude-time variations in temperature anomalies from v.3.3 of the RSS product (Mears and Wentz, 2009a; Mears and Wentz, 2009b) for estimates from the lower troposphere (bottom) to the lower stratosphere (top).

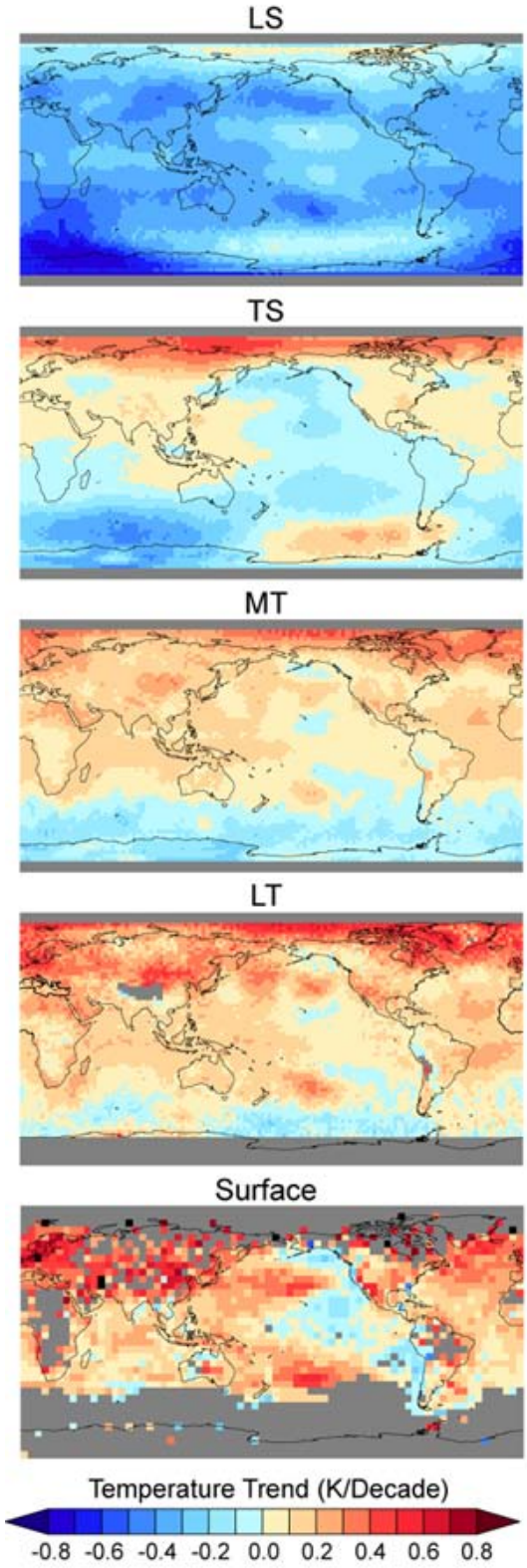

Figure 2.24: Trend maps from the surface (HadCRUT3, Brohan et al., 2006) and four atmospheric layers from MSU/AMSU (RSS v. 3.3, Mears and Wentz, 2009a, 2009b) over the period 1979–2009 (except for TS which is 1987–2009).

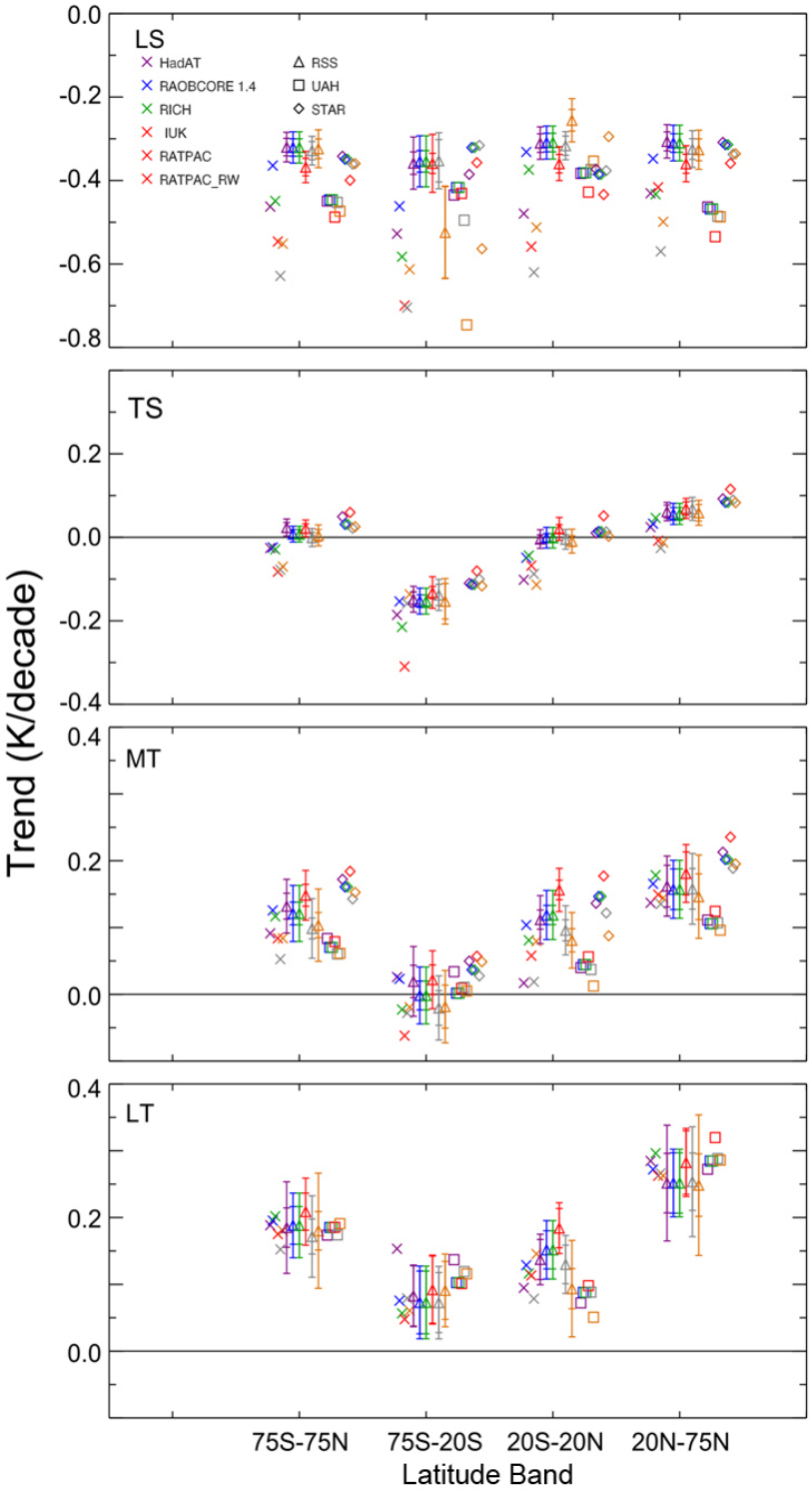

Figure 2.25: Trend estimates for MSU datasets sampled as the radiosonde datasets in space and time (hence multiple estimates for each MSU product) and the radiosonde datasets for a quasi-global average excluding the highest latitude and three sub-domains. For the RSS product internal uncertainty estimates as given in Mears (2011) are shown as whiskers (2 standard deviations). RATPAC RW is for a subsampled set of RATPAC following Randel and Wu (2006) who found potential issues for a number of RATPAC records in the stratosphere.

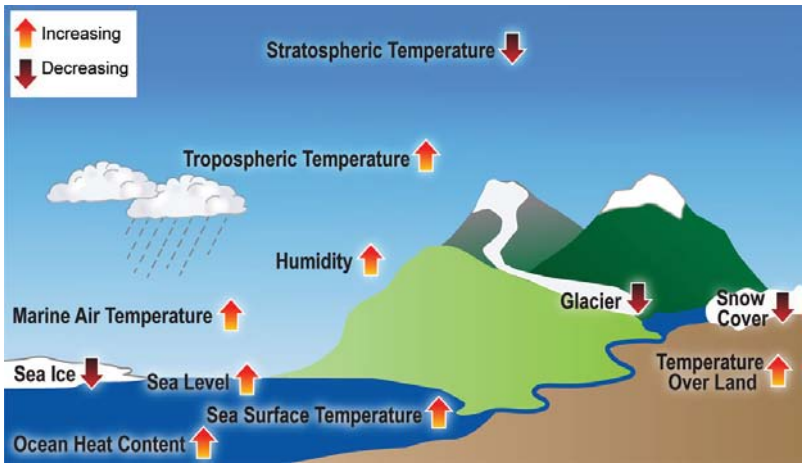

FAQ 2.1, Figure 1: Schematic of those climate elements that have been measured quasi-globally and on multi-decadal timescales that would be expected to change if the world were indeed warming; and the direction in which they would be expected to change.

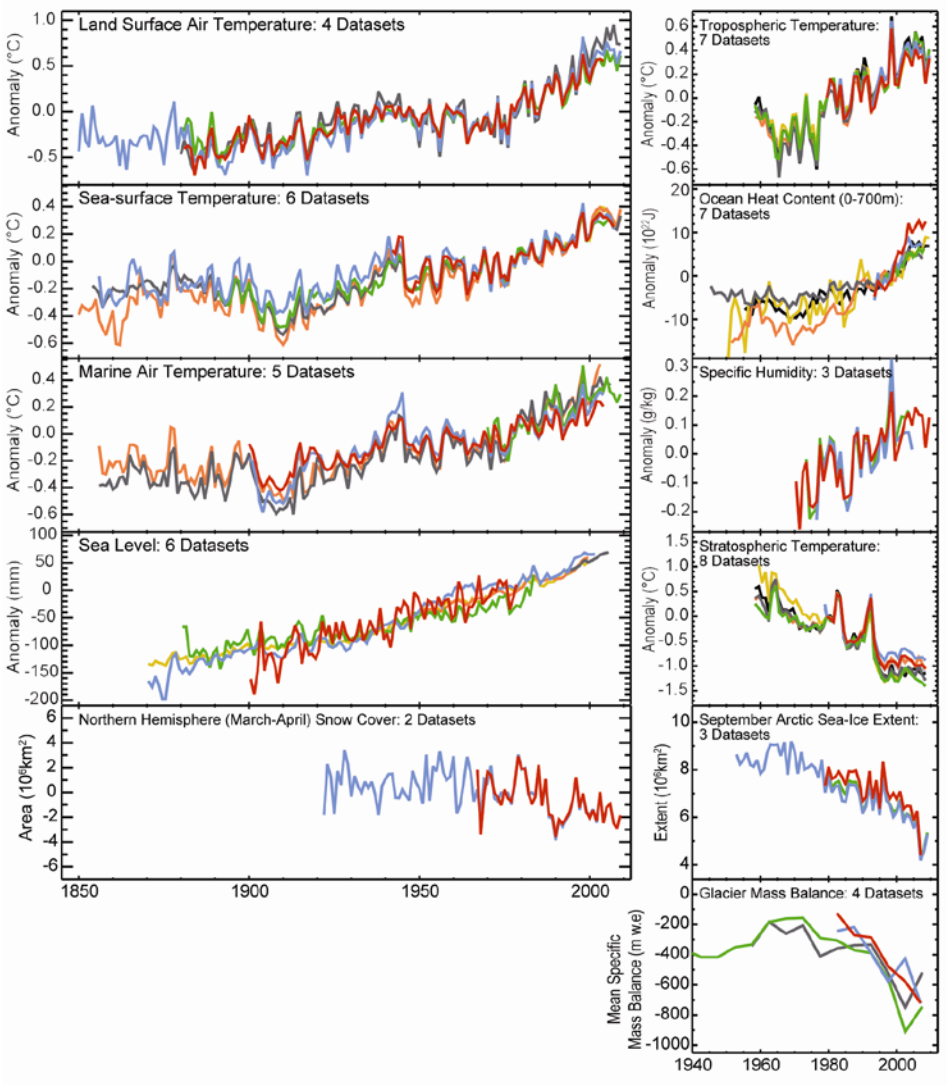

FAQ 2.1, Figure 2: Multiple redundant indicators of a changing global climate. Each line represents an independently derived estimate of change in the climate element. All publically available, documented, datasets known to the authors have been used in their latest version with no further screening criteria applied. Further details are given in Baringer et al. (2010).

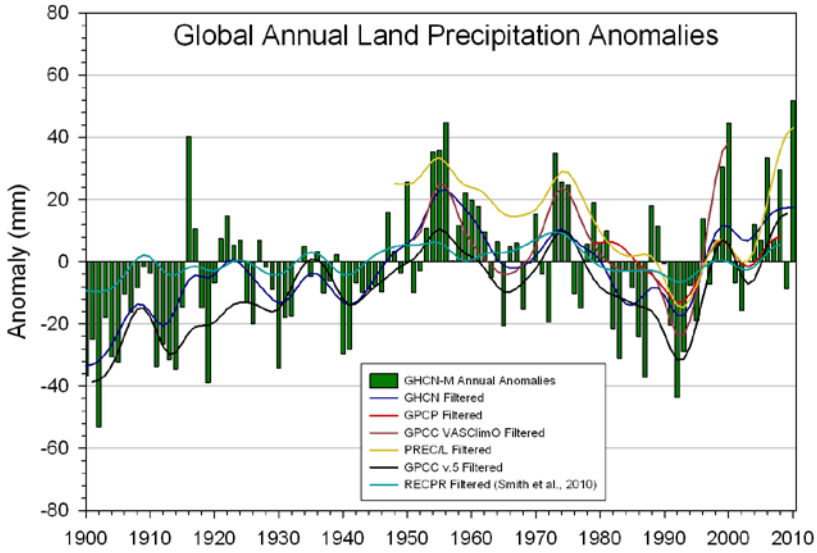

Figure 2.26: Globally averaged annual precipitation over land areas from GHCN (green bars) with respect to the 1981–2000 base period. Smoothed curves (see Appendix 3.A from Trenberth et al., 2007)) for GHCN and other global precipitation data sets as listed.

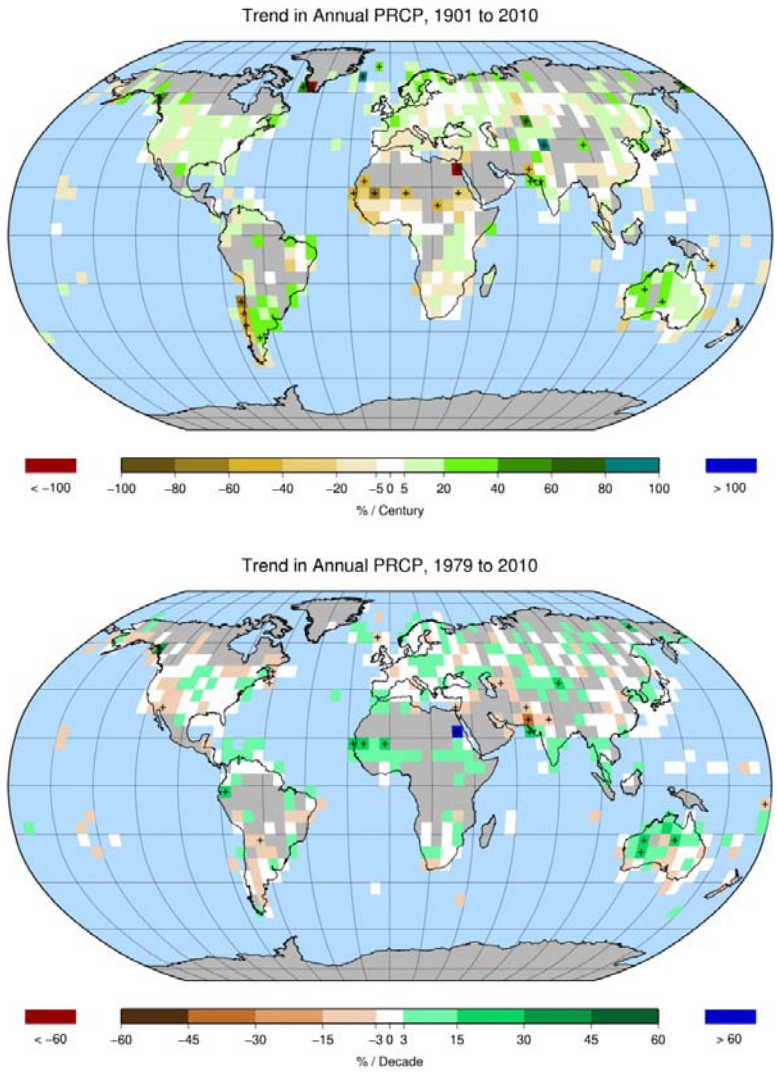

Figure 2.27: Linear trend, in % per century for annual precipitation from the GHCN data set for 1901–2010 (top) and 1979–2010 (bottom). Grid boxes with statistically significant trends at the 95% level are indicated by +.

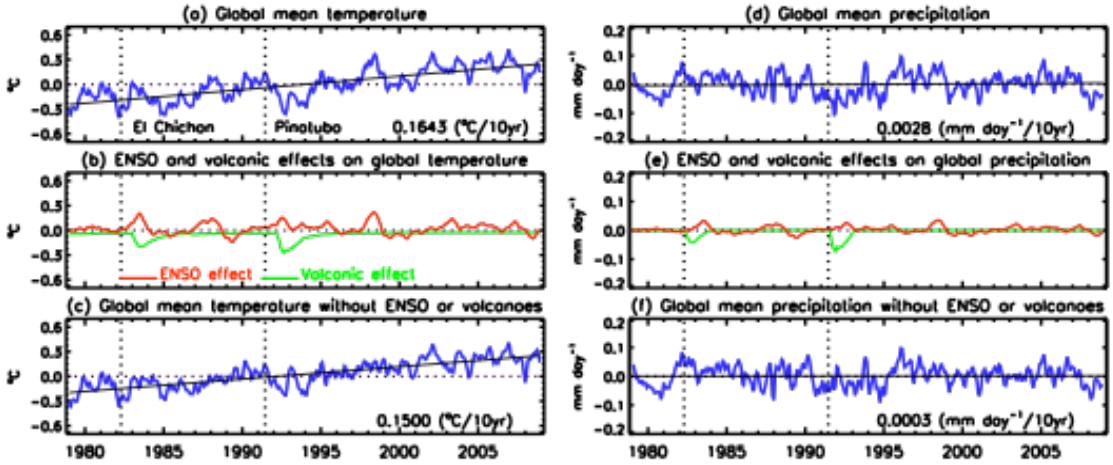

Figure 2.28: a) and d) are time series of global mean temperature and precipitation anomalies during 1979–2008, respectively. b) and e) are their corresponding ENSO and volcanic effects. c) and f) are time series of global mean temperature and precipitation anomalies with ENSO and volcanic effects removed. Also shown in a), c), d) and f) are estimated linear trends during the time period.

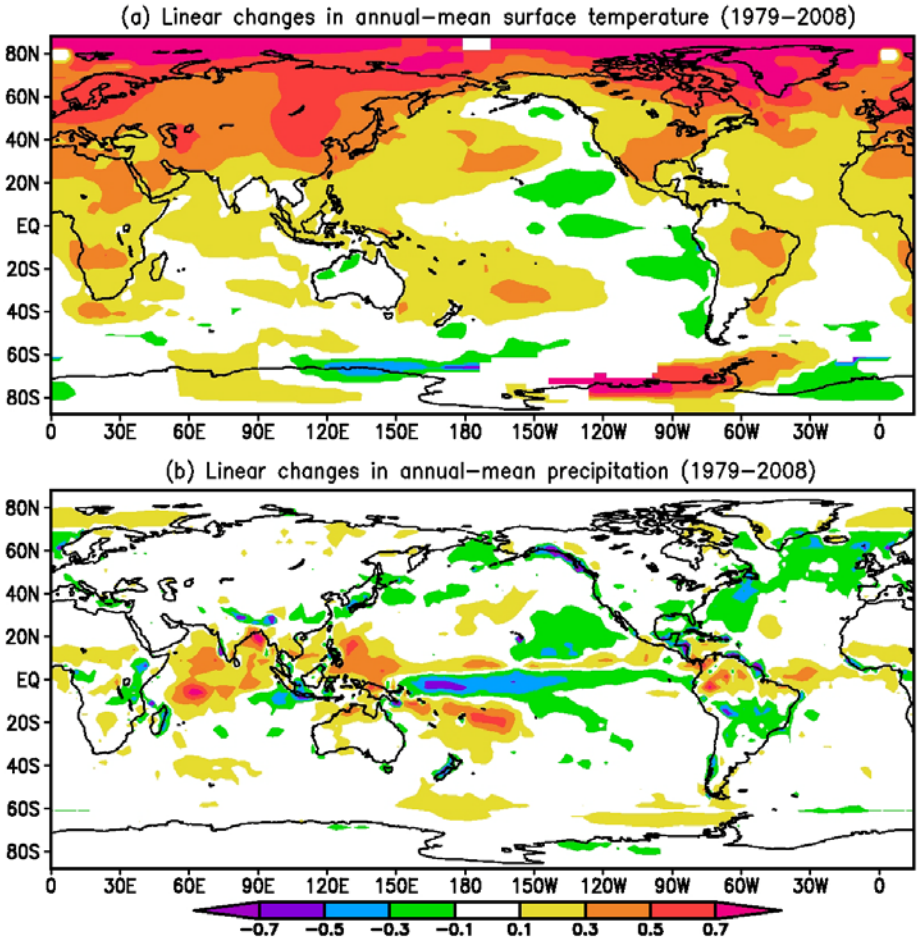

Figure 2.29: Linear changes of annual-mean a) surface temperature and b) precipitation during 1979–2008.

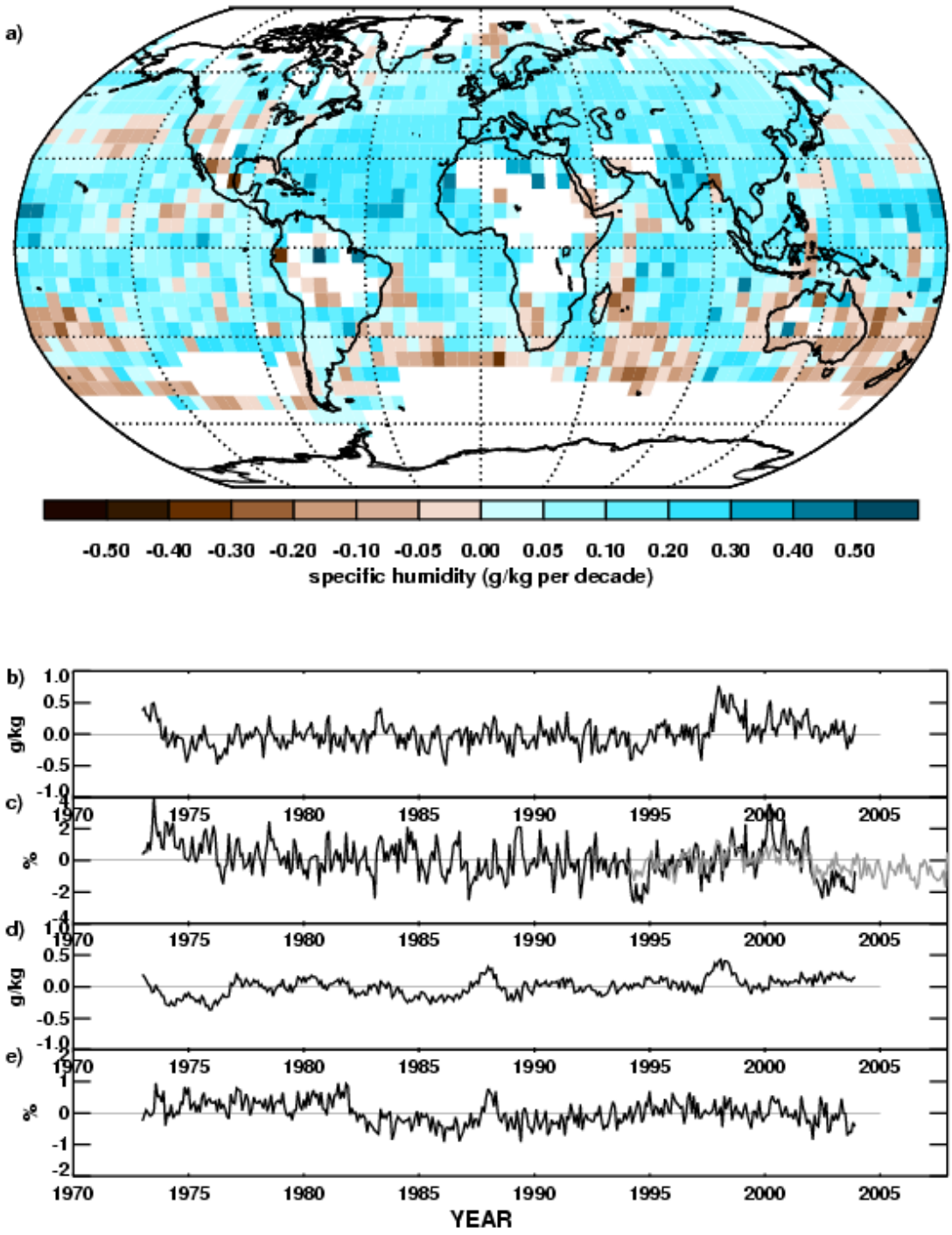

Figure 2.30: Trends and variability in surface humidity. a) Decadal trends in surface specific humidity in g kg^{-1} per decade from HadCRUH over 1973–2003. b) Globally averaged monthly mean anomaly time series of land surface specific humidity. c) Globally averaged monthly mean anomaly time series of land surface relative humidity. d) Globally averaged monthly mean anomaly time series of marine surface specific humidity. e) Globally averaged monthly mean anomaly time series of marine surface relative humidity. Time series show data from HadCRUH (solid thick black), HadCRUHext (solid thick grey), Dai (dotted red), ERA 40 (long dashed light blue), ERA interim (dot dashed royal blue) and Berry & Kent (solid thick orange).

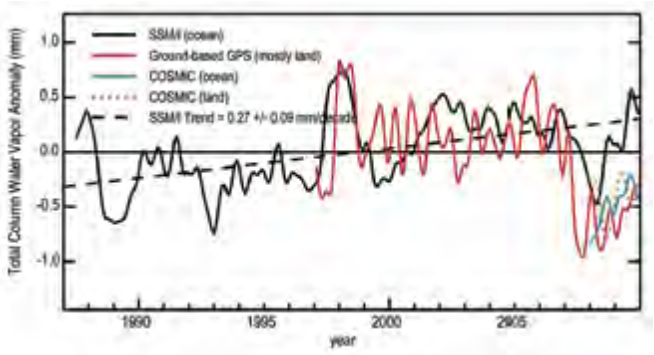

Figure 2.31: Global Anomalies in Water Vapour (from State of Climate Report).

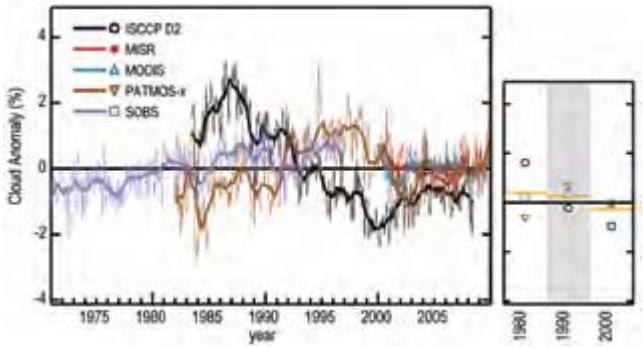

Figure 2.32: Global Anomalies in Cloud Cover (from State of Climate Report).

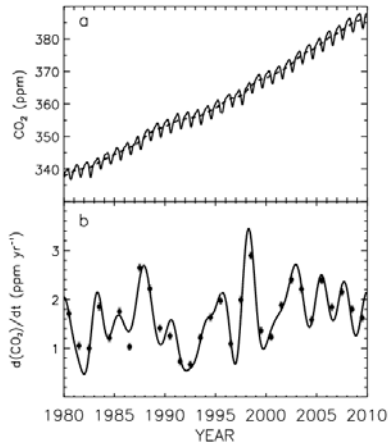

Figure 2.33: a) Solid line shows globally averaged CO_2 dry air moles fractions; dashed line is a deseasonalized trend curve fitted to the global averages. b) Instantaneous growth rate for globally averaged atmospheric CO_2 (solid line; dashed lines are ±68% confidence limits). The growth rate is the time-derivative of the dashed line in a). Symbols are annual increases from January 1 in one year to January 1 in the next year, plotted in the middle of the year.

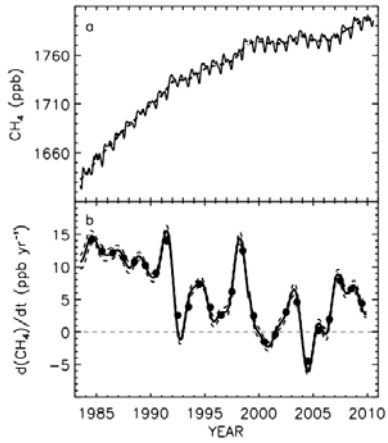

Figure 2.34: a) Solid line shows globally averaged CH_4 dry air moles fractions; dashed line is a deseasonalized trend curve fitted to the global averages. b) Instantaneous growth rate for globally averaged atmospheric CH_4 (solid line; dashed lines are ±68% confidence limits). The growth rate is the time-derivative of the dashed line in a). Symbols are annual increases from January 1 in one year to January 1 in the next year, plotted in the middle of the year.

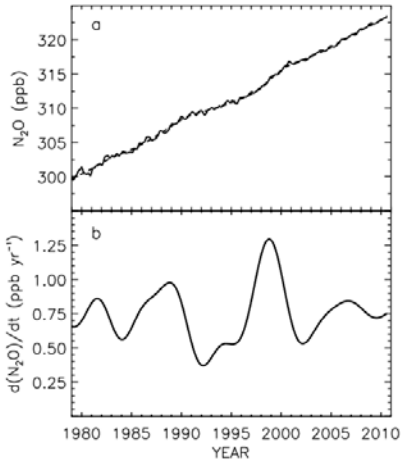

Figure 2.35: a) Solid line shows globally averaged N_2O dry air moles fractions; dashed line is a deseasonalized trend curve fitted to the global averages. b) Instantaneous growth rate for globally averaged atmospheric N_2O. The growth rate is the time-derivative of the dashed line in a).

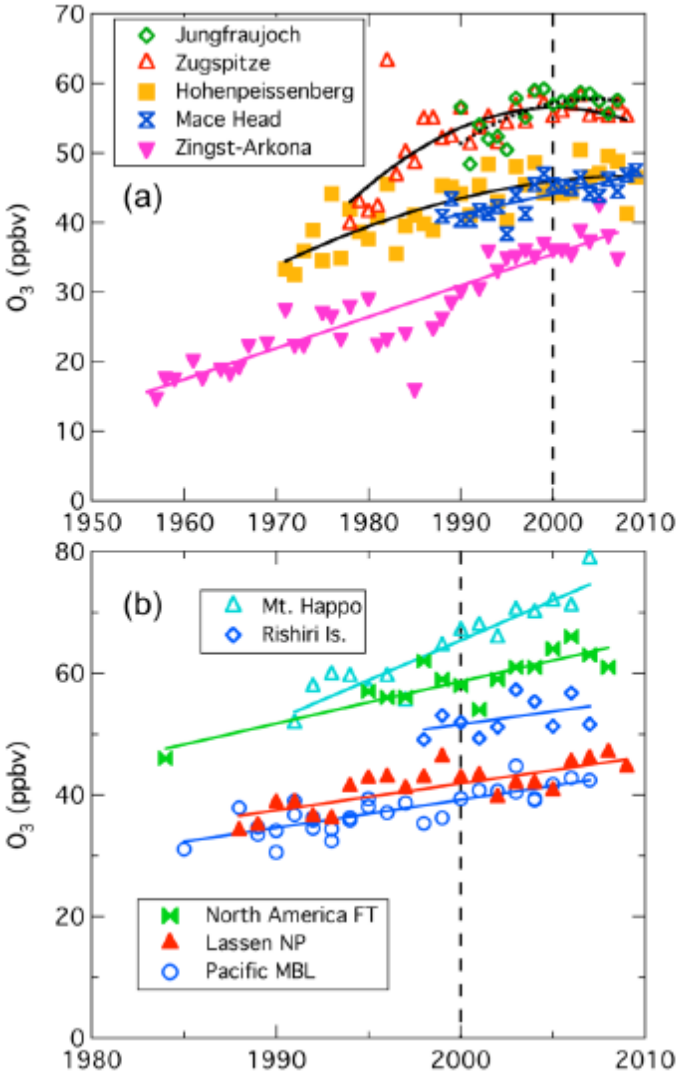

Figure 2.36: Springtime trends in O_3 concentrations measured in a) Europe and b) western North America and Japan. The lines (in colour) indicate the linear regressions to the data, and the curves (in black) indicate quadratic polynomial fits to the three central European sites over the time span of the lines. Arkona and Zingst are two sites located close to the Baltic Sea. Mace Head is located at the west coast of Ireland. Hohenpiessenberg (1.0 km asl) and Zugspitze (3.0 km asl) are in southern Germany, and Jungfraujoch (3.6 km asl) is in Switzerland. The North American data are from several sea level Pacific coastal sites and Lassen National Park (1.8 km asl) near the west coast, and from the free troposphere over the western part of the continent. The Japanese data are from Mt. Happo (1.9 km asl) on the Japanese mainland and Rishiri, a northern (45N) sea level island site (HTAP, 2010).

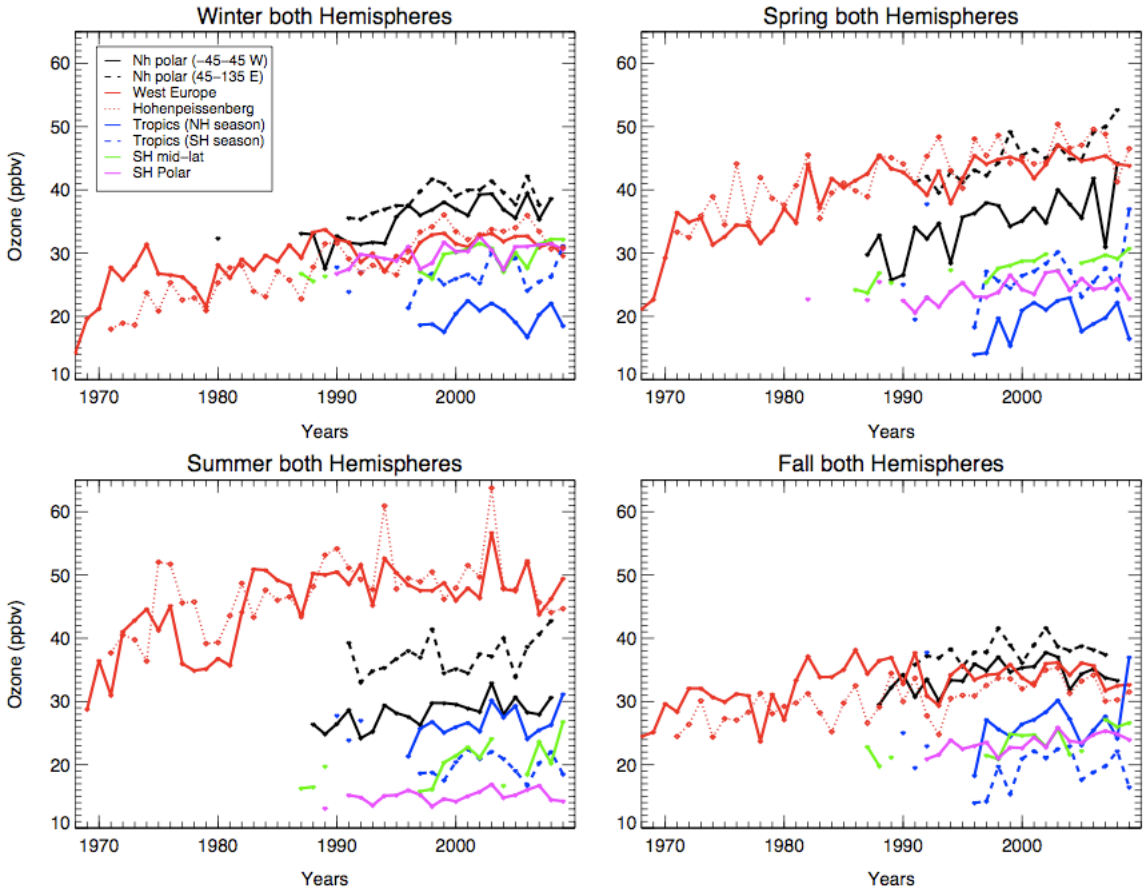

Figure 2.37: Seasonal and regional ozone from soundings at 850–950 hPa pressure levels between 1968 and 2009. Each seasonal data point represents the median statistics of >10 soundings. Winter refers to NH December-January-February and SH, July-August-September, etc.

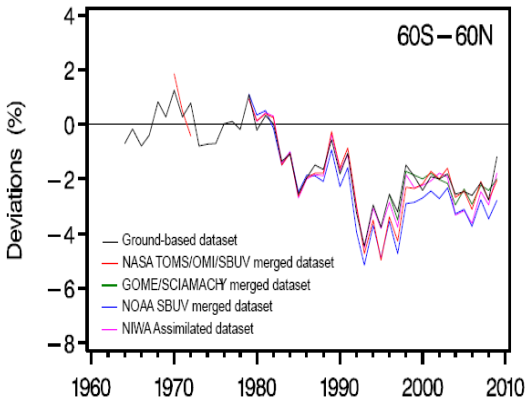

Annual mean area-weighted total ozone deviations for 60°S–60°N estimated from different global datasets: ground-based (black), NASA TOMS/OMI/SBUV(/2) merged satellite dataset (red), National Institute of Water and Atmospheric Research (NIWA) assimilated dataset (magenta), NOAA SBUV(/2) (blue), and GOME/SCHIAMACHY merged total ozone data (green). Each dataset was deseasonalized with respect to the period 1979–1987. The average of the monthly-mean anomalies for 1964–1980 estimated from ground-based data was then subtracted from each anomaly time series. Deviations are expressed as percentages of the ground-based time average for the period 1964–1980.

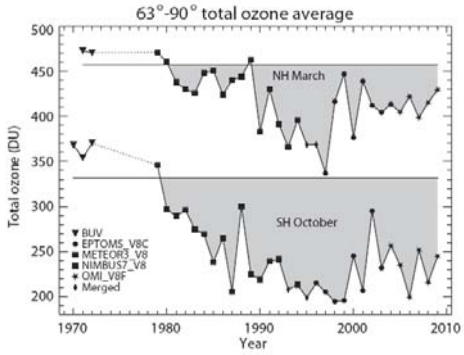

Figure 2.38: Trends in midlatitude a) and polar b) stratospheric ozone. Total ozone average of 63°–90° latitude in March (NH) and October (SH). Symbols indicate the satellite data that have been used in different years. The horizontal grey lines represent the average total ozone for the years prior to 1983 in March for the NH and in October in the SH.

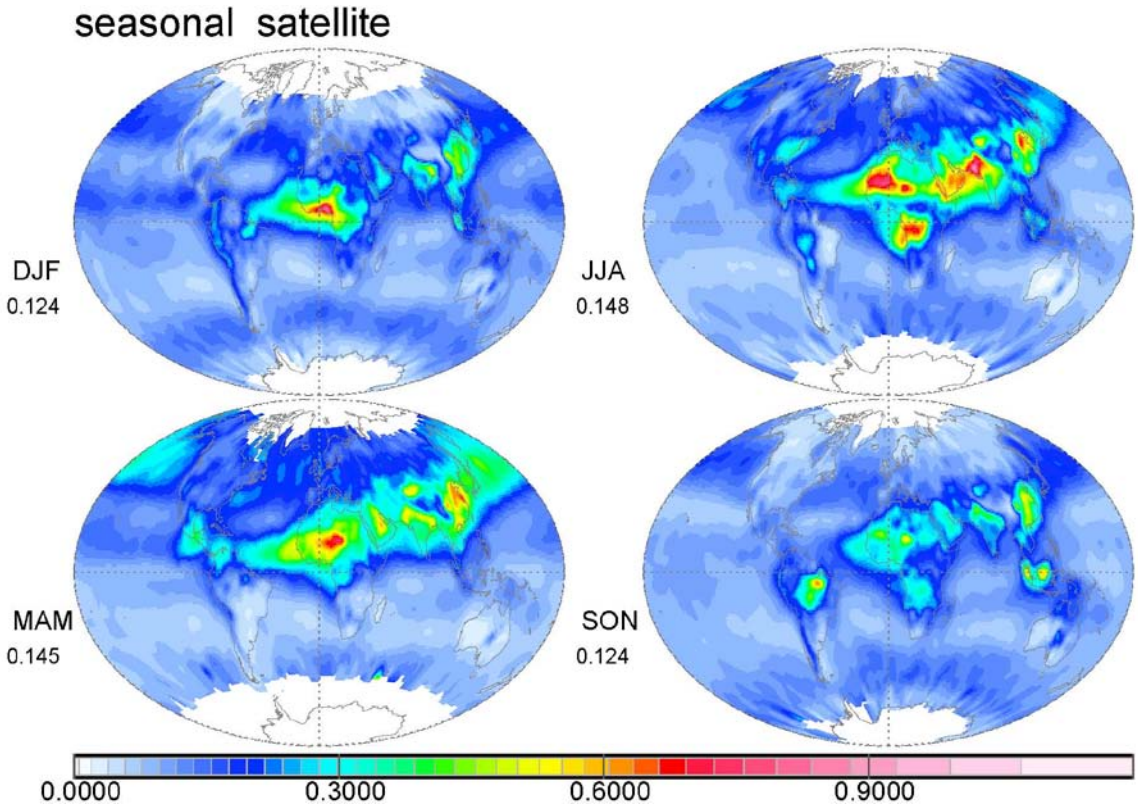

Figure 2.39: Global seasonal maps for aerosol optical depth (AOD) distributions at 550nm based a multi-annual satellite sensor retrievals by MODIS, MISR and AVHRR (after validations against ground-based sun-photometry). Strongest aerosol loads are caused by a) biomass burning during DJF in western Africa and during SON in southern America, southern Africa and Indonesia, b) by dust during MAM and JJA in northern Africa and during MAM also over the mid-east and eastern Asia and c) by pollution in MAM and especially during JJA over the industrial centers of the Northern Hemisphere.

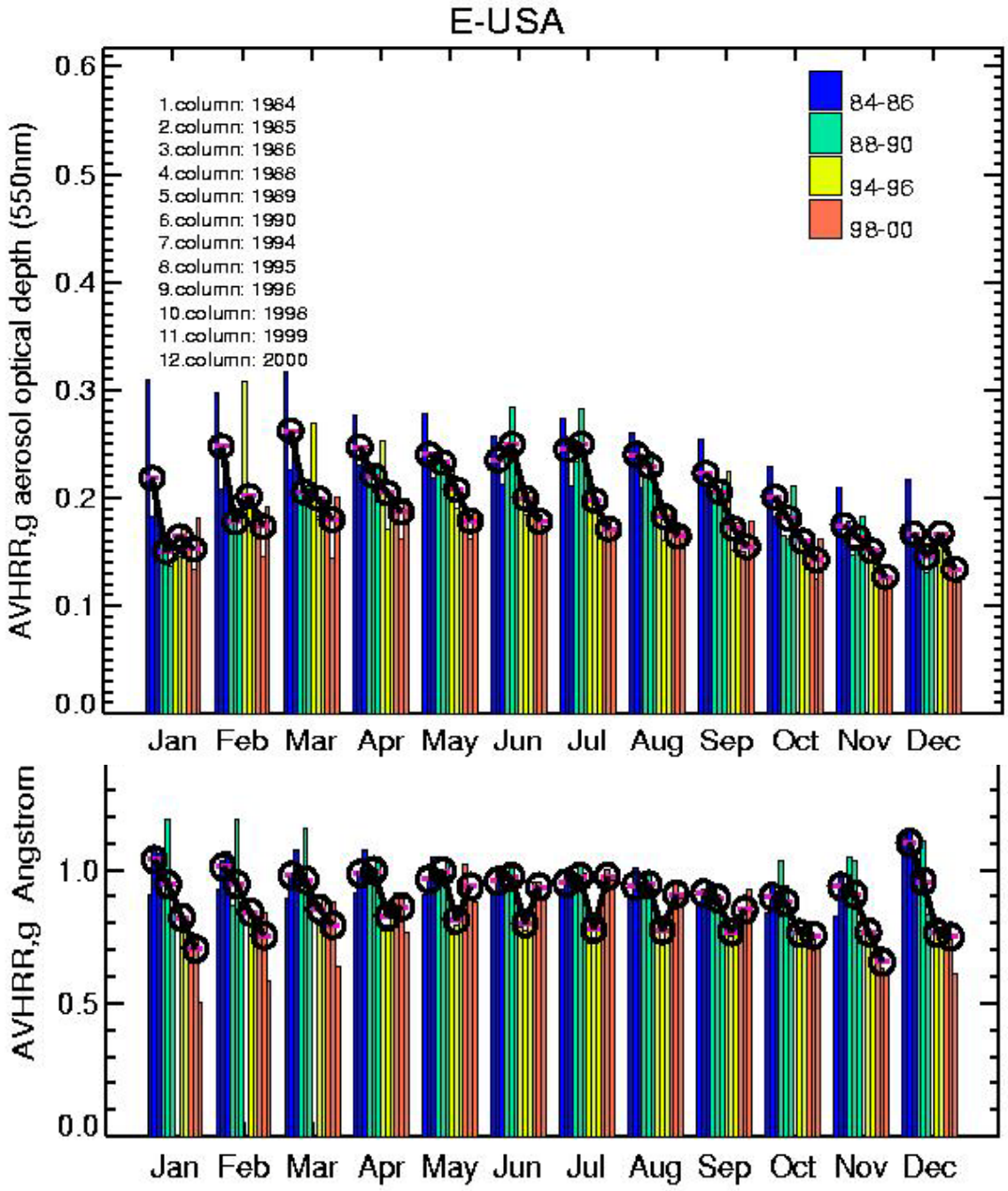

Figure 2.40: Comparison of AVHRR based trends between 1984 and 2000 for mid-visible AOD (amount) and Angstrom parameter (size) based on data off the US east coast. The data show continued decreases for AOD over the entire annual cycle and also reduction to particles size in winter (smaller Angstrom coefficient), suggesting temporal trends for the reduction of fine-mode aerosol particles over the eastern US.

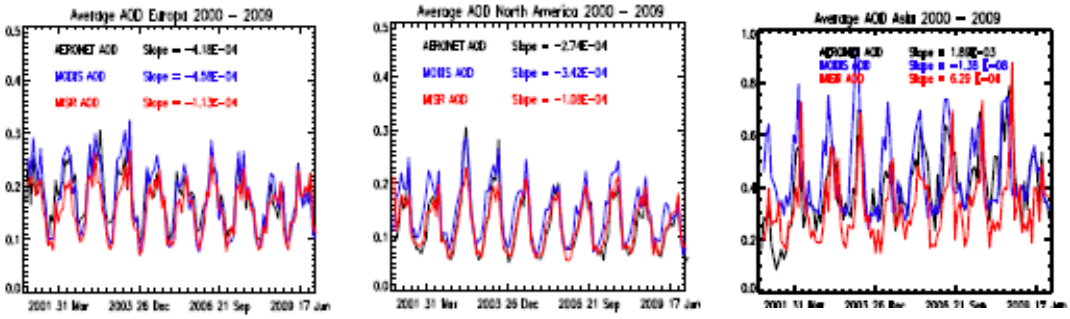

Figure 2.41: Average AOD temporal profiles from MODIS (Level 3), MISR (level 3) and AERONET (Level 2) for the 2000–2009 time period in Europe, North America and Asia. Level 2 and 3 refer to the amount of temporal, spatial, or spectral aggregration/processing of the data.

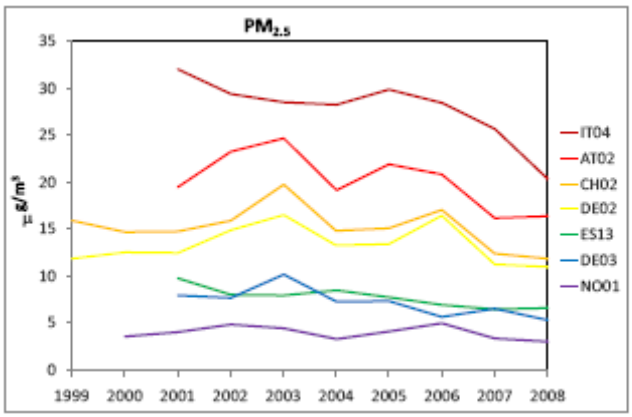

Figure 2.42: Time series of annual average PM2.5 (ug/m^3) in Europe (IT Italy;AT Austria; CH Switzerland; DE Germany; ES Spain; NO Norway).

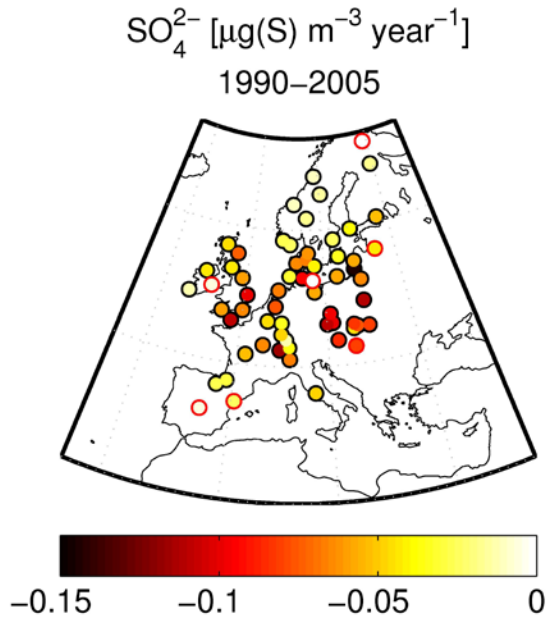

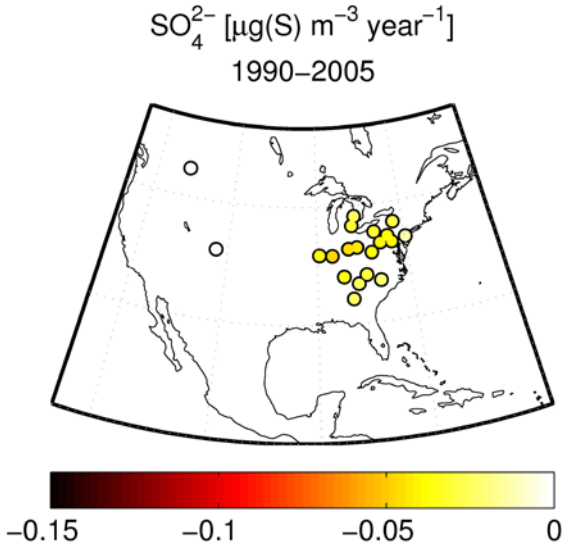

Figure 2.43: Observed SO_4 trends 1990–2005 (ug S/m^3 yr^{-1}) in Europe and the US. Not significant trends are denoted with red circle (Pozzoli et al., 2011).

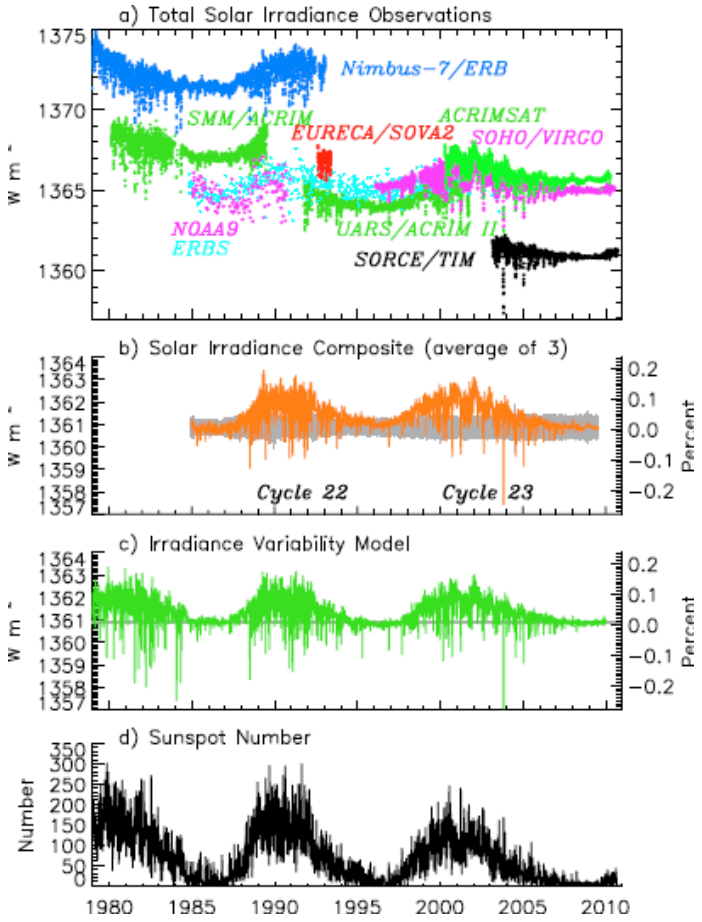

Figure 2.44: Space-borne total solar irradiance (TSI) measurements are shown in a) in "native" scales with offsets attributable to calibration errors. Instrument overlap allows corrections for offsets and the creation of a composite TSI record. Plot b) shows the average of three different reported composites [ACRIM, PMOD, and RMIB] adjusted to match the SORCE/TIM absolute scale. The grey shading indicates the standard deviation of the three composites. Shown in c) are irradiance variations estimated from an empirical model that combines the two primary influences of facular brightening and sunspot darkening with their relative proportions determined via regression from direct observations made by SORCE/TIM. The daily sunspot numbers shown in d) indicate fluctuating levels of solar activity for the duration of the database [(from Kopp and Lean, 2010, in press)].

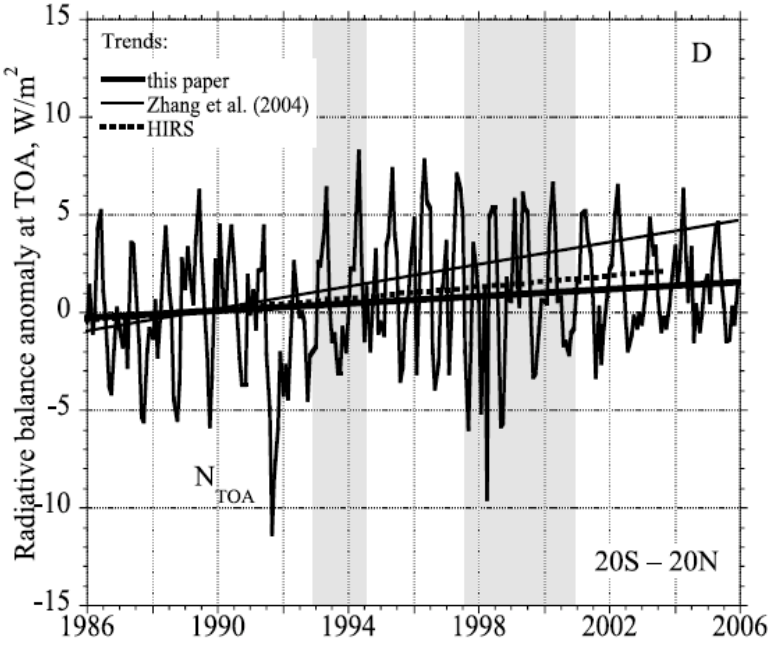

Figure 2.45: Net TOA flux anomaly from 1985–2005 for 20S–20N from merged ERBS and CERES Terra (thick solid line). The thin solid and dotted lines are derived using SW measurements from ERBS/CERES and LW observations from ISCCP-FD (Zhang et al., 2004) and HIRS (Lee et al., 2007; Lee et al., 2004). Anomalies are relative to the average over 1985–1989. From Andronova et al., (2009).

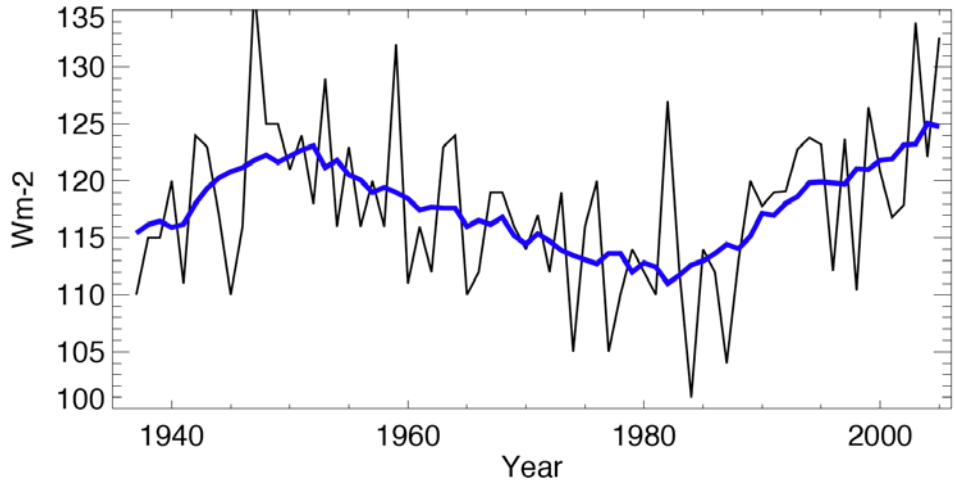

Figure 2.46: Annual mean surface solar radiation (in W m^{-2}) as observed at Potsdam, Germany, from 1937 to 2006. Five year moving average in blue. Distinct phases of inclines (1930s–1940s, "early brightening"), declines (1950s–1980s, "dimming") and renewed inclines (since 1980s, "brightening") can be seen. From Wild (2009).

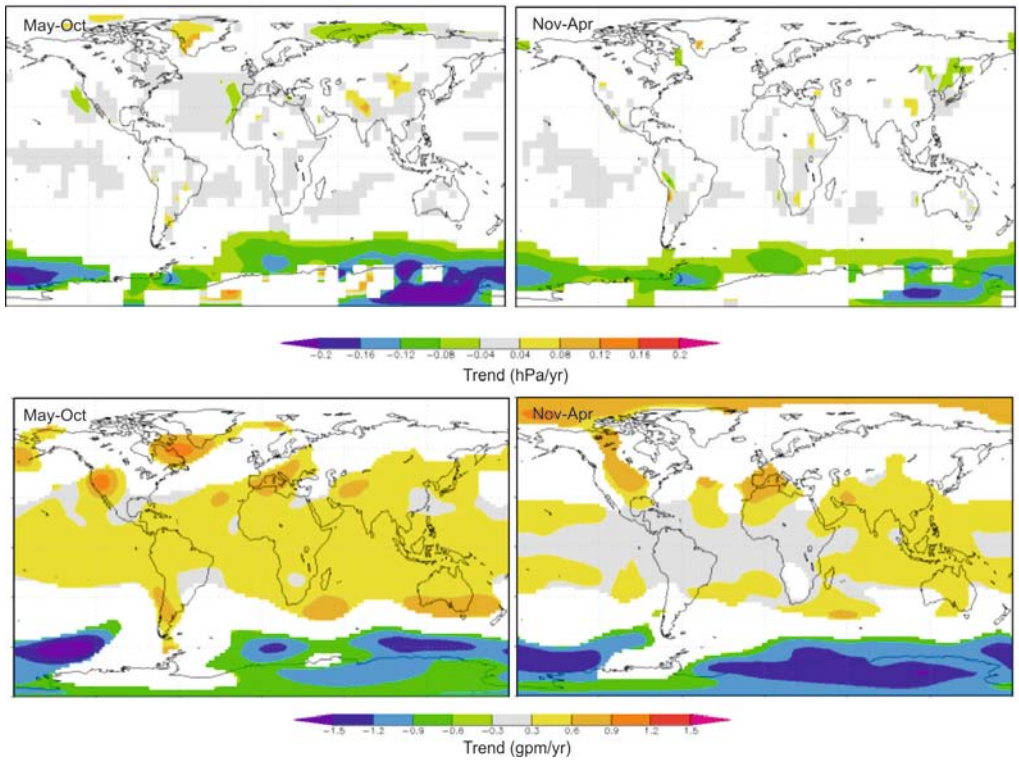

Box 2.2, Figure 1: Top: Linear trends in SLP from HadSLP2 (Allan and Ansell, 2006) between 1970 and 2010 (top) and 500 hPa GPH from 20CR (Compo et al., 2011) between 1970 and 2008 (bottom) for May-October season (left) and November-April (right). Only trends that are significant at the 10% level are shown.
[THIS IS A SIMPLE KNMI CLIMATE EXPLORER STRAWMAN; NEEDS TO BE REDONE WITH TREND ESTIMATE.]

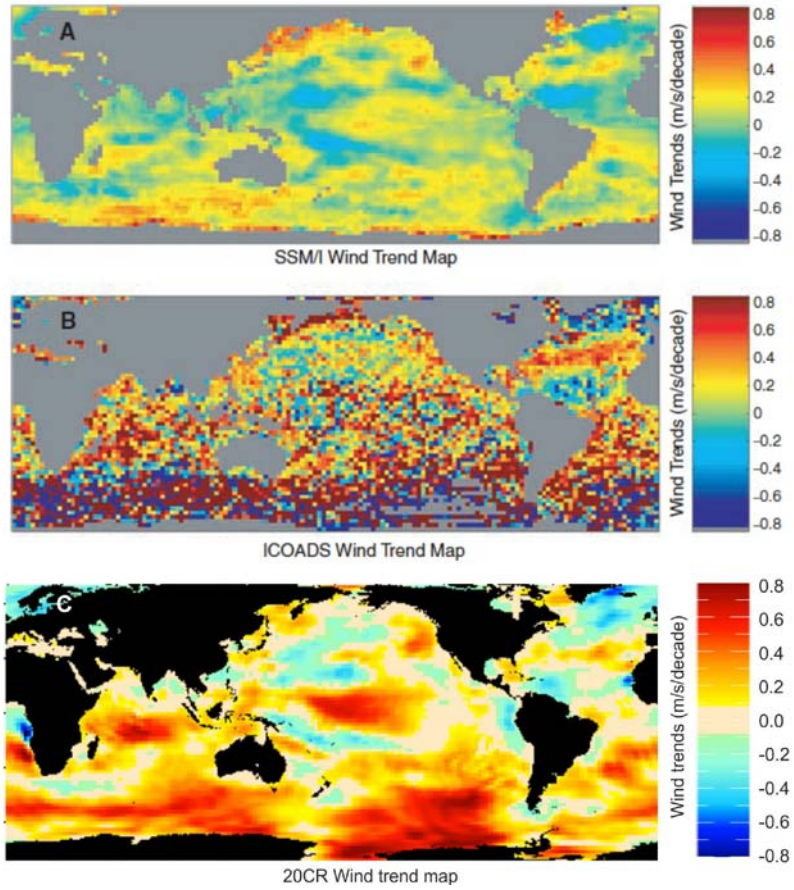

Figure 2.47: Surface wind trends for the period July 1986 to August 2006 computed at a spatial resolution of 2.5°. a) SSM/I wind trends, b) ICOADS wind trends (Wentz et al., 2007), c) 0.995 sigma level wind trend from 20CR.
[THIS IS A STRAWMAN FIGURE: PANELS B AND C COULD BE COMPLEMENTED WITH LAND SURFACE WINDS FROM ANEMOMETERS AND 20CR, RESPECTIVELY, BUT NEEDS FURTHER EFFORT.]

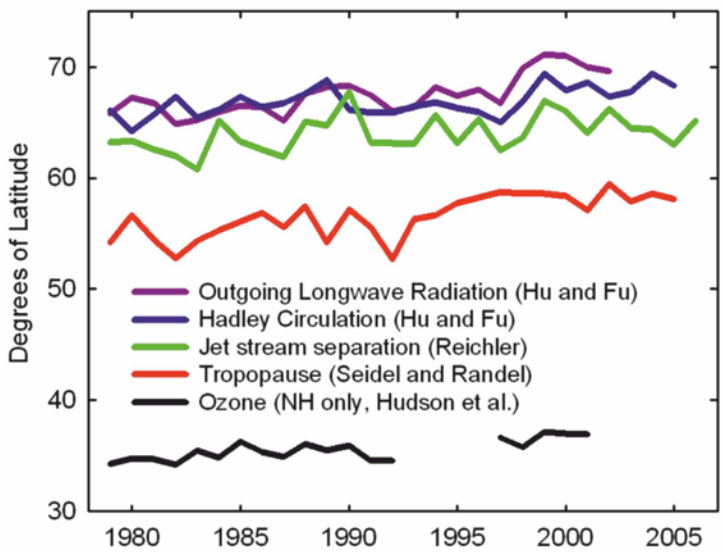

Figure 2.48: Width of the tropical belt as seen in various observation-based data sets (Seidel et al., 2008). [THIS IS A STRAWMAN FIGURE; I SUGGEST UPDATING IT AND ADDING INDICES ON STORM TRACKS.]

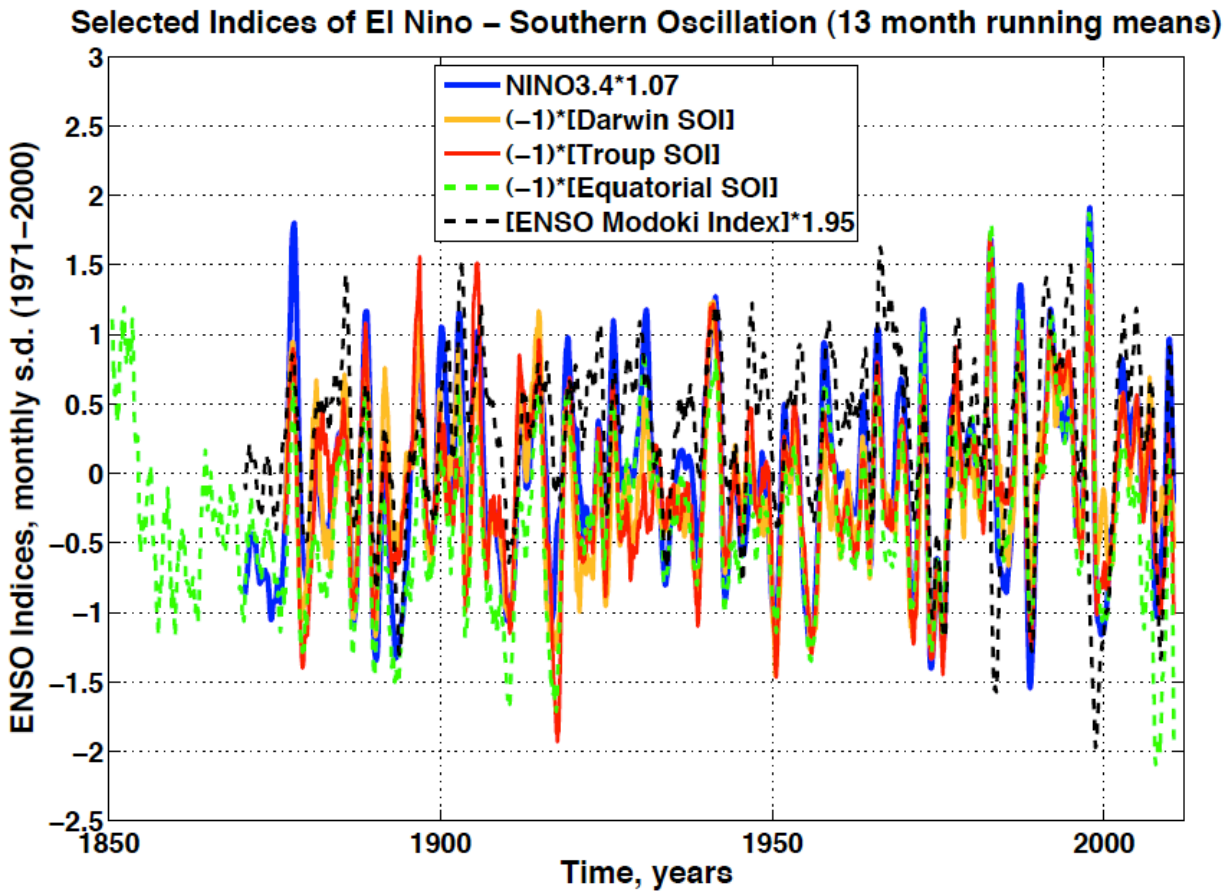

Box 2.3, Figure 1: Selected indices of ENSO as defined in Box 2.3, Table 1. To ease visual comparison, sign is inverted for all SOI versions; 13-month-running-means filter is applied to all indices. SOIs are standardized over 1971–2000 period by construction; temperature-based indices NINO3.4 and ENSO Modoki Index (EMI) are standardized here over the same period. Their standardization factors (in units of $1/^{o}C$) are specified in the legend.

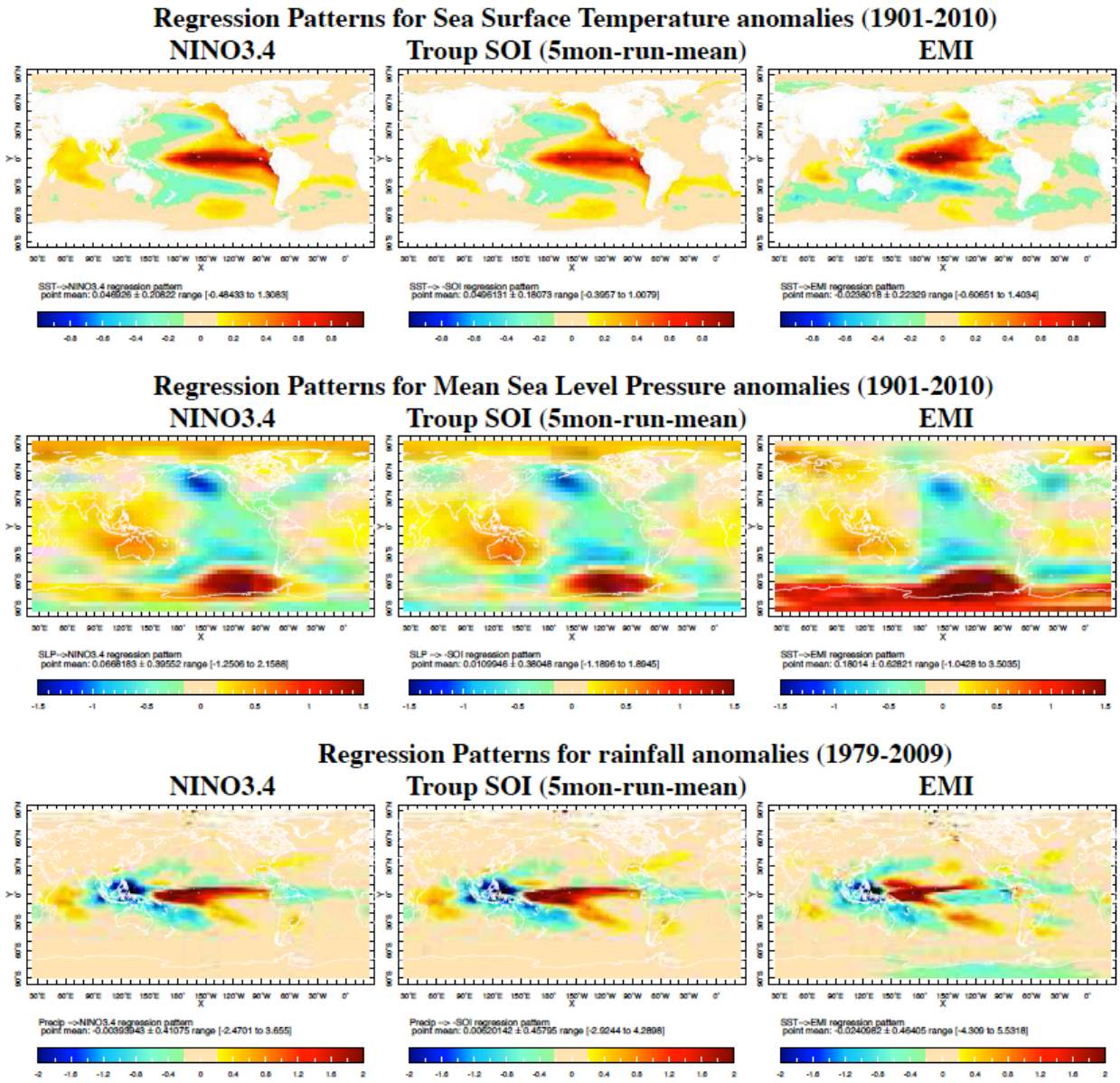

Box 2.3, Figure 2: ENSO-related variability patterns in SST, MSLP, and rainfall corresponding to the three of ENSO indices shown in Box 2.3, Figure 1: NINO3.4, Troup SOI, and EMI. Patterns are obtained by regressing monthly mean fields of these variables on each of the indices. HadISST1 and HadSLP2r for 1901–2010 period are used for SST and MSLP data respectively, and Xie and Arkin's CMAP precipitation data set is used for the rainfall fields (January 1979 – August 2009). Units of regression patterns for SST, MSLP, and rainfall, on either of temperature indices (NINO3.4 and EMI) are unitless, mb/^{o}C, and mm/day/^{o}C, respectively, and ^{o}C, mb, and mm/day per one standard deviation for SOI. Regression patterns on NINO3.4 and SOI are very similar: these are viewed as traditional ENSO impact patterns. Patterns corresponding to EMI are somewhat different, since the EMI indexes a non-canonical type of El Niño: Modoki, or Central Pacific El Niño.

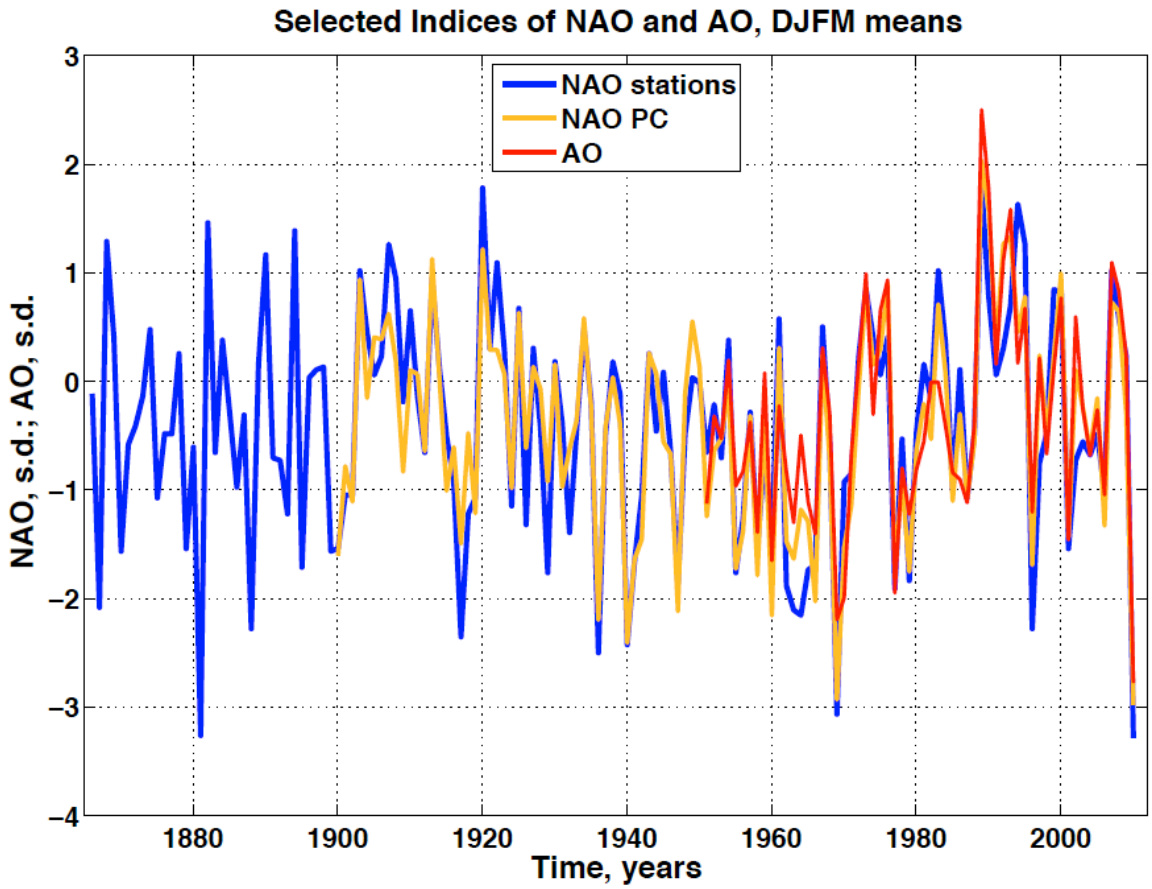

Box 2.3, Figure 3: Selected indices of NAO and AO (a.k.a. NAM) as defined in Box 2.3, Table 1. Station-based (Lisbon/Ponta Delgada minus Stykkisholmur/Reykjavik) and PC-based NAO indices are according to Hurrell (1995a), and AO index is computed by CPC on the basis of NCEP/NCAR Atmospheric Reanalysis. All indices are standardized for the 1971–2000 period. The last value in the plot corresponds to the 2009–2010 DJFM average is formally a record low in the data interval 1865 to present that is shown here (although it is very close to the previous record, set in 1880–1881 winter). The 2010–2011 DJFM value (not shown) is expected to be similarly low.

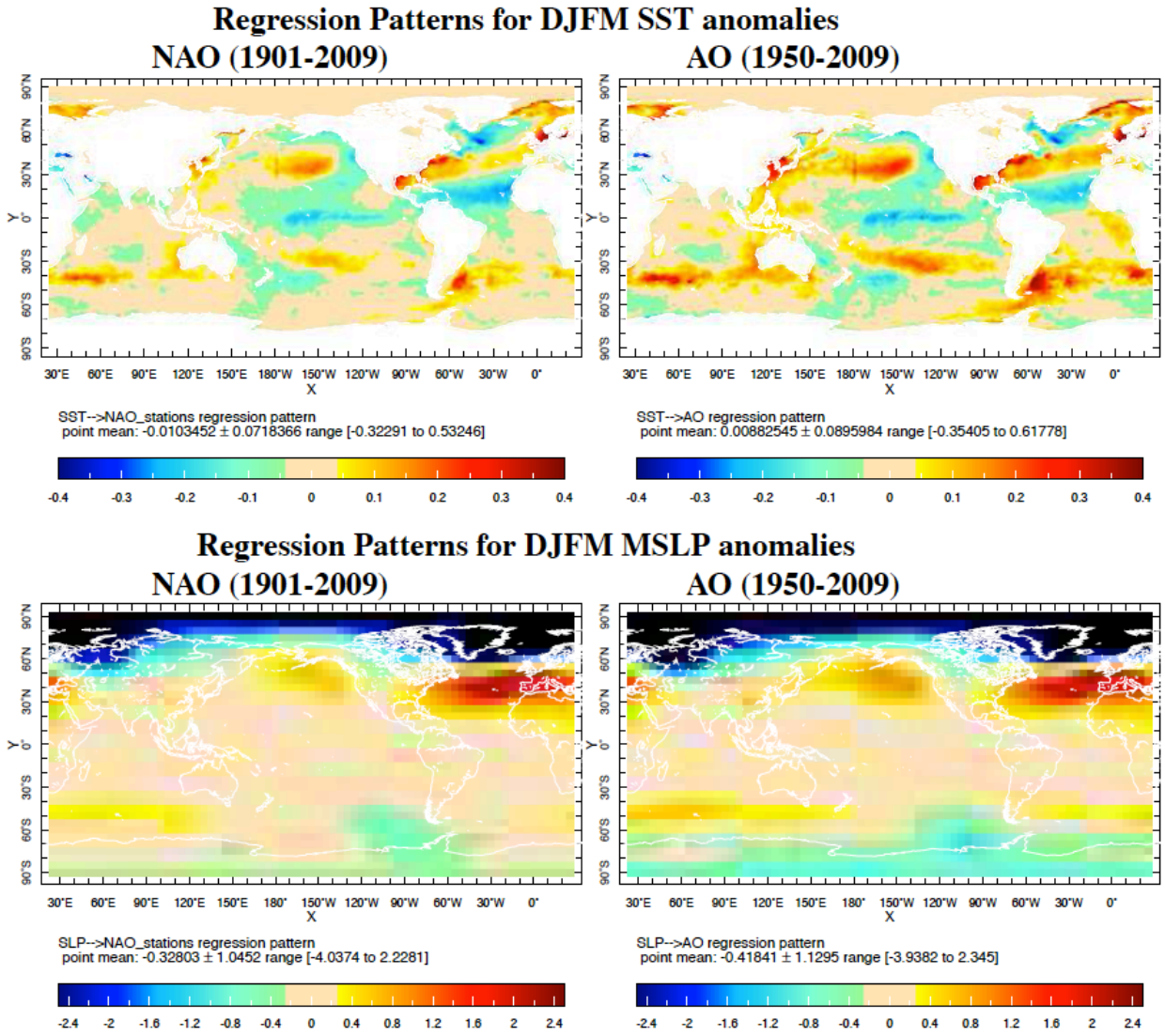

Box 2.3, Figure 4: NAO- and AO-related variability patterns in the SST and MSLP. The patterns are obtained by regressing monthly mean fields of these variables on the NAO station-based index from Hurrell (1995a) and the AO index from the CPC. Regressions are performed for the DJFM averages. HadISST1 and HadSLP2r for 1901–2010 period are used for the SST and MSLP data, respectively. Units in the regression patterns for SST and MSLP are ^{o}C/s.d and mb/s.d., respectively.